UNIVERSITY
of
GLASGOW

Department of Civil Engineering

Incipient Motion of Streambeds

by

Andrey B. SHVIDCHENKO

Thesis submitted to the University of Glasgow
in candidacy for the degree of
Doctor of Philosophy

GLASGOW
THE UNITED KINGDOM

September 2000

To my parents

Declaration

I declare that this thesis is a record of the original work carried out solely by myself in the Department of Civil Engineering at the University of Glasgow, United Kingdom, during the period of October 1997 to September 2000. The copyright of this thesis therefore belongs to the author under the terms of the United Kingdom Copyright Acts. Due acknowledgement must always be made of the use of any material contained in, or derived from, this thesis. The thesis has not been presented elsewhere in consideration for a higher degree.

Andrey B. Shvidchenko

September 2000

Acknowledgements

I would like to express my sincere gratitude to Dr G. Pender for his supervision, support and encouragement during my period of research. I am grateful to Prof N. Bicanic, Head of the Department for the provision of considerable experimental facilities. I also thank Prof D. A. Ervine, Prof R. Bettess (Hydraulics Research Ltd, Wallingford, U.K.), and Dr T. B. Hoey (Department of Geography and Topographic Science, University of Glasgow) for helpful discussions of ideas and research results. Further thanks are due to Mr K. McColl, Mr S. McLean and Ms J. McCulloch for the assistance with computing and experimental facilities, and Mr T. Montgomery and Mr W. Henderson for their technical support.

My research in Glasgow was supported financially by a University of Glasgow scholarship and an Overseas Research Student Award from the Committee of Vice-Chancellors and Principals of the Universities of the United Kingdom, which is greatly appreciated. The experimental work undertaken at Hydraulics Research Ltd, Wallingford, U.K. (HR Wallingford) was supported by an EU Human Capital and Mobility Program grant and by HR Wallingford Ltd, for which I am also very grateful. A part of research concerned the development of a computer model for graded sediment transport was funded by an Engineering and Physical Science Research Council grant. Computer software ISIS Flow/Sediment and training in its use was provided by Halcrow Group Ltd, U.K.

The data on sediment transport made available by Prof A. E. Peterson (University of Alberta, Edmonton, Canada), Prof M. Church (University of British Columbia, Vancouver, Canada), and Prof R. Bettess (HR Wallingford Ltd) is also acknowledged.

Finally, my deepest gratitude to my wife Irina for her understanding and patience, and to my daughter Tanya and son Boris whose being provided me with great moral support.

Abstract

Results of an experimental study of the incipient motion of streambeds are reported. The experiments were conducted in an 8 m long, 0.30 m wide by 0.30 m deep glass-walled tilting flume and an 18 m long, 0.80-1.10 m wide by 0.15 m deep trapezoidal concrete channel. The purpose of the experiments was to determine flow conditions associated with the initiation of bed sediment motion and to investigate near-to-threshold bedload transport. Uniform and graded natural sands and gravels were used as bed material.

A new approach to the description of critical state of the bed based on the intensity of sediment motion, or transport intensity, is proposed. This approach describes the state of the streambed mobility in terms of the fraction of bed particles mobilized in unit time, which eliminates the subjectivity in defining threshold conditions and provides a probabilistic description of the process of sediment entrainment.

On the basis of the flume data obtained for uniform sediment, a relationship between the intensity of particle motion and sediment transport rate is established. This relationship allows any measured transport rate to be expressed in terms of the probability of sediment entrainment.

The experiments reveal that critical bed shear stress for incipient motion of uniform sediment depends not only on the grain size, but also on the bed slope. This is explained by the effect of relative depth (depth to grain size ratio) on overall flow resistance. It is also shown that the value of critical dimensionless bed shear stress is not constant for rough turbulent flow, as is usually assumed, but gradually reduces for coarser gravel. The same conclusion follows from the measurements of turbulence characteristics near the bed. A revised Shields diagram relating critical stress, grain Reynolds number and bed slope is derived for different intensities of sediment motion (or, alternatively, different probabilities of sediment entrainment). The experimental results are formalized to provide a generalized method for calculating the bedload transport rate and critical Shields stress of coarse uniform sediments.

The experiments with graded sediment demonstrate that incipient motion of individual size fractions within a mixture is controlled by their relative size with respect to median size, mixture median size, and sediment sorting. The present findings are consistent with the available flume and field data. It also appears that the shear stress at

incipient motion of median-sized particles in relatively narrow graded mixtures is the same as for uniform sediment of the same size. For mixtures with a wide grading, the critical shear stress of median-sized particles is higher compared to uniform sediment. This is explained by the siltation effect reducing the overall mobility of the bed material. A technique for calculating the transport rate and critical shear stress of individual size fractions within a graded sediment is proposed.

As entrainment and motion of bed particles is largely controlled by the flow turbulence, a complementary experimental study of the turbulent structure of open-channel flow over a mobile gravel bed was undertaken in an 8 m long, 0.3 m wide by 0.3 m deep tilting flume. A flow visualization technique was used and complemented by measurements of flow velocity fluctuations near the bed. The experiments reveal that turbulent flow can be viewed as consisting of a sequence of large-scale eddies with a vertical size close to the flow depth, an average length equal to 4-5 depths, and a width of about two depths. The downstream motion of these eddies causes quasi-periodic fluctuations of the local flow velocity components. The development of longitudinal troughs and ridges on the mobile bed and preferential transport of bed particles along the troughs could be related to the effect of the turbulent eddies. The experimental results indicate that the depth-scale eddies are an important turbulence mechanism contributing to bed sediment mobilization.

The relationships derived for predicting fractional transport rates in sediment mixtures are implemented in a hydrodynamic simulation package ISIS Flow/Sediment and tested on the experimental graded sediment transport data. It is shown that the proposed model of bedload transport significantly improves the results of the simulation compared to the available sediment transport formulas and shows reasonable agreement with the actual data.

The data obtained have implications for the calculation of sediment transport rates, design of stable alluvial channels, and physical hydraulic modelling. Further work on sediment transport mechanics is suggested proceeding from the results of the present study.

Table of Contents

List of Tables

Appendix

List of Figures

4 Incipient Motion of Coarse Uniform Sediments

5 Incipient Motion of Graded Sediments

6 Turbulent Structure of Open-Channel Flow over Gravel Beds

7 Implementation and Testing of Bedload Transport Model

Notation

A	area of bed for transport observations; cross-section area
A_{gr}	threshold value of F_{gr} at initial motion
$a,\ a_{50}$	particle mobility factor for d and d_{50}
B	width
b	mixture mobility factor
b_i	hiding factor
C	Chezy coefficient; empirical parameter
$c_1,\ c_2,\ \ldots$	numerical coefficients
c_p	particle resistance coefficient
c_U	velocity coefficient
c_Δ	bed roughness height coefficient
d	mean grain size
d_a	scaling grain size
$d_m,\ d_g$	arithmetic and geometric mean sizes for sediment mixture
d_{50}	median grain size of bed surface
$d_{16},\ d_{84},\ \ldots$	grain size for which 16%, 84%, etc of sediment is finer
d_i	mean size of fraction i
d_*	dimensionless grain diameter
e	exponent in hiding function
F	hydrodynamic force
F_D	drag force
F_L	lift force (direct lift)
F_{DL}	lift force (dynamic lift)
$F_{gr},\ F_{gr\,i}$	Ackers and White particle mobility parameter for d and d_i
Fr	Froude number
f	friction factor; function
f_0	coefficient of static friction
f_i	proportion of d_i in bed surface

G	grain weight; bedload discharge
G_{gr} , $G_{gr\,i}$	Ackers and White sediment transport parameter for d and d_i
g	gravitational acceleration
H	water surface elevation above datum
h	flow depth
I	intensity of sediment motion (transport intensity)
$I\ mean$	mean intensity for duration of experiment
$I\ steady$	intensity for period of steady sediment motion
I_c	critical value of I representing sediment threshold
i	fraction number; time index
J	slope
j	flow parameter
K	Kramer grain size distribution coefficient; channel conveyance
k	kinematic viscosity of water; position index
L	length of particle displacement
L_E	turbulent eddy length
M_L	particle mobility parameter associated with direct lift F_L
m	number of particle displacements; empirical parameter
N	number of bed surface particles in area A
N_C	characteristic number
n	Manning roughness coefficient; empirical parameter
n_g	grain roughness coefficient
n_w	wall roughness coefficient
P	wetted perimeter
P_b	bed wetted perimeter
P_w	wall wetted perimeter
p	bed porosity
p_i	proportion of d_i in transport
Q	water discharge
q_b	bedload transport rate per unit width (dry weight)
$q_b\ corrected$	transport rate for period of steady sediment motion
$q_b\ measured$	mean transport rate (measured) for duration of experiment

q_{bi}	fractional bedload transport rate per unit width (dry weight)
q_b^*, q_{b50}^*, q_{bi}^*	Einstein bedload parameter for d, d_{50}, and d_i
q_c, q_{c50}, q_{ci}	critical unit water discharge for d, d_{50}, and d_i
q_l	lateral water inflow
R	hydraulic radius
R_b	bed hydraulic radius
Re	flow Reynolds number
Re_*	grain Reynolds number
$S_0 = \sqrt{d_{75}/d_{25}}$	sediment sorting coefficient
s	specific density of sediment
T	time period of observation
T_E	time period of turbulent eddy motion
t	time
U	mean streamwise flow velocity
U_c, U_{ci}	critical mean flow velocity for d and d_i
U_*	shear velocity
u	streamwise component of instantaneous point flow velocity
u'	fluctuation of u
V_s, V_{si}	settling velocity for d and d_i
v	vertical component of instantaneous point flow velocity
v'	fluctuation of v
v_{95}	95th percentile of v
W^*, W_i^*	Parker bedload parameter for d and d_i
x	longitudinal distance
Y_i	proportion of entrained grains for ith size fraction
z	bed elevation
α	angle of inflow
β	momentum correction coefficient
Δ	bed roughness height
Δt	time step
Δx	distance step

Δz	change in bed elevation
ε_i	hiding function
$\phi_i = \tau_i^* / \tau_{c\,i}^*$	normalized Shields stress
$\gamma = \rho g$	fluid specific weight
$\gamma_s = \rho_s g$	sediment specific weight
λ	Schoklitsch grain shape coefficient
θ	Romanovsky grain shape coefficient; weighting factor
ρ	fluid density
ρ_s	sediment density
$\sigma_g = \sqrt{d_{84}/d_{16}}$	geometric standard deviation
$\sigma_u = \sqrt{\overline{(u')^2}}$	turbulent intensity in streamwise direction
$\sigma_v = \sqrt{\overline{(v')^2}}$	turbulent intensity in vertical direction
τ	bed shear stress
τ_c, $\tau_{c\,i}$	critical bed shear stress for d and d_i
τ^*, τ_i^*	Shields stress for d and d_i
τ_c^*, $\tau_{c\,i\,uni}^*$, $\tau_{c\,50\,uni}^*$	critical Shields stress for uniform sediment of size d, d_i, d_{50}
$\tau_{c\,i}^*$, $\tau_{c\,m}^*$, $\tau_{c\,50}^*$	critical Shields stress for d_i, d_m, and d_{50} in mixture
$\tau_{c\,\sigma}^*$	critical Shields stress for $d_\sigma = d_g\ \sigma_g$
ω	unit stream power
ω_c	critical value of ω for sediment motion
$\Psi = 1/\tau^*$	Einstein flow intensity parameter

1

Introduction

"The sediments are a sort of epic poem of the Earth."

(Rachel Carson)

"Researchers have already cast much darkness on the subject, and if they continue their investigations we shall soon know nothing at all about it."

(Mark Twain)

1.1 Problem Statement

Determination of critical or threshold flow conditions for incipient motion of streambeds is of considerable interest to river engineers. Related engineering problems include the calculation of sediment transport, prediction of the processes of selective sorting and bed armouring, stable channel design, river regulation and restoration, operation of canal systems, protection against erosion and scour, predicting the effects both upstream and downstream of dam construction, flushing flows, determining the effect of river training works, choosing suitable sites for river crossings and water intakes, and the assessment of aquatic habitat.

Incipient motion of bed sediment has been extensively investigated for almost a century. A vast quantity of experimental data has been collected in laboratory flumes and rivers. Unfortunately, as is often the case when additional data is collected, they do little more than add scatter to the original graphs and diagrams. Instead of clarifying the subject, each additional investigation often only complicates matters and increases uncertainty of the experimental results.

The present state of knowledge on threshold conditions of uniform sediments is illustrated in Figure 1.1. This shows the well-known Shields (1936) diagram relating the critical value of dimensionless bed shear stress to grain Reynolds number. Some data collected by different researchers for natural uniform sediments (compiled by

Buffington and Montgomery 1997) are also shown on Figure 1.1. It is seen that the scatter of the experimental data is significant and is hardly acceptable for practical use.

Differences among the various studies in Figure 1.1 may be caused by a variety of reasons. These include subjectivity in defining the beginning of sediment movement, differences in experimental conditions, the effect of sediment non-uniformity, differences in grain shape, the effect of the fluid turbulence, ignoring the influence of friction from the flume sides, and effect of relative depth (depth to grain size ratio). Although these factors have been recognised and discussed in the literature (Gessler 1971, Miller et al. 1977, Buffington and Montgomery 1997), their influence on sediment threshold has not been systematically examined.

The complexity of the problem has resulted in a number of methods for predicting the threshold of bed sediment movement being proposed. These are presented in the form of equations, graphs, or tables, and relate different critical flow characteristics (velocity, shear stress, stream power, and water discharge), associated with the initiation of bed sediment transport, to physical properties of sediment (size, density, and sorting) (e.g., Graf 1971, Karaushev 1977, Garde and Ranga Raju 1987, Carson and Griffiths 1985, 1987). However, all the existing methods are limited in their application and usually give satisfactory results only for the data from which they were derived. When applied to the same data, the results from the different prediction methods can be wide ranging. An example is given in Figure 2.1. This shows a comparison of different formulas for critical bed shear stress made by Chien (1956). Obviously, the range of the calculated results in Figure 2.1 is too wide for design practice. The design engineer often faces the dilemma of selecting the most appropriate formula for his specific needs. At best the existing formulas serve as guides to planning and usually the engineer is forced to rely heavily on experience and judgment in such work.

Most of the experimental studies conducted were devoted to reasonably uniform sediment. Natural sediments, however, are usually composed of mixed-size particles, and their behaviour differs from that of the beds composed of uniform sediment. It is now generally accepted that sediment fractions in a mixture do not behave independently. Available studies of incipient motion of graded sediment have demonstrated that the effect of a mixture of grain sizes is to reduce the mobility of the smaller particles due to their sheltering by coarser grains, and to increase the mobility of the larger grains due to their increased exposure and instability, as compared to a uniform sediment of the same size (e.g., Richards 1990, Gomez 1995, Komar 1996,

Powell 1998). However, opinions differ on the entrainment mobility of different sizes within a mixture. There are some field and laboratory studies which have demonstrated that entrainment of different sizes in sediment mixtures is dominated by strong relative size effects where most sizes begin to move at about the same shear stress (Parker and Klingeman 1982, Andrews 1983, 1994, Wilcock and Southard 1988). In some cases different degrees of size selective entrainment were observed (Komar, 1987a, Ashworth and Ferguson 1989, Church et al. 1991, Ashworth et al. 1992, Petit 1994, Wathen et al. 1995, Wilcock and McArdell 1997). Apparently, mobility of individual fractions is related to the range of sizes in a mixture and sediment size distribution, but the character of this relationship is not clear at present.

In spite of the extensive research studies undertaken on sediment transport mechanics, a proper, general description of the incipient motion of natural streambeds is not possible yet. Uncertainty about the hydraulic conditions required to entrain a given particle size remains large, especially for streams with coarse bed material. The reasons for this are the highly complex nature of the bed sediment dynamics in rivers, deterministic uncertainty of the process of sediment entrainment, insufficient knowledge of factors controlling sediment motion, as well as the difference in research methods and techniques used. Additional experiments covering a wider range of sediment grading and flow conditions are needed. These should be conducted using advanced measuring equipment and analysis techniques. A single improved research method eliminating uncertainties of the previous studies and providing comparability of data from different experiments should be used. Experiments with uniform sediments should be made prior to studying the behaviour of graded sediments to provide a basis for comparison. A combined experimental study of incipient sediment motion and flow turbulent structure is desirable to provide an understanding of the effect of the flow turbulence on bed material mobility.

1.2 Research Aims

The experimental study reported here was undertaken with the general aim of improving the understanding of the physical processes controlling the incipient motion of streambeds composed of natural sands and gravels, with emphasis on gravel-bed streams. The specific aims of the research were:

- Develop a new approach to defining the critical state of the bed eliminating the subjectivity and providing the probabilistic description of the process of sediment entrainment.
- Study incipient motion and near-to-threshold transport of a wide range of coarse uniform sediments in a laboratory flume.
- Measure the mobile proportion of bed particles with respect to the bed surface population at different flow strengths.
- Study the effect of bed slope and relative depth on sediment mobility.
- Study the bed features developed in uniform sediments.
- Study the turbulent structure of the flow over beds composed of coarse uniform sediment in relation to the incipient motion of bed material.
- Reanalyse the available incipient motion data for uniform sediment and compare them with the data obtained in this study.
- Check the validity of the Shields (1936) threshold curve for uniform sediment.
- Derive a revised threshold diagram for uniform sediment.
- Study incipient motion and near-to-threshold transport of graded sediment with different size distributions in laboratory flumes.
- Study bed forms developed in graded sediments.
- Compile and reanalyse available incipient motion data for graded sediment.
- Develop a method of predicting the threshold of motion for individual size fractions within sediment mixtures.
- Develop a method of predicting incipient motion of median-sized grains in sediment mixtures.
- Develop a computer code for the calculation of graded sediment transport and incorporate it into the existing mobile bed simulation program ISIS Sediment.
- Test the performance of the modified ISIS Sediment for simulating equilibrium and non-equilibrium graded sediment transport.

The ultimate aim of the research was to derive a new method of predicting both incipient motion and near-to-threshold transport of natural uniform and graded sediment. This method should be based on the probabilistic description of the process of sediment entrainment and should account for the effect of relative depth on sediment incipient motion.

The present research was undertaken not only to study the details of the mechanism of sediment entrainment, but also to provide tools for practical calculations. The author hopes that the research work undertaken is not among those for which the words of Mark Twain (given at the beginning of this chapter) are applicable and that it is an example of an optimistic view in the generally difficult situation presently prevailing in sediment transport.

1.3 Layout of Thesis

This thesis contains eight chapters, the contents of which are summarized below.

In Chapter 1, a brief introduction to the problem is given, research aims are outlined, and a brief preview of the thesis chapters is provided.

In Chapter 2, a literature review of incipient motion of uniform and graded sediments is given. The most commonly used predicting methods are described, and possible reasons for the difference among the methods are analysed.

In Chapter 3, experimental programme, research facilities, measuring equipment, and bed materials used in this study are described.

In Chapter 4, a new approach providing a simple objective definition of the threshold for motion of uniform sediment is introduced, experimental procedure and results for uniform sediments are then presented and analysed. Factors controlling bed material entrainment and transport are investigated. A compilation of the present and other available data is used to derive a revised Shields diagram for different states of bed mobility. A formulisation of the experimental data is also developed. Bed features developed on the movable bed are described. Finally, conclusions regarding incipient motion of uniform sediments are drawn from the experimental results.

In Chapter 5, a research method used to define threshold conditions and an experimental procedure for graded sediments are described. Experimental results obtained for graded sediments and data from other relevant studies are presented and analysed, and factors influencing the behaviour of the entire sediment mixture and individual size fractions are examined. A set of equations describing the behaviour of graded sediments is derived and compared with available field and laboratory data. Bed forms developed in graded sediments are briefly described. Then, conclusions on the incipient motion of mixed-size sediments are drawn.

In Chapter 6, results of flow visualisation experiments and flow velocity fluctuations are presented. A strong effect of flow turbulence on bed particle destabilization and bed pattern developed is established. A model of macroturbulent structure of open-channel flow is proposed and compared with data from other investigations.

In Chapter 7, sediment transport relationships derived in this study are implemented in a hydrodynamic simulation computer program ISIS Flow/Sediment. The performance of the modified program is tested on graded sediment transport data collected by Glasgow and Aberdeen Universities in the HR Wallingford tilting flume.

In Chapter 8, a summary of the conclusions from the research undertaken is given, and some suggestions for future study are also considered.

All the main data measured during the present experimental study are given in appendices.

The results of this study are presented in a set of conference and journal papers (Shvidchenko 1999, Shvidchenko and Pender 2000a, 2000b, 2000c, and Shvidchenko et al. 2000).

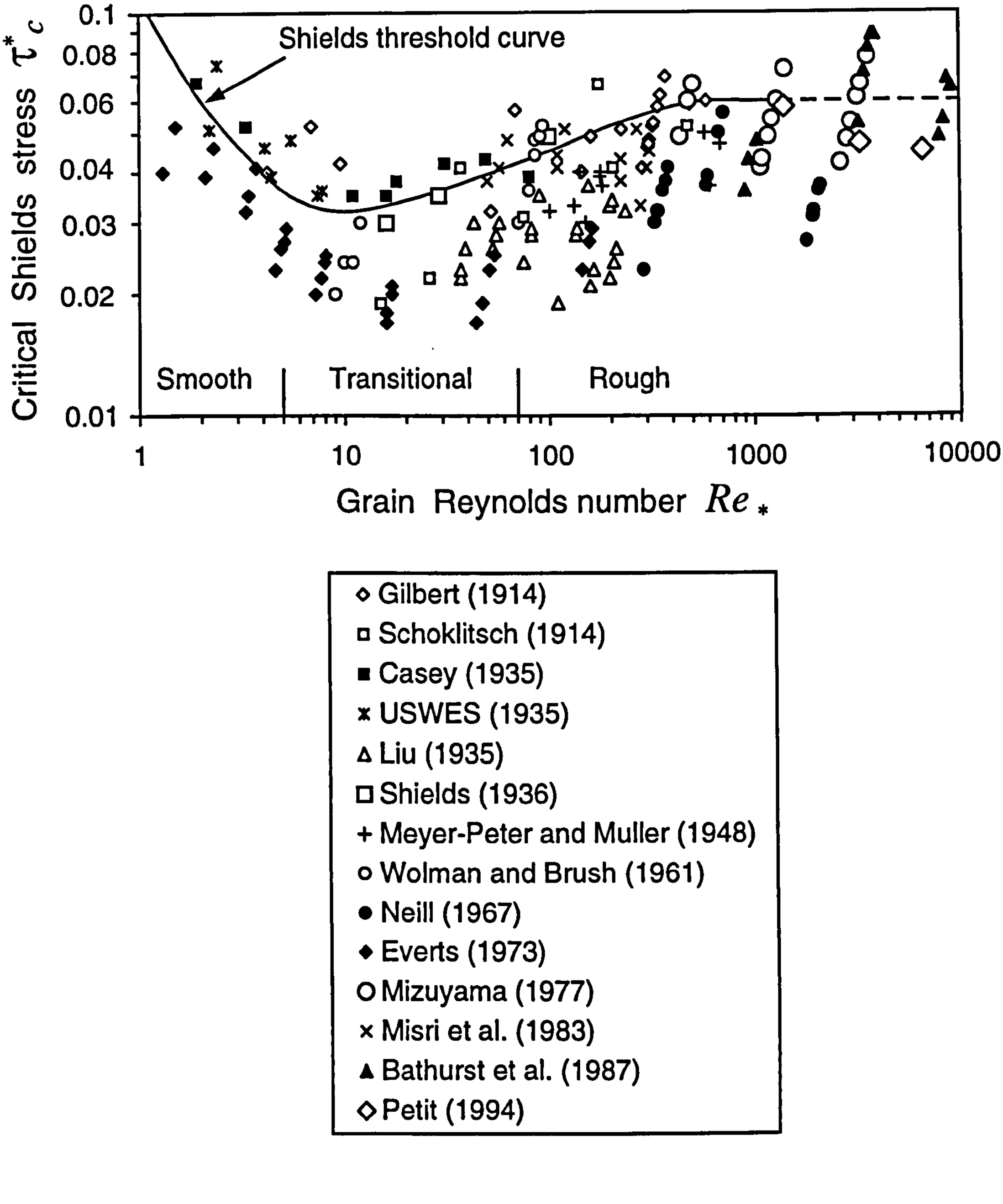

Figure 1.1 Shields diagram.

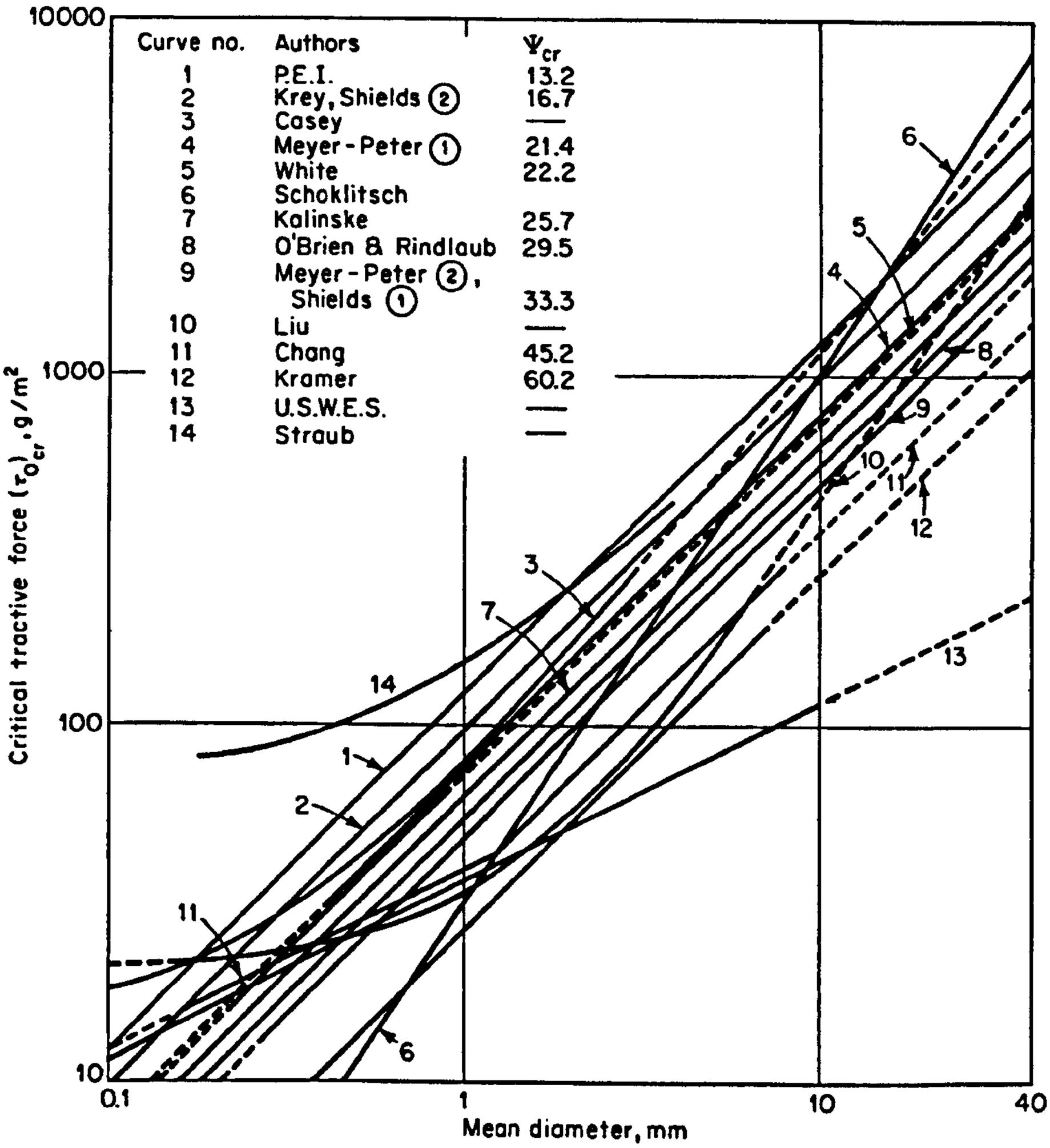

Figure 1.2 Critical bed shear stress as function of grain diameter: a comparison (after Chien 1956).

2

Incipient Motion Studies: A Literature Review

"Engineering problems associated with sediment transport by alluvial streams can be likened in many respects to a chronic skin disease... Until the profession becomes more discriminating in judging what earlier work warrants further investigation and development ... and brings more ingenuity to bear on producing genuinely new and rigorous approaches to the problems, the sediment 'itch' will continue to be the source of much irritation to hydraulic engineering."

(Jack Kennedy)

Consider an open-channel steady uniform flow over a plane mobile bed composed of a well-packed granular material. For a very small water discharge the bed material will be immobile. This flow condition is similar to that over a fixed bed. However, when water discharge is gradually increased, it will be found that at some stage bed particles will start moving. Hydraulic conditions required to initiate the motion of bed sediment are referred as "critical" or "threshold" flow conditions. Numerous publications are devoted to incipient motion of bed material. In the following sections, the most important and interesting studies from a practical point of view are reviewed, and the most commonly used prediction methods are described. All the equations throughout the thesis are given in m-kg-s units. Possible reasons for discrepancies among the different studies and methods are discussed.

2.1 Critical Mean Velocity

The earliest observations of critical or threshold conditions for the initiation of motion of sediments were reported in terms of velocity. The pioneering works on

determination of a critical velocity date back as far as the 18th century. These are mostly theoretical in character and are summarized in Forchheimer (1914), Fortier and Scobey (1926), and Heyndrickx (1948). The Hjulstrom (1935) curve, relating the critical mean flow velocity to particle size, is probably the best known of the early contributions, though the attendant scatter in the original data is rarely shown. This curve is limited to particles smaller than 100 mm and does not account for the flow depth.

Velikanov (1949) related similar variables in the following equation:

$$U_c = \sqrt{9.81\,(14\,d + 0.006)} \tag{2.1}$$

where U_c is the critical mean flow velocity for sediment motion, and d is the mean grain size.

However, where the concept of critical velocity is concerned, it is the near-bed velocity that really controls the entrainment of bed material, and this varies, for fixed mean velocity, with depth. Thus either critical near-bed velocity should be used (which is impractical) or the mean velocity should be corrected for the flow depth (or hydraulic radius). Such a correction has been employed by most subsequent researchers. For example, Goncharov (1938) derived the following formula for critical mean flow velocity:

$$U_c = 3.9\,R^{0.2}(d + 0.0014)^{0.3}\left(\frac{d}{d_{95}}\right)^{0.2} \tag{2.2}$$

where R is the hydraulic radius, and d_{95} is the grain size for which 95% of sediment is finer. The last term in this formula accounts for the effect of sediment non-uniformity on critical velocity. According to Goncharov (1938), this formula shows good results for d in the range 0.35-60 mm. This formula is very popular in Russia and is considered as one of the most reliable.

Later Goncharov (1954) proposed another formula based on flume tests with d up to 10 mm:

$$U_c = 1.41 \log\left(\frac{8.8\,h}{d_{95}}\right)\sqrt{\frac{2\,g\,(s-1)\,d}{3.5}} \tag{2.3}$$

where h is the flow depth, g is the gravitational acceleration, $s = \rho_s/\rho$ is the specific density, ρ_s is the sediment density, and ρ is the fluid density.

Levi (1957) deduced a formula, which reads

$$U_c = 1.4\,a\sqrt{g\,d} \tag{2.4}$$

where $a = \log(12R/d_{90})$ for $R/d_{90} \geq 60$, $a = 0.8 + 0.67\log(10R/d_{90})$ for $10 \leq R/d_{90} < 60$, and $a = 1$ for $R/d_{90} < 10$. The formula is based on flume data with uniform sediments and can be applied for $d > 1.5$ mm. In the case of non-uniform sediments, Levi (1957) suggests using the correction procedure adopted by Goncharov (1938).

Shamov (1959) proposed a relationship given by

$$U_c = 4.4\,d^{1/3}h^{1/6} \tag{2.5}$$

This relationship was originally derived from laboratory experiments and then verified on field data from sand and gravel rivers. This formula is applicable for $d > 0.2$ mm and is widely used in Russia.

Gvelesiani (1946) obtained the following formula for gravel-bed rivers with $d > 1.5$ mm:

$$U_c = 1.41\frac{\log\left(\frac{8.8\,h}{d}\right)}{\log\left(\frac{12\,d_{95}}{d}+1\right)}\sqrt{\frac{2\,g\,(s-1)\,d}{2.8}} \tag{2.6}$$

Neill (1967) conducted experiments with 5.0-29.1 mm uniform gravel and artificial balls in a 5 m long by 0.9 m wide flume, and proposed a "conservative design curve" in the form

$$\frac{U_c^2}{(s-1)\,g\,d} = 2.50\left(\frac{d}{h}\right)^{-0.20} \tag{2.7}$$

Garde (1970) analysed the available data on critical conditions and found that for hydrodynamically rough surfaces

$$\frac{U_c}{\sqrt{(s-1)\,g\,d}} = 0.50\log\left(\frac{h}{d}\right)+1.63 \tag{2.8}$$

Talmaza and Kroshkin (1968) suggested the following relationship for gravel-bed rivers:

$$U_c = 2\,\frac{(a-1.5)}{(a+1)}\left(\frac{h}{d}\right)^{1/a}\sqrt{(s-1)\,g\,d} \tag{2.9}$$

where $a = 2.24\log(h/d) - 0.21\,[\log(h/d)]^2 + 2.52$. This formula is based on a large amount of field and laboratory data.

Yang (1973) found that for grain Reynolds number $Re_* < 70$

$$\frac{U_c}{V_s} = \frac{2.5}{\log(Re_*)-0.06}+0.66 \tag{2.10}$$

where V_s is the settling velocity of particle. Yang (1973) argues that for rough turbulent flow ($Re_* > 70$) U_c/V_s is no longer a function of Re_* and the formula reduces to

$$\frac{U_c}{V_s} = 2.05 \tag{2.11}$$

This finding is obviously in contradiction with most other equations in which the critical velocity is not only a function of the grain size but also of the depth.

Only a few methods have been developed for calculating critical flow velocities of individual size fractions within graded sediments. Rossinsky (1968) derived a formula applicable to both uniform and graded sediments

$$U_{ci} = \frac{2.35\left(\frac{d_m}{d_{90}}\right)^{0.2} b_i \sqrt{(s-1)\, g\, d_i}}{c_U} \tag{2.12}$$

where U_{ci} is the critical mean flow velocity for *i*th size fraction (d_i), d_m is the mean size of the bed sediment, b_i is the hiding factor which can be approximated by

$$b_i = \left(\frac{d_i}{d_m}\right)^{-0.23} \tag{2.13}$$

c_U is the velocity coefficient (ratio of near-bed velocity to mean velocity) based on the logarithmic velocity distribution

$$c_U = \frac{\log\left[11.7\left(\frac{d_i}{d_m}+0.50\right)\right]}{\log\left[6.15\left(\frac{h}{\Delta}+0.35\right)\left(\frac{h}{0.35\,\Delta}+1\right)^{\frac{0.35\,\Delta}{h}}\right]} \tag{2.14}$$

and Δ is the bed roughness height ($\Delta \approx 0.7\, d_m$). The hiding factor (2.13) is analogous to the hiding function employed in the critical shear stress concept discussed below. It accounts for relative size effects in sediment mixtures, reducing the mobility of grains smaller than mean size and increasing mobility of coarser particles.

Romanovsky (1974) from his laboratory experiments suggested a formula for coarse graded sediments ($d_i \geq 2$ mm):

$$U_{ci} = V_{si} \sqrt{\frac{j\, f_0\, N_C}{c_U^2\, N_C + j\, f_0}} \tag{2.15}$$

where V_{si} is the settling velocity of particle of size d_i calculated by

$$V_s = (2.4\,\theta - 0.7)\sqrt{(s-1)\,g\,d_i} \tag{2.16}$$

θ is the grain shape coefficient ($\theta = 0.48$ for flat particles, =1.00 for sphere) with typical value of 0.75 for natural rounded gravel, j is the flow parameter

$$j = \begin{cases} \left(10\,\theta^2 - 9.2\,\theta + 2.16\right)^{-1} + 0.6 & \text{for} \quad \theta < 0.8 \\ 1.35 & \text{for} \quad \theta \geq 0.8 \end{cases} \tag{2.17}$$

N_C is the characteristic number

$$N_C = \frac{(0.7\,C + 6)\,C}{g} \tag{2.18}$$

$$c_U = \frac{1.11\,C\sqrt{1 - a\left(\dfrac{2\,h - d_i}{2\,h}\right)^2}}{C - 1} \tag{2.19}$$

$$a = \begin{cases} 0.57 + \dfrac{3.3}{C} & \text{for} \quad 10 \leq C \leq 60 \\ 0.0222\,C - 0.000197\,C^2 & \text{for} \quad C > 60 \end{cases} \tag{2.20}$$

C is the Chezy coefficient, f_0 is the coefficient of static friction depending on d_i/Δ and θ (Table 2.1), $\Delta = c_\Delta\,d_m$, d_m is the mean size for the bed surface, c_Δ is the bed roughness height coefficient depending on sediment sorting coefficient $S_0 = \sqrt{d_{75}/d_{25}}$ (Table 2.2), d_{75} and d_{25} are the grain sizes for which 75% and 25% of sediment is finer, correspondingly.

The concept of critical flow velocity is widely used in engineering practice. It is preferable over the critical shear stress approach (discussed below) in rivers with complicated channel form, e.g. meandering and braided rivers, in which local water slope (required for calculating shear stress) is usually misleading because of non-uniformity of flow. However, most of the existing methods for determining U_c are derived for reasonably uniform sediment and are inapplicable for fractionwise calculations in widely graded sediments. But even for uniform sediment these methods

give a wide range of critical flow conditions. Figure 2.1 shows critical values of mean flow velocity for motion of uniform sediment obtained using some of the above formulas. Obviously, agreement among them is not very good. It is seen that the predicted critical flow velocity for grain size d=10 mm ranges between 0.95 m/s and 1.35 m/s (a 42% difference), and for d=100 mm between 1.96 m/s and 3.71 m/s (a 89% difference). These ranges of the calculated results are hardly acceptable for design practice.

The Rossinsky (1968) and Romanovsky (1974) formulas for critical flow velocity are the only ones known to be developed specially for graded sediment calculations, the latter formula also accounting for the effect of grain shape. However, these two formulas are based on limited laboratory data sets and have not been thoroughly checked in natural gravel-bed streams.

The concept of critical flow velocity has been validly criticized by some researchers. It is argued that the critical velocities are influenced by a large number of factors, which has an adverse effect on accuracy (Bogardi 1965). The unanswered questions as to what is meant by near-bed velocity and what is a proper relationship between near-bed velocity and mean velocity have led many researchers to accept a more convenient and easier to measure in flumes and straight channels quantity of the bed shear stress as an incipient motion criterion.

2.2 Critical Bed Shear Stress

Bed shear stress (or tractive stress) is defined as

$$\tau = \rho\, g\, R_b\, J \tag{2.21}$$

where R_b is the hydraulic radius of the bed corrected for the effect of walls (for very wide flows $R_b \approx h$), and J is the slope. The bed shear stress can be directly related to the velocity distribution near the bed and the viscosity of the fluid. The advantage of using the bed shear stress as a predictor for incipient motion of bed sediment was identified in the 18th century (Graf 1971), but it did not become popular prior to the work of Schoklitsch (1914) who advanced an experimentally based formula

$$\tau_c = \sqrt{0.201\,\gamma_s\,(\gamma_s - \gamma)\lambda\,d^3} \qquad (2.22)$$

where τ_c is the critical value of bed shear stress for bed material motion, $\gamma_s = \rho_s\, g$ and $\gamma = \rho\, g$ are the specific weights of sediment and water, respectively, and λ is the grain shape coefficient ranging from $\lambda = 1$ for spheres to $\lambda = 4.4$ for flat grains.

Since then many laboratory and field studies have been carried out, and a number of empirical relationships for calculating τ_c have been proposed (e.g., Graf 1971, Garde and Ranga Raju 1987). Among these the relationship of Krey (1925)

$$\tau_c = 0.076\,(\gamma_s - \gamma)\,d \qquad (2.23)$$

is often quoted. Many other formulas do not differ considerably from (2.22) and (2.23), especially as far as their form is concerned.

An improvement over the foregoing studies was Kramer's (1935) suggestion to relate critical shear stress to the mean diameter of bed material d and the character of grain size distribution. Kramer (1935) carried out experiments in a 14 m long and 0.81 m wide flume using quartz grains of relative density 2.70. On the basis of these experiments and data available from other sources, he proposed the following equation for critical bed shear stress:

$$\tau_c = 0.0167\,(\gamma_s - \gamma)\frac{d}{K} \qquad (2.24)$$

where K is the Kramer grain size distribution coefficient, defined as the ratio of two areas above the cumulative grading curve divided by a 50% horizontal line. This equation is based on data with d ranging from 0.24 mm to 6.52 mm, and a uniformity coefficient K varying from 0.265 to 1.00. Many equations proposed later by other investigators have used the Kramer coefficient K (Garde and Ranga Raju 1987) thereby accounting for the effect of gradation on sediment mobility.

Schoklitsch (1962) reanalysed a large amount of available data and suggested using two relationships for critical shear stress, given in Figure 2.2. For grains coarser

than 6 mm, an equation (2.23) established by Krey (1925) is suggested, whereas for 0.1-3 mm grains, Schoklitsch suggested his own equation:

$$\tau_c = 0.000285\,(\gamma_s - \gamma)\,d^{1/3} \qquad (2.25)$$

According to Schoklitsch, the cause for the "strange shape" shown in Figure 2.2 – the shape of the Shields threshold curve described later comes into mind – cannot be explained. Referring to the grain size distribution coefficient *K*, Schoklitsch attributes no advantage in using it.

The formulas listed above and many other similar earlier empirical relationships (summarized in Graf 1971 and Garde and Ranga Raju 1987) can yield the approximate critical bed shear stress for the entire sediment mixture. These formulas are limited in their application and are not recommended for practical use, as they give a wide range of critical flow conditions, as shown in Figure 1.2. Further, these formulas are based on the mean grain diameter. There is no evidence that the mean diameter represents most correctly the composition of a sediment mixture. Parameters, such as the Kramer (1935) grain size distribution coefficient *K*, have not become very popular (Graf 1971). Finally, these formulas are purely empirical and do not throw any light on the mechanism of movement of sediment particles. An insight into such mechanism is essential for solving more complex problems in fluvial hydraulics.

There are also certain limitations of the critical shear stress approach. A major practical objection to the use of a shear stress criterion is that in natural streams it is difficult to determine the effective shear stress on the bed grains because local slopes are affected by several factors besides bed grain friction. Nevertheless, this approach has proved to be very popular among design engineers.

2.3 Shields Diagram

A revolutionary work on incipient motion of bed sediment was made by Shields (1936). The story of this research conducted in very difficult conditions in Nazi Germany is described in Kennedy (1995), and some details of his experimental methods and results (Shield's original laboratory data were lost during World War II) are reported in Buffington (1999). Shields (1936) was apparently the first to study the

beginning of motion of sediment particles after considering the forces acting on bed particles and then applying the principles of similarity. After over five decades, the threshold diagram derived by Shields is still often quoted and used widely. The diagram refers to the incipient transport of uniform sediment on a flat bed by a two-dimensional uniform turbulent flow and relates dimensionless bed shear stress, or Shields stress,

$$\tau^* = \frac{\tau}{g\,(\rho_s - \rho)\,d} = \frac{R_b\,J}{(s-1)\,d} \tag{2.26}$$

and grain Reynolds number

$$Re_* = \frac{U_* d}{k} \tag{2.27}$$

where $U_* = \sqrt{\tau/\rho}$ is the shear velocity, and k is the kinematic viscosity of water. Shields (1936) empirically established a functional relationship between dimensionless critical bed shear stress τ_c^* and grain Reynolds number Re_* using his own and additional flume data (Figures 1.1 and 2.3). The relationship has a distinct form for hydraulically smooth, transitional, and rough surfaces, indicating a minimum value of $\tau_c^* \approx 0.03$ at $Re_* \approx 10$ and a constant value of $\tau_c^* \approx 0.06$ above $Re_* \approx 400$, with the latter value of τ_c^* based on a single data point at high values of Re_*. Shields (1936) originally drew a band of critical shear stresses of appreciable width on his diagram. Rouse (1939) replaced this band with a single mean curve termed the Shields threshold curve (Figures 1.1 and 2.3).

A drawback of the Shields diagram is that the bed shear stress τ appears on both axes. Iterative calculations must be made to determine critical flow characteristics (slope or bed hydraulic radius) for a given grain size. For the convenience of practical use, the Shields threshold curve has been presented as a combination of τ_c^* and dimensionless grain diameter (Bonnefille 1963, Yalin 1972, Miller et al. 1977):

$$d_* = d\left[\frac{g\,(s-1)}{k^2}\right]^{1/3} \tag{2.28}$$

The Shields threshold curve in τ_c^* versus d_* coordinates is expressed by the following relationships (Rijn 1984):

$$\tau_c^* = \begin{cases} 0.24\, d_*^{-1} & \text{for } d_* \le 4 \\ 0.14\, d_*^{-0.64} & \text{for } 4 < d_* \le 10 \\ 0.04\, d_*^{-0.10} & \text{for } 10 < d_* \le 20 \\ 0.013\, d_*^{0.29} & \text{for } 20 < d_* \le 150 \\ 0.055 & \text{for } d_* > 150 \end{cases} \tag{2.29}$$

The advantage of (2.29) is that d_* can be calculated from known fluid and grain parameters, and thus the critical value of Shields stress τ_c^* can be determined directly, while as mentioned previously the use of original Shields diagram requires iterative calculations.

The Shields threshold curve has been confirmed by many experimenters (Bogardi 1965, Egiazaroff 1967, Taylor and Vanoni 1972) and has been widely accepted as a suitable criterion for the initiation of uniform sediment motion. However, the high degree of scatter in the experimental data collected by subsequent researchers (see Figure 1.1) has resulted in attempts to reconsider the threshold value of dimensionless shear stress and to modify the diagram. For example, experiments of White (1940) in a small flume (100 cm long by 5.08 cm wide) with 0.122-5.6 mm well-sorted sand and steel shot have demonstrated independence of τ_c^* on Re_* for laminar and turbulent flows, with individual values of τ_c^* ranging between 0.064 and 0.18. Based upon their flume measurements with coarse bed material (up to 28.6 mm in size), Meyer-Peter and Muller (1948) concluded that the correct τ_c^* value for true initial motion of uniform bed material was about 0.03. Knoroz (1953) undertook experiments in a 0.625 m wide flume with 0.182-1.482 mm sand and obtained a threshold curve without the characteristic dip in the transitional zone. According to the Knoroz (1953) findings, hydraulically rough flow is observed for $Re_* > 25$ with $\tau_c^* \approx 0.025$. Egiazaroff (1967) estimated using different experimental data that the original Shields curve was placed 15-25% higher than it should be due to Shields' use of insufficiently uniform material. Neill (1967) conducted experiments with coarse bed material and observed the variation of τ_c^* (between approximately 0.03 and 0.05) with the relative roughness (grain size to depth

ratio) in fully-rough turbulent flow. He was also unable to detect any rise of τ_c^* for $Re_* > 70$ as is given by the Shields curve (Neill 1968a).

Doubts upon the rise of the Shields curve in the region of rough beds have also been expressed by Ackers and White (1973), who summarized a large volume of experimental data for sand and gravel ranging in size between 0.04 mm and 28.1 mm. The threshold curve derived by Ackers and White (1973) is close to the Shields curve in the transitional zone. However, at the coarse grain end of the scale results of Ackers and White (1973) agree with Neill (1967) data grouping around $\tau_c^* \approx 0.03$.

Miller et al. (1977) modified and extended the Shields curve by using carefully selected additional flume data from various sources. The compiled data allowed an extension of τ_c^* versus Re_* curve by three orders of magnitude of Re_* over the original curve presented by Shields (1936). The modified threshold curve was drawn in the middle of a rather wide data envelope, with a shape similar to that of the Shields graph but with a lower value of $\tau_c^* \approx 0.045$ for rough turbulent flow. A similar graph was derived by Yalin and Karahan (1979) by employing the most recent results of flume studies at that time. Both data sets compiled by Miller et al. (1977) and Yalin and Karahan (1979) show considerable scatter, with individual τ_c^* values for rough turbulent flow ranging from about 0.020 to 0.065. Other values that have been proposed for the constant τ_c^* at large Re_* include 0.047, 0.015, 0.009 and 0.007 (Zeller 1963, Bogardi 1965, Helland-Hansen 1971, and Paintal 1971).

It has also been established that the critical value of Shields stress is not constant for rough turbulent flow but increases for steeper slopes and lower depth to grain size ratios (Neill 1967, Ashida and Bayazit 1973, Mizuyama 1977, Bathurst et al. 1983, Misri et al. 1983). Graf and Suszka (1987) from flume experiments with 12.2 and 23.5 mm uniform gravels derived the following empirical relationship for slopes in the range $0.005 \leq J \leq 0.025$:

$$\tau_c^* = 0.042 \times 10^{2.2J} \tag{2.30}$$

Modifications of the Shields diagram at low values of Re_* (smooth sediment beds) have also been proposed by Grass (1970), White (1970), Mantz (1977), Unsold (1982). Some of the threshold curves concerning the entrainment of coarse uniform

sediments are presented in Figure 2.3. As one can see, for high values of Re_* these curves give a wide range of threshold flow conditions.

2.4 Critical Stream Power

The stream power (mean rate of energy dissipation per unit length of channel) is a third criterion for the threshold of bed material movement introduced and developed by Bagnold in a long series of papers. In one of his latest works (Bagnold 1980), a constant value of critical Shields stress $\tau_c^* = 0.04$ was used for rough turbulent flow to derive an equation

$$\omega_c \approx 290\, d^{1.5} \log\left(\frac{12\,h}{d}\right) \tag{2.31}$$

where ω_c is the critical value of unit steam power $\omega = \rho\, h\, J\, U$ for incipient motion of bed sediment. The formula employs a modal grain size and is valid only for natural sediments ($\rho_s = 2600$ kg/m^3). In case of bimodal bed material, Bagnold (1980) suggests using the geometric mean value between the two modes $\overline{\omega}_c = \sqrt{\omega_{c1}\, \omega_{c2}}$, where ω_{c1} and ω_{c2} are the threshold values of ω for the individual modes d_1 and d_2 in the grain size distribution. Bagnold (1980) applied equation (2.31) in conjunction with his bedload transport formula to a variety of sand and gravel-bed rivers and demonstrated a reasonable agreement between measured and calculated data.

Ikeda (1983) undertook experiment with 6.5 mm gravel in a 160 m long, 4 m wide by 2 m deep flume and observed variation of threshold stream power with bed slope. The steeper the slope was set, the lower the value of threshold stream power was observed. In the experiments of Ikeda (1983), however, the bed was not levelled before each run, and therefore bed features remaining from the previous runs could have had some effect on sediment threshold.

It should be mentioned that the concept of critical stream power has not been developed for predicting behaviour of individual size fractions within sediment mixtures and is not very popular among the researchers concerned with bedload transport.

2.5 Critical Water Discharge

In his later research, Schoklitsch (1962) abandoned the concept of critical bed shear stress developed in his earlier works (see above), stating that "there is not too much known about it". He suggested the use of water discharge as incipient motion criteria, which can be easily derived from the Shields-type equations through substitution in a flow-resistance relationship. Based on laboratory and river data, Schoklitsch (1962) proposed the following dimensional relationship:

$$q_c = 0.26\,(s-1)^{5/3}\,\frac{d^{3/2}}{J^{7/6}} \tag{2.32}$$

where q_c is the critical unit water discharge. For sand mixtures, the use of d_{40} (grain size for which 40% of sediment is finer) is suggested.

Bettess (1984) derived another relationship for gravel streams:

$$q_c = \frac{0.104}{J}\log\left(\frac{1.221}{J}\right)\sqrt{(s-1)\,g\,d^3} \tag{2.33}$$

This equation can be used to determine critical conditions for natural sediment with $\rho_s/\rho = 2.65$, and grain size greater than 2.5 mm.

Bathurst et al. (1983, 1987) conducted experiments in a 16.8 m long and 0.6 m wide flume with reasonably uniform gravels (median diameters $d_{50} = 11.5$, 22.2, and 44.3 mm) and observed an increase of critical Shield stress for steep slopes and low relative depths ($h/d < 10$). This demonstrated the failure of the traditional assumption of the constant value of critical Shields stress for rough turbulent flow. Bathurst et al. (1987) concluded that for these conditions critical water discharge is a better predictor for gravel threshold than the Shields approach, and derived an empirical equation

$$q_c = 0.15\,g^{0.5}\,d^{1.5}\,J^{-1.12} \tag{2.34}$$

This relationship is shown to agree with available flume data for gravels and is recommended for use with essentially uniform sediments for the range of slopes $0.0025 \leq J \leq 0.20$. For mountain rivers with slopes in the range 0.0025-0.10, Bathurst et al. (1987) suggested using

$$q_c = 0.21\, g^{0.5}\, d_{16}^{1.5}\, J^{-1.12} \tag{2.35}$$

where d_{16} is the grain size for which 16% of sediment in the surface layer is finer.

All the above equations show approximate agreement with the uniform sediment data. In the case of graded sediment, however, these predict general behaviour of the entire sediment mixture.

Bathurst (1987) has attempted to expand the concept of critical water discharge to predicting entrainment of individual size fractions within sediment mixtures [see also Komar (1996)]. Data from gravel-bed streams were used to examine the relationship between fractional critical discharge q_{ci} and fraction size d_i. It was found that the individual data sets have trends that cross the curve of equation (2.34) approximately at the median diameters of the distributions, so that the data could be normalized as

$$\frac{q_{ci}}{q_{c50}} = \left(\frac{d_i}{d_{50}}\right)^t \tag{2.36}$$

where q_{c50} is the critical unit discharge for median size d_{50} determined from equation (2.34). Based on data from two rivers, Bathurst determined that exponent t is of the order of 0.2-0.4, and further suggested that its value might depend on the sorting of the gravel within the bed material as evaluated by the d_{84}/d_{16} ratio. The relationship (2.36) is analogous to the hiding function in the critical shear stress concept. More field and laboratory data are required to better establish the discharge-based equations for fractional threshold calculations in graded sediments, and analyses are needed to explore its relationship to the stress-based hiding function theory.

2.6 Hiding Functions

In the classical procedure of calculating transport of graded sediment it is assumed that each size fraction is not affected by the presence of other fractions and that each fraction is distributed uniformly in the bed. However, it has been experimentally established that sediment fractions in a mixture do not behaviour independently and that there are strong intergranular effects. Smaller particles are shielded by coarser grains and need higher flow strength for mobilization if compared with uniform sediment of the same size. Conversely, larger particles are entrained at lower threshold than in a bed of uniform sediment due to increased exposure and instability. The combination of these effects is often referred to as the "hiding phenomenon" and can be described by a "hiding function". A hiding function is a correction of the mobility of individual size fractions d_i within a mixture for relative size effects with respect to either uniform sediment of that size or a characteristic grain size of the mixture.

The first hiding function, introduced by Einstein (1950), was used to extend the application of his statistically based uniform sediment bedload formula to graded sediment. From the flume experiments, he derived an empirical hiding function by matching the computed and measured total load transport rates. This function reduced the applied shear stress for particles of relative size $d_i/d_{50} < 1.3$, while the coarser fractions were considered to be unaffected by hiding.

Day (1980) and White and Day (1982) investigated threshold conditions for size fractions in graded sediment in an 18 m long by 2.46 m wide tilting flume. The experimental results complemented by other available data were analysed in terms of sediment transport parameter G_{gr} and particle mobility parameter F_{gr} introduced by Ackers and White (1973). For a given size fraction and flat bed conditions, these parameters may be defined as

$$G_{gr\,i} = \frac{q_{b\,i}}{f_i\, \rho_s\, d_i\, U}\left(\frac{U_*}{U}\right)^n \tag{2.37}$$

and

$$F_{gr\,i} = \sqrt{\tau_i^*} \tag{2.38}$$

where U is the mean flow velocity, n=0.0 for dimensionless grain diameter $d_* > 60$, and $n = 1.0 - 0.56 \log(d_*)$ for $1 \le d_* \le 60$. The beginning of motion of the bed material (or reference transport rate) was taken as $G_{gr\,i} = 10^{-4}$. The results led to the hiding function:

$$\sqrt{\frac{\tau^*_{c\,i}}{\tau^*_{c\,i\,uni}}} = 0.4 \left(\frac{d_i}{d_a} \right)^{-0.5} + 0.6 \qquad (2.39)$$

where $\tau^*_{c\,i}$ and $\tau^*_{c\,i\,uni}$ are the critical values of Shields stress for size d_i in a mixture and in uniform sediment of size d_i, respectively, $\tau^*_{c\,i\,uni} = 0.029$ for $d_* > 60$, $\tau^*_{c\,i\,uni} = \left(0.23\, d_*^{-0.5} + 0.14\right)^2$ for $1 \le d_* \le 60$, and d_a is the scaling grain size in the mixture which begins to move under the same conditions as a uniform bed material. The scaling size is given by

$$\frac{d_a}{d_{50}} = 1.6 \left(\frac{d_{84}}{d_{16}} \right)^{-0.28} \qquad (2.40)$$

The study of Day (1980) and White and Day (1982) indicated that the position of the size fraction within the grading curve is more important than the overall grading of the sediment mixture, i.e. $\sqrt{\tau^*_{c\,i} / \tau^*_{c\,i\,uni}}$ is more sensitive to d_i / d_{50} than d_{84} / d_{16}. However, a physical explanation of the relationship (2.40) has not been found.

A number of researchers have demonstrated that the relative variation of the critical value of dimensionless bed shear stress for different grain sizes within graded sediment is largely controlled by a central value of the grain size distribution, commonly the mean size, d_m, or the median size, d_{50}:

$$\frac{\tau^*_{c\,i}}{\tau^*_{c\,m}} = \text{function}\left(\frac{d_i}{d_m} \right) \quad \text{or} \quad \frac{\tau^*_{c\,i}}{\tau^*_{c\,50}} = \text{function}\left(\frac{d_i}{d_{50}} \right) \qquad (2.41)$$

where $\tau^*_{c\,m}$ and $\tau^*_{c\,50}$ are the critical values of Shields stress for sizes d_m and d_{50} in a mixture, respectively. For example, Egiazaroff (1965) proposed a relationship, which can be expressed as:

$$\frac{\tau^*_{c\,i}}{\tau^*_{c\,m}} = \left[\frac{\log(19)}{\log(19\,d_i/d_m)}\right]^2 \tag{2.42}$$

where a value of $\tau^*_{c\,m} = 0.06$ is recommended for coarse material. This equation is based on a limited amount of Russian and other experimental data.

Ashida and Michiue (1971) modified the Egiazaroff relationship for $d_i/d_m \le 0.4$ as:

$$\frac{\tau^*_{c\,i}}{\tau^*_{c\,m}} = 0.85\,\frac{d_m}{d_i} \tag{2.43}$$

Hayashi et al. (1980) recommended the following equations for calculating critical Shields stress in sediment mixtures:

$$\frac{\tau^*_{c\,i}}{\tau^*_{c\,m}} = \begin{cases} \left(\dfrac{d_i}{d_m}\right)^{-1} & \text{for} \quad d_i/d_m \le 1 \\ \left[\dfrac{\log(8)}{\log(8\,d_i/d_m)}\right]^2 & \text{for} \quad d_i/d_m > 1 \end{cases} \tag{2.44}$$

These relationships demonstrate that all particles finer than d_m are entrained at the same bed shear stress τ, while coarser particles experience size-selective entrainment.

Parker et al. (1982) analysed bedload transport data from Oak Creek, a small, flume-like gravel-bed stream in Oregon, U.S.A., with the median size of the surface material $d_{50} = 54$ mm. They introduced the bedload parameter (for *i*th size fraction)

$$W^*_i = \frac{(s-1)\,g\,q_{b\,i}}{f_i\,\rho_s\left(\dfrac{\tau}{\rho}\right)^{3/2}} = \frac{q^*_{b\,i}}{\tau^{*3/2}_i} \tag{2.45}$$

where

$$q_{bi}^{*} = \frac{q_{bi}}{f_i \rho_s \sqrt{(s-1)g d_i^3}} \tag{2.46}$$

is the normalized Einstein bedload parameter (Einstein 1942), q_{bi} is the fractional transport rate computed as $p_i q_b$, p_i is the proportion of fraction i in the transport (=1 for uniform sediment), q_b is the bedload transport rate per unit width (dry weight), f_i is the proportion of fraction i in the bed surface (=1 for uniform sediment), d_i is the mean size of fraction i, and τ_i^* is the Shields stress for d_i. Plotting measured fractional transport rates as W_i^* versus τ_i^* and using arbitrary chosen value of $W_i^* = 0.002$ as a reference transport rate corresponding to threshold conditions, Parker with colleagues derived the following surface-based hiding function for the whole range of grain sizes in the bed material in Oak Creek (Parker and Klingeman 1982):

$$\frac{\tau_{ci}^*}{\tau_{c50}^*} = \left(\frac{d_i}{d_{50}}\right)^{-e} \tag{2.47}$$

where e=0.982 is the exponent in hiding function, and $\tau_{c50}^* = 0.035$ is the critical Shields stress for the median size of the bed surface. Here the mobility of individual fractions is related to the median value of the grain size distribution. In the above equation, the value of e is close to unity, which indicates that critical shear stresses τ_{ci} for particles of various sizes comprising the bed in Oak Creek were practically independent of particle size ($\tau_{ci} \propto d_i^{0.018}$) and that motion of different size fractions in sediment mixtures was dominated by strong relative size effects, eliminating almost entirely size-selective transport (in case of pure size-selective entrainment, as implied by the classical approach, the exponent would be equal to zero). This allowed Parker et al. (1982) to propose their "equal mobility" concept as a first approximation for predicting behaviour of graded sediments [see also Andrews and Parker (1987)]. This concept can be viewed as consisting of two parts: "equal entrainment mobility" and "equal transport mobility". Equal entrainment mobility is defined as the case when all

particle sizes comprising the bed material begin to move at nearly the same flow strength. Equal transport mobility refers to the situation where all particle sizes are transported according to their relative proportions in the bed material, so that the bedload and bed material grain size distributions are identical. As Kuhnle (1992) noted, if one condition of equal mobility for a given channel is fulfilled it does not imply that the other one is. The equal entrainment mobility was observed earlier by Ashida and Michiue (1971) and Hayashi et al. (1980), but only for fine fractions in the mixtures.

Andrews (1983) used bedload transport data collected in the East Fork River ($d_{50}=1.3\,\mathrm{mm}$), the Snake River ($d_{50}=54\,\mathrm{mm}$), and the Clearwater River ($d_{50}=74\,\mathrm{mm}$) to derive a relationship $\tau^*_{ci}/\tau^*_{c50}=(d_i/d_{50})^{-e}$ with e=0.872. The hiding function of Andrews (1983) is based on the "largest-grain method", i.e. on the assumption that the dimensionless bed shear stress, τ^*_i, computed for the largest bedload particle at a given discharge approximates the critical value, τ^*_{ci}, as long as larger particles are available on the riverbed. Andrews (1983) also indicated an average value of $\tau^*_{c50}=0.033$ for the median particle in the bed surface of 24 self-formed gravel-bed rivers in Colorado. Although based on a different analysis method, the exponent in the hiding function obtained by Andrews (1983) is very similar to that of Parker et al. (1982) derived using independent sets of data, thus supporting the equal entrainment mobility hypothesis.

Diplas (1987) reanalysed the Oak Creek data and found that the Parker et al. (1982) bedload parameter W^*_i actually depends on the grain size d_i. He suggested a new similarity parameter defined as $\tau^{*(d_i/d_{50})^{0.3214}}_i$. Plotting W^*_i against this parameter and using $W^*_i=0.0025$ as a reference transport rate, Diplas derived a subsurface-based hiding function $\tau^*_{ci}/\tau^*_{c50}=(d_i/d_{50})^{-e}$ with e=0.943. This result demonstrated that despite strong relative size effects there actually was some degree of size-selective entrainment in Oak Creek.

Komar (1987a) reanalysed some of the same river data used by Parker and his colleagues and claimed that there is no common threshold at all for the motion of gravels, hence that equal mobility of all sizes certainly does not hold near the threshold for sediment motion. From the data on the maximum particle diameter transported under the various water discharges, Komar (1987a) found for Oak Creek $\tau_{ci}\propto d_i^{0.57}$

[see also Komar and Shih (1992)], which is equivalent to $\tau^*_{ci}/\tau^*_{c50} = (d_i/d_{50})^{-e}$ with e=0.43 and $\tau^*_{c50} = 0.030$ for the bed surface, whereas Parker et al. (1982) found essentially no dependence of τ_{ci} on d_i. Komar (1987a) also reanalysed data sets collected by Carling (1983) in a small gravel-bed stream (Great Eggleshore Beck, England), Hammond et al. (1984) in a tidal channel, and Day (1980) in a laboratory flume. The data of Carling (1983) and Hammond et al. (1984) were fitted by $\tau^*_{ci}/\tau^*_{c50} = (d_i/d_{50})^{-e}$ with e=0.68 and =0.71, respectively, and $\tau^*_{c50} = 0.045$ in both cases (Komar 1987a, 1987b). Considering the significant scatter of the Oak Creek data, Komar (1987a) mentioned that the use of e=0.68 in the hiding function would also show reasonable agreement. This demonstrated a high degree of uncertainty when fitting relationships to the scattered field data. The measurements of Day (1980) were found to follow non-linear trends. However, attempts to fit the Egiazaroff non-linear equation (2.42) to these measurements were not successful. Therefore, relationships of the form of $\tau^*_{ci}/\tau^*_{c50} = (d_i/d_{50})^{-e}$ were fitted to the data of Day (1980) for $d_i/d_{50} > 1$ only. These gave a range of values of e from 0.29 to 0.66, with τ^*_{c50} ranging between 0.026 and 0.047. The results obtained by Komar implied a significant degree of size-selective entrainment in graded sediments, i.e. different size fractions are entrained at different bed shear stresses. These disagreed with the results of Andrews (1983) and Andrews and Erman (1986) who used the same largest-grain approach and concluded that all sizes are mobilized at effectively the same shear stress. Komar and Shih (1992) and Komar (1996) also argued that equality e=1 in hiding function $\tau^*_{ci}/\tau^*_{c50} = (d_i/d_{50})^{-e}$ cannot be interpreted as a demonstration of equal mobility of different sizes on its own, as this may be significantly influenced by plotting on the log-log graph of random data collected for coarse grains at low flow strength. Subsequently, however, Komar and Carling (1991) presented improved flow-competence assessments based on the largest particle sizes transported in Oak Creek and Great Eggleshore Beck. The corresponding equations are $\tau_{ci} \propto d_i^{0.361}$ (Oak Creek) and $\tau_{ci} \propto d_i^{0.185}$ (Great Eggleshore Beck), yielding e=0.639 and e=0.815 in $\tau^*_{ci}/\tau^*_{c50} = (d_i/d_{50})^{-e}$, respectively.

Ashworth and Ferguson (1989) studied entrainment of mixed size gravel bed material in several reaches of two streams in Scotland (Allt Dubhaig and River Feshie) and one in Norway (Lyngsdalselva). The largest-grain method gave the averaged

surface-based relationship $\tau^*_{ci}/\tau^*_{c50} = (d_i/d_{50})^{-e}$ fitted to the rather scattered data from these rivers, with e=0.74 and $\tau^*_{c50} = 0.089$. Application of the Parker et al. (1982) reference transport method yielded the following surface-based values of e and τ^*_{c50}: 0.65 and 0.072 for Allt Dubhaig (d_{50} =23-98 mm), 0.67 and 0.054 for Feshie (d_{50} =52-63 mm), 0.92 and 0.087 for Lyngsdalselva (d_{50} =69 mm), respectively. It is seen that the application of different methods gave strikingly different results. Nevertheless, Ashworth and Ferguson (1989) concluded that their results indicated unequal mobility of different sizes of bedload as opposed to the equal entrainment mobility concept. Subsequently Wathen et al. (1995) collected additional bedload transport data in Allt Dubhaig and, using the reference transport method, derived somewhat different surface-based values of e=0.90 and $\tau^*_{c50} = 0.086$. The results of Wathen et al. (1995) indicated significantly lower degree of size-selective entrainment in Allt Dubhaig, compared to those obtained earlier by Ashworth and Ferguson (1989). This discrepancy of the results obtained for the same river reflects the natural variability of bedload transport, generally low accuracy of data collected in natural gravel-bed streams, and effect of subjectivity in fitting transport rating curves to significantly scattered data points.

Ferguson et al. (1989) undertook measurements of gravel transport in a braided reach of the pro-glacial White River, Washington, U.S.A. They determined threshold conditions using the largest-grain approach and derived a hiding function $\tau^*_{ci}/\tau^*_{c50} = (d_i/d_{50})^{-e}$ with e=0.88 and $\tau^*_{c50} = 0.047$ for the bed surface. It should be noted here, that in braided streams entrainment and motion of bed material could be significantly influenced by irregular spatial geometry of the channel (Carson and Griffiths 1987). Yet another study concerning entrainment of gravel in braided streams is that of Ashworth et al. (1992) in the Sunwapta River, Canada. Use of the largest-grain method gave e=0.69 and surface-based $\tau^*_{c50} = 0.049$, while the reference transport method of Parker et al. (1982) resulted in e=0.79 and $\tau^*_{c50} = 0.061$. The results obtained by the two different methods were considered very similar and implied unequal (i.e., size-selective) entrainment of bed particles of different sizes.

Church et al. (1991) sampled bedload in the gravel-bed Harris Creek and observed entrainment of gravel at stages significantly higher than those that moved sand, with sand portion moving with near equal mobility (i.e., composition of moving sand was the same as of the composition of sand contained in the bed).

Wilcock (1992, 1993) presented the results of extensive experiments in 22 m long by 0.6 m wide and 11 m long by 0.6 m wide flumes with a wide range of different bed materials including uniform sediments, unimodal sediment mixtures with different sorting, and bimodal sediments with different proportion in each mode and spread between modes. Some of the earlier results were presented in Wilcock and Southard (1988). The reference transport method of Parker et al. (1982) was used to determine the critical shear stress for each size fraction. The experimental results combined with previously published data indicated that incipient motion occurred at nearly the same shear stress for all size fractions in skewed, lognormal, and rectangular unimodal distributions and weakly bimodal distributions, with the exponent e in hiding function $\tau^*_{ci}/\tau^*_{c50} = (d_i/d_{50})^{-e}$ varying between 0.81 and 1.09. For these sediments the critical shear stress for d_{50} fell within a factor of 1.4 of the Shields threshold curve. Mixture sorting was demonstrated to have no effect on the critical shear stress. For strongly bimodal mixtures the size independence of the fractional critical shear stress was no longer maintained: finer fractions began moving at a shear stress considerably smaller than the coarse fractions. The values of critical shear stress for different fractions in strongly bimodal sediments were found to be influenced by the proportion present in each mode.

Kuhnle (1992, 1993a) measured fractional transport rates of bedload on Goodwin Creek having weakly bimodal grain size distribution. Applying the Parker et al. (1982) reference method, he obtained a hiding function $\tau^*_{ci}/\tau^*_{c50} = (d_i/d_{50})^{-e}$ based on subsurface bed material, with e=0.805. Laboratory experiments of Kuhnle (1993a, 1993b) with sand-gravel sediment mixtures has demonstrated that in strongly bimodal sediments, the critical shear stress for the sand fractions is nearly constant and increases with increasing size for the gravel fractions.

Andrews (1994) studied marginal bedload transport in the gravel-bed Sagehen Creek ($d_{50} = 58$ mm) and, applying the Parker et al. (1982) reference-transport method to define threshold for different size fractions, arrived at e=0.887 and $\tau^*_{c50} = 0.0384$ for the surface bed material. These values were similar to that obtained for Oak Creek by Parker et al. (1982) and Parker and Klingeman (1982).

Petit (1994) undertook a series of experiments in 6 m long by 0.5 m wide flume with fixed and mobile beds composed of essentially uniform well-rounded gravel ranging in size from 12.8 to 39.2 mm. With these different beds, experiments were

carried out at different slopes and discharges, using marked 10-65 mm pebbles. Nearly one hundred marked particles were used, and Petit documented the local bed stresses for those pebbles that did not move as well as for the pebbles that were entrained. Graphs of dimensionless shear stresses τ^*_{ci} versus d_i/d_{50} were developed for each experiment, and lines for the "onset of movement" and "generalized movement" were established. The hiding functions $\tau^*_{ci}/\tau^*_{c50} = (d_i/d_{50})^{-e}$ so derived for the "onset of movement" had values of e ranging from 0.66 to 0.81, while τ^*_{c50} determined as the proportionality coefficients in τ^*_{ci} versus d_i/d_{50} graphs ranged from 0.045 to 0.058. Petit recommended use of e=0.70 and $\tau^*_{c50} = 0.050$ based on the complete series of experiments.

Wilcock et al. (1996) measured gravel entrainment in the Trinity River, California using large tracer gravel installations and concluded that the transition from complete immobility to entrainment of the entire bed surface occurred over a narrow range (10-15%) of the bed shear stress. The value of $\tau^*_{c50} = 0.039$ was obtained for gravel $d_{50} = 36$ mm using the Parker et al. (1982) reference transport method.

Wilcock and McArdell (1993, 1997) studied mobilization thresholds of a widely graded, multi-modal sediment ($d_{50} = 5.2$ mm, size range 0.21-64 mm, geometric standard deviation $\sigma_g = \sqrt{d_{84}/d_{16}} = 7.4$) in a 7.9 m long by 0.60 m wide flume and observed entrainment of different size fractions over the seventeen-fold range of bed shear stress. The critical shear stresses were determined using Parker et al. (1982) reference transport method from fractional transport rates scaled by the grain size distribution of the bed surface. The experimental data demonstrated that for $d_i > 2$ mm critical bed shear stress τ_{ci} for size d_i is approximated by $\tau_{ci} = 30.4\, d_i^{0.55}$, which is equivalent to e=0.45 in $\tau^*_{ci}/\tau^*_{c50} = (d_i/d_{50})^{-e}$. This result yielded a pattern of increasing reference threshold stresses with grain size. This was strikingly different from many previous observations obtained with the same reference transport method and a variety of other sediments, in which values of exponent e around unity were typical. The result was consistent, however, with similar trends observed with strongly bimodal sediments (Wilcock 1992, 1993). Wilcock and McArdell (1997) and Wilcock (1997a) also presented results of measuring the active proportions Y_i of different size fractions (painted at different colours) with respect to the bed surface population. The results

obtained using time series photographs of the bed indicated that the active proportion of a fraction decreases with grain size at reference transport conditions from $Y_i \approx 0.8$ for d_{50} to $Y_i \approx 0.2$ for fractions larger than 22.6 mm. That is, Parker et al. (1982) reference transport method does not provide equal mobilized proportion for different size fractions at incipient motion. This agrees with the earlier conclusion of Komar and Shih (1992) who demonstrated that Parker et al. (1982) reference transport criterion $W_i^* = 0.002$ involves the motion of thousands of sand-size grains and only a few coarse gravel grains. The shear stress corresponding to fractional mobility $Y_i = 0.5$ is approximated by $\tau_{ci} = 53.5\, d_i^{0.67}$ for d_i greater than about 5 mm, which can be converted into hiding function $\tau_{ci}^*/\tau_{c50}^* = (d_i/d_{50})^{-e}$ with e=0.33. This hiding function differs from others in that it corresponds to the bed state when 50% of the grains in a size fraction are mobilized. This is an entirely different measure compared to the reference transport method and the largest-grain method (Wilcock 1997).

Attempts have been made to relate the variation of critical shear stress for individual size fractions in sediment mixtures to sediment sorting and flow characteristics. For example, Nakagawa et al. (1982) proposed a theoretical relationship, in which they added the geometric standard deviation of the mixture as the third parameter. Misri et al. (1984) used experimental data to develop a correction factor for calculating effective shear stress acting on bed particles of different sizes, which depended on the Kramer (1935) grain size distribution coefficient. Pender and Li (1995) applied a non-linear optimisation technique to the data on graded sediment transport of Day (1980) and USWES (1935) and developed two different hiding functions. The first one was derived following the work of White and Day (1982) and corrected fractional critical shear stress relative to that for uniform sediment of the same size. The second function was developed following Parker et al. (1982) and corrected critical shear stress for each size fraction relative to that for the geometric mean grain size in the mixture. Additional parameters in these hiding functions were mixture geometric standard deviation $\sigma_g = \sqrt{d_{84}/d_{16}}$ and Froude number Fr. The functions were included in a numerical model for predicting graded sediment behaviour under unsteady flow conditions. The model was tested against independent flume data and performed reasonably well when the second hiding function was used.

An interesting experimental study was undertaken by Patel and Ranga Raju (1999). They observed initiation of motion and transport of different fractions in unimodal sediment mixtures ($d_{50} = 2.59 - 3.70$ mm, $\sigma_g = 1.73 - 2.90$) in a 12 m long by 0.40 m wide flume. The experimental data obtained using the reference transport method of Parker et al. (1982) and the largest-grain method for the coarsest fractions deviated from any of the existing hiding functions. Analysis of the experimental results and other available data resulted in a new empirical relationship for unimodal and weakly bimodal sediment mixtures:

$$\frac{\tau^*_{ci}}{\tau^*_{c\sigma}} = \left(\frac{d_i}{d_\sigma}\right)^{-0.96} \tag{2.48}$$

where $d_\sigma = d_g\ \sigma_g$, d_g is the geometric mean size defined as $\log(d_g) = \sum f_i \log(d_i)$, f_i is the proportion of fraction d_i in the bed, $\sigma_g = \sqrt{d_{84}/d_{16}}$ is the geometric standard deviation, $\tau^*_{c\sigma}$ is the critical Shields stress for the size d_σ. It was found that $\tau^*_{c\sigma}$ is a function of σ_g. This function is presented graphically in Figure 2.4.

There have been also a few attempts to incorporate hiding and exposure effects into formulas for calculating fractional critical flow velocity (Rossinsky 1968, Romanovsky 1974) and critical water discharge (Bathurst 1987). However, these methods are not well elaborated and need a thorough practical verification.

Thus, there is a significant number of publications devoted to the development of hiding function theory. There are many laboratory and field studies that have demonstrated near equal entrainment mobility of different size fractions. However, in many cases significantly different degrees of size-selective entrainment have been observed. Comparison of some of the hiding functions proposed in the literature is presented in Figure 2.5 for a typical range of d_i/d_{50} found in natural gravel-bed streams. It is seen that there is a considerable discrepancy in the results, with almost a ten-fold difference in the critical Shields stress for the end size fractions. It appears, therefore, that the tendency to either size-selective entrainment or equal entrainment mobility is dependent on local hydraulic and sedimentological conditions, and that hiding functions should not be based on aggregated data, nor applied uncritically to other rivers. Size-dependent and size-independent entrainment may, therefore, represent

ends of a spectrum of possible initial motion conditions. The general consensus that have emerged over the past few years is that particle mobility in sediment mixtures is governed more by particle relative size than absolute size such that entrainment of different size fractions is closer to the equal entrainment mobility end of the spectrum (Powell 1998). Coarser particles are therefore slightly less mobile than finer particles, at least at the low excess shear stresses and transport intensities that predominate in gravel-bed rivers. In spite of the completed studies, however, a reliable method for estimating the relative variation of critical shear stress for different fractions in a mixture has yet to be proposed. There is also no method for predicting the values of $\tau^*_{c\,m}$ or $\tau^*_{c\,50}$ which is needed for fractionwise calculations when using hiding function of the form of (2.41). As is shown on Figure 2.6, values of $\tau^*_{c\,50}$ for median grain size d_{50} obtained by different researchers differ significantly. Attempts have been made to relate $\tau^*_{c\,50}$ to the Shields threshold curve (Shields 1936) derived for uniform sediment (Neill 1968b, Wilcock and Southard 1988, Wilcock 1992, Kuhnle 1993a, 1993b). In many studies, however, large departures of $\tau^*_{c\,50}$ from the Shields curve have been observed (e.g., Parker and Klingeman 1982, Misri et al. 1983, Komar 1987a, Garde and Ranga Raju 1987, Ashworth and Ferguson 1989, Andrews 1984, 1994, Patel and Ranga Raju 1999). In Figure 2.6, the Shields threshold curve is also shown for comparison. It has been concluded that the relative variation of $\tau^*_{c\,i}$ within a mixture can be estimated with more accuracy than the actual value of $\tau^*_{c\,i}$ for a particular size fraction, e.g., $\tau^*_{c\,50}$ (Misri et al. 1983, Garde and Ranga Raju 1987, Wilcock 1993). Thus, the development of a method of determination of $\tau^*_{c\,m}$ or $\tau^*_{c\,50}$ requires further research.

2.7 Discussion

It is evident from the literature review presented that there are significant differences among the various studies on incipient motion of streambeds. This can be seen in all the figures presented above. The most important reasons for these differences are briefly discussed herein.

One of the most obvious sources of the scatter in experimental results is the difference in incipient motion definitions. The four most common methods of defining

incipient motion are: (a) visual observation, (b) reference transport method, (c) largest-grain method, and (d) probabilistic approach. Visual observation is a direct method but can be subjective depending on one's definition of how much movement constitutes initial motion. The subjectivity arises because the entrainment of sediment is not a sudden event but a gradual process of bed mobilization characterized by increasing frequency of particle displacement as flow strength rises. Various researchers have used different qualitative definitions of critical (or threshold) conditions such as "first displacement" of a single particle (Neill 1967), "first movement of a plane sediment bed" (White 1970), "onset of movement" and "generalized movement" (Petit 1994), "scattered particle movement" (Rathburn and Guy 1967), "1-2 grains start to move" and "more or less continuous weak movement of grains" (Rakoczi 1975), "incipient transport" (Mantz 1977), "weak movement" (Chiew and Parker 1994), "the most exposed particle moves" (Laursen 2000), and "general movement on the bed" (USWS 1935, Quraishy 1943, Misri et al. 1983). Kramer (1935) defined four levels of visual bed movement as follows:

1. None
2. Weak – ("... several of the smallest particles are in motion, in isolated spots, and in countable numbers.")
3. Medium – ("... grains of mean diameter are in motion in numbers too large to be countable ... movement is no longer local in character. It is not strong enough to affect bed configuration and does not result in transportation of an appreciable quantity of material.")
4. General – ("... grains up to and including the largest are in motion and movement is occurring in all parts of the bed at all times. It is sufficiently vigorous to change the bed configuration ...")

Experiments conducted at Delft Hydraulics, Delft, Netherlands (Rijn 1989) and by Graf and Pazis (1977) have demonstrated that determined values of critical shear stress may vary significantly depending on what degree of bed mobility is set as the threshold of sediment motion (Figure 2.7). For example, Kramer's (1935) definitions of visual grain motion (weak, medium, and general) represent a two-fold difference in τ_c^* values. It is thus not surprising that the experimental data based on visual estimations of threshold exhibit a considerable scatter (see Figure 1.1).

The second method is based on extrapolation of bedload transport rates to either a zero or low reference value. Shields (1936) determined critical shear stress corresponding to "zero sediment transport" by extrapolating backward measured transport rating curves. As has been demonstrated by Paintal (1971), this method can lead to erroneous conclusions if based on insufficient transport data. His flume tests with 2.5-22.2 mm gravel have shown that actually there is no single value of bed shear stress below which no sediment motion is observed. Experiments by Taylor and Vanoni (1972) and Unsold (1982) indicated that the Shields curve corresponds not to zero transport but to a small observable transport rate. Standardized definitions of incipient motion have been proposed on the basis of the number of grains in motion, the area of bed observed, and the duration of observation (Neill and Yalin 1969, Yalin 1972, Wilcock 1988, Bunte 1992); however, these definitions have not been widely adopted, probably because of the difficulty of their practical application. Ackers and White (1973) and Parker et al. (1982) suggested relating the beginning of bed movement to some small practically measurable sediment transport rate expressed in dimensionless form, "below which no significant transport is considered to take place". The reference transport approach is objective and provides a deterministic description of first sediment motion. The Parker et al. (1982) reference transport criterion (described above) is now widely used by other investigators (e.g., Wilcock and Southard 1988, Wilcock 1992, 1993, Kuhnle 1992, 1993a, 1993b, Wilcock and McArdell 1993, 1997, Wathen et al. 1995, Wilcock et al. 1996, Andrews 1994). On the other hand, Parker et al. (1982) criterion is criticised as giving higher mobilized proportion of fine grains compared to coarse grains (Komar and Shih 1992, Wilcock and McArdell 1997). Also, values determined from the reference transport approach are sensitive to the extrapolation method used and the particular reference transport value chosen. Differences in the choice of dimensionless reference transport rate used to define incipient motion can result in a three-fold variation of reference-based τ_c^* values [see, for example, experimental results of Paintal (1971)]. Despite this potential for variation, however, Wilcock (1988) found that reference-based τ_c^* values determined from the Parker et al. (1982) and Ackers and White (1973) methods differed by only 5% for the same data set. Kuhnle (1995) used the both reference transport methods for determination τ_{ci}^* in his experiments with sand-gravel sediment mixtures and obtained very similar results. Close agreement between different reference-transport methods in these studies demonstrates the potential reliability of reference-transport approach in defining

incipient motion of sediment. The reference transport approach, although deterministic, but at least free from subjectivity, is now widely used for studying graded sediment behaviour, but nobody has attempted its application to uniform sediment.

The largest-grain method relates critical flow conditions to the largest grain size transported (e.g., Andrews 1983, Carling 1983, Komar 1987a, 1987b, Ferguson et al. 1989). This method is sensitive to the size and efficiency of the sediment trap, sample size, sampling strategy, duration of the measurements, and availability of coarse grain sizes. Wilcock (1988) pointed out that the maximum size of sediment transported is likely to be underestimated because there is a low probability that the biggest particle moving over an area of bed will be sampled in a finite time, even if the sampler is big enough. Furthermore, the largest-grain method is inappropriate for sediment that exhibits equal mobility, as the largest-grain approach relies on selective transport. The advantage of this method is its applicability to streams in which direct measurements of bedload transport are impossible and the only way to investigate flow competence is the use of tracers (e.g., Wilcock 1997b).

The probabilistic approach is a relatively new method used to define incipient motion of streambeds. Recent studies have demonstrated that the stochastic nature of fluid turbulence and the variability of the grain geometry introduce a random element into sediment entrainment (Grass 1970, Gessler 1971, Lavelle and Mofjeld 1987). This requires a probabilistic description of the phenomenon in terms of the probability of sediment entrainment or, in other words, percentage of bed surface in motion. Attempts have been made to related threshold conditions to the active proportion of the bed particles. Based on the experimental data, Wilcock and McArdell (1997) and Wilcock (1997a) concluded that the active proportion of each size fraction of 0.5 (i.e., 50% of grains in a given fraction are moving) approximates threshold conditions close to that predicted by the Parker et al. (1982) reference transport method. However, the relationship of mobilized proportion of particles to flow characteristics and bedload transport rate has not been fully examined. There are also few studies devoted to quantitative definition of the probability of sediment entrainment. For example, Cheng and Chiew (1998) presented a theoretically derived probability formulation for sediment entrainment and demonstrated that critical Shields stress $\tau_c^* = 0.05$ was equivalent to the probability of entrainment of approximately 0.6%. Recently, Keshavarzy and Ball (2000) investigated the influence of turbulence on the entrainment of 2 mm sand particles in a 35 m long by 0.61 m wide tilting flume, using motion picture photography

and modern image processing techniques. They obtained probability density functions for instantaneous shear stress and for the instantaneous number of entrained particles, which were used to modify the Shields diagram through the addition of the probability distribution function of particle motion. This modification enabled the entrainment of particles with a defined probability of occurrence to be obtained from the Shields diagram. According to Keshavarzy and Ball (2000) findings, the Shields threshold curve at $Re_* \approx 70$ corresponds to about 10% of all bed surface particles entrained, with an exceedance probability of 50% (Figure 2.8). Their results were in agreement with the percentage of bed area in motion obtained by Petroff (1993) for 4.8 mm particles ($Re_* \approx 300$). The deficiency of these studies is the limited experimental basis and absence of a time element in their definitions of proportion of mobilized grains and entrainment probability. However, because of randomness and intermittence of sediment motion, the percentage of the entrained particles (or probability of a given grain mobilization) will depend on the observation period (Einstein 1942, Yalin 1972).

Differences in incipient motion definitions among and within the different methods are apparently the major contributors to the observed scatter of experimental data and differences among the various studies (Miller et al. 1977, Wilcock 1988, Buffington and Montgomery 1997). The use of different initial motion methods described above can produce strikingly different estimates of critical flow conditions for sediment incipient motion, and therefore results of studies employing different methods should not be mixed together and should not be used to confirm or deny each other. Despite the importance of the incipient motion of streambeds in hydraulic engineering, no generally accepted definition of sediment threshold exists.

Initial bed conditions may also influence the experimental results. It is known that the stability of a bed particle is significantly affected by its relative protrusion above the mean bed level. Fenton and Abbott (1977) demonstrated experimentally that the critical Shields stress τ_c^* for grains resting on the top of an otherwise flat bed in a turbulent stream was about 0.01 – considerably lower than values of 0.03-0.06 for beds where all grains were at the same level. As the protrusion of a test particle decreased, the critical Shield stress τ_c^* increased rapidly. When the top of the test particle was 0.2 times the particle diameter below the bed surface, τ_c^* had increased by thirty-fold, to a value of 0.3. The importance of relative protrusion and bed pocket geometry for incipient motion of bed particles is also evident from the analysis of Wiberg and Smith (1987). Church

(1978) produced a summary of critical Shields stresses τ_c^* for gravel-bed rivers and suggested that τ_c^* may vary between 0.02 for "loose" gravel to 0.10 for a "compacted" bed material. Therefore, threshold for an artificially prepared "over-loose" bed with many protruding particles will be significantly lower compared to threshold for a well-packed water-worked bed.

Another source of experimental data scatter can be the difference in grain shape. Quraishy (1943) established experimentally that in turbulent rough flow critical shear stress is higher for flat grains ($\tau_c^* \approx 0.100$) compared to near spherical grains ($\tau_c^* \approx 0.045$). Li and Komar (1986) and Komar and Li (1986) measured variations of pivoting angles with grain shape and demonstrated that, for a given grain size, the order of increasing flow strength required for entrainment is spheres, ellipsoidal grains, angular grains, and imbricated ellipsoids. Gomez (1994) observed the generally lower mobility of flat gravel particles compared to angular and rounded gravel in a laboratory flume. He also mentioned that hiding functions might vary with particle shape. The effect of grain shape on sediment mobility is taken into account in formulas of Schoklitsch (1914) for critical shear stress and Romanovsky (1974) for critical flow velocity. However, Carling (1983) concluded from field measurements in two small gravel-bed streams that the influence of grain shape was not important in the initiation of bed material motion, given the limited range of natural grain shapes. Natural alluvial deposits are usually composed of angular sand and sub-rounded gravel. Extreme shapes (flat and spherical particles) are not common in rivers and are unlikely to be used by experimentalists studying incipient motion of natural sediments.

Ignoring the influence of friction from the flume sides and bed forms is yet another reason for the data scatter. In many publications, especially in earlier ones, there is no clear indications whether the corrections for the effect of sidewalls and bed forms were made or not (see, for example, data summary in Buffington and Montgomery 1997). Some researchers argued that the flow in the channel centre was the most important for sediment transport and the effective hydraulic radius of the bed R_b in this region could be approximated by the total flow depth h (e.g., Shields 1936). However, neglecting the sidewall effect in flume studies with low width to depth ratio (i.e., $B/h < 10$) may potentially result in erroneous estimations of critical flow conditions. Carling (1983) demonstrated that critical Shields stress τ_c^* in narrow natural gravel-bed

streams is considerably higher than τ_c^* in broad streams, thus showing the importance of using hydraulic radius instead of depth for calculating τ_c^* at small values of B/h.

Ignoring the presence of bed forms in natural streams may cause 10-75% overestimation of the actual bed shear stress (Parker and Peterson 1980, Prestegaard 1983, Hey 1988, Wilcock 1993). Although in flume experiments initially planar bed surfaces are normally used, during the experiments with sediment transport different bed forms may appear. If the reference transport method is used, then the results of extrapolation of sediment rating curves may be influenced by the presence of these bed forms, and extrapolated values may be higher than that actually needed to initiate movement in the absence of bed forms.

It has also been recognized that an apparent contributor to the systematic differences among the data sets for the various investigations is the influence of relative depth (depth to grain size ratio, h/d) on the threshold of grain motion. It is often argued that relative depth has little or no effect on the initiation of sediment motion in relatively deep flows (Gessler 1971, Yalin 1972). Conversely, flume studies with coarse sand and gravel of Neill (1967), Ashida and Bayazit (1973), Bathurst et al. (1983, 1987), and Misri et al. (1983), and field measurements of Carling (1983) demonstrated that the influence of relative depth on reported values of critical shear stress can be significant, especially for steep, shallow flows where the grain size is comparable with the flow depth. The results of their studies clearly show that the critical value of Shields stress increases systematically as the ratio of critical depth to grain size is reduced and that the rate of increase depends on channel slope (see also Shields 1936, Cheng 1970, Aksoy 1973, Mizuama 1977, Torri and Poesen 1988). It should be noted here that Shields (1936) originally assumed that his threshold diagram should be restricted to $h/d > 40$. Attempts have been made to develop a relationship between critical Shields stress and relative depth (e.g., Ashida and Bayazit 1973, Carling 1983, Bathurst et al. 1983, Bettess, 1984, Graf and Suszka 1987). However, an insufficient volume of data together with the uncertainty arising from the subjective definition of critical conditions in most studies prevented direct comparison of the data collected and, as a result, did not allow derivation of a generalized relation for the effect of relative depth.

In comparing different hiding functions, critical Shields stresses for median size in the distribution τ_{c50}^* based on both bed surface and subsurface material are often mixed altogether (e.g., Petit 1994, Komar 1996), which lead to erroneous conclusions. Some

researchers (e.g., Petit 1994) compared hiding functions obtained using different analysis methods, which is also misleading. In most flume studies, fractional thresholds required to obtain a hiding function have been derived using fractional transport rating curves fitted to the data collected at different slopes (e.g., Misri et al. 1984, Samaga et al. 1986, Wilcock and Southard 1988, Wilcock 1992, Kuhnle 1993a, 1993b, 1995, Wilcock and McArdell 1993, 1997, Petit 1994, Patel and Ranga Raju 1996, 1999). Given the possible effect of the relative depth described above, this may lead to erroneous results. It has also been demonstrated that the observed variations in hiding functions can be attributed to the difference in the character of the bed material size distribution (Nakagawa et al. 1982, Wilcock 1993, Kuhnle 1993b, Pender and Li 1995, Patel and Ranga Raju 1999). However, the relationship of mobility of individual size fractions to the grain size distribution is not clear at present.

Finally a word of caution. It has been recognized that the critical flow conditions for the beginning of bed material movement is significantly higher than that needed to maintain movement once particles have been entrained by the flow. For example, flow velocity for the cessation of motion is lower (1.2-1.4 times) than the critical velocity for bed material entrainment (e.g., Goncharov 1938, 1954, Shamov 1959). Reid et al. (1985) demonstrated that in the gravel-bedded Turkey Brook the depositional threshold, on average, is only 35% of the entrainment threshold when expressed in terms of bed shear stress, and 20% when expressed in terms of stream power. Thus, these two different phenomena should not be confused.

2.8 Conclusions

Despite almost a century of incipient motion studies there remains a lack of knowledge on sediment thresholds appropriate for fully turbulent flow and steep slopes with low relative depth typical of gravel-bed rivers. The literature review given above demonstrates that there is a number of empirical and semi-theoretical methods for calculating different critical flow characteristics (flow velocity, bed shear stress, stream power, and water discharge) for incipient motion of streambeds. Among the methods available, the Shields threshold diagram is one of the most widely used for predicting threshold conditions for incipient motion of uniform sediments. The Shields diagram is based on the critical shear stress concept, which is much better elaborated than others.

One of the advantages of this approach is the use of geometric flow characteristics (depth and slope), which are relatively easier to measure compared to dynamic characteristics (velocity). This makes the shear stress approach attractive for design practice. The main deficiencies of the Shields threshold diagram are the absence of a strict objective definition of the threshold conditions and non-consideration of the effect of relative depth on sediment mobility. These two factors are apparently the major contributors to the scatter of experimental data in the diagram, resulting in a wide range of threshold conditions for rough turbulent flow being proposed. To improve the accuracy of predictions and to eliminate the subjectivity, it is necessary to approach the problem probabilistically and to investigate experimentally in detail the effect of relative depth, which has received little attention in the literature to date. A combined experimental study of incipient sediment motion and flow turbulent structure is desirable to improve understanding of the effect of the flow turbulence on bed material mobility.

The threshold of individual fractions within graded sediments is determined using hiding functions, accounting for hiding and exposure effects. It is now generally established that the behaviour of different size fractions is largely controlled by their relative size with respect to the median grain size. However, opinions differ on the character of the hiding function and its relation to the grain size distribution. Proposed functions give a wide range of fractional thresholds, and none of them is generally accepted. There is also no reliable method for predicting the threshold for median-sized particles in a sediment mixture, which is required for fractionwise calculations. More investigations on the matter are needed. These should cover a wide range of grain size distributions and flow conditions. A probabilistic description of incipient motion of different size fractions should be provided. Scaling on the bed surface data should be made, as the surface layer is the direct source for bedload transport. Bedload transport data should be collected at a variety of bed slopes to study the effect of the relative depth on mobility of different size fractions within graded sediments.

Clarifying the problems outlined above comprise the main objectives of this thesis.

Table 2.1 Coefficient of Static Friction f_0 (Romanovsky 1974)

d_i/Δ	Grain shape coefficient θ					
	0.55	0.60	0.70	0.80	0.90	1.00
0.7	2.70	2.70	2.60	2.40	2.40	2.30
0.8	2.30	2.20	1.90	1.60	1.60	1.30
0.9	1.85	1.72	1.55	1.38	1.10	0.80
1.0	1.67	1.58	1.40	1.20	0.92	0.70
2.0	1.10	1.01	0.90	0.75	0.58	0.34
3.0	0.93	0.88	0.79	0.66	0.48	0.27
4.0	0.85	0.82	0.73	0.61	0.45	0.24
5.0	0.82	0.78	0.70	0.58	0.42	0.22
6.0	0.80	0.75	0.67	0.56	0.40	0.21
7.0	0.77	0.74	0.66	0.55	0.40	0.20
8.0	0.75	0.73	0.64	0.54	0.39	0.20
9.0	0.74	0.72	0.63	0.53	0.39	0.20
10	0.73	0.70	0.62	0.52	0.38	0.20
20	0.70	0.65	0.58	0.49	0.36	0.19
30	0.67	0.63	0.56	0.47	0.35	0.18
40	0.65	0.62	0.54	0.45	0.34	0.18
50	0.64	0.60	0.53	0.44	0.33	0.18
60	0.62	0.57	0.51	0.43	0.33	0.17
70	0.61	0.56	0.50	0.42	0.32	0.17
80	0.60	0.56	0.50	0.41	0.32	0.17
90	0.60	0.56	0.49	0.41	0.32	0.17
100	0.59	0.55	0.49	0.40	0.31	0.17
200	0.54	0.50	0.45	0.38	0.29	0.16
300	0.50	0.47	0.43	0.37	0.27	0.16
400	0.48	0.45	0.42	0.36	0.26	0.16
500	0.46	0.44	0.40	0.35	0.25	0.15

Table 2.2 Bed Roughness Height Coefficient c_Δ (Romanovsky 1974)

S_0	1.20	1.30	1.40	1.50	1.60	1.70	1.80	2.00
c_Δ	0.87	0.71	0.53	0.39	0.32	0.27	0.24	0.20

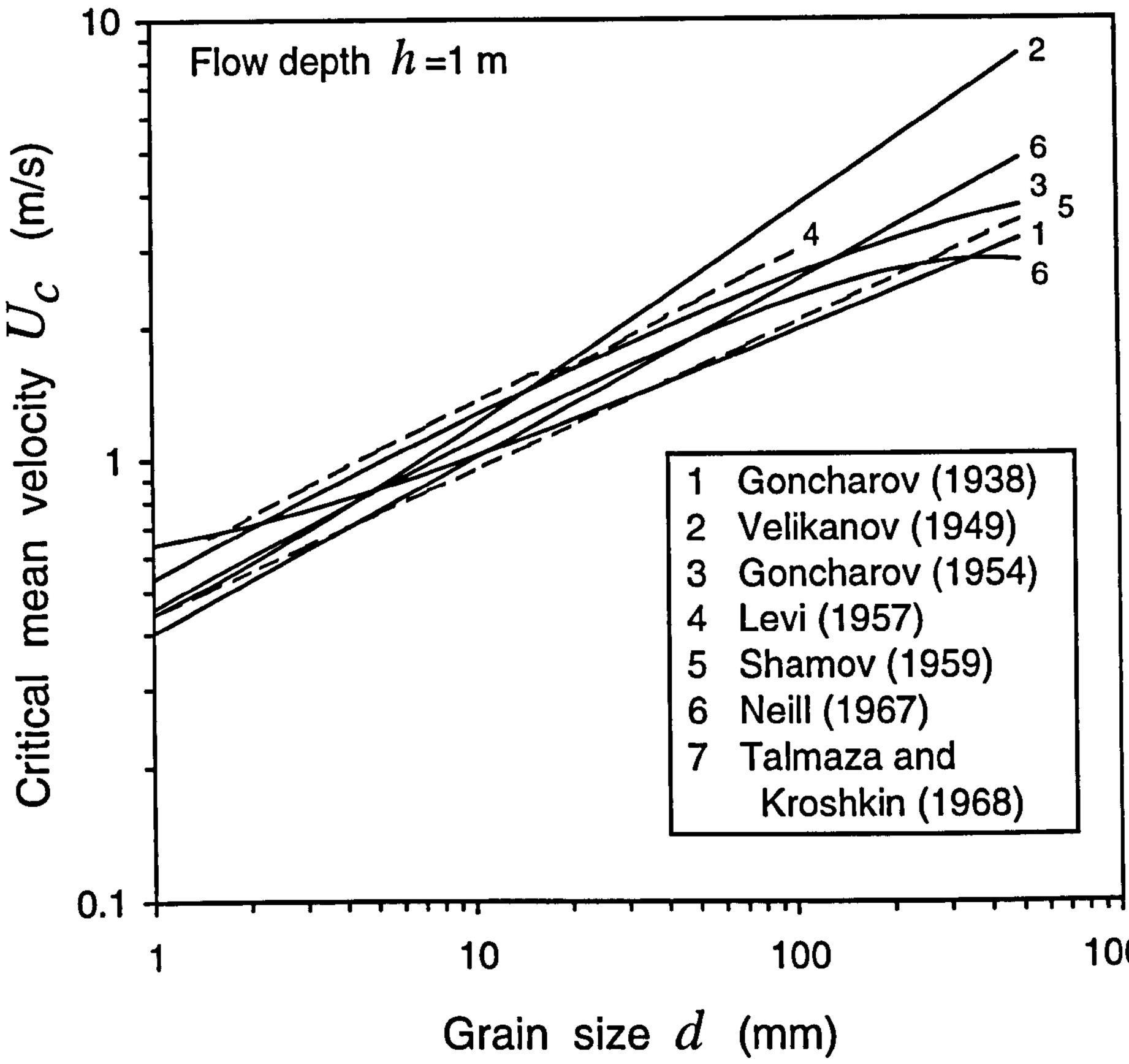

Figure 2.1 Critical flow velocity U_c versus grain size d for flow depth h=1 m (uniform sediment).

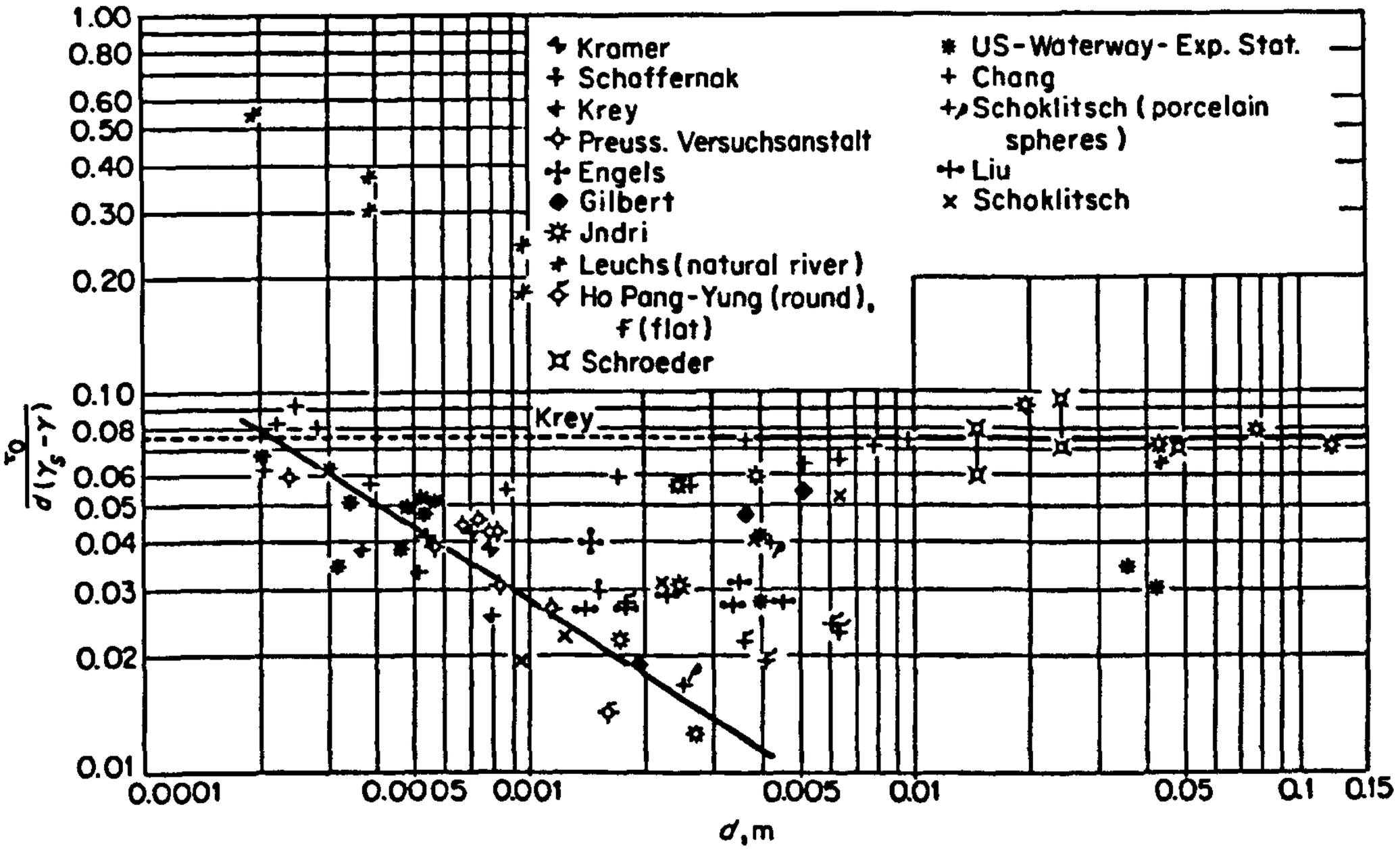

Figure 2.2 Schoklitsch diagram for critical bed shear stress (after Graf 1971).

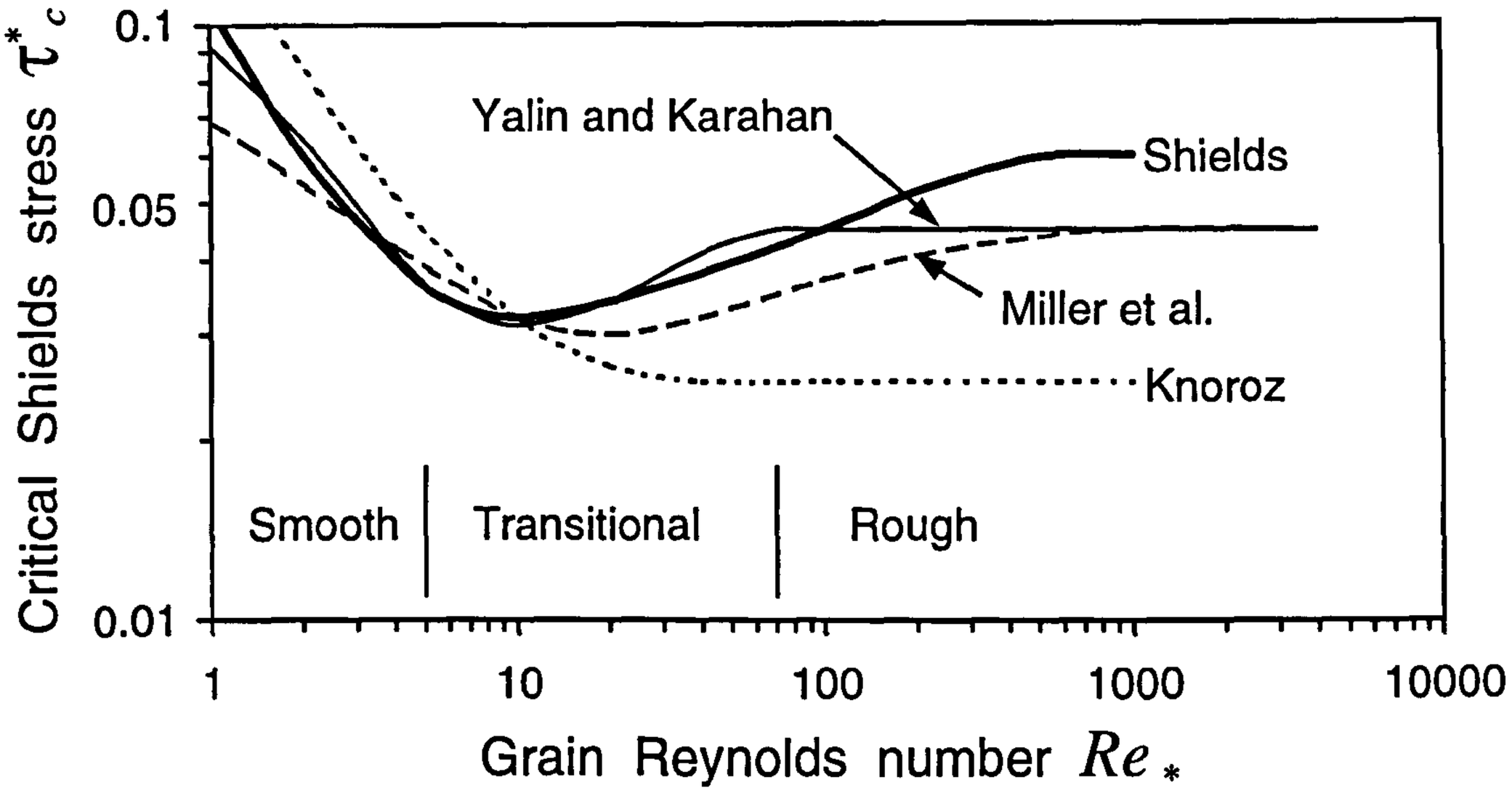

Figure 2.3 Threshold curves obtained by different researchers.

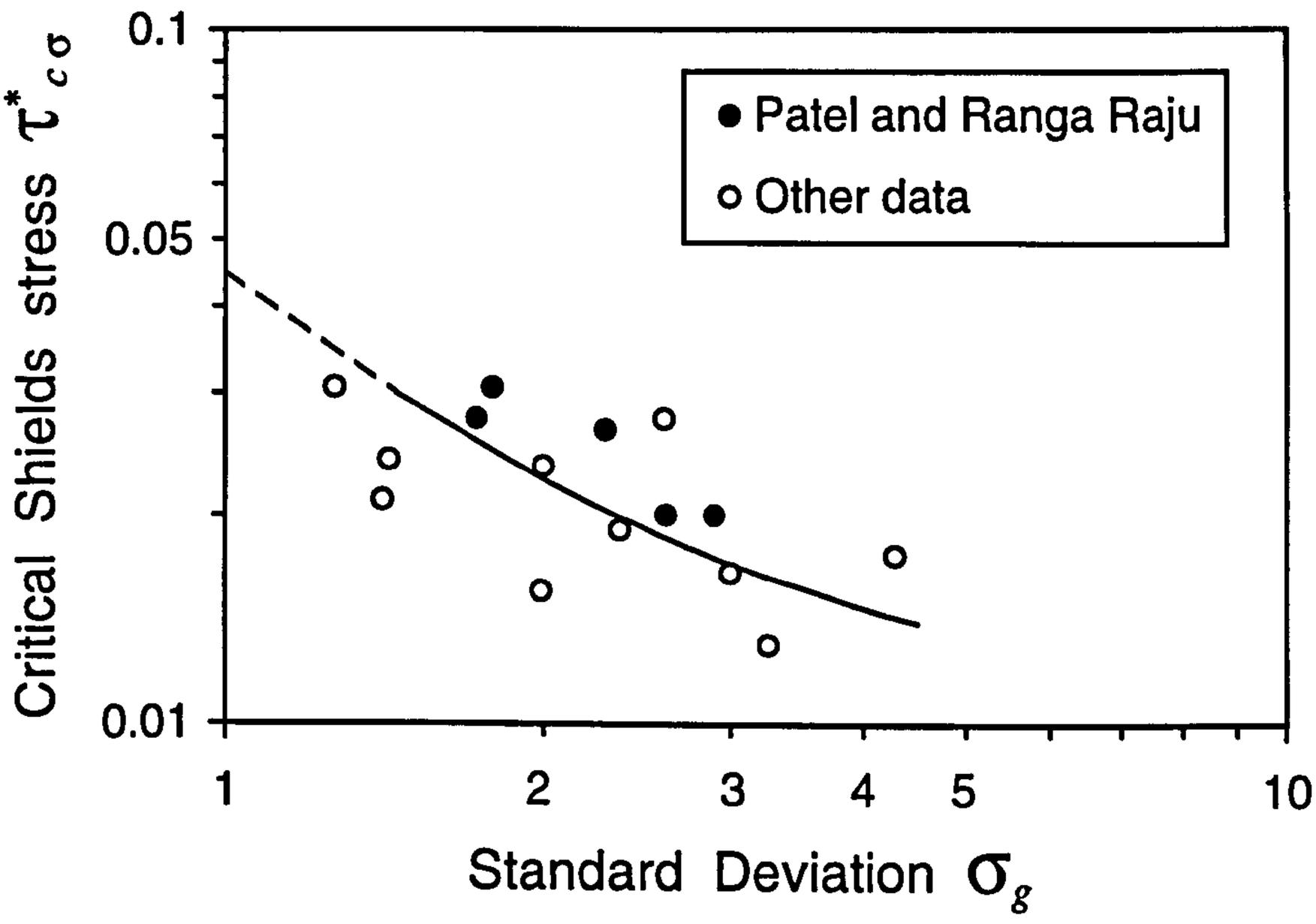

Figure 2.4 Variation of $\tau^*_{c\sigma}$ with σ_g for unimodal and weakly bimodal sediments (after Patel and Ranga Raju 1999).

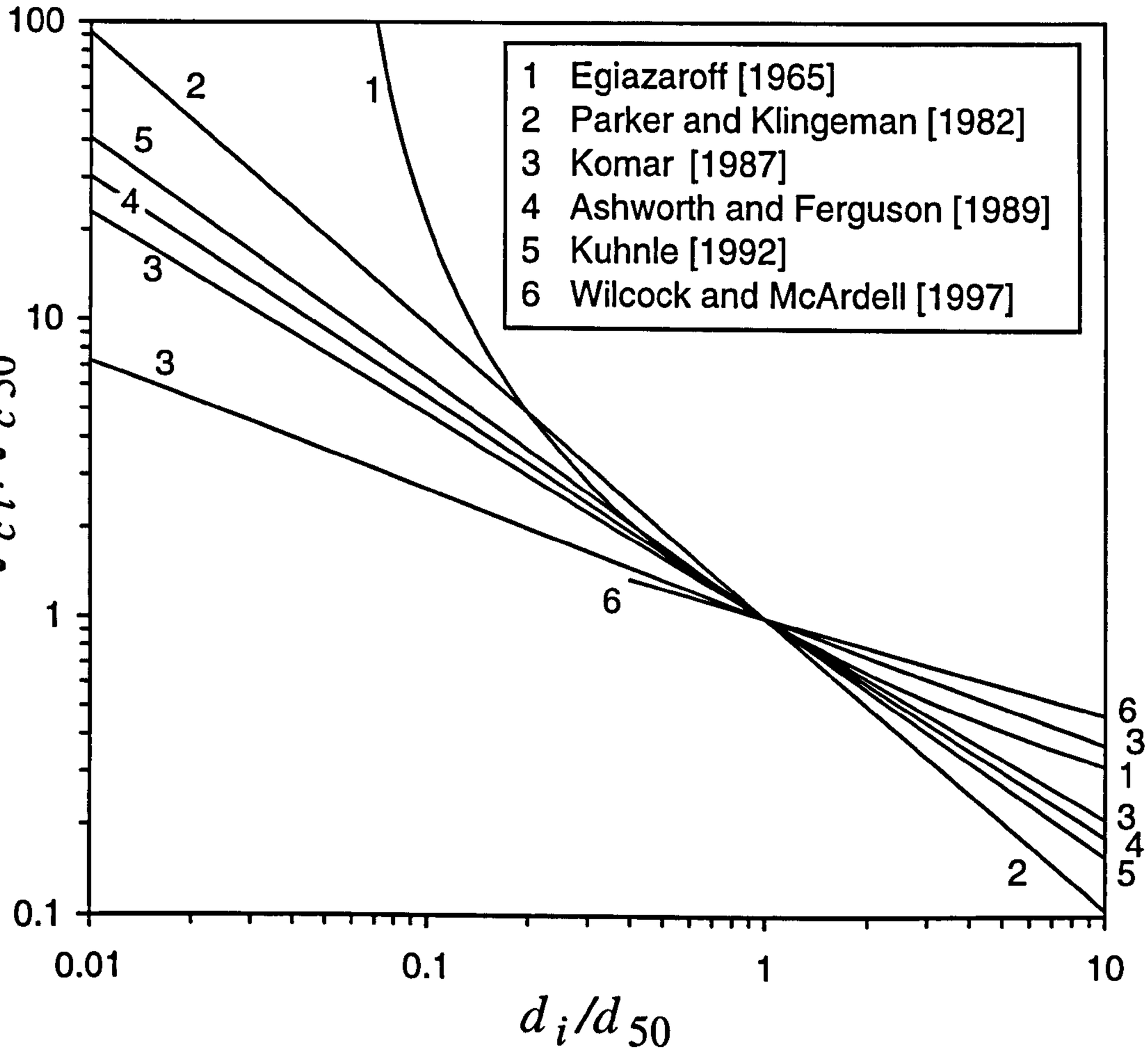

Figure 2.5 Comparison of different hiding funtions.

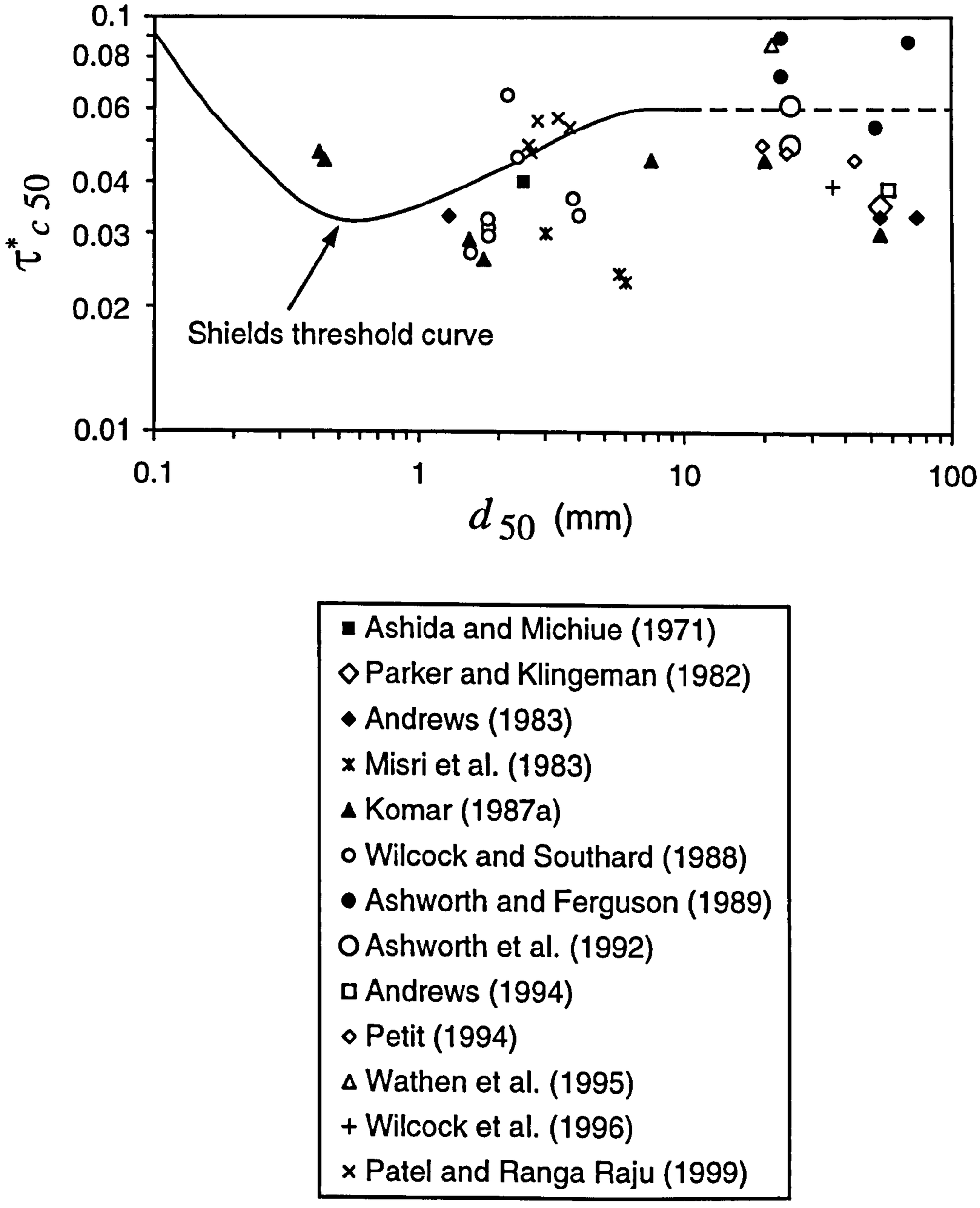

Figure 2.6 Critical Shields stress $\tau^*_{c\,50}$ for median size d_{50} in sediment mixtures.

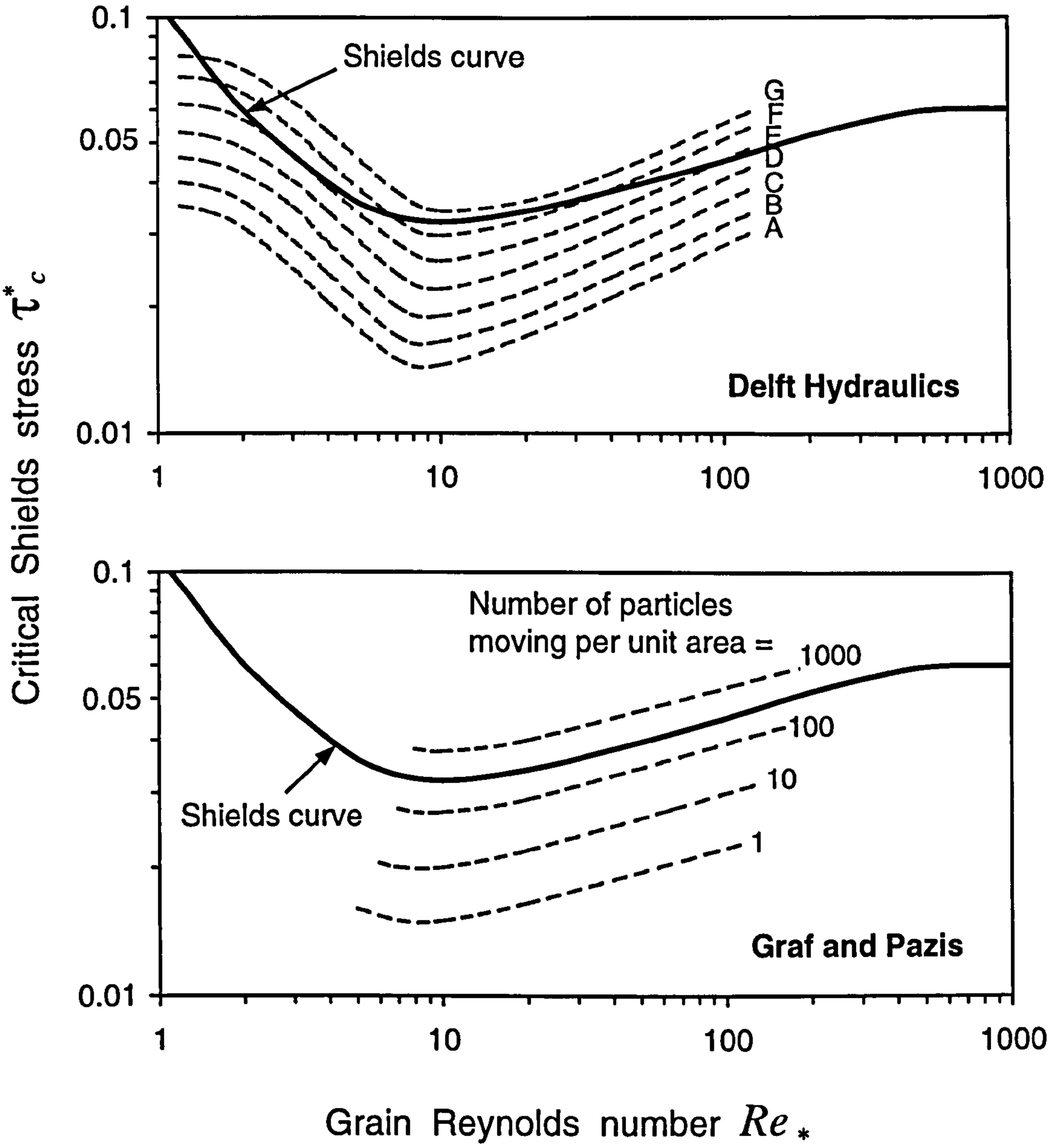

Figure 2.7 Experimental results of Delft Hydraulics (after Rijn 1989) and Graf and Pazis (1977):

A - occasional particle movement at some locations,
B - frequent particle movement at some locations,
C - frequent particle movement at many locations,
D - frequent particle movement at nearly all locations,
E - frequent particle movement at all locations,
F - permanent particle movement at all locations,
G - general transport (initiation of ripples).

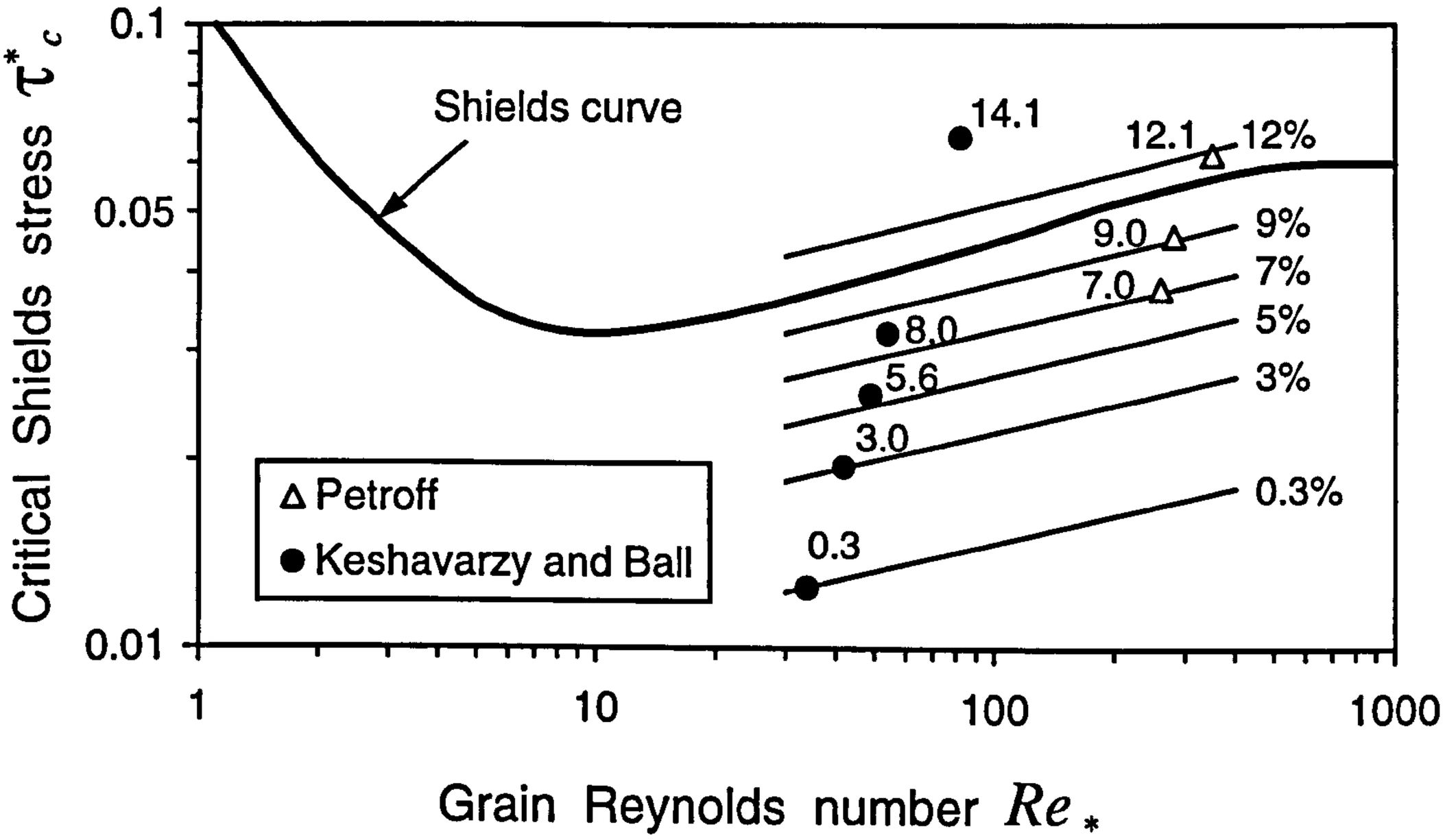

Figure 2.8 Percentage of bed area entrained with exceedance probability of 50%.

3

Experimental Programme, Research Facilities and Apparatus

3.1 Experimental Programme

The experimental part of the present study was carried out using two laboratory research facilities having different dimensions and characteristics. These facilities included a tilting Armfield flume in the Department of Civil Engineering, University of Glasgow, and a large flume at Hydraulic Research Ltd, Wallingford, U.K. (HR Wallingford). The experimental programme was designed to study various aspects of incipient motion and near-to-threshold transport for a wide range of uniform and graded sands and gravels typical of gravel-bed rivers. Three sets of experiments were conducted. The first one was concerned with coarse uniform sediments. This set of experiments was carried out in the Armfield flume and was aimed at providing a basis for studying the behaviour of graded sediments. The second set of experiments examined incipient motion of sediment mixtures having different grain size distributions. The major part of the experiments was conducted in the Armfield flume, with supplementary tests undertaken in the HR Wallingford flume. During the experiments with both uniform and graded sediments, several flume slopes were used and, for each, a number of runs were made with the flow varying between a very low one with almost no sediment transport, and one which moved a substantial portion of the bed material. The variables measured were bed slope, water discharge, flow depth, water temperature, active proportion of the bed particles (only for uniform sediments), sediment transport rate, bedload grading (for graded sediments), initial and final composition of bed surface (for graded sediments), and bed topography. The third set of experiments was undertaken to study the turbulent structure of the flow over the flat bed composed of uniform gravels. This set included flow visualisation experiments and measurements of flow velocity fluctuations near the bed at different states of bed mobility. The experiments were conducted in the Armfield flume using a flow

visualisation technique developed at the Department of Civil Engineering, University of Glasgow. The experimental programme for each set of experiments was initially designed in very general terms and then was constantly corrected and modified according to the results obtained, which were difficult to predict given existing uncertainty in the subject.

Additional graded sediment transport data analysed in the present study were collected during a series of experiments undertaken by Universities of Glasgow and Aberdeen in the same HR Wallingford flume during 1995-96 (Fuller 1998). These experiments were designed to produce a marginal transport of a widely graded bed material when only selective fractions of the bed were transported. The aim of these experiments was to study equilibrium and non-equilibrium graded sediment behaviour under different flow conditions. The experiments were conducted in the same HR Wallingford flume using the same apparatus as in the present experimental study. The author of this thesis actively participated in these experiments during a four-month scientific visit to HR Wallingford in 1996.

The following is a description of the flumes and apparatus used for collecting the experimental data, and bed materials investigated. All the measuring equipment employed in HR Wallingford tests was commissioned by the Universities of Glasgow and Aberdeen (Fuller 1998). Experimental procedures were different for each set of experiments and used different measuring equipment. The experimental procedures are detailed later in the appropriate chapters: Chapter 4 for with uniform sediments, Chapter 5 for graded sediments, and Chapter 6 for flow turbulence.

3.2 Armfield Flume

3.2.1 Installation

The Armfield flume is 8 m long (effective working length 6.5 m), 0.3 m wide and 0.3 m deep (Figures 3.1 and 3.2). The flume is rectangular in cross-section, with glass walls and a smooth steel floor. The flume is supported on a pivot at the centre and a manually operated mechanical jack at the upstream end. It can be tilted about the pivot to slopes between –0.0050 and 0.0350. The slopes can be approximately set using a graduated scale and then have to be checked and corrected using levelling.

The flume is a closed system in which water is re-circulated by means of an electrically powered pump capable of producing a flow up to about 30 litres per second. Water is pumped from two sumps beneath the flume to a head tank at the upstream end of the flume through a return pipe. The head tank is filled with ~20 mm diameter glass spheres to minimize turbulence at the entrance. In addition, an array of cylindrical flow straightening tubes is placed at the flume entrance. The water flow enters the head tank from beneath, then passes down the flume, falls into a collection tank, and returns to the sumps. The water level in the flume can be controlled by means of an adjustable tailgate at the outlet end of the flume. The tailgate is operated as a cable-draw bridge with a crank handle.

A sediment bed was laid in the flume and levelled using a screed board supported on cylindrical instrument rails installed on the top of flume sides parallel to the flume bed. To prevent local scour, 0.7 m of the bed near the inlet and 0.2 m near the outlet were made immobile. The total length of the sediment bed in the flume was 5.6 m, the thickness being about 5 cm.

3.2.2 Bedload sampling equipment

The flume is equipped with a removable transparent sediment trap for sampling bedload (Figure 3.3). The trap is 100 cm deep by 15 cm wide with a streamwise length of 30 mm, and it is located at a distance of 5 m from the inlet end of the flume. The trap was placed on a jack and, when jacked, was pressed firmly to an opening in a cylindrical valve fitted beneath a 150 x 30 mm sampling slot cut in the flume floor. A perspex box open at the bottom and top was fixed above the sampling slot. The upper edge of this box was made adjustable and was set about half of the grain diameter lower than the average level of the top of the bed particles. During the runs, the trap could be isolated from the flow by means of the cylindrical valve, which allowed collection of a series of consecutive bedload samples without disturbance to the flow and sediment transport. The volume above the valve was used to accumulate bedload during exchanging and emptying the trap.

Bedload samples collected were weighed using electrical scales (accuracy 0.1 g) and, when required, sieved using a set of standard sieves.

3.2.3 Flow measuring equipment

Water discharge in the flume is determined using a built-in current meter in the flow return pipe. The current meter is connected to a calibrated pointer indicator. The readings are in litres per second, with the minimum measurable flow of about 0.3 L/s and accuracy of 0.1 L/s.

Supplementary measuring equipment includes a moving pointer gauge used to measure bed and water surface elevations with accuracy of 0.1 mm.

A mini-propeller meter was also used to measure time-averaged streamwise flow velocity. This measuring device consisted of a propeller meter installed inside a 14 mm ring on the end of a long thin rod and a digital data logger. The readings were in Hertz and could be converted to the local flow velocity using a calibrated chart.

A measuring tape was attached along the flume for the identification of the flume and bed areas investigated. In addition, vertical scales were attached to the flume walls at different locations along the flume for measuring flow depth.

Water temperature was measured to 0.1 ^{0}C by means of a thermometer.

3.2.4 Apparatus for registration of fluorescent tracer motion

A still camera was used to detect the motion of particles coated with fluorescent paint during some of the experiments. The photographs were taken in ultra-violet light with different exposure, which allowed tracking moving fluorescent tracers on the photographs. The camera attached on the top of a metal supporting frame and ultra-violet (UV) lamps used for registration of fluorescent particle motion is shown in Figure 3.4.

3.2.5 Flow visualization apparatus

Special equipment was designed and constructed at the Department of Civil Engineering, University of Glasgow, for flow visualization studies. A movable carriage in the form of a closed metal box having dimensions 65 x 40 x 25 cm was made and contained two 2000 W halogen lamps covered above with a reflective sheet and two fans for air-cooling (Figure 3.5). The bottom of the box had a long and narrow slot producing about 0.5 m long by 5 mm wide light sheet from the lamps. The bottom plate was made movable in cross-sectional direction so that the light sheet could be positioned at any location across the flume. The light sheet was used to illuminate a thin vertical slice of the flow seeded with neutrally buoyant 0.5-1.5 mm spherical plastic

beads to highlight the turbulent structure of the flow (Figure 3.6). The carriage was supported on C-shape bearings providing a smooth movement of the carriage along the flume's cylindrical instrument rails. The movement of the carriage was controlled with a computer monitored stepper motor attached to the carriage and running on a rack fixed to the flume. The motor was driven at the desired pre-set speed, which provided a facility for the "sliding filming" of the flow. Recordings of the neutrally buoyant tracer motion were made through the transparent flume wall with a digital video camera operating at 25 frames per second (Figure 3.7) and a digital still camera using a ¼ sec exposure mounted on a supporting frame attached to the carriage. Both cameras were controlled using a computer. The videos and images were directly downloaded to the computer in a digital format for subsequent analysis. Simultaneously, they were projected on a large TV-screen to provide tuning of the recording equipment and for demonstration purposes.

3.2.6 Flow turbulence apparatus

Turbulence characteristics of the flow were measured using a down-looking three-dimensional computer operated SONTEK Acoustic Doppler Velocimeter, or ADV (see Figure 3.1). The ADV system consists of a signal conditioning module, a probe with an acoustic transmitter and three acoustic receivers, and an ADV processor (Figure 3.8). The sampling volume is located 5-6 cm below the transmit transducer. The ADV operates at sampling rate of 25 Hertz and provides collection of instantaneous local flow velocity data in three directions (streamwise, vertical, and transverse).

3.3 HR Wallingford Flume

3.3.1 Installation

HR Wallingford flume is 25 m long by 2.46 m wide (Figure 3.9). The flume is rectangular in cross-section with metal walls. It can be tilted by means of mechanical jacks operated by two electrically driven shafts. A calibrated revolution counter, on the electric motor, enabled the flume slope to be set.

Water is re-circulated through the flume using three electrically powered pumps. Two of the pumps have a maximum discharge of 100 litres per second and the third, smaller pump, a maximum discharge of 10 litres per second. The pumps are located at

the downstream end of the flume, downstream of the sump. Water is pumped from the sump to the upstream end of the flume through a pipe network beneath the flume. At the upstream end of the flume the two larger pump discharges are split, and enter the flume symmetrically either side of the flume centre line. The small pump discharge enters along the centre line. A woven fibre (hairlock) barrier was installed at the flume entrance to provide a stilling basin and some dampening of the flow turbulence. The flow then passes down the flume, through the test section, and returns to the sump. A tailgate is placed across the full width at the downstream end of the flume and is operated as a cable-draw bridge with a crank handle. This is used to control the water surface profile in the flume.

Box section instrument rails were installed on the top of the flume walls and were made parallel to each other and parallel to the flume bed. A steal measuring tape was attached to each of the rails with 0.0 m chainage at the upstream end of the channel. This enabled the identification of areas of the flume by rail chainage.

Within the flume an 18.7 m long trapezoidal concrete straight channel with symmetrical flood plains was cast and filled with a 17.5 cm layer of bed material (Figure 3.10). The channel had a top width of 1.10 m, 45^0 side slopes, a movable bed width of 0.80 m, and a depth of 0.15 m. After the bed material to be examined was placed in the channel, it was levelled using two screed boards of successively lower levels. Both screed boards rested on the concrete flood plains so the initial prepared bed for each experiment was at the same level below the flood plains. Coarse non-transportable gravel was placed in the channel at the upstream end to accelerate the development of a turbulent flow. A concrete block was cast across the channel just downstream of the traps (described below) to provide a common datum for in-channel measurements. The block was slightly lower in height than the sediment bed level so that it would cause minimal disturbance to the flow around the trap location.

3.3.2 Bedload transport traps

A trap system was installed transversely across the whole mobile bed width at chainage 16.7 m to provide collection of all bedload transported. The system consisted of three transparent traps beneath the flume, a waste box, and barrel valves (Figure 3.11). Each trap was 70 cm deep and 19.6 cm wide with a 25 mm sampling slot. The traps were open at the top and bottom, and during the sampling were connected to the valves orifice and the opening in the waste box. The sampling was controlled by the

barrel valves and sliding guillotines at the bottom of the traps. When required, the traps could be isolated from the flow in the channel by means of the barrel valves. When this was done, each trap could be removed and the sample recovered without disturbance to the flow and sediment transport. The waste box was used to store material collected during the initial stages of the experiments, when required flow regime was being established, and during non-continuous sampling. This trap system was developed at the University of Glasgow, U.K., from the system proposed by Hardwick and Willetts (1991).

3.3.3 Instrument carriages

The flume was equipped with two movable instrument carriages, supported on roller bearings and running along the full length of the experimental channel on the instrument rails. (Figure 3.12). This allowed various measurements to be made at any position along and across the channel. The first carriage was made of aluminium angles and gusset plates in the form of a bridge truss. From this instrument carriage flow velocity, water surface elevations, and longitudinal bed profiles were measured.

The second smaller instrument carriage, in the form of a flat bridge across the flume, was used as a base for taking photographs of the bed surface texture during the experiments. This carriage was equipped with a photographic frame and an adjustable suspended glass plate enabling photographs to be taken through the water surface without reflection.

3.3.4 Flow measuring apparatus

Water discharge in the flume was determined using orifice plates contained in flow return pipes beneath the flume. By measuring the head loss across the orifice plates it was possible to calculate the discharge through the network. Measurement of the head difference was taken using a computer monitored pressure transducer. Before the measurements, the air had to be bled from the downstream side of the orifice plates, the pipes connecting the two sides of the orifice plates to the pressure transducer, and the pressure transducer itself. This was done using bleed valves on the pipe network and the through flow facility on both sides of the pressure transducer. Once all the air was removed from the system, discharge through each of the pipes in use was measured for a period of time and averaged.

Water surface profiles were taken using a pointer gauge mounted on a moving instrument carriage (Figure 3.13). Additional measurements were made using pressure tappings moulded into the channel banks at various chainages down the flume. The outer ends of these tappings were connected to stilling pots from which water surface levels could be monitored using digital pointer gauges.

Flow velocity distributions were measured by means of three miniature propellers attached to the upstream side of the instrument carriage (Figure 3.13). The centre of each propeller was at the same horizontal level across the channel. The transverse position of the propellers was fixed, but they could be moved vertically by means of an electronic stepper motor. Data acquisition for the velocity profiles and vertical movement of the mini-propellers were all computer monitored.

Water temperature was measured using an electronic temperature probe to 0.1 ^{0}C.

3.3.5 Longitudinal bed profile apparatus

Longitudinal bed profiles were measured using three lasers and a wire potentiometer, all mounted on the instrument carriage (Figure 3.14). LAS-8010V lasers were used with a measurement range of +/- 40 mm, a resolution of 50 µm, an ellipsoid spot diameter less than 1 mm, and a response time of 20 ms. The lasers were housed in stream lined farings attached to a frame on the downstream side of the instrument carriage. This frame was driven by an electric motor to position the lasers above the water surface within reading distance from the bed. The wire from the potentiometer was attached to the instrument carriage and fixed to the upstream end of the flume. During the bed profiling, the instrument carriage was pushed along the flume. The readings from the lasers were recorded in a personal computer and related to a potentiometer reading, and therefore a chainage. By starting each longitudinal bed profile over the concrete block datum it was possible to relate bed profiles to each other and to the water surface.

3.3.6 Sediment feeder

The flume was equipped with a mechanical conveyor belt feeder for feeding sediment at the upstream end of the flume. The speed of the conveyor belt could be changed according to the required sediment feed rate.

3.4 Bed Materials

The sediments used in the experiments consisted of natural sand and well-rounded gravel typical of alluvial bed material (relative density 2.60-2.65). The sediments were thoroughly sieved to obtain eight essentially uniform fractions ranging in size from 1 mm to 14 mm, which were then mixed in required proportions to get mixtures of predetermined gradation. The graded bed materials were thoroughly mixed using hand measured quantities of each size fractions either manually or in a small, clean mixer. The mixing was made in small amounts at a time to reduce the likelihood of a badly mixed bed material. The physical characteristics of experimental uniform sediments are given in Table 3.1. The experimental graded bed materials are summarized in Table 3.2, where mixture geometric standard deviation is defined as $\sigma_g = \sqrt{d_{84}/d_{16}}$.

The range of graded sediments was designed to study the influence of the parameters defining the shape of sediment grain size distribution (e.g., mixture sorting, skewness, and bimodality) on the mobility of individual size fractions. The effect of mixture sorting alone was examined using three mixtures, N-1, N-2, and N-3, having the same median size (4.3-4.5 mm) as one of the uniform sediments tested and a similar character of grain size distribution (normal), but with different values of mixture standard deviation. Two sediment mixtures, F and C, had skewed distributions, with modes in the fine and coarse ends of the mixtures, accordingly. Mixture B was characterized by bimodal grain size distribution. Grain size distributions of the experimental sediment mixtures are given in Tables 3.3-3.4 and in Figure 3.15. Cumulative grading curves are shown in Figure 3.16.

The incipient motion of all uniform sediments and the six sediment mixtures was studied in the Armfield flume. The experiments in the HR Wallingford flume were undertaken to investigate the behaviour of a widely graded, weakly bimodal sediment (mixture HR in Table 3.2 and Figures 3.15-3.16) with grain sizes ranging from 0.25 to 22.2 mm. This mixture was mainly composed of the same material used in the Armfield flume tests with adding fine and medium sand fractions.

The use of uniform and graded sediment of the same origin provided a direct comparison between the experimental results.

Table 3.1 Experimental Uniform Sediments

No.	Sediment	Size Range (mm)	Mean Size d (mm)	Density ρ_s (kg m^{-3})	Porosity p	Grain Shape
1	Coarse sand	1.0-2.0	1.5	2650	0.47	angular
2	Fine gravel	2.0-2.8	2.4	2600	0.38	angular
3	"Pea" gravel	2.8-4.0	3.4	2650	0.47	rounded
4	"Pea" gravel	4.0-5.0	4.5	2650	0.47	rounded
5	"Pea" gravel	5.0-6.3	5.65	2650	0.47	rounded
6	Marine gravel	6.3-8.0	7.15	2600	0.38	rounded
7	Marine gravel	8.0-10.0	9.0	2600	0.38	rounded
8	Marine gravel	10.0-14.0	12.0	2600	0.38	rounded

Table 3.2 Experimental Graded Sediments

No.	Designation	Size Distribution			Geometric Standard Deviation	Mixture Type
		d_{16} (mm)	d_{50} (mm)	d_{84} (mm)	σ_g	
1	N-1	3.7	4.5	5.8	1.25	Normal
2	N-2	2.7	4.5	6.9	1.60	Normal
3	N-3	2.2	4.3	8.0	1.91	Normal
4	F	1.4	2.6	6.0	2.07	Skewed (fine)
5	C	3.8	6.4	8.6	1.50	Skewed (coarse)
6	B	1.7	4.1	7.7	2.13	Bimodal
7	HR*	0.83	4.3	7.36	2.98	Weakly bimodal

* HR Wallingford flume

Table 3.3 Size Distribution of Sediment Mixtures as Percentage of Total

Mix	Size Range							
	1.0-2.0 (mm)	2.0-2.8 (mm)	2.8-4.0 (mm)	4.0-5.0 (mm)	5.0-6.3 (mm)	6.3-8.0 (mm)	8.0-10.0 (mm)	10.0-14.0 (mm)
N-1	1.10	2.95	15.70	49.10	17.55	8.90	2.75	1.95
N-2	6.10	9.83	17.70	26.90	15.50	13.27	6.37	4.33
N-3	12.47	12.50	13.87	15.60	12.63	14.03	10.77	8.13
F	34.65	19.85	14.45	11.00	7.55	6.25	3.20	3.05
C	3.05	3.20	5.95	11.20	16.45	31.65	18.75	9.75
B	20.65	14.10	8.25	9.00	10.00	24.55	7.10	6.35

Table 3.4 Size Distribution of Sediment Mixture HR

Size Range (mm)	<0.25	0.25-0.36	0.36-0.5	0.5-0.71	0.71-1.0	1.0-1.4
Percentage	4.50	4.91	3.20	2.42	1.72	1.67
Size Range (mm)	1.4-2.0	2.0-2.8	2.8-4.0	4.0-5.6	5.6-8.0	8.0-9.5
Percentage	2.16	4.57	19.90	26.41	17.09	4.08
Size Range (mm)	9.5-12.7	12.7-15.9	15.9-19.1	19.1-22.2	>22.2	
Percentage	3.56	2.16	0.65	1.00	0.00	

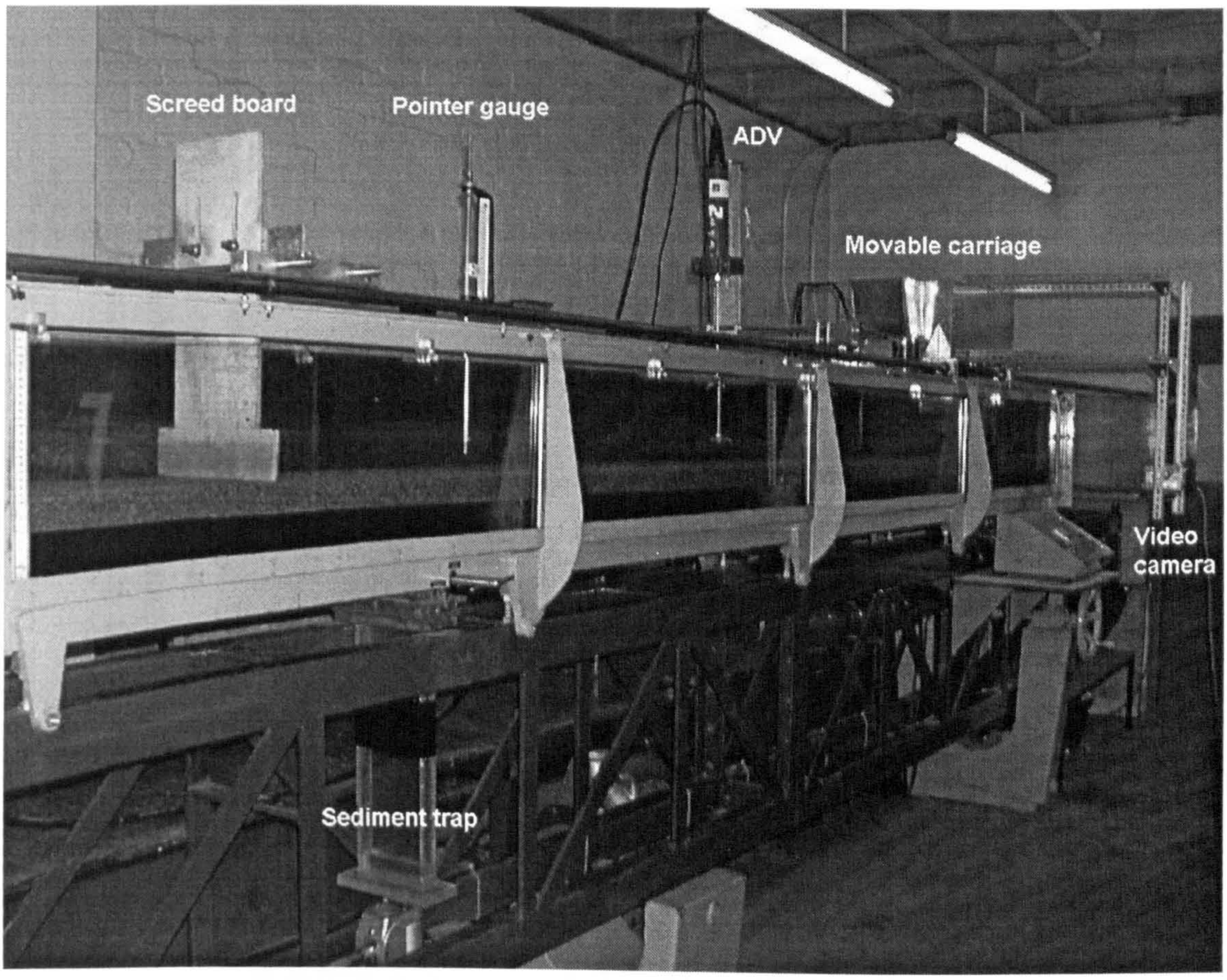

Figure 3.1 General view of Armfield flume (University of Glasgow).

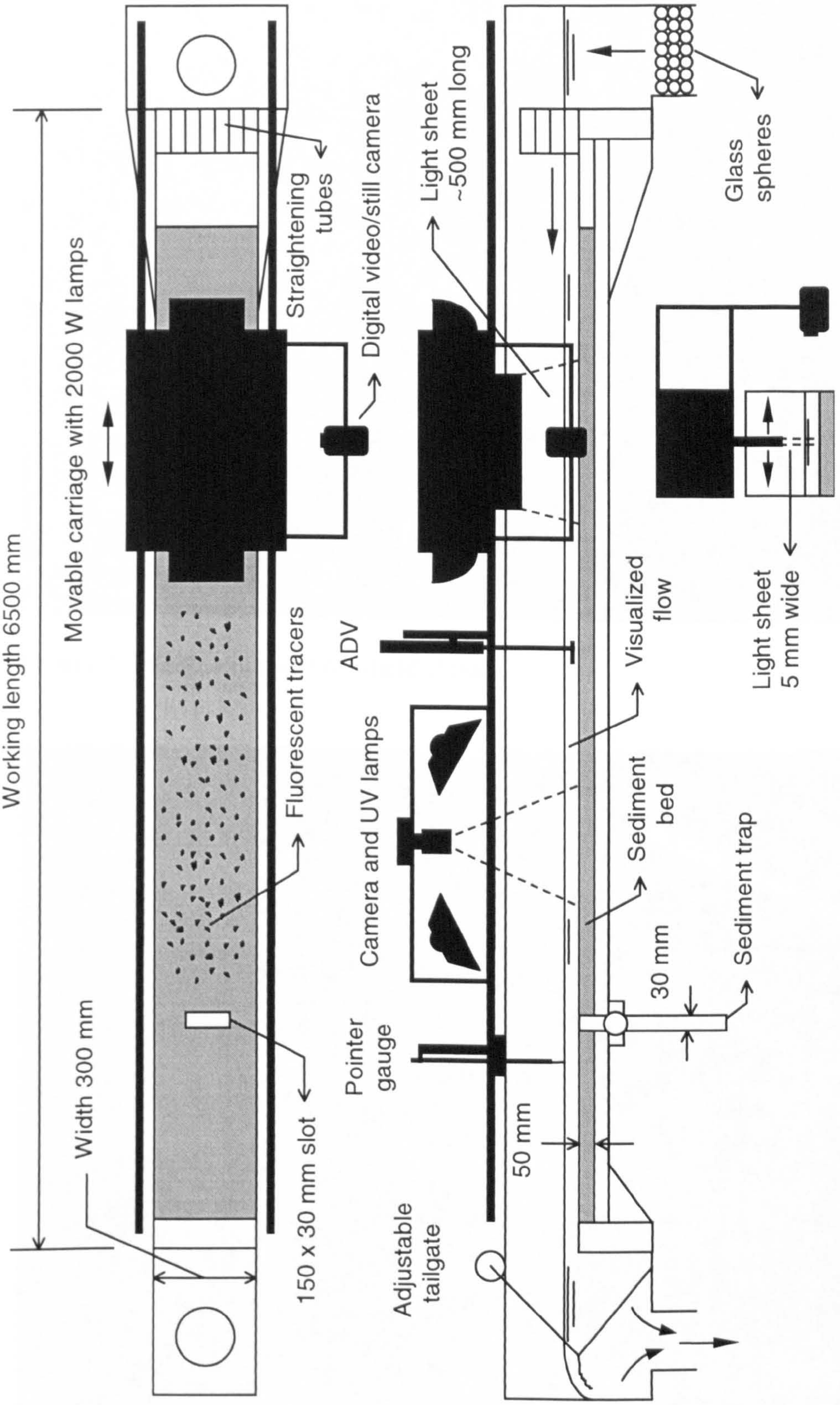

Figure 3.2 Measuring equipment (Armfield flume).

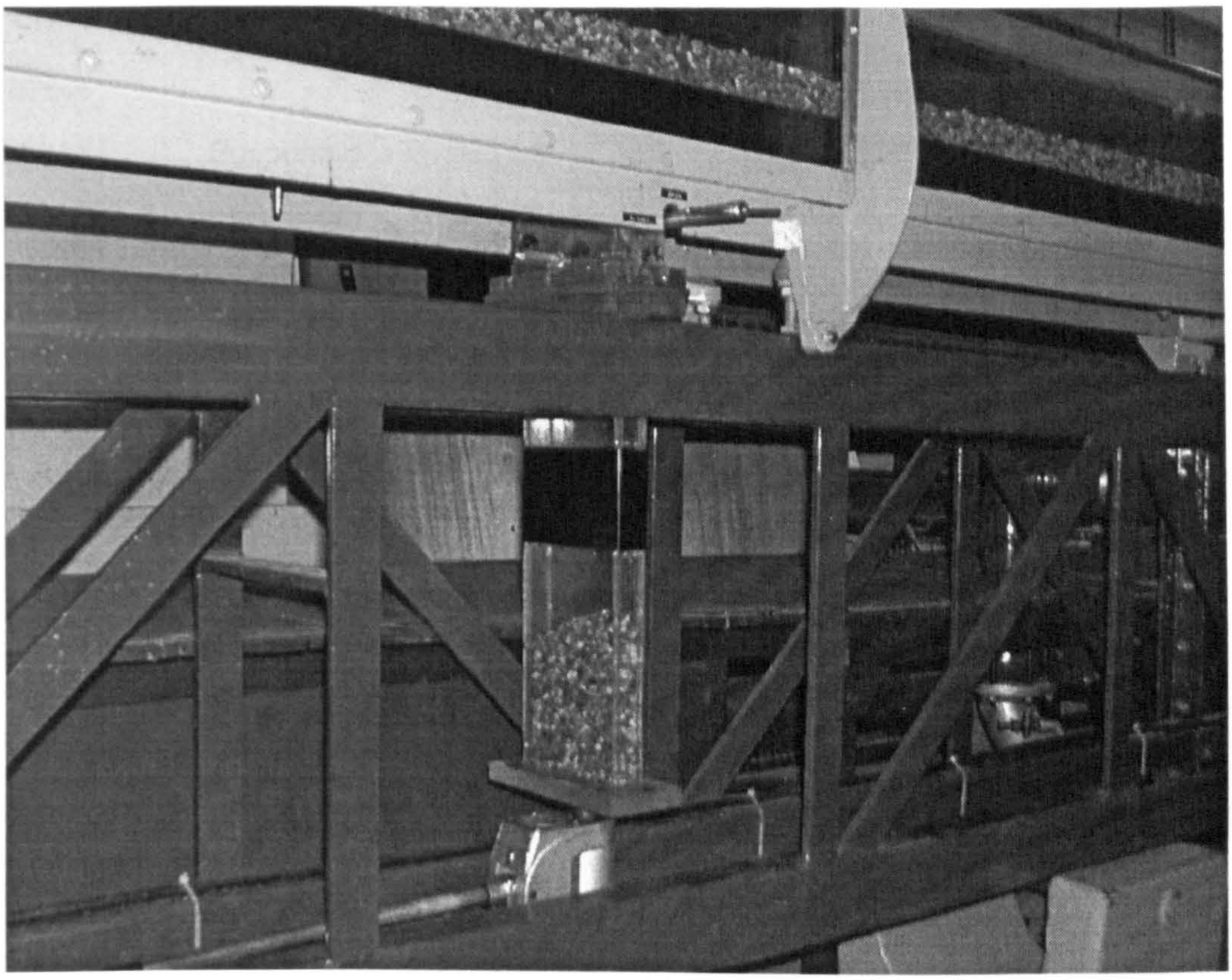

Figure 3.3 Sediment trap (Armfield flume).

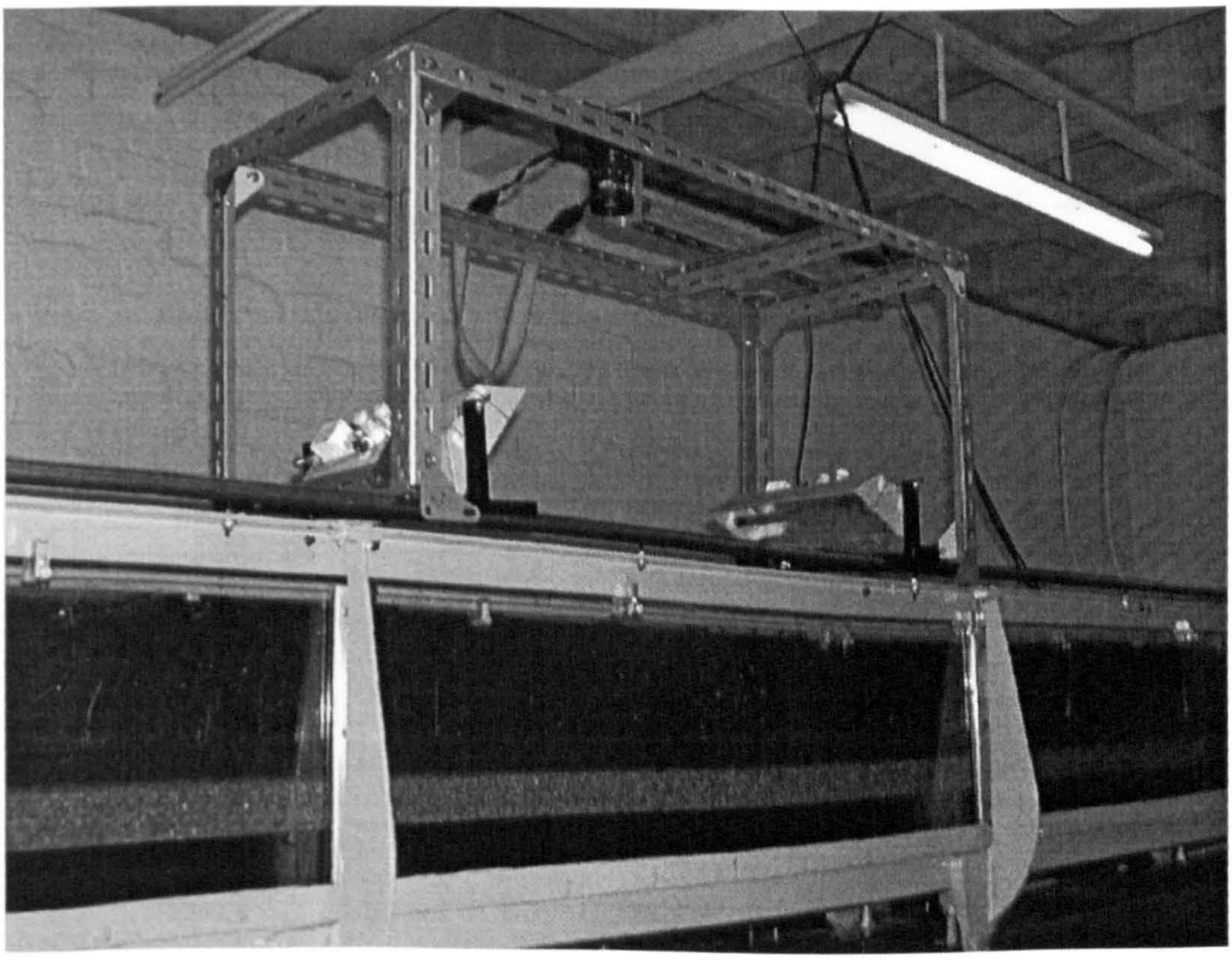

Figure 3.4 Camera and ultra-violet lamps used for registration of fluorescent particle motion (Armfield flume).

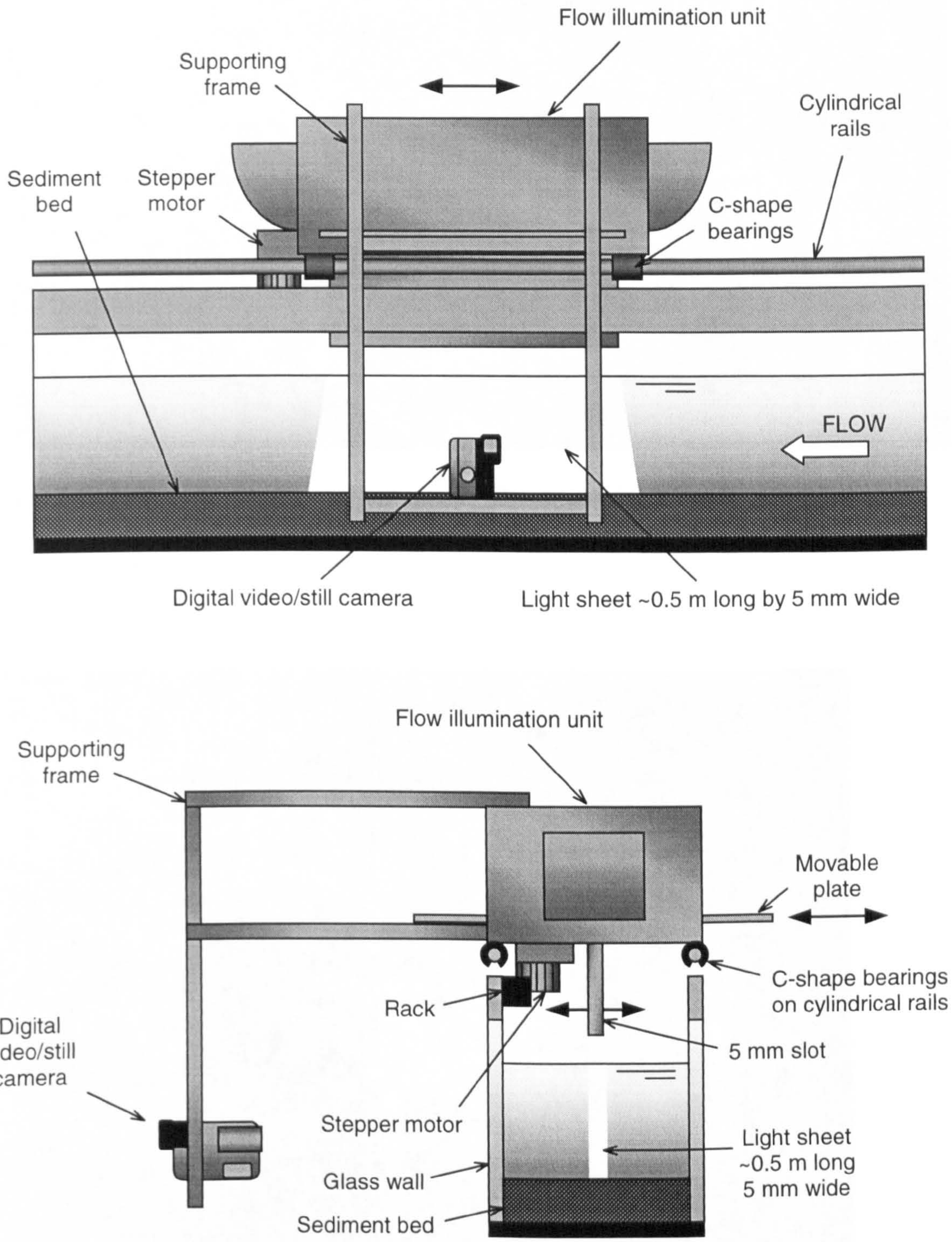

Figure 3.5 Diagram of flow illumination unit.

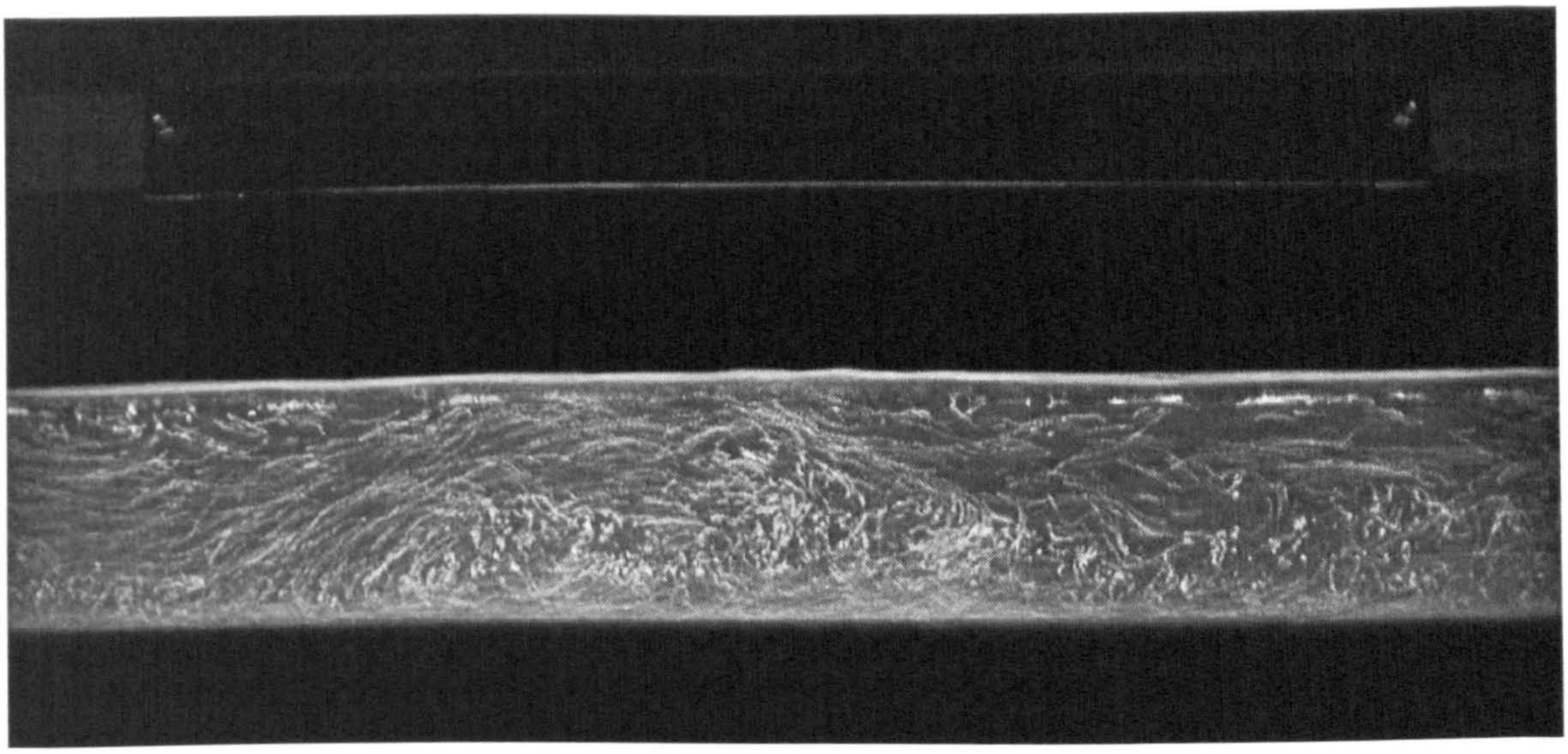

Figure 3.6 Motion of neutrally buoyant tracers illuminated by 0.5 m long and 5 mm wide light sheet produced by halogen lamps contained inside movable carriage (Armfield flume).

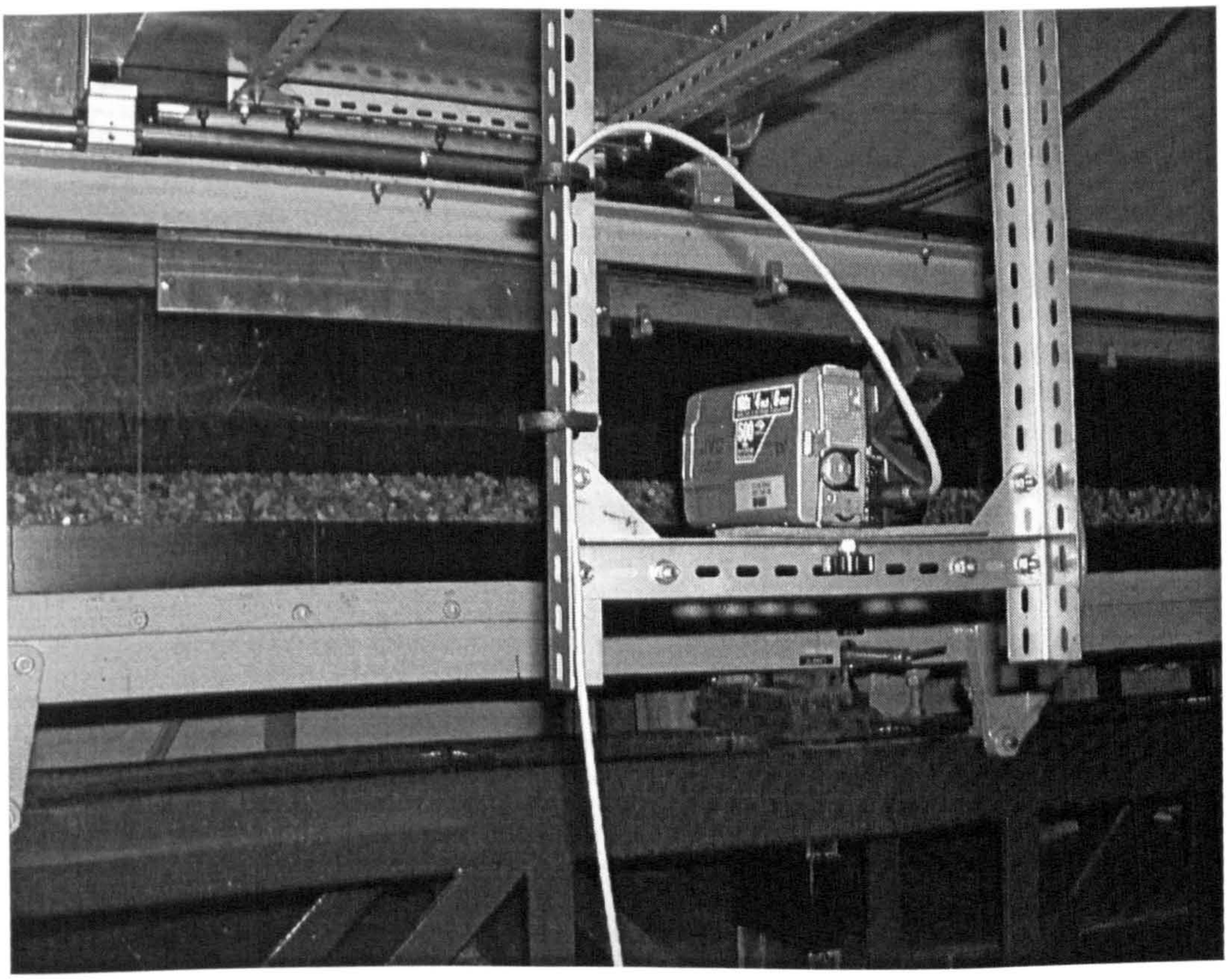

Figure 3.7 Digital video camera attached to movable carriage for registration of neutrally buoyant tracer motion (Armfield flume).

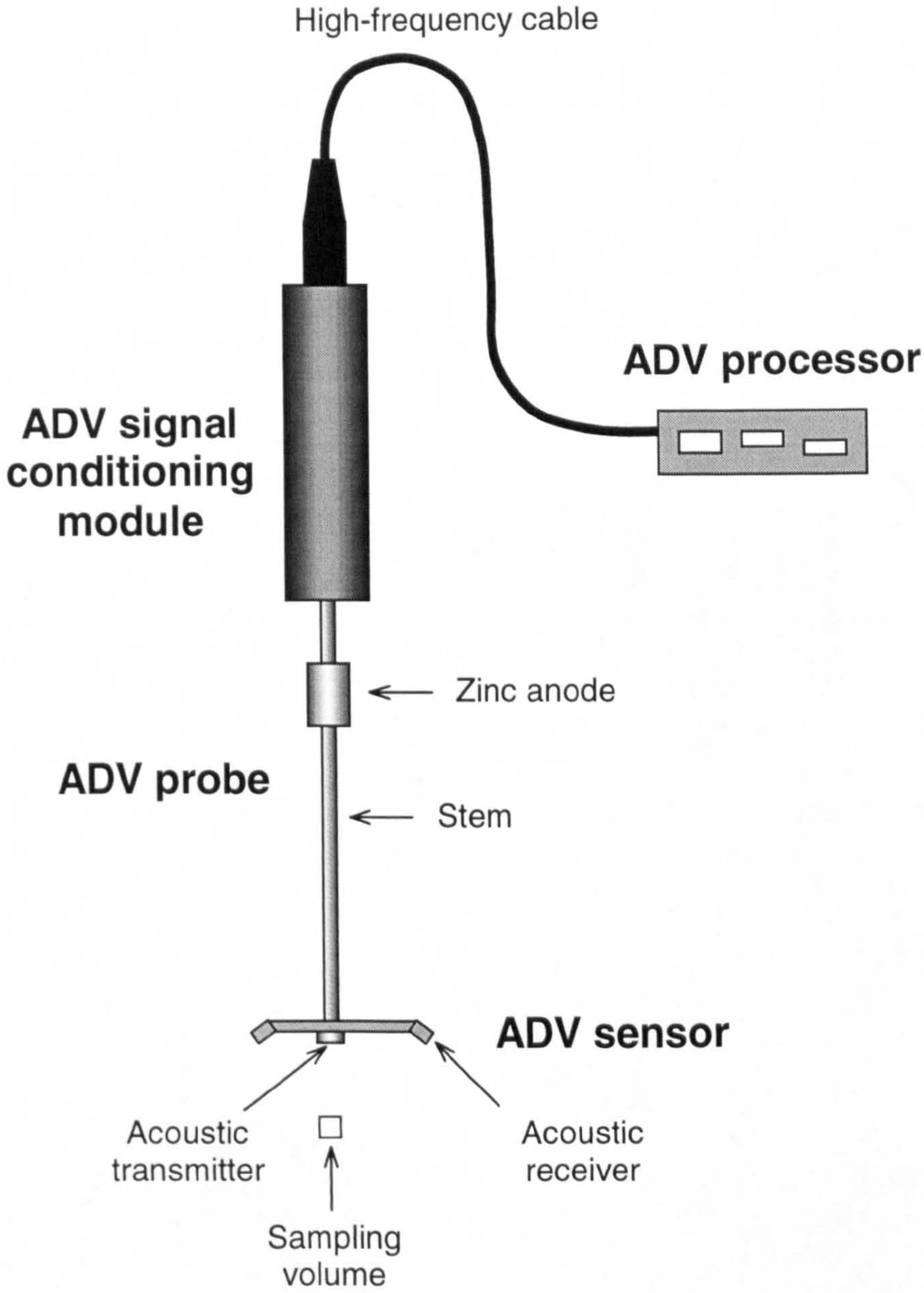

Figure 3.8 Acoustic Doppler Velocimeter (diagram).

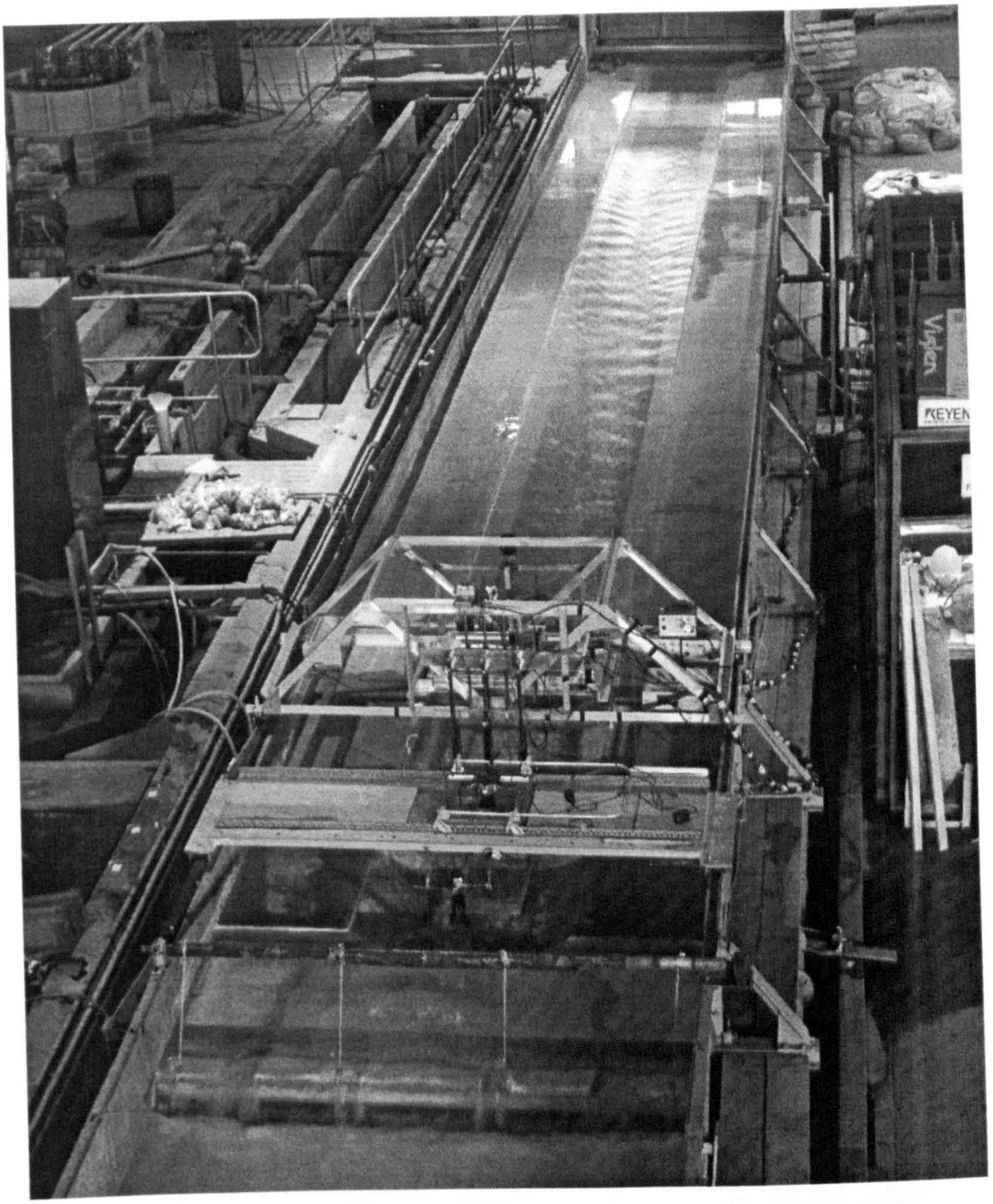

Figure 3.9 HR Wallingford flume (looking upstream).

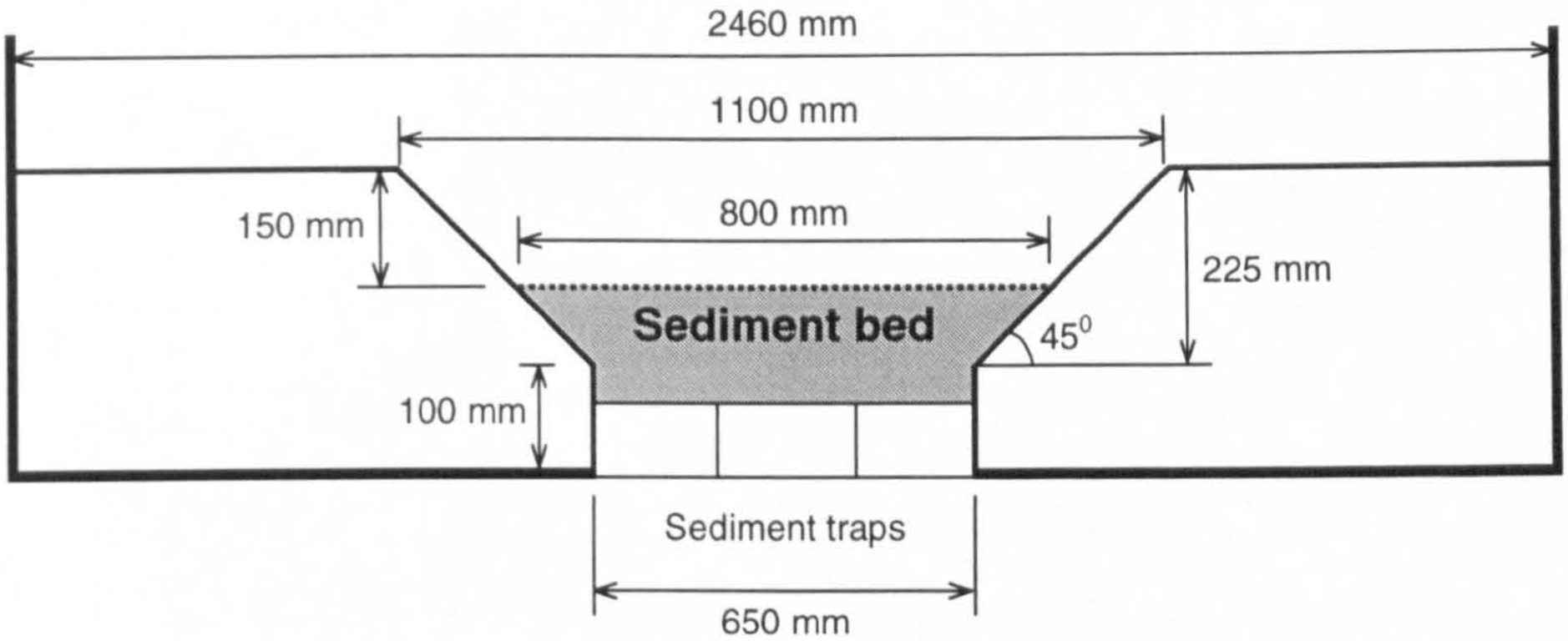

Figure 3.10 Channel cross-section (HR Wallingford flume).

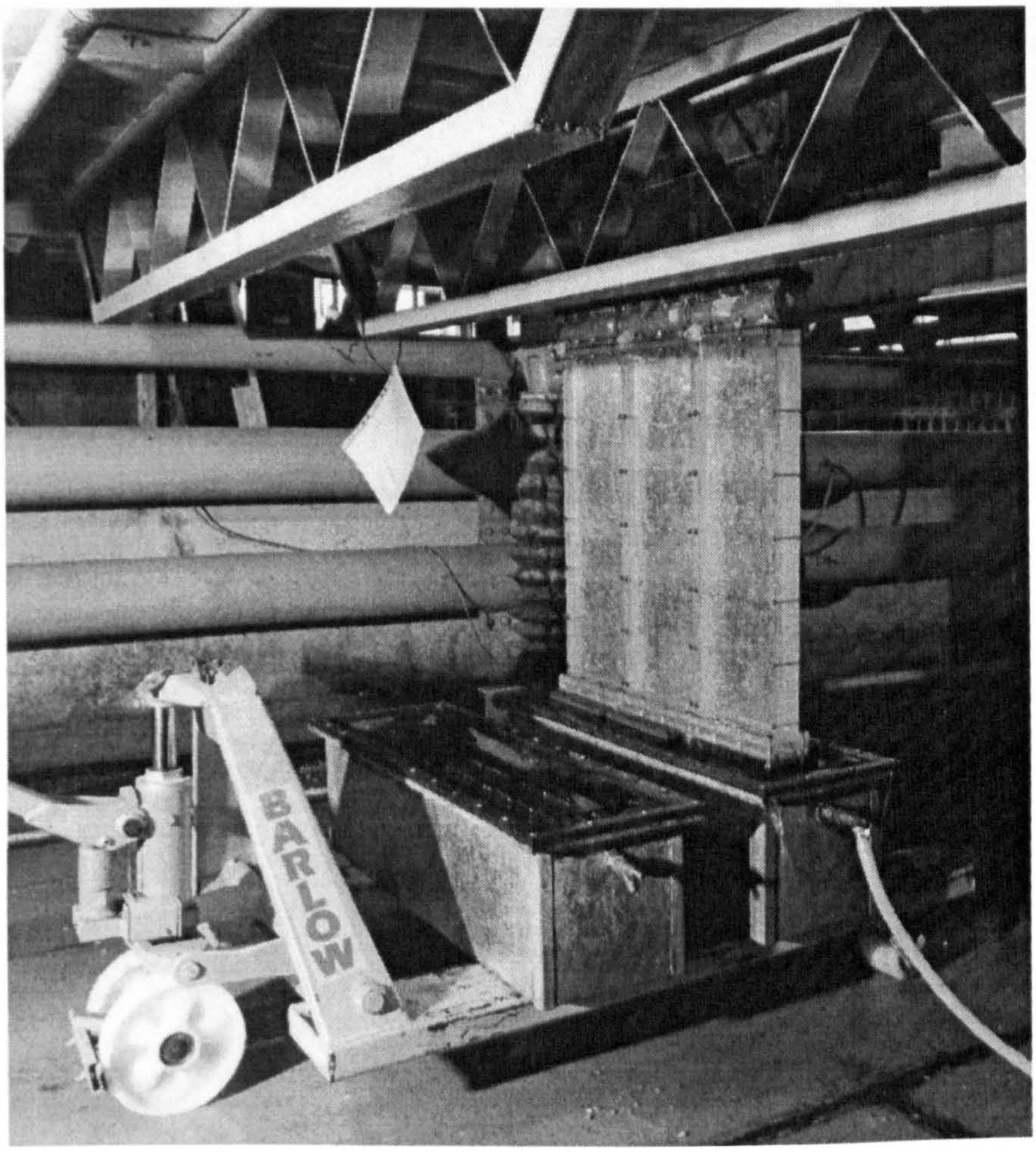

Figure 3.11 Sediment traps (HR Wallingford flume).

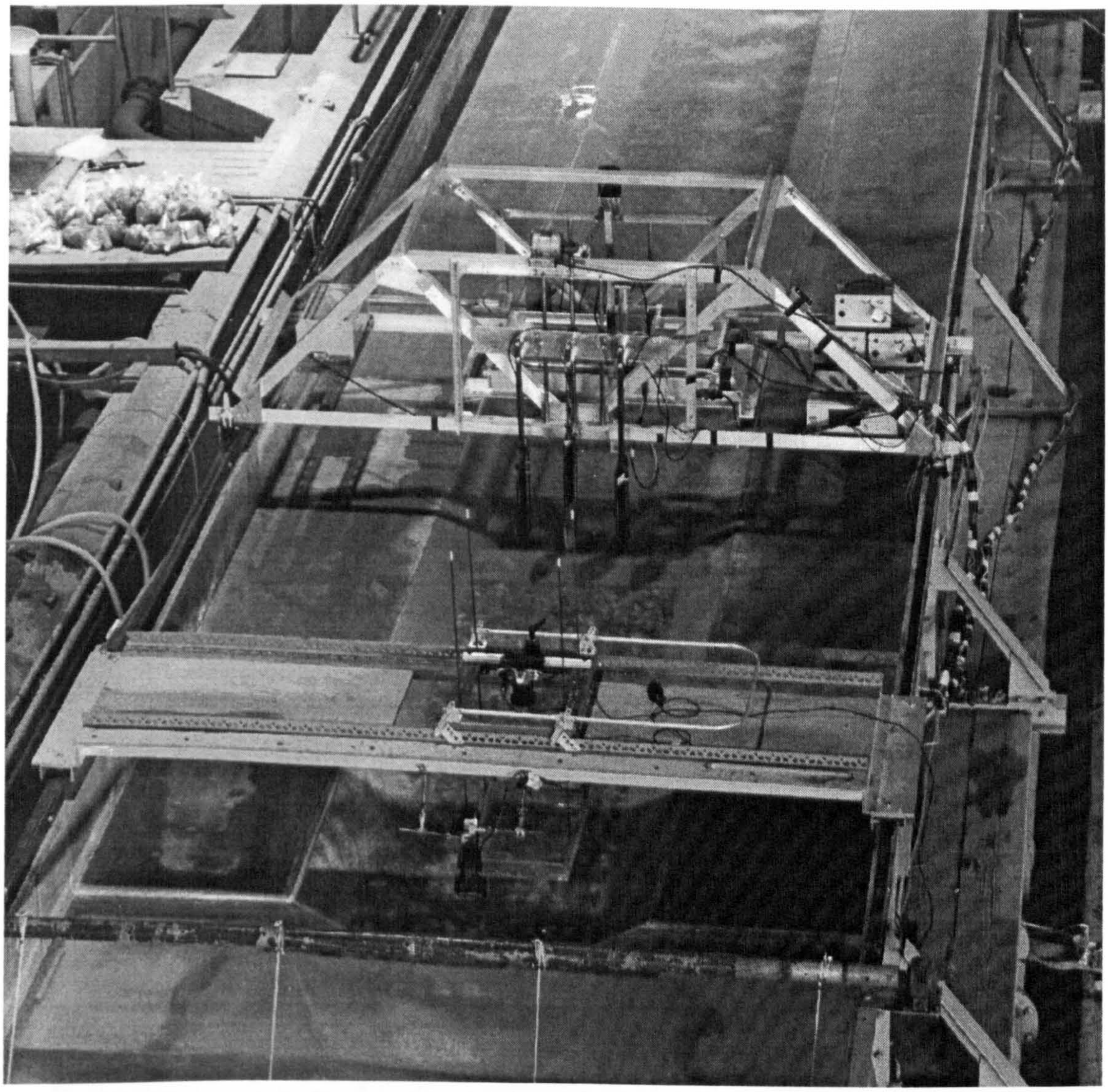

Figure 3.12 Instrument carriages (HR Wallingford flume).

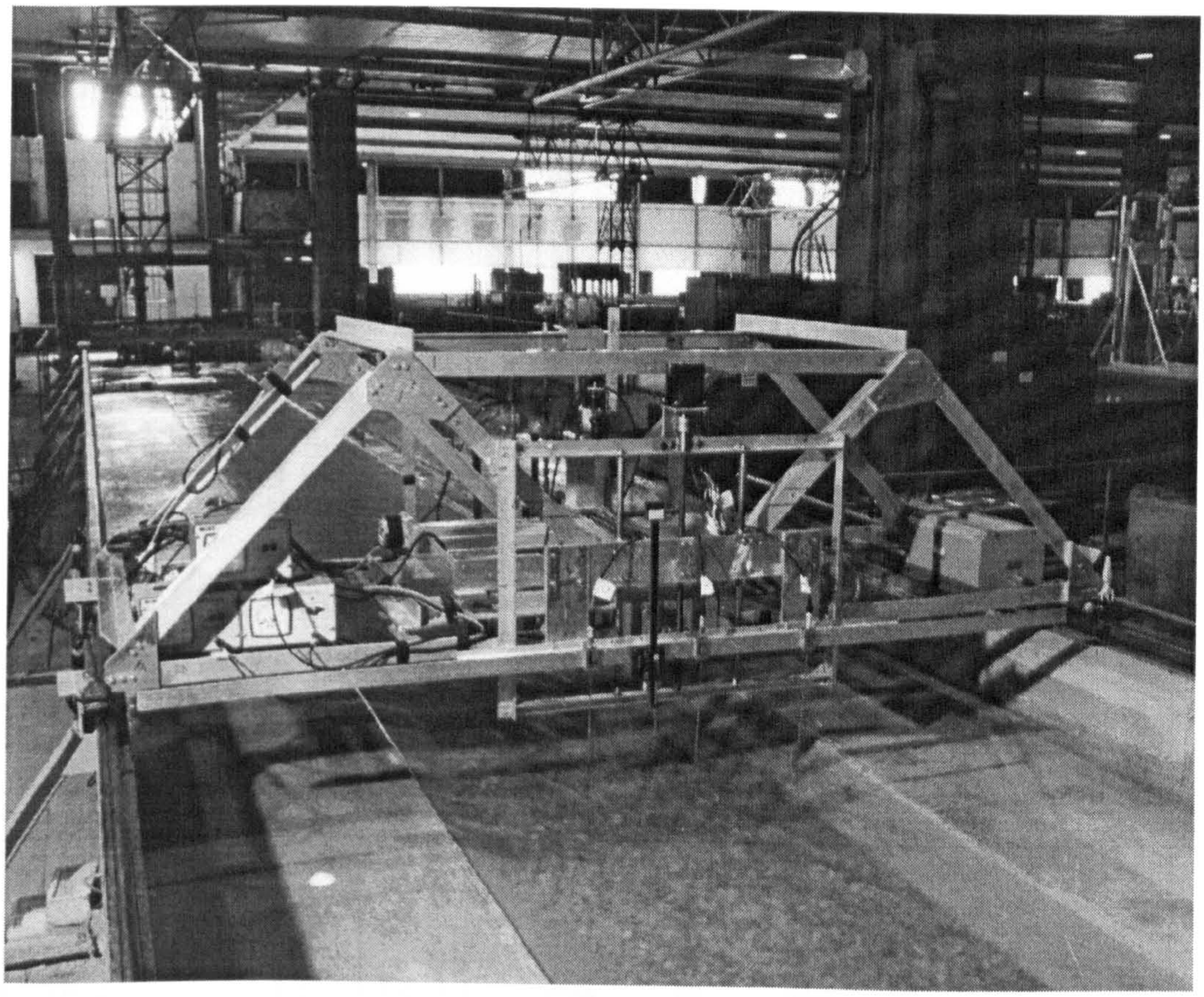

Figure 3.13 Mini-propellers and water surface pointer gauge (HR Wallingford flume).

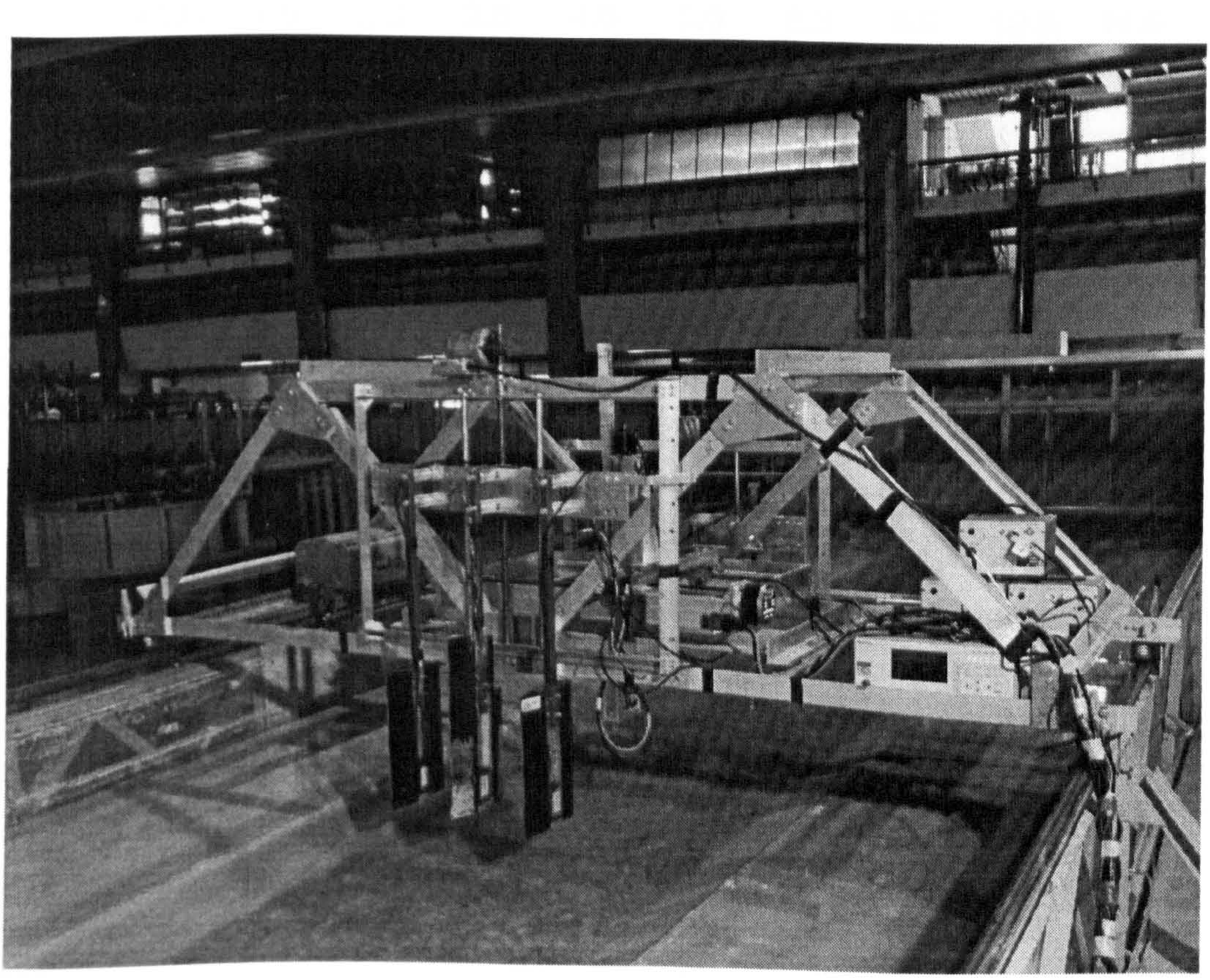

Figure 3.14 Longitudinal lasers (HR Wallingford flume).

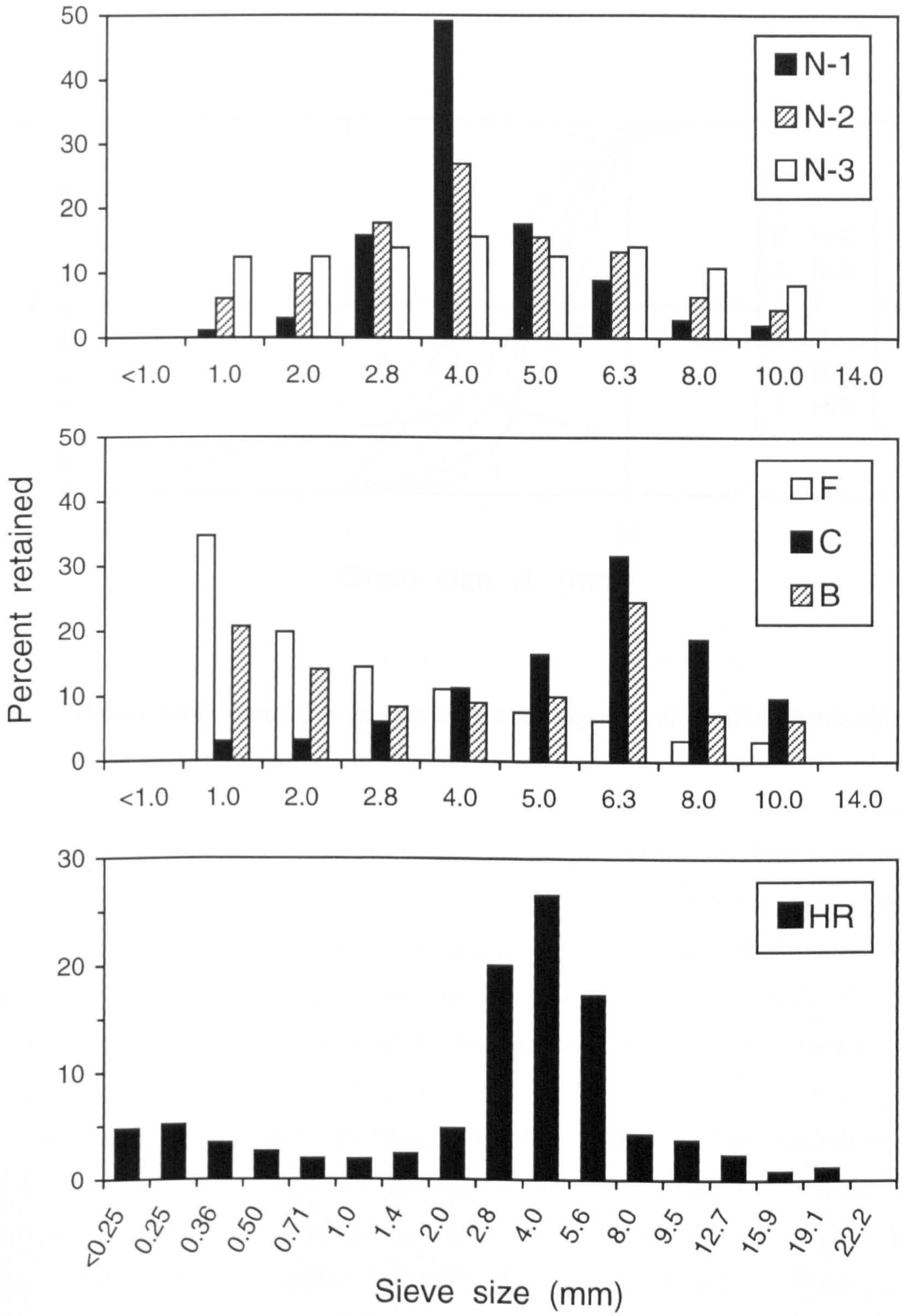

Figure 3.15 Grain size distributions for experimental sediment mixtures.

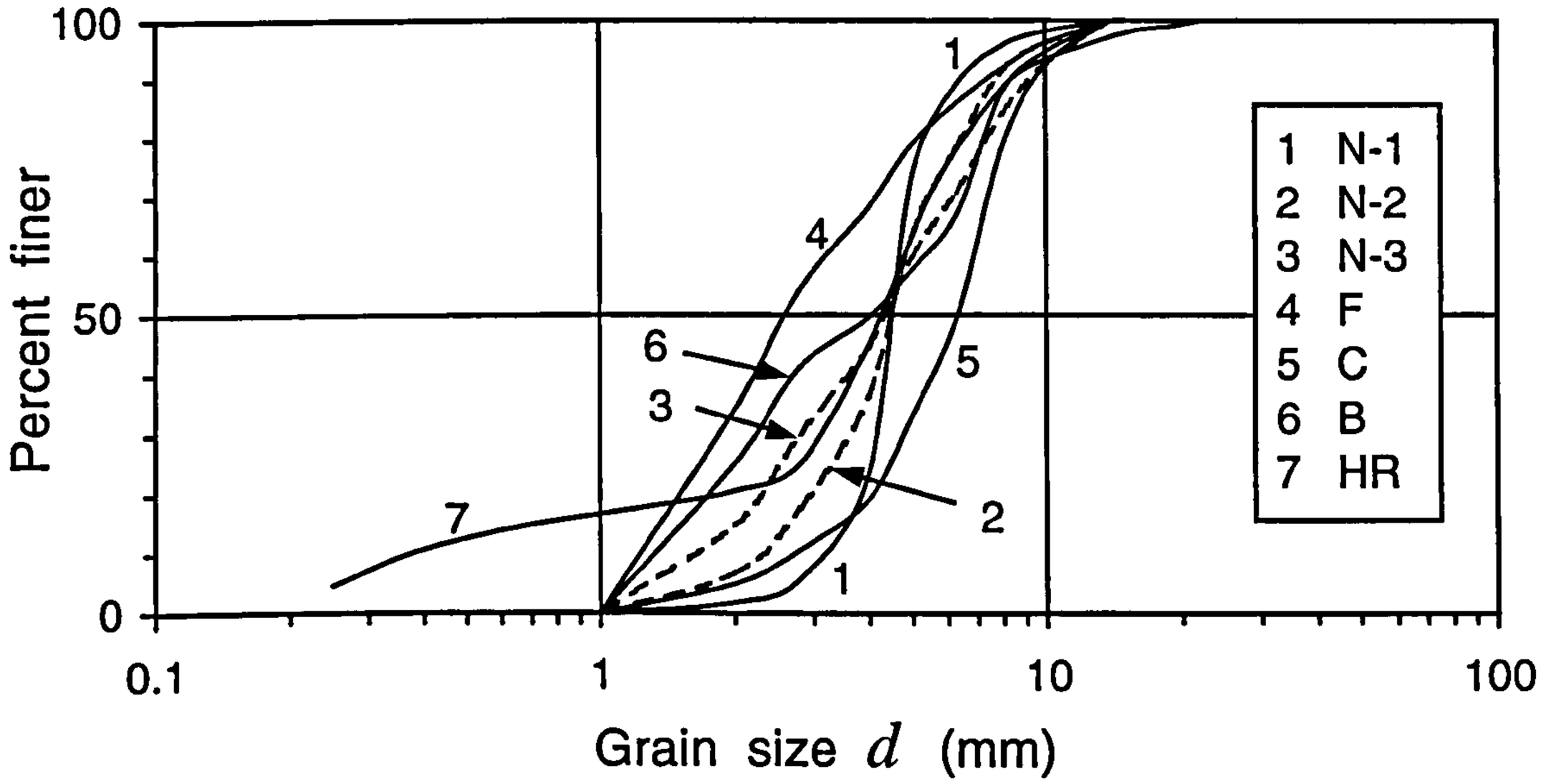

Figure 3.16 Cumulative grading curves for experimental sediment mixtures.

4

Incipient Motion of Coarse Uniform Sediments

"When you try to explain the behaviour of water, remember to demonstrate the experiment first and the cause next."

(Leonardo da Vinci)

4.1 Threshold Conditions

Consider a plane bed consisting of cohesionless uniform particles with turbulent water flowing over it. The flowing water will exert fluctuating hydrodynamic forces on the bed particles that tend to displace them. When a bed particle is unable to resist the destabilising hydrodynamic forces, it is entrained and starts to move. The entrainment threshold for each particle resting in the top layer of the bed is controlled by the grain's size, shape, and location among the surrounding particles. Because both turbulent fluctuations and individual grain characteristics are randomly distributed, the process of sediment entrainment has a random and intermittent character (Grass 1970). The greater the flow strength, the higher the level of turbulence and the higher the probability that a given grain will be entrained.

Practically, it is difficult to establish the flow strength below which no particle motion occurs. There is always some probability that even at a very low flow, maximum turbulent pulsations will be strong enough to cause the displacement of some grains (Paintal 1971, Lavelle and Mofjeld 1987). Hence, incipient motion of sediments is inherently a stochastic process characterised by a gradual increase of frequency of particle displacements as flow strength rises. Prediction of grain entrainment, therefore, requires an appropriate probabilistic description of the phenomenon.

In the present study the concept of threshold conditions for streambed movement is linked to the probability of sediment entrainment through the intensity of sediment

motion. The intensity of sediment motion is expressed as a relative number of particles displaced in unit time (Figure 4.1):

$$I = \frac{m}{N\,T} \tag{4.1}$$

where I is the intensity of sediment motion (or transport intensity), m is the number of particle displacements observed during the time interval T on the area A of the surface of a mobile bed, and N is the number of surface particles in the area A. The transport intensity I has the dimension s^{-1} and, in other words, is the fraction of all particles in the bed surface displaced every second. The number of particles N in the surface layer one grain diameter d thick can be estimated from

$$N = \frac{A\,d\,(1-p)}{\frac{\pi\,d^3}{6}} \tag{4.2}$$

where p is the bed porosity.

The rate of sediment transport can be expressed as (Yalin 1972)

$$q_b = \frac{m}{A\,T}\,G\,L \tag{4.3}$$

where G is the grain weight and L is the length of displacement of a grain after detachment. Rearranging (4.1) and substituting into (4.3), we obtain the transport rate expressed in terms of intensity of sediment motion

$$q_b = \frac{N}{A}\,I\,G\,L \tag{4.4}$$

Following analysis by Einstein (1942), the intensity I in (4.4) may also be interpreted as the probability that a particle in a bed area with the length L and unit width will start moving in any given second. Thus the parameter I also provides a probabilistic description of the process of sediment motion, and this parameter can be measured

experimentally. An important point is that the "critical value" of I is not fixed and can be chosen depending upon the design context.

The use of relative number of mobilized particles for determining I eliminates the necessity to change the area of observation A when changing sediment size, which is required when using other approaches (Neill and Yalin 1969, Yalin 1972). This ensures comparability of experimental data obtained for different grain sizes, provided the bed area of observation A and the time of observation T are large enough to obtain a stable mean value of transport intensity I. It should be noted that there are no strict definitions of what the area and time scales associated with observation of particle entrainment should be in each particular case. As the incipient motion of sediment is considered as a spatially and temporally random process of particle displacement under turbulent fluctuations, it is necessary that the area of observation A should be "large" in comparison to the grain area, and the time T of the observation should be "large" in comparison to the time average period of turbulent fluctuations (Yalin 1972). The choice of A and T in any particular study depends on the flume dimensions, measuring equipment, method of observation, and the range of grain sizes and flow conditions investigated.

4.2 Experimental Procedure

The experiments with uniform sediments (listed in Table 3.1) were conducted in the Armfield flume, University of Glasgow. Prior to each experiment, the sediment bed was carefully levelled using the screed board. Then the flume was set to the experimental slope, the tailgate was raised, and the bed was slowly flooded with water from the downstream end of the flume. After this the pump was started, the tailgate was opened, and after a short period of sub-threshold flow to remove unstable grains, the flow was gradually increased to the desired value. Care was taken to ensure that uniform flow was always maintained in the flume. The flume was long enough for the uniform flow to be self-established in most of the experiments. Only for high flows was the tailgate used to compensate for the recession curve at the outlet of the flume.

After uniform flow was established, the waste sediments collected in the trap were removed and sediment sampling was begun. Owing to the very low sediment transport rates in most cases the sampling period coincided with the duration of the experiments.

The bedload samples collected in the trap were subsequently dried and weighed to obtain the time-averaged bedload transport rate for the duration of each experiment.

In addition to the trapping of transported sediment the intensity of sediment motion was determined (every 3-10 min, depending on sediment transport rate) by either visual or photographic methods. The visual method consisted of counting the number of particle displacements from a 0.3x0.3 m^2 bed area 0.6 m upstream of the trap. The choice of the area of observation was restricted by the flume width and the physical ability of an observer to conduct the "observation". The area of observation contained between 740 grains (12 mm gravel) and 27,000 grains (1.5 mm sand). The time of a single observation varied from 15 s to 5 min depending on sediment discharge and was set individually for each experiment to average out the pulsing character of particle displacement caused by turbulent fluctuations. The area and time of observation in the experiments were large enough to obtain a stable mean value of transport intensity.

The photographic method was used to gain information on the intensity of sand-size particle motion during relatively active sediment transport when visual counting was impractical. A series of photographs of a 0.3x0.7 m^2 bed area with randomly distributed particles (normally about two thousand) labelled with fluorescent paint (four different colours were used) were taken in ultra-violet light. Comparative measurements showed that the use of the fluorescent paint did not change the sediment properties (density, fall velocity, and angle of repose). Displaced fluorescent particles were clearly identified as coloured streaks on the photographs taken with 1 s exposure (Figure 4.2). Counting the number of displaced and immobile fluorescent particles on the photographs gave an estimate of the intensity of sediment motion.

Other measured characteristics included water discharge, bed and water surface elevations, flow depth, and water/air temperature. Water discharge was determined using the built-in current meter in the flow return pipe. The functioning of the current meter and the manner in which the readings had to be made (using the pointer indicator) were considered to be unreliable and unsatisfactory for precise measurements. Therefore, the measured water discharge was taken as an approximate. Bed surface elevations were measured before and after each experiment using the moving pointer gauge. Water levels were continuously recorded during the experiments using the pointer gauge. Flow depth was controlled using vertical scales attached to the glass walls. Water and air temperatures were measured at the beginning and the end of the

experiments to give an average value. After each experiment bed surface topography was surveyed and photographed.

The experiments were conducted at a range of fixed bed slopes (0.0019-0.0287) for a variety of water discharges (0.3-29.3 L s^{-1}) with different intensity of sediment motion (5×10^{-6} - 6×10^{-2} s^{-1}). The duration of a single experiment depended on sediment transport rate and varied from a few minutes to 2.5 hours, most lasted for about one hour. During all the experiments, sediment transport was by bedload only, i.e. by rolling and sliding along the bed. Because of the generally low rates of sediment transport and relatively short duration of the experiments, no sediment was re-circulated or fed into the flume during the tests. The volume of sediment stored in the bed was very large in comparison with the volume mobilized, so that it constituted, in effect, an inexhaustible supply. No noticeable change of flow conditions or bed erosion took place during the experiments, so it is assumed that the sediment transport phenomenon in $\approx$2-3 m long measuring reach upstream of the trap approximated an equilibrium process for the duration of the measurements (i.e., the number of particles leaving the observation reach was equal to that entering).

4.3 Experimental Results

A total of 312 experiments (237 hours) with uniform sediment were performed. A summary of the hydraulic conditions and sediment transport rates observed in the experiments is presented in Table 4.1. All the measured data for uniform sediments are given in Table A.1 (Appendix A).

4.3.1 Intensity of sediment motion

During the initial stages of the experiments a gradual reduction of the intensity of sediment motion was usually observed (Figure 4.3). This reflected the rearrangement of the initial artificial bed structure arising from the bed construction. As time progressed, the intensity of grain motion stabilized and approached some steady value taken to correspond to the equilibrium transport for a water worked bed in the measuring reach.

Mean values of the intensity of sediment motion for the duration of the experiments are closely related to measured sediment transport rates. The relationship

between transport intensity I and sediment transport rate expressed as dimensionless Einstein bedload parameter

$$q_b^* = \frac{q_b}{\rho_s \sqrt{(s-1)gd^3}} \tag{4.5}$$

is presented in Figure 4.4. The correlation coefficient of the I versus q_b^* relationship is 0.98. The relationship appears to be independent of the bed slope and can be fitted by the straight line

$$\boxed{I = q_b^*} \tag{4.6}$$

This equality has significant practical value as it allows any measured bedload transport rate to be expressed in terms of the intensity of sediment motion or, alternatively, the probability of sediment entrainment. Hence, the proposed probabilistic approach to the description of the process of sediment entrainment actually reduces to the simple reference transport method based on the use of bedload transport relations. This has implications for the practical application of the probabilistic approach in the situations where only bedload transport data are available.

4.3.2 Bed shear stress

The bed shear stress concept is used in the present study to define incipient motion of the bed material. This concept has certain advantages and is better elaborated for fractionwise calculations in graded sediments compared to other approaches (discussed in Chapter 2). The bed shear stress is calculated as $\tau = \rho\, g\, R_b\, J$ using the hydraulic radius of the bed R_b and the slope J. The sidewall correction procedure used in this study to define R_b is based on the Manning roughness coefficients of the bed grains (n_s) and of the walls (n_w). The principal assumption is that the cross-sectional water area can be divided into bed area and wall area having the same energy gradient (equal to the bed slope) and mean flow velocity U of the total section. Applying the Manning formula $U = R^{2/3} J^{1/2} / n$ to each part of the water area, we obtain

$$R_b = R\left(\frac{n_g}{n}\right)^{3/2} \tag{4.7}$$

and

$$n = \frac{\left(P_b n_g^{3/2} + P_w n_w^{3/2}\right)^{2/3}}{P^{2/3}} \tag{4.8}$$

Here $R = B\,h/P$ is the hydraulic radius of the total area, B is the flow width, h is the flow depth, n is the equivalent Manning roughness coefficient, $P = B + 2h$ is the wetted perimeter of the complete section, $P_b = B$ is the wetted perimeter of the bed, $P_w = 2h$ is the wetted perimeter of the flume walls. The grain roughness is expressed by the Strickler formula $n_g = 0.048 d^{1/6}$ (Carson and Griffiths 1987) and the roughness of the glass walls is taken as $n_w = 0.010$ (Chow 1959).

The above wall-correction procedure is chosen to avoid the use of the mean flow velocity. In design practice, flow velocity is usually to be determined, and the Manning formula is widely used for the calculations. Thus the employment of the roughness coefficients for the sidewall correction provides direct applicability of the results of the flume study to solving practical problems. However, the present method and commonly used Vanoni and Brooks method (Vanoni et al. 1971) have shown comparable results differing by less than 5%.

4.3.3 Bedload transport

To account for the artificially high initial period of sediment transport (see Figure 4.3), measured transport rates (mean for the duration of the experiments) were corrected as follows:

$$q_b corrected = q_b measured\,\frac{I\ steady}{I\ mean} \tag{4.9}$$

This gave sediment transport rates for the period of steady particle motion. The corrected transport rates are plotted as the Einstein bedload parameter q_b^* against dimensionless Shields stress $\tau^* = \tau/[(\rho_s - \rho)\,g\,d]$ in Figure 4.5.

It is evident from Figure 4.5 that the bedload relations obtained for different bed slopes experience a systematic shift, that is, the steeper the slope is, the higher the shear stress must be to produce a given sediment transport rate. This is also obvious from Figure 4.6, constructed using graphs shown in Figure 4.5 for a fixed transport rate $q_b^* = 10^{-4}$ and relating Shields stress τ^* with bed slope for different grain sizes. Figure 4.6 demonstrates that for a given grain size, the value of τ^* required to produce a given transport rate increases consistently with bed slope and that the rate of increase depends on the slope.

The observed phenomenon can be explained in terms of the effect of relative depth (R_b/d for narrow channels with width to depth ratio B/h less than ≈ 10) on overall flow resistance. It is known that for transitional and rough turbulent flow the hydraulic resistance strongly depends on relative depth. The relationship between friction factor

$$f = 8\frac{U_*^2}{U^2} = 8\frac{\tau}{\rho U^2} \tag{4.10}$$

and relative depth R_b/d has been established by Nikuradze (1933) for artificially roughened pipes and by Zegzhda (1938) for open channel flow. They derived very similar diagrams relating friction factor f to flow Reynolds number Re and the value of R_b/d. These diagrams clearly demonstrate that for transitional and rough turbulent flow, friction factor f progressively increases with decreasing R_b/d. The increase of friction resistance for shallower flows is due to the increased effect of the wake eddies, shed by the bed particles, on the overall flow resistance. This effect is most significant for bed particles and their eddies comparable with the flow depth [R_b/d < 30-50 (Zegzhda 1938)]. Obviously, this effect of relative depth on flow resistance is reflected in the results of the present experiments. For a given grain size d and a given bed shear stress $\tau = \rho g R_b J$ the increase of slope J and the corresponding decrease of bed hydraulic radius R_b (and therefore decrease of R_b/d) cause a greater flow resistance and, accordingly, lower flow velocity U and lower sediment transport rate. As a result, a higher value of Shields stress $\tau^* = \tau/[(\rho_s - \rho) g d]$ is required to produce a given sediment transport rate for steeper slopes (Figure 4.5). The relationship between values

of τ^* and R_b/d corresponding to $q_b^* = 10^{-4}$ for different grain sizes is presented in Figure 4.7. The effect of relative depth on sediment mobility has proved to be quite significant. In the present experiments, for example, decrease of R_b/d from about 25 to 5 caused an almost twofold increase of τ^* corresponding to a given transport rate (Figure 4.7).

It is obvious that beyond some critical value, further increase of bed slope will cause the opposite effect, that is, decrease of τ^* for a given transport rate. This will happen for very steep slopes approaching the angle of repose for the bed material, when sediment mobility is increased by the effect of gravitation. Such extreme situations have been studied by others [e.g., Cecen and Bayazit (1973), Luque and van Beek (1976), Smart (1984), Chiew and Parker (1994)] and are beyond the scope of the present study.

4.3.4 Threshold diagram

To derive a threshold diagram based on the above probabilistic description of the process of bedload transport, it is necessary to choose a "critical" value of the intensity of sediment motion. It has been already mentioned that determined values of Shields stress corresponding to threshold conditions may vary significantly depending on how much movement is assumed to constitute incipient motion of the sediment (see Figures 2.7 and 2.8). This is also clearly demonstrated by Figure 4.8 based on the results of the present experiments with 3.4 mm gravel. Figure 4.8 shows a rather wide range of the variation of Shields stress for the intensity of sediment motion varying from "rare displacement of single particles" up to "frequent particle movement".

Obviously, the solution of different engineering problems may require different degrees of bed stability. For example, the critical state of the bed that is suitable for the accurate calculation of sediment transport may be too conservative for use in stable channel design. Therefore, in the present study two "critical" values of transport intensity are chosen as representative of the threshold of sediment movement: (a) $I = 10^{-4}$ s^{-1} (one of 10,000 surface particles is entrained every second) and (b) $I = 10^{-2}$ s^{-1} (one of 100 surface particles is entrained every second). The first transport intensity is close to the practical lower limit of sediment transport rate that can be reliably measured in open-channel experiments and which can be visually defined as "occasional particle movement at some locations" (Rijn 1989) or "weak" sediment transport ["several particles are in motion, in isolated spots, and in countable numbers"]

(Kramer 1935). The second one corresponds to "frequent particle movement at many locations" (Rijn 1989) or "general movement" on the bed (Kramer 1935). These two chosen "critical" values are also shown in Figure 4.8 as "threshold 1" and "threshold 2", respectively.

Given the linear relationship between transport intensity I and bedload parameter q_b^* [Figure 4.4, equation (4.6)], the experimental bedload relations can be used to determine values of Shields stress τ^* for different bed slopes corresponding to the two chosen "critical" values of the transport intensity: $I = 10^{-4}$ s^{-1} (or $q_b^* = 10^{-4}$) and $I = 10^{-2}$ s^{-1} (or $q_b^* = 10^{-2}$). The values of "critical" Shields stress τ_c^* were read by eye from the experimental q_b^* versus τ^* relations (Figure 4.5). Plots of τ_c^* on the Shields diagram as a function of grain Reynolds number Re_* together with the corresponding values of bed slope are presented in Figures 4.9 and 4.10. The Shields threshold curve is also shown in these figures for comparison.

To complement and extend the results of the present experiments, a search for data available in the literature was undertaken. Analysis of the existing large volume of data sets on sediment transport (e.g., Brownlie 1981, Gomez and Church 1988) revealed that in spite of extensive flume and field studies, surprisingly few data are available for incipient motion of coarse uniform ($\sqrt{d_{84}/d_{16}} < 1.5$) sediments. The only data sets which could be presented in the form of q_b^* versus τ^* relations for fixed bed slopes and which cover a sufficiently wide range of sediment transport rates to be analysed in accordance with the above method are those collected in flumes by Casey (1935), Bogardi and Yen (1936), Ho (1939), Paintal (1971), Taylor and Vanoni (1972), Ikeda (1983), Bathurst et al. (1984), and Graf and Suszka (1987). A summary of the additional data used for the present analysis is given in Table 4.2 and some of the bedload relations are shown in Figure 4.11. Most of the experimental data collected at different bed slopes, especially those of Bathurst et al. (1984) and Graf and Suszka (1987), demonstrate an apparent dependence of bedload transport rate on the slope, as was observed in the present experiments (compare Figures 4.5 and 4.11). Some of the data collected by Bathurst et al. (1984) for 22.2 mm and 44.3 mm gravel, and by Graf and Suszka (1987) for 23.5 mm gravel are also presented in Figures 4.6 and 4.7, showing variation of Shields stress τ^* required to produce a transport rate of $q_b^* = 10^{-4}$ with slope and relative depth, respectively.

The additional data sets were used to determine values of τ_c^* corresponding to $q_b^* = 10^{-4}$ ("threshold 1") and $q_b^* = 10^{-2}$ ("threshold 2") for a variety of bed slopes and grain sizes (Figure 4.11). These values of Einstein bedload parameter q_b^* are the equivalents of "critical" transport intensities $I = 10^{-4}$ s^{-1} and $I = 10^{-2}$ s^{-1}, respectively (see Figure 4.4). The values of τ_c^* determined for the additional data plotted on the Shields diagram are shown in Figures 4.9 and 4.10. As one can see, the available data from the other flume studies generally support and complement the results of the present experiments.

The compiled data set makes it possible to draw a family of threshold curves for different bed slopes (Figures 4.9 and 4.10). On this graph a number of interesting facts can be observed. At once the similarity of the general pattern of the present graph and the friction diagrams by Nikuradze (1933) and Zegzhda (1938) for transitional and rough turbulent flow is obvious [see also Moody (1944) and Chow (1959)]. This does suggest that the observed variation of τ_c^* for a given grain size simply reflects the dependence of the friction resistance on the relative depth. As one can also see from Figures 4.9 and 4.10, the experimental threshold curves follow approximately the shape of the Shields curve for $Re_* < 170$, show maximum critical Shields stress for $170 < Re_* < 300$ ($d \approx 4-5$ mm), and demonstrate an apparent gradual reduction of τ_c^* for large values of Re_*. Increase of τ_c^* with Re_* in the transitional zone ($Re_* \approx 10-300$) is usually explained by the destruction of the laminar sub-layer covering bed particles and the associated increase of hydraulic resistance. However, the observed subsequent reduction of τ_c^* with Re_* for rough turbulent flow is very surprising since one would expect τ_c^* to be independent of Re_* in this zone, as is generally acknowledged and is shown by all the existing threshold curves (Figure 2.3). To find a possible explanation of such behaviour, the experimental results shown in Figure 4.9 are presented in terms of relative depth (R_b/d) in Figure 4.12. It is seen from this figure that the Shields stress $\tau^* = R_b\, J/[(s-1)d]$ required to produce a given transport intensity ($I = 10^{-4}$ s^{-1}) at a given R_b/d value reduces for high values of Re_*. This means that in rough turbulent flow larger particles offer relatively lower resistance to the flow compared to finer grains. This is in contradiction with all the known friction diagrams showing invariability of the friction factor for a given relative depth in the

rough turbulent region [e.g., Nikuradze (1933), Zegzhda (1938), Moody (1944), Chow (1959)].

It is interesting to note, however, that data given by Misri et al. (1983) generally support the above observations. Misri et al. (1983) studied incipient motion of uniform sediment ranging in size between 1.67 mm and 4.36 mm using a visual definition of threshold as "general movement". Their experimental results demonstrated both decrease of τ_c^* with increase of R_b/d for a given sediment size and gradual reduction of τ_c^* for high values of Re_* for a given R_b/d value.

The present conclusion is also in agreement with the experimental results of Klaven and Kokovin (1987) who observed entrainment of a special artificial particle from a bed composed of uniform gravels. The experiments were conducted in an 8 m long by 0.10 m wide tilting flume, at a constant flow depth of 0.05 m and variable flume slopes. The bed material ranged in size from 2.5 mm and 6.5 mm, the thickness of the bed being 6 cm. The artificial particle was a conical washer placed in an appropriate-shaped nest (both made of perspex) level with the bed surface. The observation demonstrated that the artificial particle was entrained from the 2.5 mm gravel bed at mean flow velocity of U=0.770 m s^{-1} (slope J=0.0132), from the 4.5 mm gravel at U=0.550 m s^{-1} (J=0.0070), and from 6.5 mm gravel at U=0.514 m s^{-1} (J=0.0066). That is, the coarser the gravel, the lower flow strength was required to entrain the artificial particle. This is generally consistent with the results of the present experiments.

The observed variation of τ_c^* with Re_* in rough turbulent region can be explained by the fact that the wake eddies, which are shed by the bed particles and which interact with the flow turbulence, actually depend on the absolute size of the particles (Bathurst 1982). For the same value of R_b/d, change in absolute size of bed material apparently results in a change of the character of the turbulent field near the bed affecting the overall flow resistance. This effect must be especially pronounced for the relatively shallow flows investigated in the present flume study.

As one can see from Figures 4.9 and 4.10, the commonly used Shields threshold curve is more appropriate for the conditions of "general movement" on the bed. If "weak" sediment motion is chosen as a critical state of the bed, the Shields threshold curve shows agreement with the experimental data only for steep slopes (of the order of 0.010-0.020) and significantly overestimates critical flow conditions (up to 90%) for bed slopes less than 0.010, especially in the rough turbulent zone. The coarser is the bed

material, the greater is the overestimation obtained using the Shields curve. By extrapolating the experimental threshold curves, one may conclude that for a bed composed of 50 mm gravel and having slope of 0.005 (the values typical of many natural gravel-bed streams) the use of the Shields threshold curve would overestimate critical flow depth by more than 200%. It should be noted, however, that there is an obvious lack of data at high Re_* values. Further experiments with very coarse bed material and moderate slopes with large values of R_b/d would significantly clarify the situation. Although the difference in the shape of sand size sediment (angular particles) and gravel (well-rounded particles) in the present experiments could have some effect on the sediment mobility and therefore the shape of the threshold curves for $Re_* < 150$, this is believed to reflect the natural situation in rivers where sand bed material is unlikely to be rounded.

Thus the results obtained clearly demonstrate the effect of relative depth (or, alternatively, bed slope) on incipient motion of bed sediment and partly explain the scatter of data on the Shields diagram. Until now, evidence on the effect of relative depth (directly related to the bed slope) on sediment mobility was fragmentary and incomplete. The present study has summarized data for a wide range of sediment sizes (d=1.07-44.3 mm) and has resulted in comprehensive threshold diagrams for the sizes investigated (Figure 4.9 and 4.10).

As one can see from Figures 4.9 and 4.10 (see also Figures 4.6 and 4.7), the critical Shields stress for a given bed slope first increases and then decreases as sediment size increases. The change of direction in the relationship occurs at a sediment size of about 4-5 mm. The observed variation of the critical Shields stress with grain size may have implications for the practice of physical hydraulic modelling. It is believed that the process of coarse sediment transport can be faithfully reproduced at a reduced scale using sand size sediment (e.g., Yalin 1971). Many of the present theories of movable bed modelling are based on the assumption of the constancy of τ_c^* for rough turbulent flow. However, the present findings indicate that this is apparently not the case, and therefore the use of sand for studying the behaviour of coarse material needs further investigation.

It should be noted, that the Shields diagram is a useful means of evaluating the critical flow conditions as long as a single curve can be defined and, in particular, while the critical Shields stress is constant at large grain Reynolds numbers. The introduction of the dependency of critical Shields stress on both slope (or relative depth) and grain

Reynolds number has considerably reduced the ease of use of the diagram. Iterative calculations must be made to determine critical flow characteristics (slope or bed hydraulic radius) for a given grain size. The experimental results in a form more convenient for practical use are presented in Figure 4.13. The diagram in Figure 4.13 refers to the initial motion of natural uniform ($\sigma_g < 1.5$) coarse sand and well-rounded gravel on a flat bed by uniform water flow. It relates critical flow characteristics (hydraulic radius of the bed R_b and bed slope J) with grain size d for the two "critical" transport intensities $I=10^{-4}$ s^{-1} and $I=10^{-2}$ s^{-1}, corresponding to "weak" and "general" sediment motion accordingly. The difference between the values of R_b corresponding to the above transport intensities varies from 15-25% for steep slopes to 20-40% for moderate slopes. From an engineering point of view, these differences may be considered as insignificant for laboratory conditions with shallow flows. However, such differences cannot be disregarded in large rivers and canals where the depth is much greater than in experimental flumes. The diagram shown in Figure 4.13 covers a range of flow conditions typically observed in laboratory flumes, but it can be used to estimate critical conditions in larger streams by extrapolating the experimental results. Further investigations of initial motion of very coarse gravel (larger than 50 mm) at moderate bed slopes (less than 0.010) are needed to extend the threshold diagram for conditions typical of natural gravel-bed streams.

4.3.5 Formalization of results

The threshold diagrams presented graphically in Figures 4.9, 4.10, and 4.13 are derived for two arbitrary chosen "critical" transport intensities. However, situations may arise in design practice when the prediction of other "critical" states of bed mobility may be required. Therefore, an attempt is made to formalize the experimental results to provide a generalized method for calculating threshold conditions of coarse uniform sediments.

Analysis of the experimental data reveals that the bedload relations obtained for $q_b^* \leq 10^{-2}$ in this study and by other investigators (listed in Table 4.2) are reasonably well represented by the following relationship (see Figures 4.5 and 4.11):

$$q_b^* = (a\,\tau^*)^{18}\, J^{-5.0} \tag{4.11}$$

where a is the particle mobility factor expressed by

$$a = -1.1\left[\log(1000\,d)\right]^3 + 4.8\left[\log(1000\,d)\right]^2 - 5.0\log(1000\,d) + 4.6 \qquad (4.12)$$

with the grain size d in metres. The above equations are derived for $1 \le d \le 44.3$ mm and $0.001 \le J \le 0.070$. The exponent 18 at τ^* in (4.11) is close to the values of 16 derived by Paintal (1971), 17.5 found by Taylor and Vanoni (1972), 15.7 recommended by Parker (1990) for very low sediment transport rates, and 15.1 obtained by Wathen et al. (1995) for the gravel-bed Allt Dubhaig. Somewhat lower values for the exponent have been obtained by Misri et al. (1984) and Swamee and Ojha (1991) (8 and 9, respectively). However, it should be remembered that the transport data used in these studies were collected at different bed slopes and none of the proposed methods account for the effect of bed slope on bed material mobility as demonstrated in Figures 4.5 and 4.11.

Parameter a in (4.11) reflects the difference in the relative mobility of different grain sizes. The variation of a with grain size d according to the experimental data is shown in Figure 4.14 together with the approximating relationship (4.12). As is seen from this figure, the value of a first decreases and then increases as sediment size increases. The minimum value of a corresponds to a sediment size of around 5 mm. This means that at a given bed slope J particles with $d \approx 5$ mm require a higher value of τ^* compared with finer and coarser grains to produce a given dimensionless transport rate q_b^*. A similar pattern is seen in the threshold diagrams in Figures 4.9 and 4.10. The cause of this behaviour is not clear at present. As is speculated above, it may be related to the dependence of the near-boundary turbulence on the absolute grain size. Further investigations are needed to clarify the phenomenon.

Bearing in mind that $I = q_b^*$ (Figure 4.4), equation (4.11) can be rearranged into a general expression for calculating critical Shields stress of coarse uniform sediments:

$$\tau_c^* = \frac{I_c^{0.0556}}{a} J^{0.278} \qquad (4.13)$$

where I_c is the "critical" value of sediment transport intensity (or probability of sediment entrainment) representing the threshold of sediment movement. The threshold

curves shown in Figures 4.9 and 4.10 are therefore described by the following two relationships:

$$\tau_c^* = \frac{0.60}{a} J^{0.278} \qquad \text{(for } I_c = 10^{-4}\text{, Figure 4.9)} \qquad (4.14)$$

and

$$\tau_c^* = \frac{0.77}{a} J^{0.278} \qquad \text{(for } I_c = 10^{-2}\text{, Figure 4.10)} \qquad (4.15)$$

The generalized equations (4.11) and (4.13) are applicable only for $I_c \leq 10^{-2}$ ($q_b^* \leq 10^{-2}$) as for higher transport rate the q_b^* versus τ^* relationship is known to change dramatically (Paintal 1971, Misri et al. 1984, Parker 1990).

4.3.6 Bed features

During most of the experiments with appreciable sediment motion longitudinal ridges and troughs were developed on the bed (Figure 4.15). The more active the sediment transport, the more pronounced were the longitudinal bed forms. The number of troughs varied from two to nine depending on the flow depth h. The troughs were about 1-2 grain diameter deep, with the width of about $2h$, which is in agreement with the existing data (e.g., Ikeda 1981, Ikeda 1983, Nezu and Nakagawa 1989, 1993). Visual observations of bed particle motion revealed that the most active sediment movement took place along the troughs. The same conclusion follows from the analysis of data on movement of bed particles labelled with fluorescent paint (Figure 4.16). This is also consistent with experimental results of Nezu and Nakagawa (1989) who observed higher streamwise velocity, bed shear stress, and bedload transport through troughs compared to along ridges developed in a sand channel. The observed preferential transport of bed particles along the troughs indicates that the motion of particles is not an entirely random process over the bed area, but concentrates along certain paths, the width of which is scaled with the flow depth. This does suggest that the particle mobilization is strongly influenced by the structure of the flowing water and that an improved understanding of sediment dynamics can only be obtained from a combined study of sediment entrainment phenomenon and flow kinematic structure.

The cause of the longitudinal bed forms is discussed in detail later in Chapter 6 concerned with the turbulent structure of the open-channel flow.

4.4 Conclusions

The following are the principal results of the present experimental study of initial motion of streambeds composed of coarse uniform sediments.

A new approach to the description of critical state of the bed based on the intensity of sediment motion, or transport intensity, is proposed. This approach describes the state of bed material mobility in terms of the fraction of bed particles mobilized in unit time, which eliminates the subjectivity in defining threshold conditions and provides a probabilistic description of the process of sediment entrainment.

On the basis of the flume data, a relationship between the transport intensity I and dimensionless bedload parameter q_b^* is established (Figure 4.4). This relationship allows any measured transport rate to be expressed in terms of the transport intensity or, alternatively, probability of sediment entrainment. The experimental bedload relations obtained for different grain sizes and bed slopes in this study (Figure 4.5) and by other researchers (Figure 4.11) are used in conjunction with the I versus q_b^* relationship (Figure 4.4) to derive a revised Shields diagram for two states of sediment mobility on the bed: (a) "weak" sediment motion with transport intensity $I = 10^{-4}$ s^{-1} ("threshold 1"), and (b) "general" sediment transport with $I = 10^{-2}$ s^{-1} ("threshold 2"). The appropriate threshold diagrams are shown in Figures 4.9 and 4.10, and are presented in a form suitable for practical use in Figure 4.13.

The experimental results indicate that the critical Shields stress τ_c^* strongly depends on the chosen value of "critical" intensity of sediment motion (Figure 4.8). It is shown that the Shields threshold curve is appropriate for "general" sediment movement on the bed. An almost twofold overestimation of critical flow depth may result from the use of the Shields threshold curve for predicting "weak" transport of coarse gravel at slopes less than 0.010.

The experimental data also reveal that τ_c^* for incipient motion of uniform sediment depends not only on the grain size (or grain Reynolds number) but also on bed

slope (Figures 4.9 and 4.10). The steeper the slope is, the higher is the value of τ_c^*. This effect is explained by the greater resistance of the grains caused by reduced relative depth (depth to grain size ratio) for steeper slopes.

Analysis of the results of the present and other flume studies reveals the following interesting fact. At high values of Re_* (medium to coarse gravel) critical Shields stress τ_c^* is not constant, as is usually assumed, but gradually decreases as grain size increases, which indicates lower flow resistance for coarse gravel if compared with fine gravel. This is in contradiction to all the existing theories. Further experimental study is required to clarify the phenomena observed. This should include both a detailed study of the turbulent structure of the flow over rough beds and experiments with coarse gravel at moderate slopes with high values of relative depth. Collection of additional data on incipient motion of medium and fine sand by the method used in the present study is also desirable to extend the threshold diagram (Figures 4.9 and 4.10) for low values of grain Reynolds number.

The bed particle mobilization is shown to occur not randomly over the bed area but along certain paths. This is explained by the effect of the flow kinematic structure and is discussed in detail later in the appropriate chapter.

Finally, a set of generalized equations (4.11)-(4.13) for calculating low bedload transport rates and critical Shield stress is derived for practical use by design engineers.

Table 4.1 Range of Data for Uniform Sediments in Armfield Flume Experiments

Sediment No.	Grain Size d (mm)	Width B (m)	Slope J x 10^3	Depth h (m)	Velocity U (m s^{-1})	Transport Rate q_b (g s^{-1} m^{-1})
1	1.5	0.30	1.9-14.1	0.006-0.048	0.16-0.40	0.0038-28.5
2	2.4	0.30	2.6-14.1	0.014-0.068	0.06-0.51	0.0043-51.9
3	3.4	0.30	1.9-23.8	0.013-0.135	0.16-0.75	0.014-11.8
4	4.5	0.30	2.6-28.7	0.017-0.136	0.18-0.79	0.013-23.3
5	5.65	0.30	4.1-15.7	0.033-0.124	0.49-0.87	0.024-9.28
6	7.15	0.30	4.1-23.8	0.029-0.121	0.54-0.93	0.080-62.4
7	9.0	0.30	6.5-15.7	0.051-0.114	0.62-0.96	0.059-26.7
8	12.0	0.30	11.5-28.7	0.043-0.100	0.61-1.07	0.070-37.2

Table 4.2 Summary of Other Flume Data for Uniform Sediments

Primary Source	Mean Grain Size d (mm)	Geometric Standard Deviation σ_g	Width B (m)	Slope J x 10^3	Depth h (m)	Velocity U (m s^{-1})	Transport Rate q_b (g s^{-1} m^{-1})
Casey (1935)	2.46	1.16	0.40	1.2-5.1	0.027-0.219	0.44-0.75	0.0010-59.5
Bogardi and Yen (1936)	6.85	1.11	0.30, 0.82	14.1-14.8	0.040-0.074	0.69-0.92	0.18-21.9
Ho (1939)	6.01	1.39	0.40	3.4-5.0	0.109-0.174	0.69-1.02	0.098-27.1
Paintal (1971)	2.5, 7.95, 22.2	1.08-1.11	0.91	1.2-9.6	0.029-0.203	0.39-1.38	0.00001-49.6
Taylor and Vanoni (1972)	1.07, 2.81	1.11, 1.14	0.27	0.8-3.7	0.060-0.061	0.30-0.53	0.0007-0.0421
Ikeda (1983)	6.5	1.36	4.00	2.4-5.4	0.135-0.313	0.99-1.52	0.30-254.4
Bathurst et al. (1984)	11.5, 22.2, 44.3	1.24-1.27	0.60	5.0-70.0	0.044-0.254	0.75-2.00	0.77-4667
Graf and Suszka (1987)	12.2, 23.5	1.23-1.24	0.60	5.0-25.0	0.094-0.245	0.92-1.54	0.22-514.4

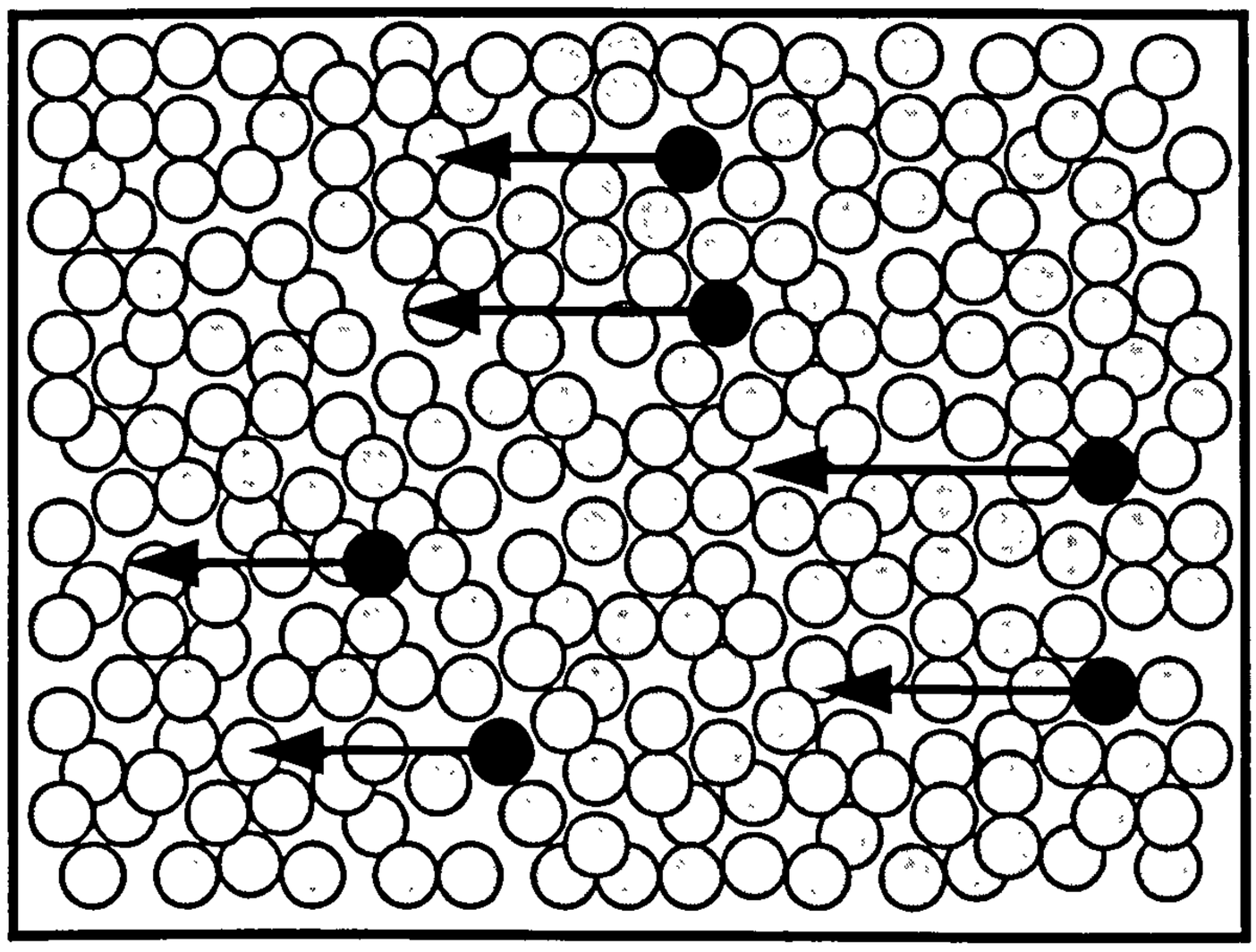

Figure 4.1 Schematic diagram of a bed area with displaced and immobile particles.

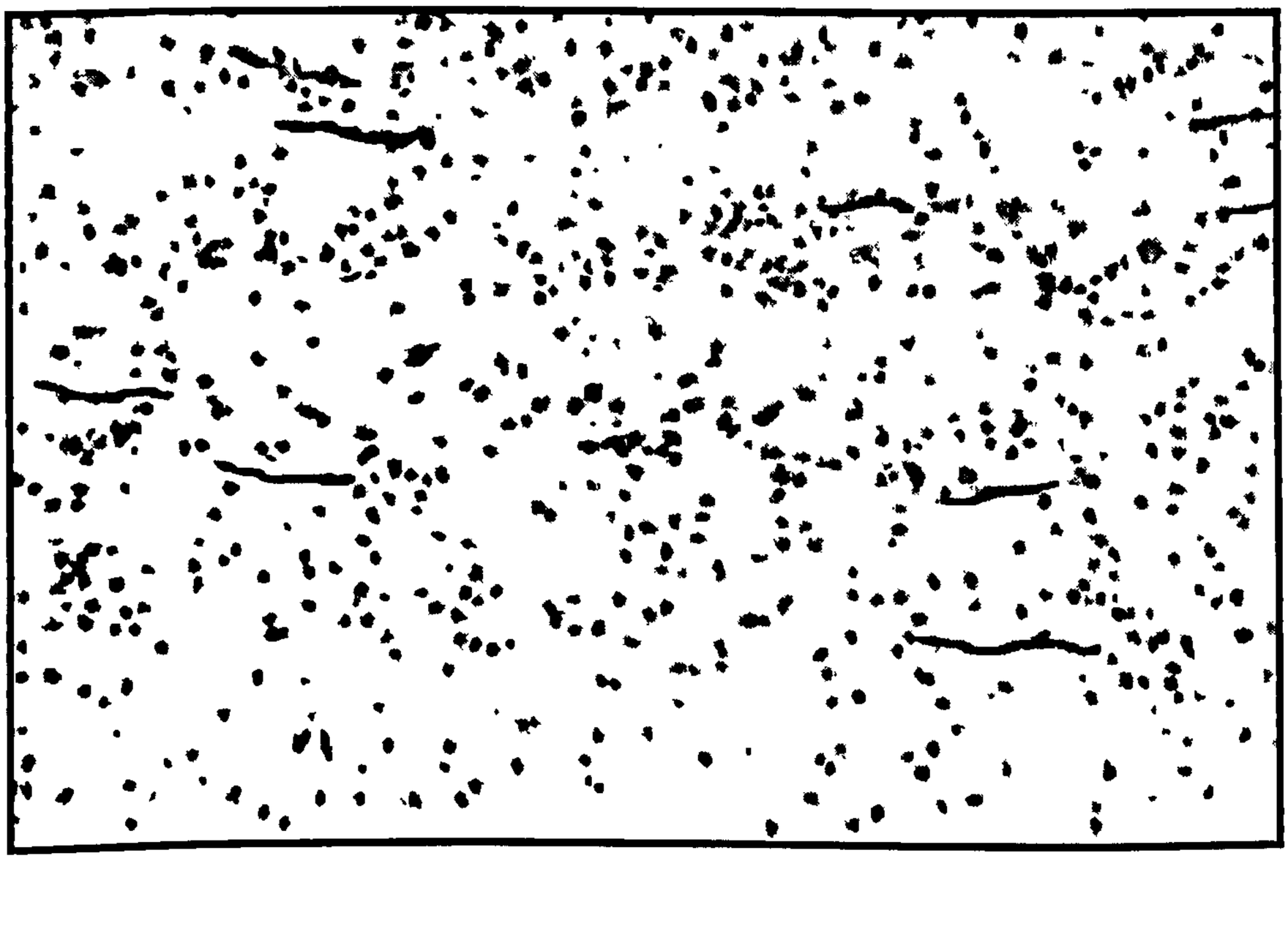

Figure 4.2 An image of the bed with displaced fluorescent particles (flow right to left).

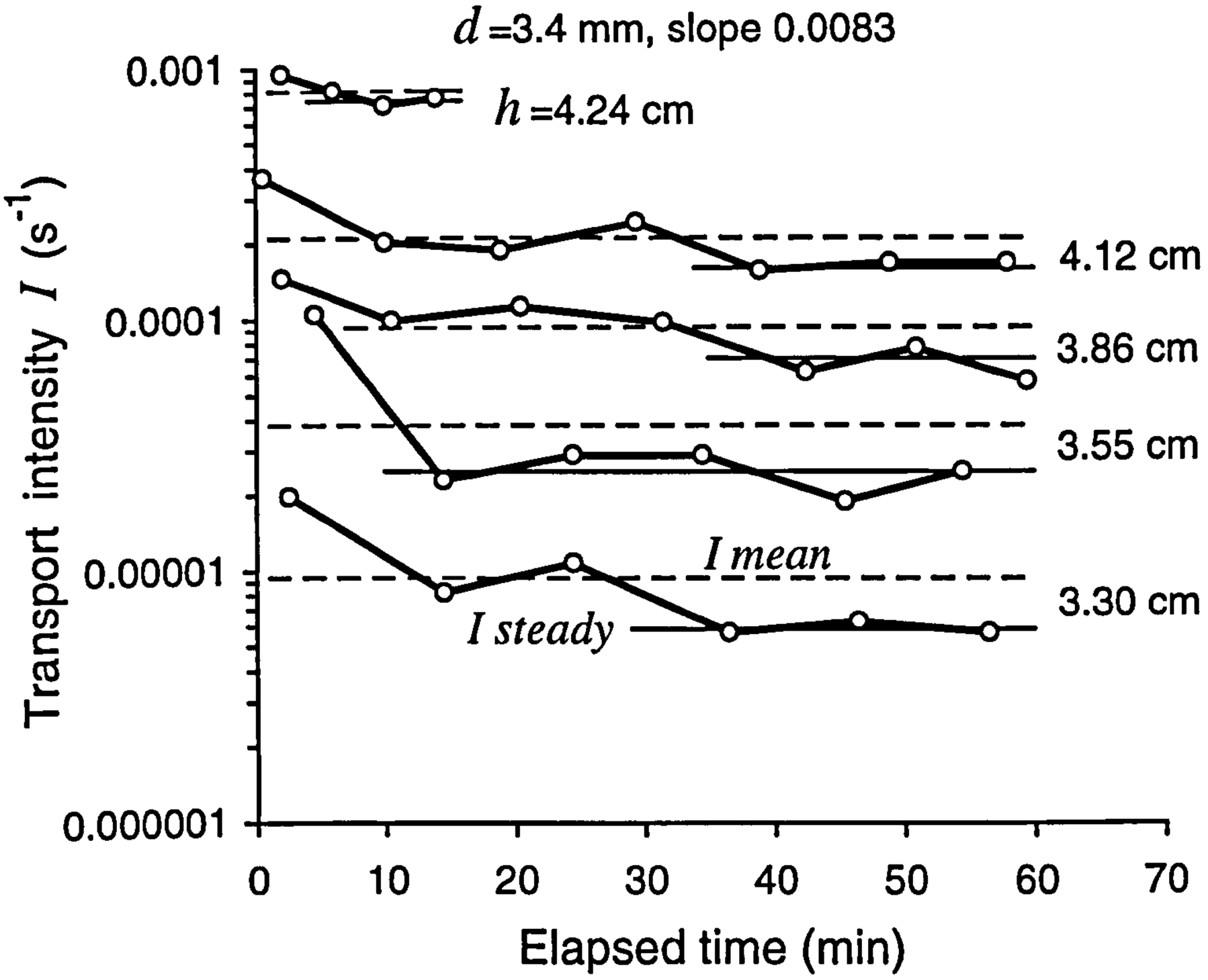

Figure 4.3 Change of transport intensity I with time.

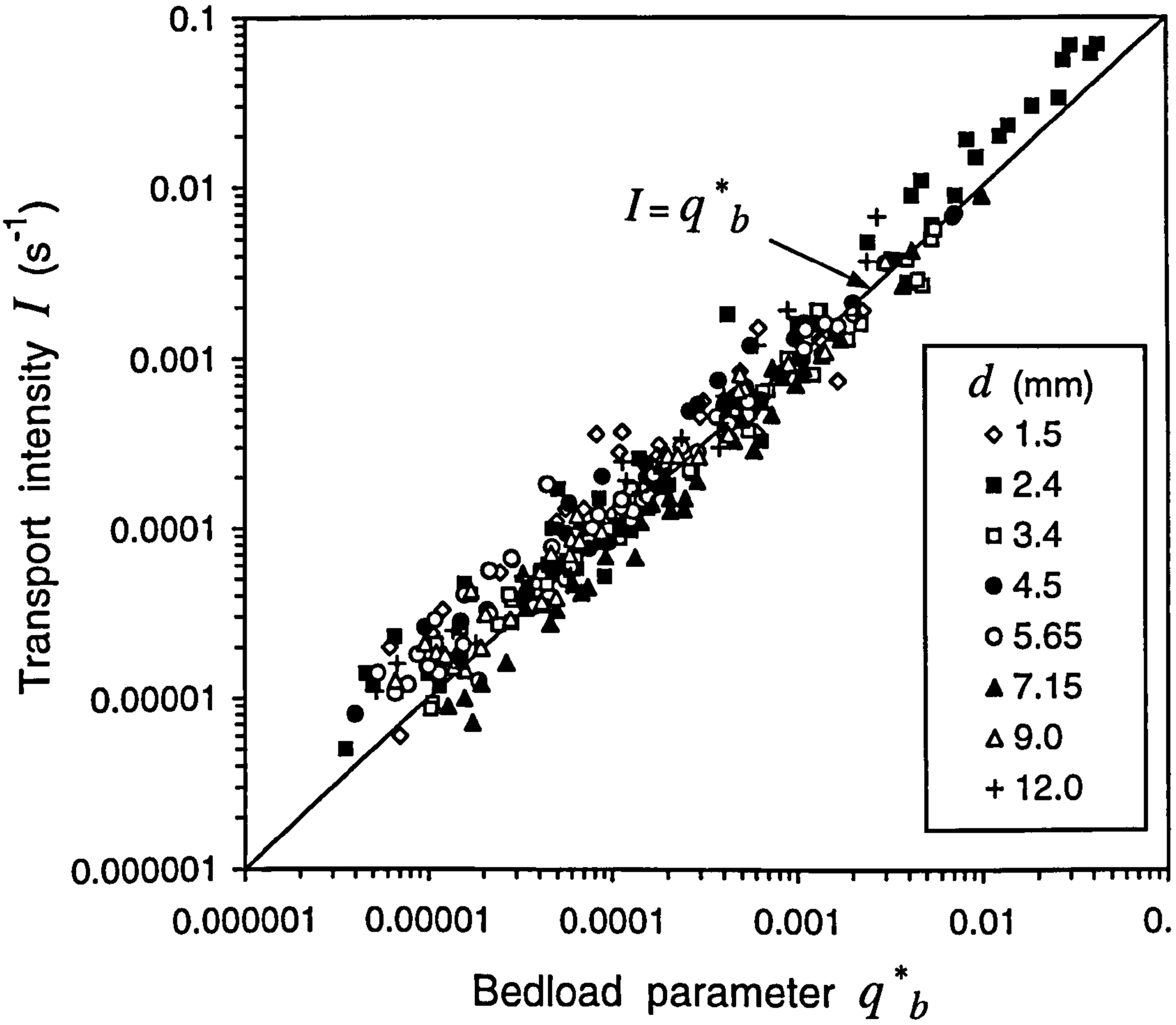

Figure 4.4 Relationship between transport intensity I and bedload parameter q^*_b.

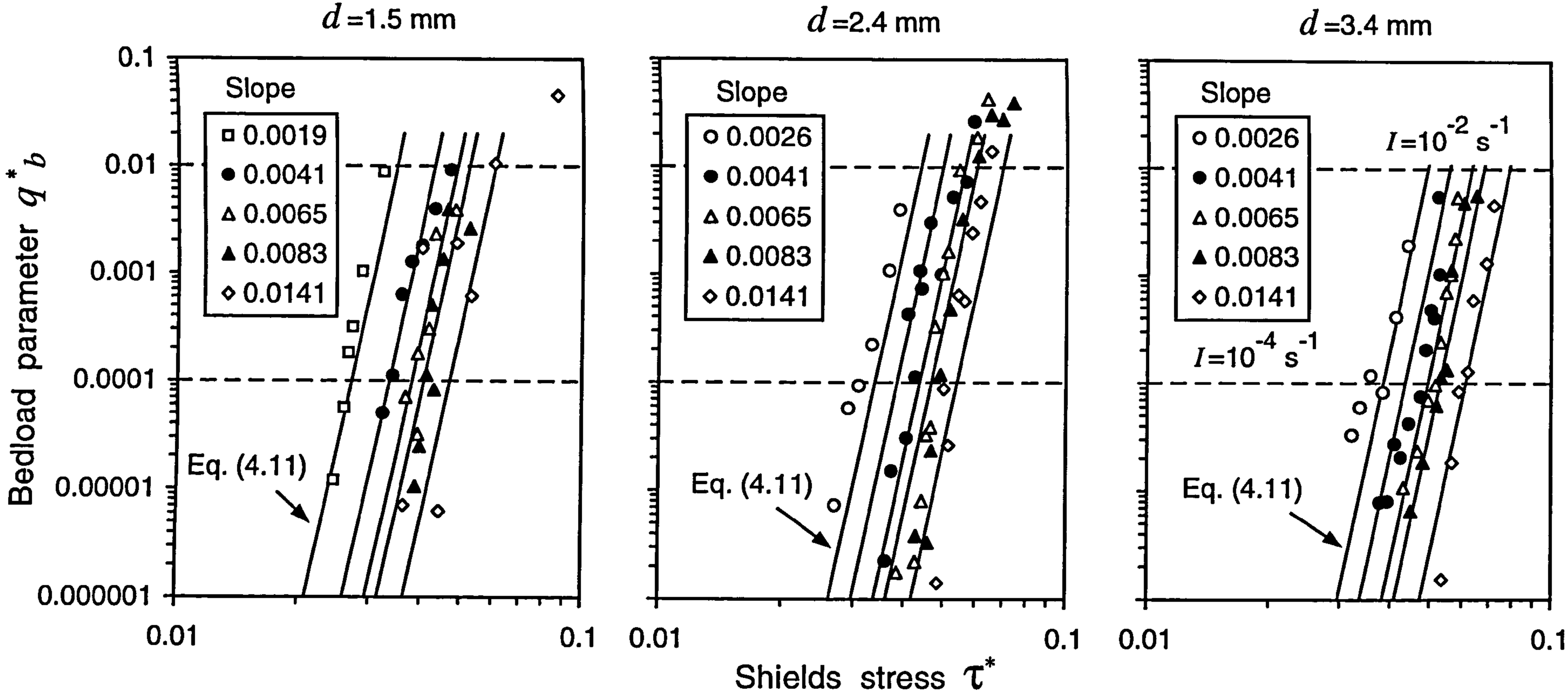

Figure 4.5 Plots of q^*_b versus τ^* for uniform sediments.

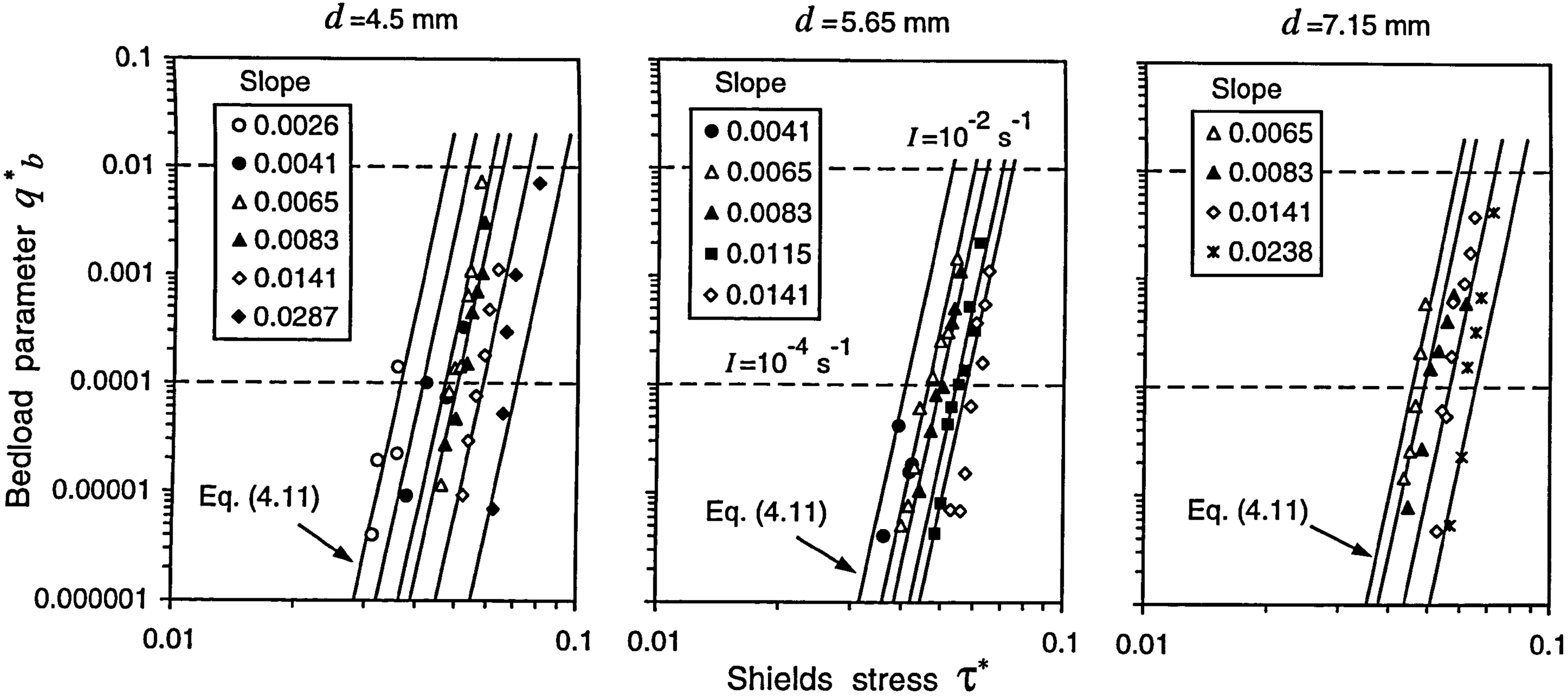

Figure 4.5 (continued).

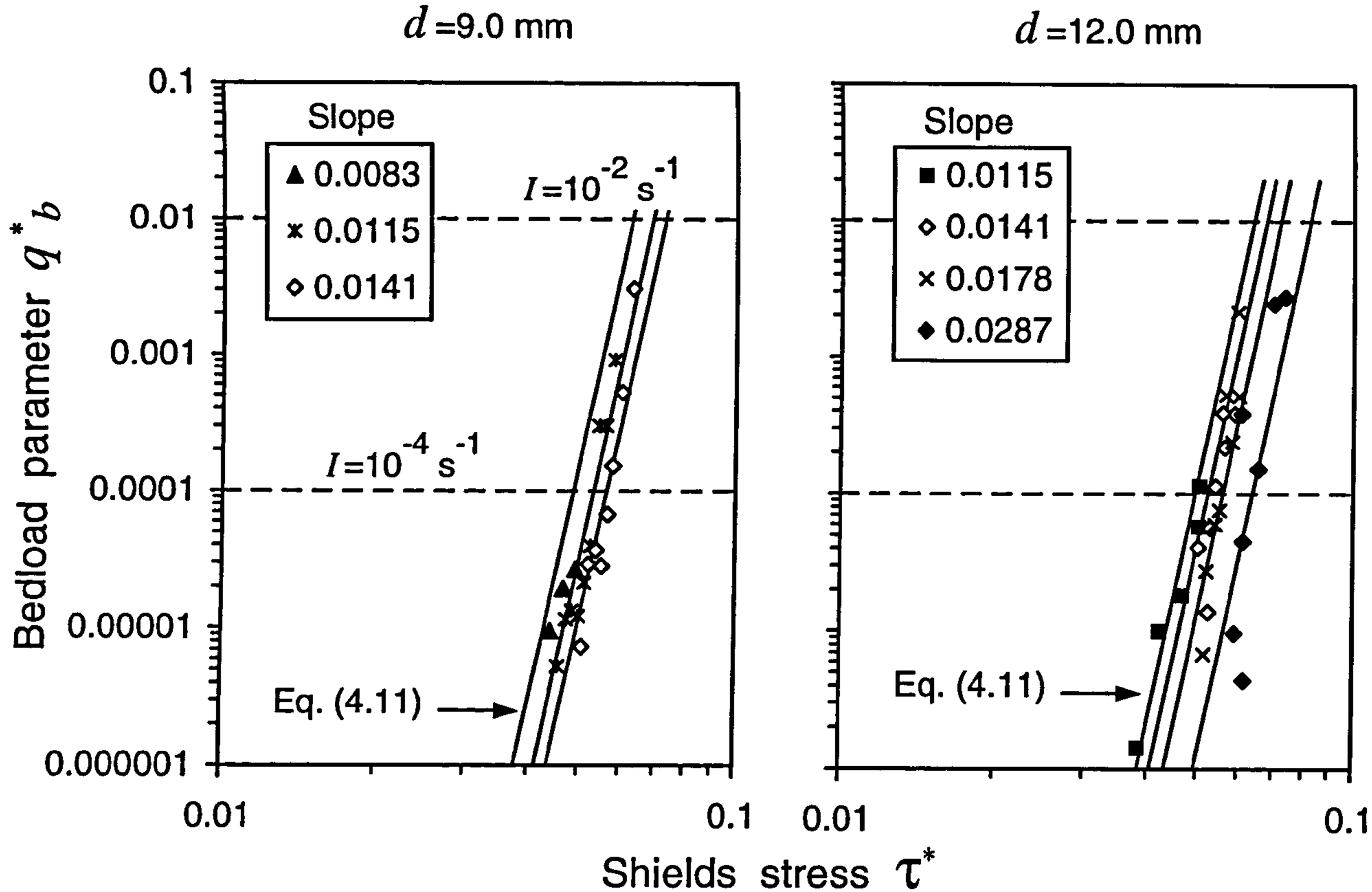

Figure 4.5 (continued).

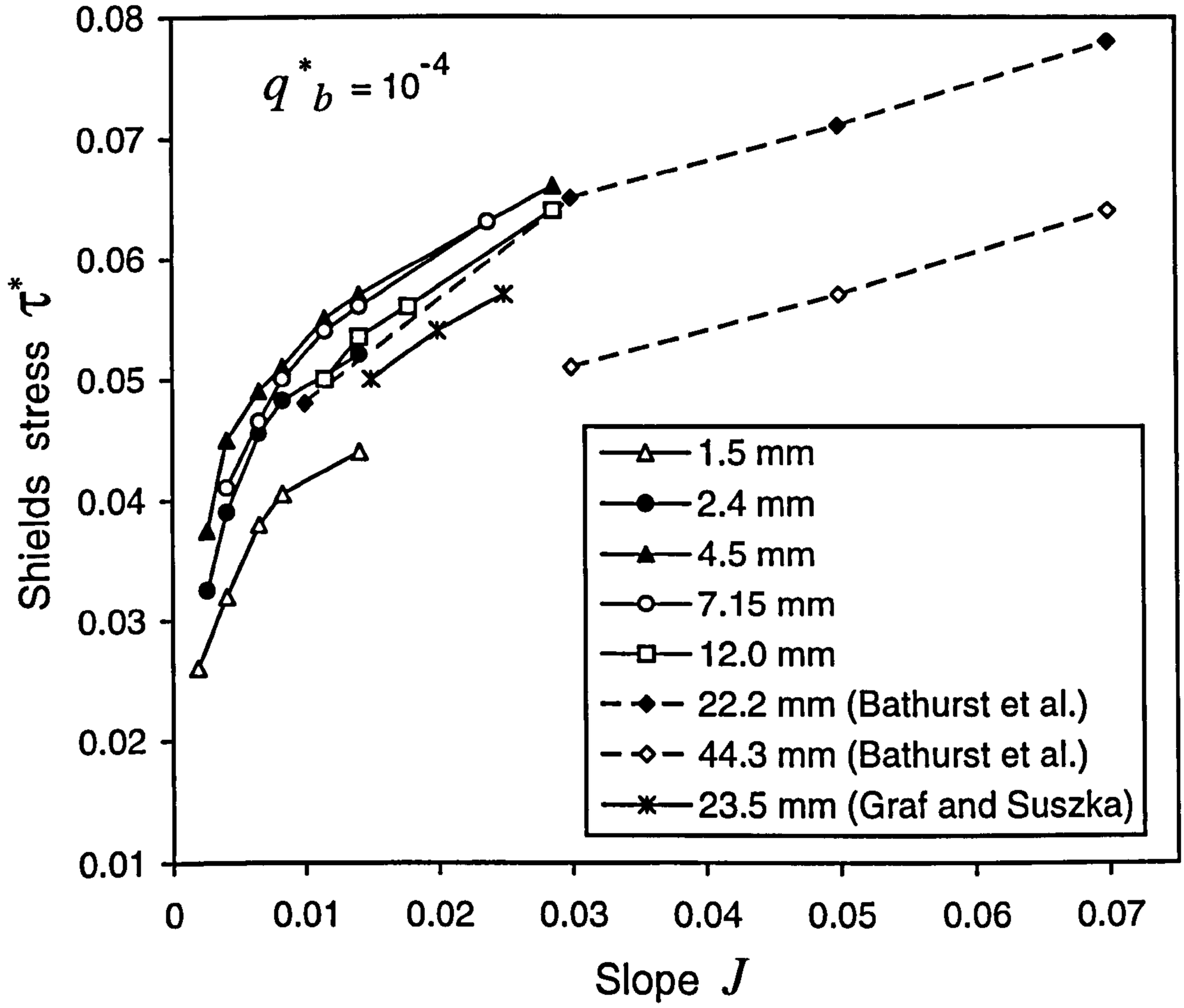

Figure 4.6 Shields stress τ^* (corresponding to $q^*_b = 10^{-4}$) as a function of slope J for different grain sizes.

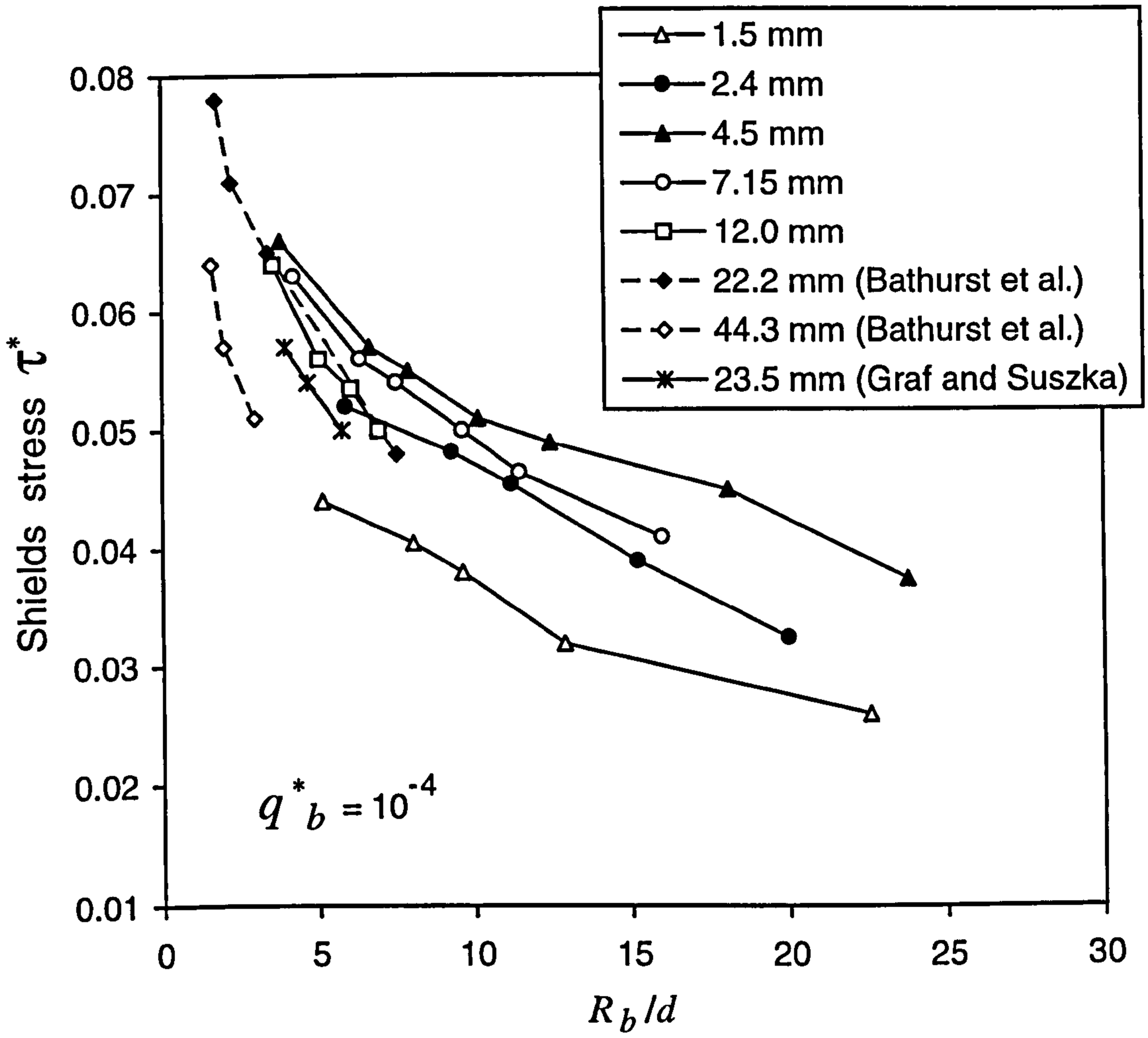

Figure 4.7 Shields stress τ^* as a function of R_b/d for different grain sizes ($q^*_b=10^{-4}$).

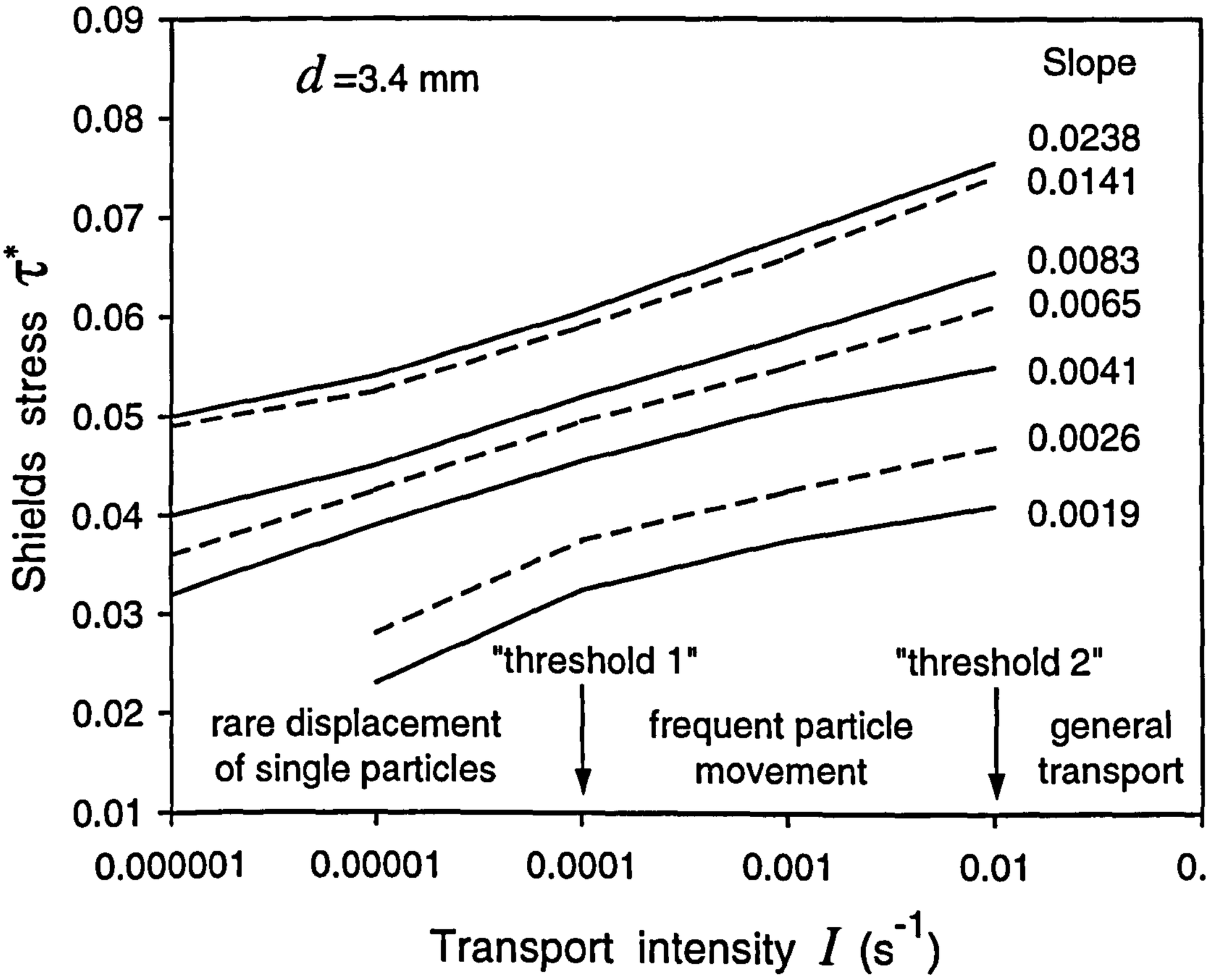

Figure 4.8 Shields stress τ^* versus transport intensity I.

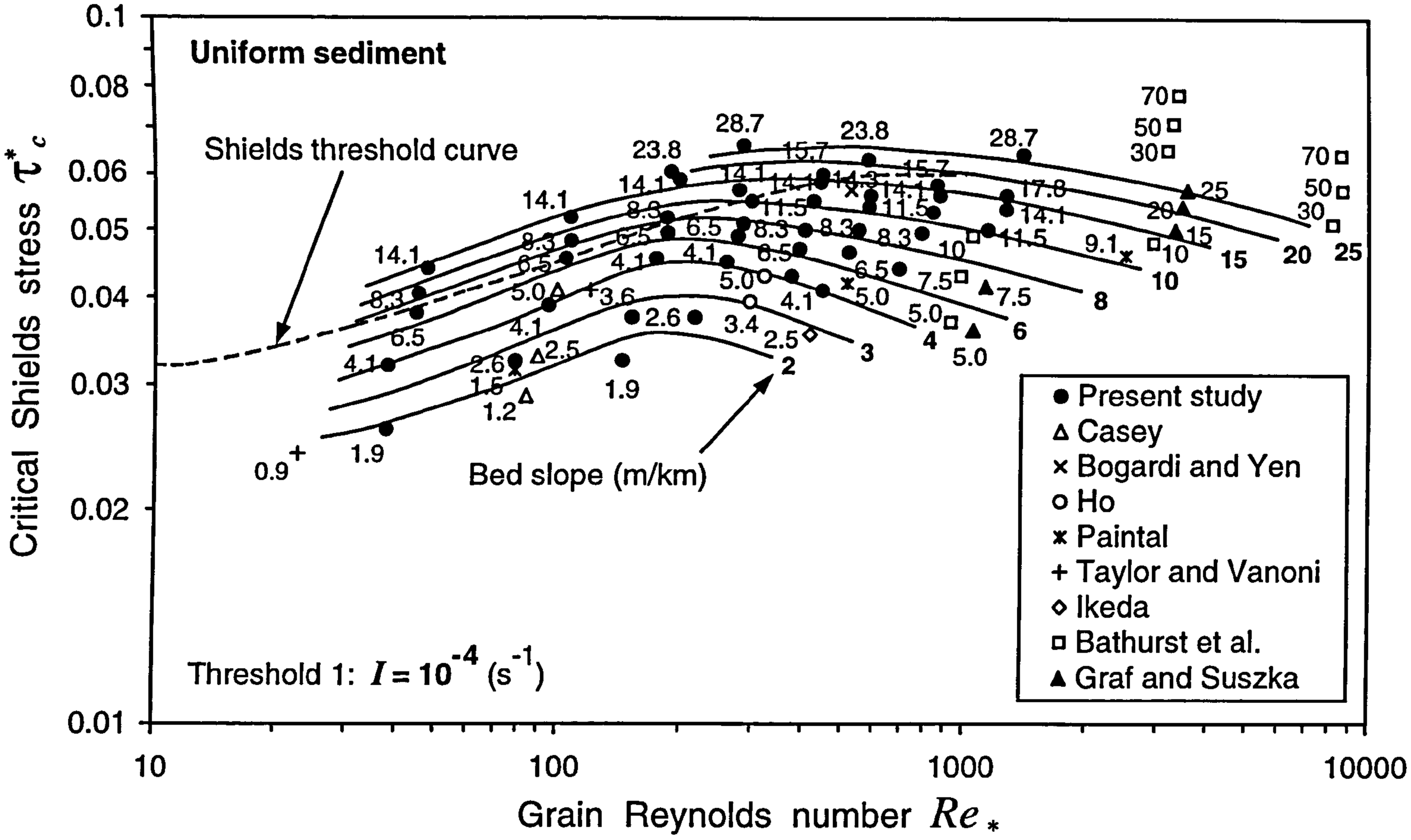

Figure 4.9 Critical Shields stress τ^*_c versus grain Reynolds number Re_* at different bed slopes for $I=10^{-4}$ s^{-1} ("weak" transport).

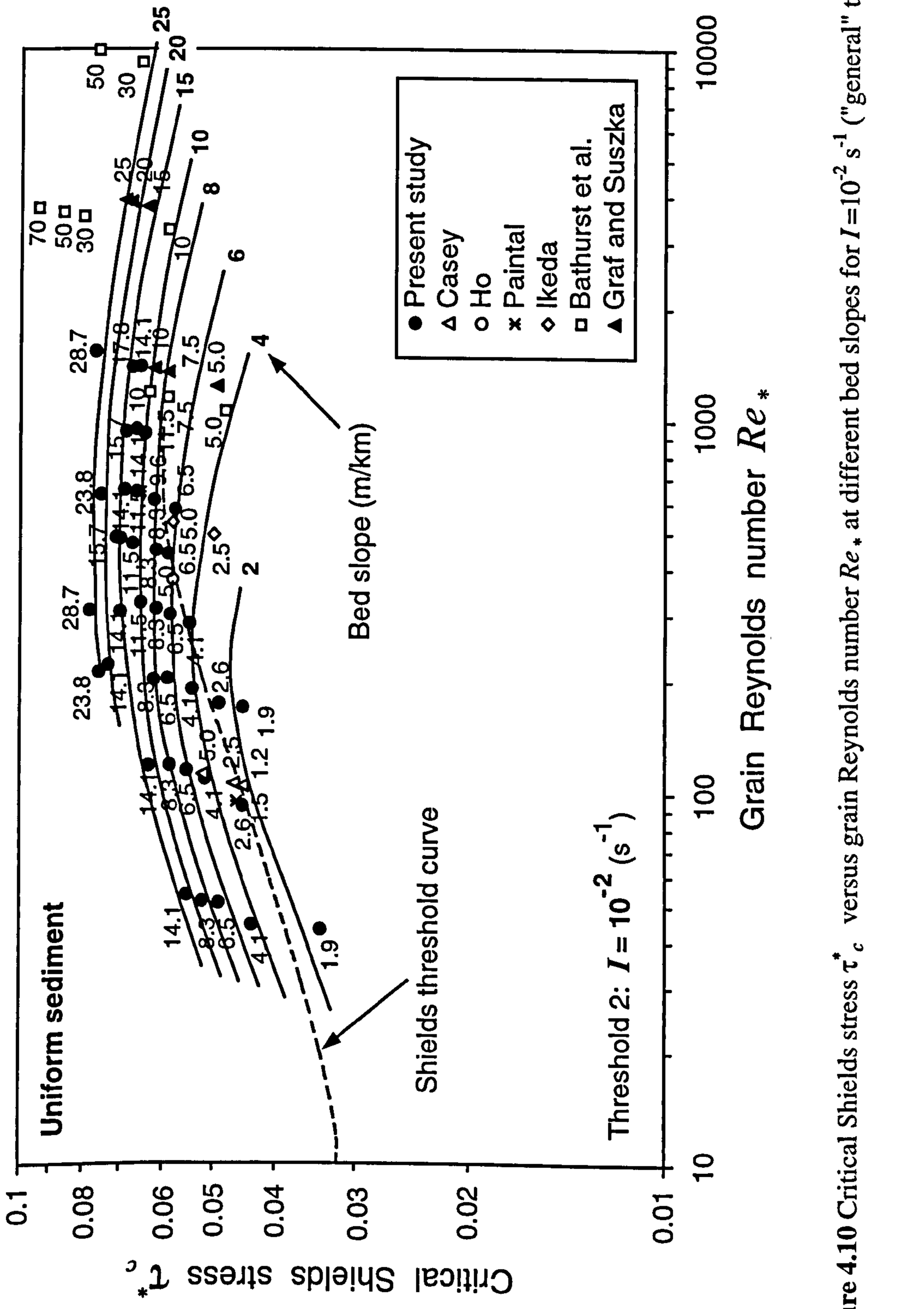

Figure 4.10 Critical Shields stress τ^*_c versus grain Reynolds number Re_* at different bed slopes for $I=10^{-2}$ s^{-1} ("general" transport).

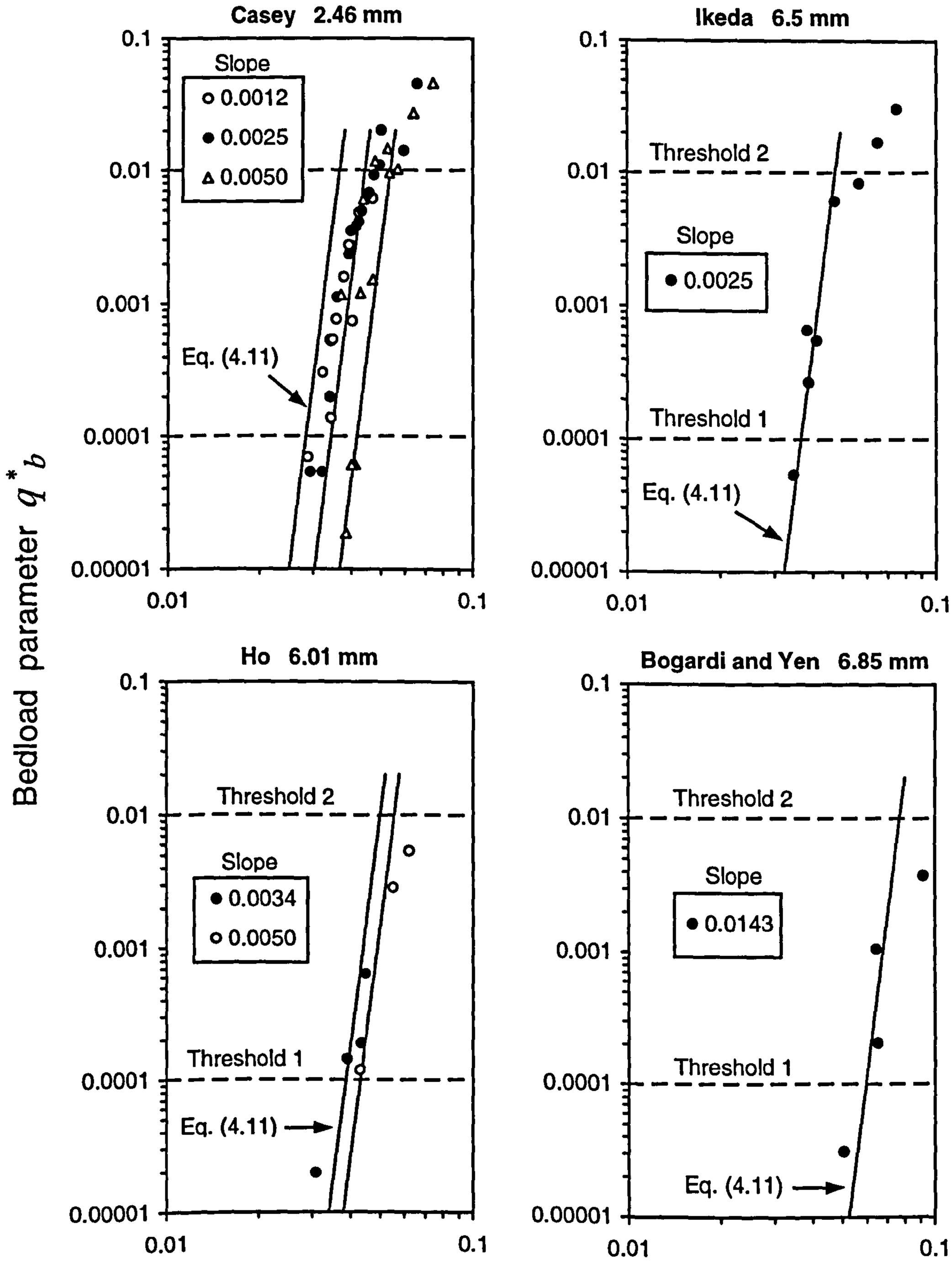

Figure 4.11 Bedload transport data for uniform sediments from other studies fitted by relationship (4.11).

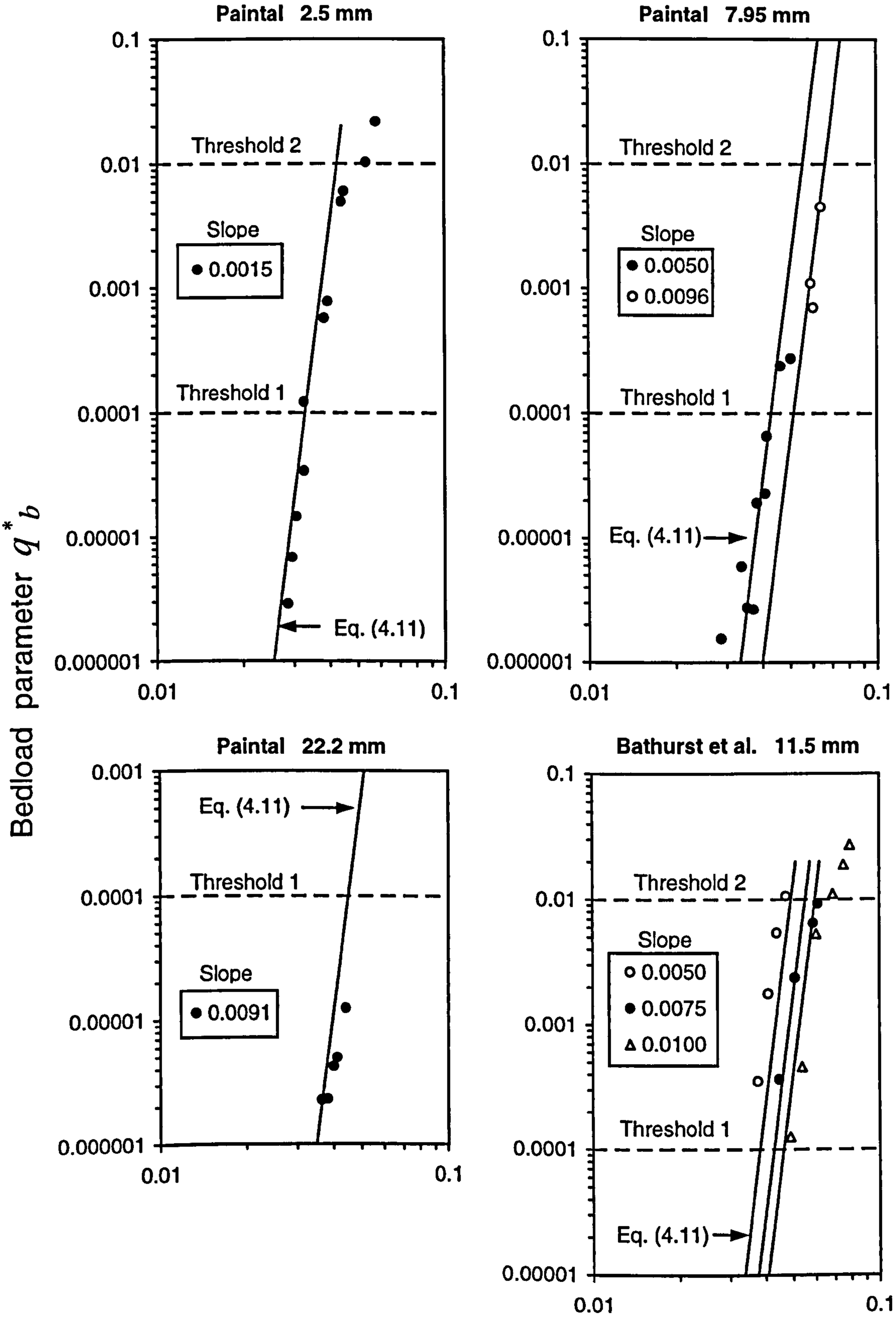

Figure 4.11 (continued).

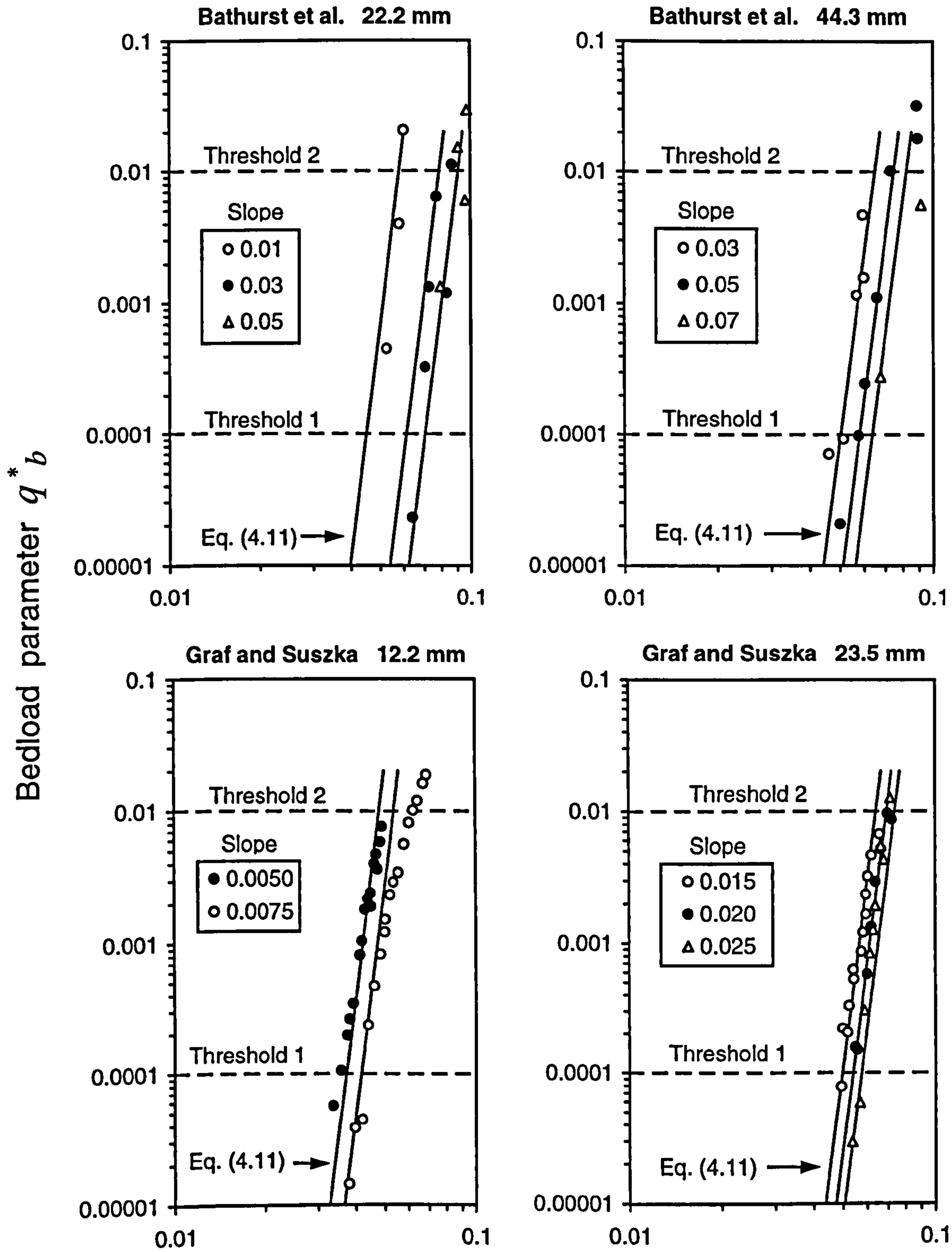

Figure 4.11 (continued).

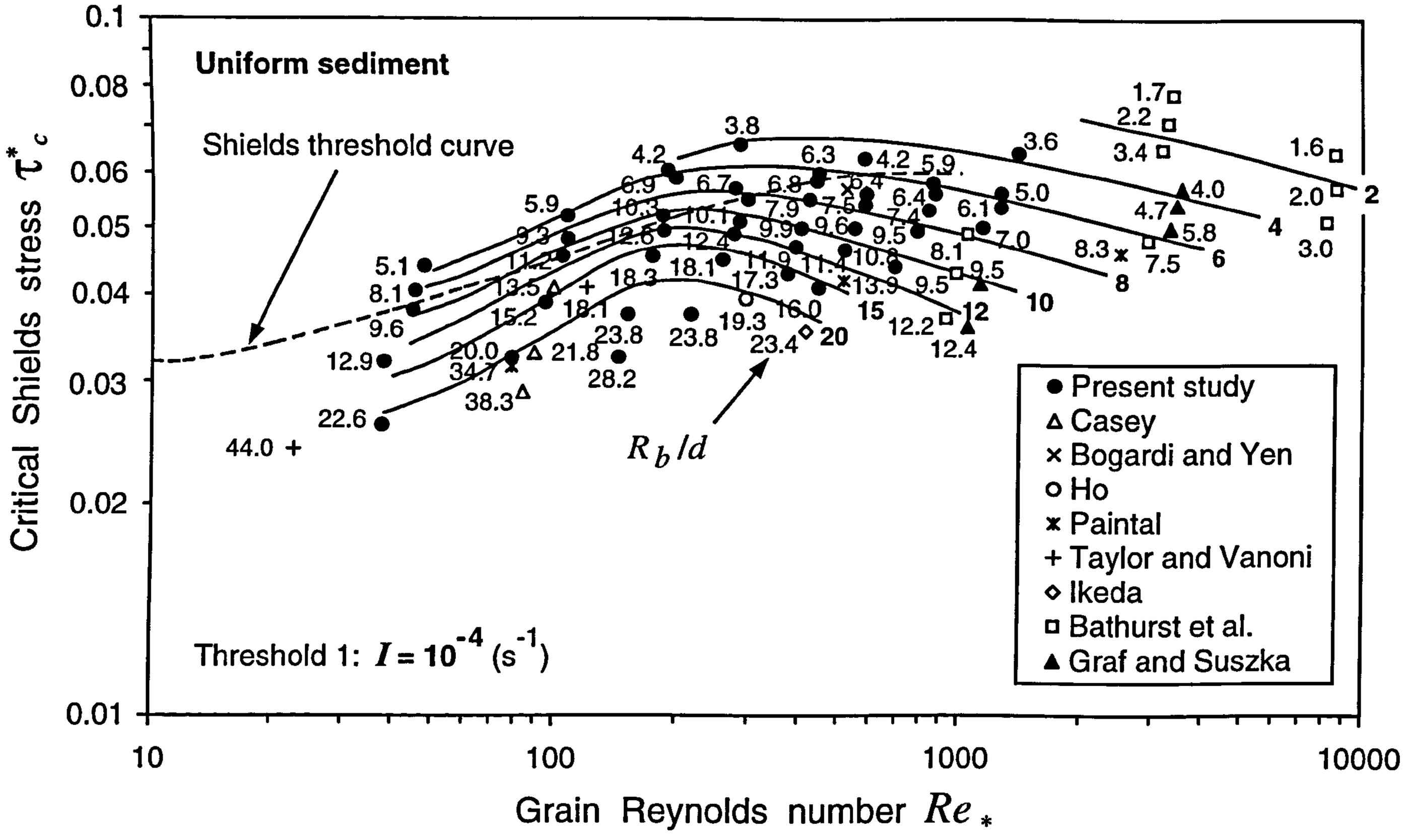

Figure 4.12 Critical Shields stress τ^*_c versus grain Reynolds number Re_* for different values of R_b/d corresponding to I=10^{-4} s^{-1}.

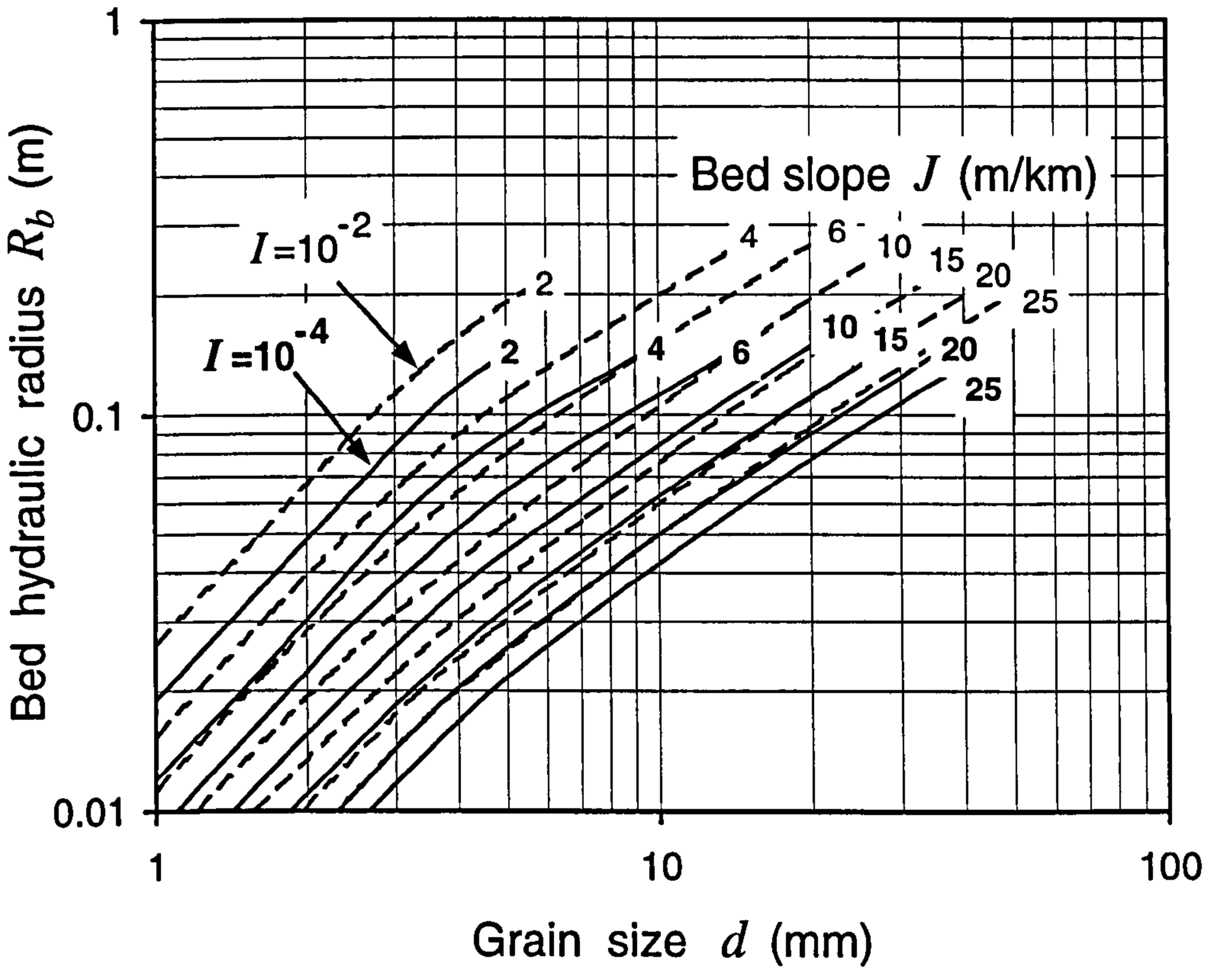

Figure 4.13 Relationship between critical flow characteristics (bed hydraulic radius R_b and bed slope J) and grain size d for two different "critical" values of intensity of sediment motion I.

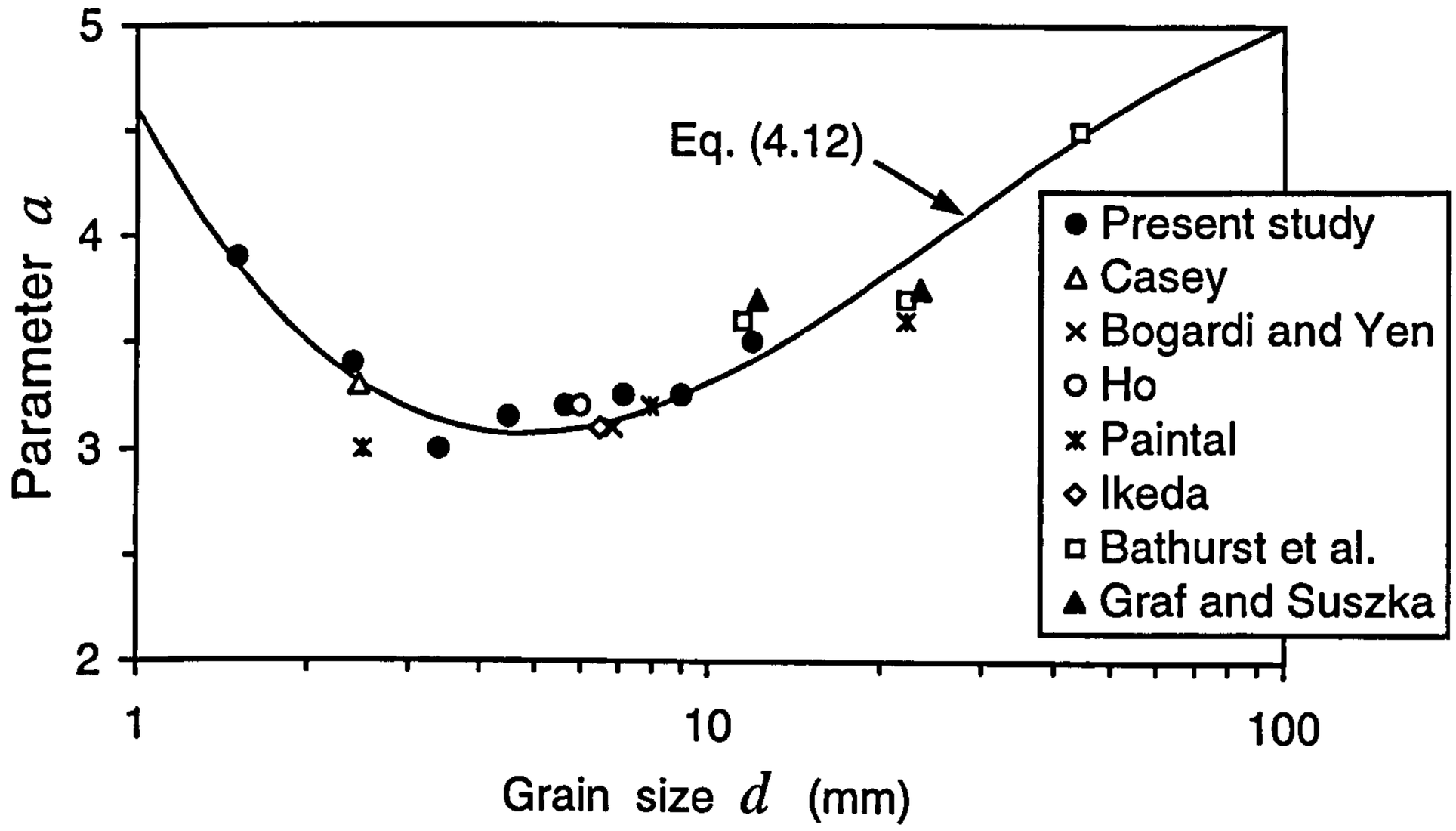

Figure 4.14 Variation of parameter a with grain size d.

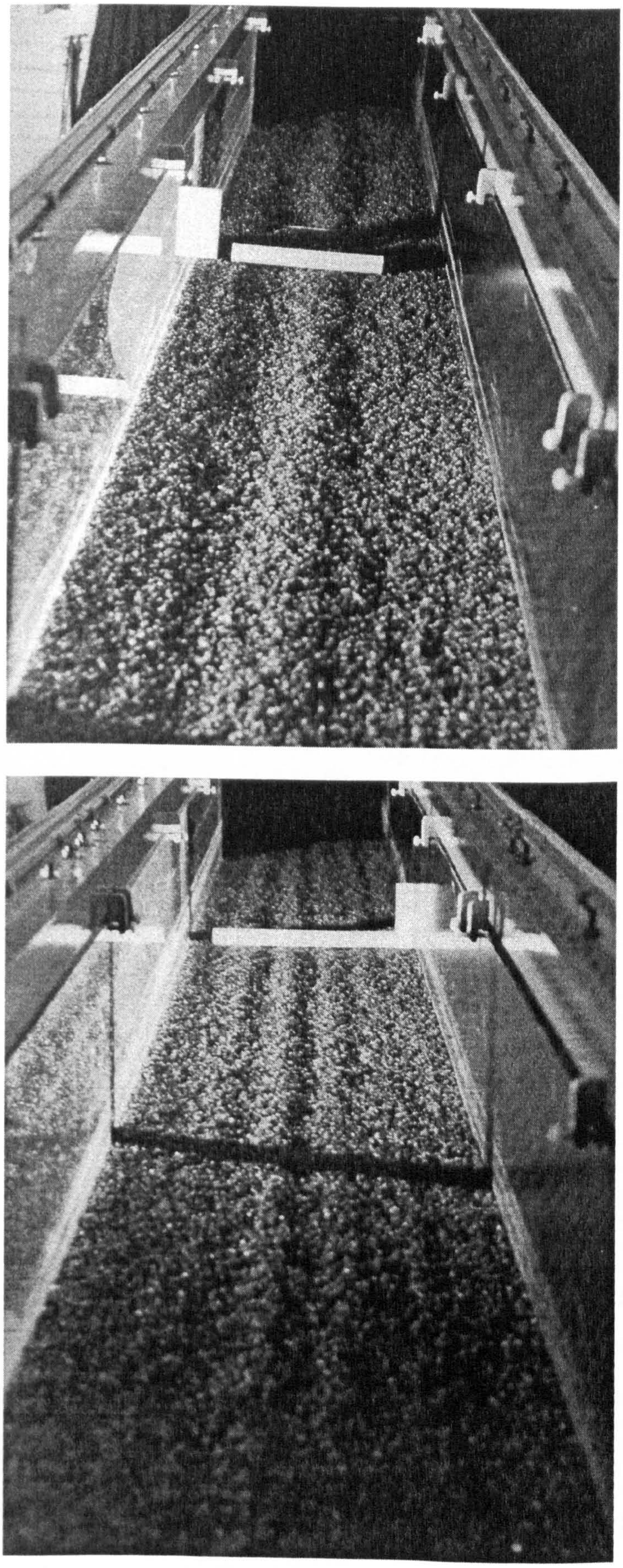

Figure 4.15 Longitudinal ridges and troughs developed in 2.4 mm sediment: (top) slope J=0.0041, depth h=0.0530 m; (bottom) J=0.0065, h=0.0305 m.

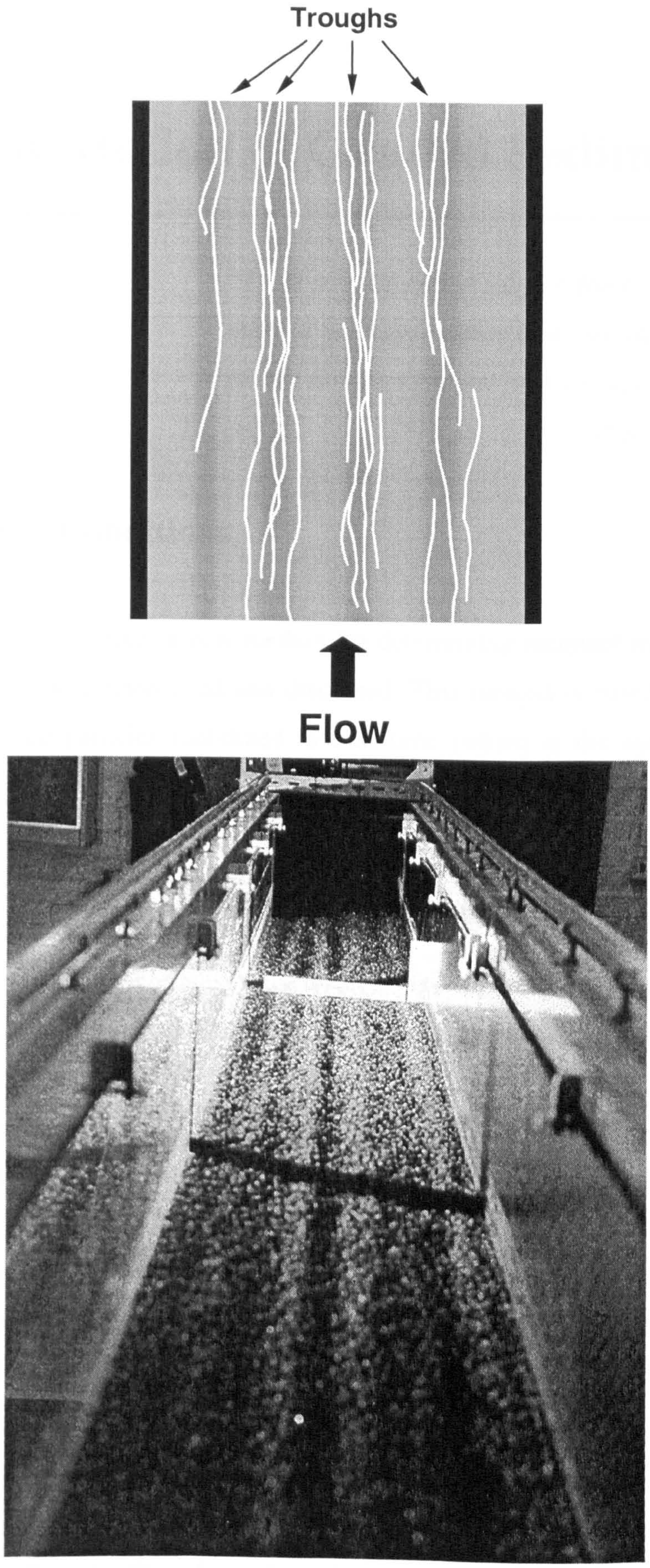

Figure 4.16 Paths of fluorescent bed particle motion (from photo taken with 10 s exposure) and longitudinal ridges/troughs in experiment with d=2.4 mm, J=0.0065, h=0.0354 m.

5

Incipient Motion of Graded Sediments

"I will treat of such a subject. But first of all, I shall make a few experiments and then demonstrate why bodies are forced to act in this manner."

(Leonardo da Vinci)

5.1 Threshold Conditions

In the previous chapter a new method for determining incipient motion of coarse uniform sediments was introduced and discussed. This method is based on measuring the fraction of bed particles mobilized in unit time (which is the equivalent of the probability of sediment entrainment) in relation to the applied shear stress. The "critical" state of the bed is estimated in terms of an admissible intensity (probability) of sediment motion. The appropriate flow conditions are called "critical" or "threshold" conditions.

Application of this probabilistic approach to beds composed of uniform sediments is relatively straightforward. However, in the case of graded sediments this approach requires estimating the active proportion of each size fraction in the sediment mixture, which is a rather difficult task. In principle, it can be done through painting the fractions in different colours and monitoring displacement of individual painted grains (e.g., Rakoczi 1987, Wilcock and McArdell 1993, 1997, Wilcock 1997a). However, this is very laborious and time consuming, given the wide range of sediment mixtures planned in this investigation. Fortunately, experiments with uniform sediments have revealed a linear relationship between the intensity of sediment motion I and the dimensionless bedload transport rate q_b^* (Figure 4.4). That is, the proposed probabilistic approach to the bed sediment entrainment actually reduces to the simple reference transport method, which is based on the use of bedload transport relations and which is readily applicable to mixed-size sediments. Therefore, the reference transport method is used here to define threshold conditions for each size fraction in graded sediments.

The reference transport method used here differs from those proposed by others (e.g., Ackers and White 1973, Parker et al. 1982) in that it relates the critical value of Shields stress for each size fraction

$$\tau_i^* = \frac{\tau}{g\,(\rho_s - \rho)\,d_i} = \frac{R_b\,J}{(s-1)\,d_i} \tag{5.1}$$

to the normalized Einstein bedload parameter

$$q_{bi}^* = \frac{q_{bi}}{f_i\,\rho_s\,\sqrt{(s-1)\,g\,d_i^{\,3}}} \tag{5.2}$$

where $\tau = \rho g R_b J$ is the bed shear stress, g is the gravitational acceleration, R_b is the hydraulic radius of the bed (corrected for the side-walls effect, see Section 4.3.2, Chapter 4), J is the slope, ρ_s is the sediment density, ρ is the fluid density, $s = \rho_s/\rho$ is the specific density, d_i is the mean size of fraction i, q_{bi} is the fractional transport rate computed as $p_i\,q_b$, q_b is the bedload transport rate per unit width (dry weight), p_i is the proportion of fraction i in the transport, and f_i is the proportion of fraction i in the bed surface. The critical Shields stress τ_{ci}^* is estimated as the stress corresponding to a reference transport rate chosen as representative of the threshold for motion of ith size fraction. To provide a flexible approach to defining the "critical" state of the streambed required for solving various engineering problems, the two different reference transport conditions used earlier for uniform sediments are considered here: (a) $q_{bi}^* = 10^{-4}$ ("threshold 1") and (b) $q_{bi}^* = 10^{-2}$ ("threshold 2"). These values of q_{bi}^* are the equivalent of fractional transport intensities (or fractional entrainment probabilities) of $I = 10^{-4}$ s^{-1} and $I = 10^{-2}$ s^{-1}, respectively (see Figure 4.4). As mentioned in Chapter 4, the value of $q_{bi}^* = 10^{-4}$ is close to the practical lower limit of measurable sediment transport rate and corresponds to the Kramer's (1935) definition of "weak" sediment transport, while the value of $q_{bi}^* = 10^{-2}$ corresponds to the Kramer's (1935) "general movement" on the bed.

There are several reasons for using the Einstein bedload parameter (5.2) as a reference transport criterion. Firstly, it is widely used in sediment transport formulas. Secondly, at low values of τ_i^*, plots of q_{bi}^* versus τ_i^* tend to be very steep, unlike, for example, Parker et al. (1982) bedload parameter $W_i^* = q_{bi}^* / \tau_i^{*3/2}$. This results the determined values of τ_{ci}^* being less sensitive to the accuracy of sediment transport measurements. Finally, the Einstein bedload parameter can be readily interpreted in terms of the proportion of mobilized particles relative to immobile particles in the bed surface, or, in other words, the probability of bed particle entrainment (Figure 4.4).

5.2 Experimental Procedures

5.2.1 Armfield flume

A major part of the experiments with the sediment mixtures designated N-1, N-2, N-3, F, C, and B (see Table 3.2, Figures 3.15 and 3.16) was conducted in the Armfield flume. The experimental procedures for the graded sediments were in general similar to those used for uniform sediments, but without direct measuring of the intensity of sediment motion as reference transport method was used to estimate threshold conditions. In addition, based on the experience from the previous tests with uniform sediments, bedload sampling during near-to-threshold flow conditions was started about 15-25 min after the uniform flow was established. At this time any artificial features arising from the screeding of the laid bed were judged to have dissipated, and the transport rate diminished from its initial peak value and approached a steady value corresponding to water worked bed conditions.

The experiments included measurements of bed slope, water discharge, flow depth, cumulative bedload transport rate, and water/air temperature. The bedload accumulated in the sediment trap was subsequently dried, weighed, and sieved to obtain the time-averaged bedload transport rate for the duration of the measurements and cumulative bedload grading. In addition, areal samples of the bed surface material were taken at different parts of the flume before and after each experiment. The bed surface samples were taken by removing a top layer material of about one centimetre thick using a thin metal plate. Care was taken to cause minimum disruption of the bed structure during the sampling procedure. The bed surface samples were then sieved to

estimate the change of the bed surface composition during the experiments. The analysis of the surface samples showed that the initial and final bed surface size distributions were practically the same for all experiments and these were also not appreciably different from the corresponding bulk-mix distributions. Thus, there was no influence of vertical sorting on sediment transport during the experiments.

The experiments were conducted at several of the flume slopes used in the tests with uniform sediments (0.0041-0.0141). Water discharge varied from 3.0 to 30.4 L s^{-1}. The duration of the experiments varied from a few minutes to 3.3 hours, depending on sediment transport rate, usually about 1-1.5 hours. As before, sediments were not re-circulated or fed into the flume during the experiments because of the generally very low sediment transport rates and relatively short duration of the experiments. After each experiment the top few centimetres of the bed were removed and replaced with newly mixed material.

A total of 130 experiments (112 hours) with graded sediments were completed in the Armfield flume. The range of hydraulic conditions and sediment transport rates observed in the experiments is given in Table 5.1. All the measured hydraulic and transport data are given in Table B.1 (Appendix B). The bedload gradings and compositions of the final bed surface are given in Tables B.2 and B.3 (Appendix B), respectively.

5.2.2 HR Wallingford flume

Supplementary experiments with the widely graded mixture designated HR (Table 3.2, Figures 3.15 and 3.16) were undertaken in the HR Wallingford flume. The pre-experimental arrangements were similar to that used in the Armfield flume. This included preparation of a flat bed, slow flooding of the bed from the downstream end of the flume, and gradual increase of water discharge until it reached an experimental value. The measured characteristics were the bed slope, water discharge, flow depth, surface flow velocity (by floats), bedload transport rate, and bedload composition.

During the experiments, a series of consecutive bedload samples were taken. Sampling time decreased with transport rate, ranging from 60 to 2 minutes. After measurement of the volume of each bedload sample (which gave mean transport rate during sampling interval), all the bedload was returned to the flow at the flume inlet. Thus, in this experiments a manual re-circulation of sediment transported was provided. Only one sample for each experiment was extracted for subsequent sieving analysis.

After each experiment the top few centimetres of the bed material were removed and new sediment added and levelled.

The experiments were conducted at a bed slope of 0.0045 and for a variety of flows with different degrees of bed mobility. The duration of the experiments varied from a few minutes to 5.4 hours. In spite of the wide grain size distribution of the mix HR, all the sediment sizes found in the bed were transported as bedload.

Altogether 12 experiments with a total duration of 20 hours were performed in HR Wallingford flume. A summary of the experimental conditions is given in Table 5.1. All the measured hydraulic and transport data, and bedload gradings are presented in Tables C.1 and C.2 (Appendix C).

5.3 Additional data

The present analysis is based on both experimental results collected as part of this study and data from previous investigations. The primary requirement used to select the additional data examined here is that the fractional transport rates were measured over a wide range of bed mobility, including very low transport rates near to incipient motion. Additionally, the data should cover a range of bed material gradings and median sediment size. Given the established effect of bed slope on incipient motion of uniform sediments (Chapter 4), a further requirement is that the fractional transport data were collected at the same bed slope (at least near incipient motion). Unfortunately, most of the published laboratory data for graded sediments were measured at significantly different slopes and presented together in an attempt to obtain a unique relationship between fractional transport rates and different flow characteristics. This significantly limits the usefulness of most of the existing sets of flume data. Although bedload transport in natural streams is measured with a much lower accuracy compared to the controlled conditions of the flume experiments, the field data are free from the effect of changing bed slope.

Only a few studies of graded sediment transport provide the required information. The nine sources of flume and field data chosen for this study include Day (1980), Misri et al. (1984), Wilcock and Southard (1988), Patel and Ranga Raju (1996), Parker and Klingeman (1982), Pozdnyakov (1987), Kuhnle (1992), Andrews (1994), and Wathen et al. (1995). Summaries of bed material characteristics and ranges in hydraulic conditions

and transport rates are given in Tables 5.2 and 5.3, respectively. Cumulative grain size distributions for all the bed materials are compared in Figure 5.1. The data were collected using different operational and measurement procedures, and differ in accuracy and reliability, but all refer to the transport of coarse sand and gravel mixtures on a reasonably flat bed by steady, uniform flow. The following is a brief discussion of the sources of the additional data chosen for the analysis.

5.3.1 Flume data

Day (1980) studied fractional transport of two weakly bimodal graded sediments made up of a natural mixture obtained from a local gravel pit. The study was undertaken in the same 18 m long by 2.46 m wide HR Wallingford tilting flume as was used in the part of the work presented in this thesis. The thickness of the sediment bed in the flume was 10-20 cm. The individual experiments were conducted at a constant water discharge and a variety of bed slopes, which allowed different transport rates to be observed. The experiments consisted of measurements of sediment transport rate, water discharge, water surface elevation, and flow depth. The bedload transported was re-circulated using a sediment return pumping system. The sediment load was measured as it re-entered the main channel through a set of nozzles at the upstream end of the flume. Although this method of sampling could introduce systematic errors, particularly as the rates of size fraction transport must differ between the main flume channel and the return system piping (32 mm diameter), it was chosen for economic reasons. Sampling suspended load via Pitot tubes indicated that even at higher transport rates the amount of suspended material was very small and its contribution to the total load was ignored. All bedload samples were taken not less than two hours after the beginning of the experiments. After each experiment the top few centimetres of the bed material was removed and replaced by fresh material so that the new experiment would not be affected by vertical sorting. As bedload was measured at different slopes, only data collected during series A experiments for fractions with median size 1.55-8.69 mm could be used for the present analysis (near-to-threshold transport rates of these fractions were measured at slopes around ~0.0010). These data presented in tabular form are used here to obtain q_{bi}^* versus τ_i^* fractional bedload relations.

Misri et al. (1984) undertook flume experiments involving measurements of the bedload transport rates of different fractions in various sediments. The experiments were carried out in a tilting flume having a length of 16.0 m, width of 0.75 m, and a

depth of 0.48 m. The sediments investigated were composed of natural sand and gravel and had different gradations. A sediment trap at the downstream end of the flume was used to collect the transported sediment. The same material was continuously fed back manually at the upstream end of the flume at a constant rate to maintain sediment equilibrium. The effective bed shear stress was defined using the hydraulic radius of the bed computed from the Manning-Strickler equation. The transport data obtained for sediment mixture N2 are presented graphically as plots of normalized Einstein bedload parameter q_{bi}^* versus Shields stress τ_i^* for a number of fractions ranging from 0.71 mm to 17.89 mm (Misri et al 1984, their Fig. 6). These data were collected for a rather narrow range of slopes (0.0038-0.0048), which allowed them to be analysed according to the present method.

Wilcock and Southard (1988) studied incipient motion of different mixed-size sediments in a 23 m long, 0.6 m wide, and 0.3 m deep tilting flume. The thickness of the sediment bed in the flume was 7 cm. The experiments consisted of measurements of a standard set of variables including water discharge, flow depth, water surface slope, and sediment transport. Uniform flow during the experiments was maintained by adjusting the flume slope. All the transported sediment fell into a trap at the downstream end of the flume and was returned, with a small discharge of water, to the head of the channel through a 2.5 cm tube using an air-driven pump. Sediment transport was sampled by passing the water-sediment mixture in the sediment return system through a sieve that trapped the sediment. Total bed shear stress was computed using the sidewall correction procedure of Vanoni and Brooks (Vanoni et al. 1971). Because bed forms were present in many runs, an estimate of the skin friction part of the total bed shear stress was also made. Fractional transport rates for MIT 1ϕ sediment mixture are presented graphically in Wilcock and Southard (1988) in their Fig. 4 in terms of the Parker et al. (1982) bedload parameter $W_i^* = q_{bi}^* / \tau_i^{*3/2}$ versus Shields stress τ_i^*. The experiments with the MIT 1ϕ sediment were conducted at different slopes, but near-to-threshold transport for all size fractions ranging from 0.77 mm to 6.17 mm was observed at slopes of about 0.0011.

Patel and Ranga Raju (1996) studied fractional bedload transport rates for five different unimodal sediment mixtures in a 12 m long, 0.40 m wide, and 0.52 m deep titling flume. The sediments were mixed from natural sand and gravel, and ranged in size from 0.60 mm to 40.00 mm. The thickness of the sediment bed in the flume was

about 7.5 cm. During the experiments re-circulation of sediment was provided by manually feeding back the sediment collected in a trap located at the downstream end of the flume. When equilibrium conditions were achieved, three bedload samples, each collected for a duration of 2 minutes to 10 minutes depending upon the sediment discharge, were taken. These samples were then dried, weighed and sieved to get the transport rates of individual fractions in a sediment mixture. The experiments were conducted at different slopes and a variety of water discharges. No bed features were observed in any of the runs. Bed shear stress was calculated in the same manner as in Misri et al. (1984). The composition of the sediment bed surface was measured before and after each run by pouring molten wax on the bed surface within a wooden frame. The analysis of the surface samples showed that the composition of the bed surface did not change noticeably during the runs and was the same as of the bulk bed material. The experimental q_{bi}^* versus τ_i^* relations obtained for 0.67-11.18 mm size fractions in mixture M3 are presented in Fig. 3 of Patel and Ranga Raju (1996). As these were measured at a narrow range of slopes of 0.0044-0.0056 (see Patel and Ranga Raju 1999), they are used for the present analysis.

5.3.2 Field data

Parker and Klingeman (1982) utilized bedload transport data collected in Oak Creek, Oregon, U.S.A. by Milhous (1973). Oak Creek is a small, steep, gravel-bottomed stream with the width of bed gravel of about 3.66 m. Bedload measurements were accomplished by means of a vortex tube extractor extending the full width of the channel. The comprehensive information concerning both bed material and bedload size distributions, the use of a measuring technique which avoids most of the efficiency problems associated with samplers, and the small scale and simple, flume-like geometry of Oak Creek, render the data collected by Milhous of special value. The 22 measurements made during the winter of 1971 appeared to correspond to conditions at which the pavement was "mobile", i.e., sizes common in the pavement were present in the bedload. These measurements were plotted as fractional bedload relations in terms of the Parker bedload parameter W_i^* based on pavement content versus Shields stress τ_i^* for the ten coarsest size fractions ranging from 0.89 to 89 mm (Parker and Klingeman 1982, their Fig. 2b). Both W_i^* and τ_i^* were calculated using the hydraulic radius. The W_i^* versus τ_i^* relationships are well defined, with the fractional transport

rates for particles coarser than about 7 mm close to the threshold chosen in the present study ($q_{bi}^{*} = 10^{-4}$).

Pozdnyakov (1987) measured bedload transport and associated flow characteristics in the gravel-bed Ala-archa River, Kirgizia, during 1985-1986. The measurements during the summer of 1985 were made using a multi-sectional bedload mesh sampler mounted on a metal rod. The sampler was 0.26 m wide and was composed of a vertical set of four metal frames with attached mesh bags for sampling bedload coarser than 5 mm at different layers of the flow (0.0-0.20 m, 0.20-0.35 m, 0.35-0.45 m, and 0.45-0.49 m above the bed). Such design of the sampler allowed not only measurement of transport rates and bedload composition, but also determination of saltation height of different size fractions. The measurements showed that between 80% and 100% of bedload was transported within 0.0-0.20 m active layer above the bed surface. The measurements during the summer of 1986 were made by means of an "extended" bedload sampler, which was a modification of the multi-sectional sampler. A total of 43 sets of tabular data on bedload transport and associated hydraulic characteristics are available. These data are used to obtain q_{bi}^{*} versus τ_i^{*} fractional bedload relations. Here τ_i^{*} corresponds to grain roughness and is defined using hydraulic radius of the bed R_b computed from the Manning formula $U = R_b^{2/3} J^{1/2} / n_g$ with the grain roughness coefficient given by the Strickler equation $n_g = 0.048\, d_{50}^{1/6}$ (Carson and Griffiths 1987).

Kuhnle (1992) measured transport rates of eight size fractions (0.35-45.25 mm) of the weakly bimodal bed material on Goodwin Creek, U.S.A., from 1984 to 1988. Bedload samples were collected with modified Helley-Smith samplers (Helley and Smith 1971) suspended from a footbridge at the upstream end of a "V"-shaped supercritical flow concrete structure installed in the stream channel. The samplers had trapezoidal inlet orifice with the area of 58.06 cm^2. Altogether 488 bedload samples were collected. Corresponding values of bed shear stress were calculated using the hydraulic radius and water surface slope measured in a 106 m straight reach 63 m upstream from the location where the samples were collected. The data were averaged to eliminate the natural variability of the bedload transport processes for gravel and to define the mean transport rate for a given flow strength. The averaged bedload relations were presented graphically as W_i^{*} versus τ_i^{*} plots (Kuhnle 1992, his Fig. 7.6). Although the fractional transport data were normalized on the composition of the sub-surface

material, the absence of the well-developed armour layer and similar grading of the bed surface and sub-surface material allowed the use of the bedload relations presented in Kuhnle 1992 for the purposes of the present analysis.

Andrews (1994) observed marginal bedload transport in gravel-bed Sagehen Creek, California, U.S.A. A study reach, approximately 160 m long, was established immediately upstream from a gauging station in order to investigate the hydraulic and sediment transport characteristics. The bedload was sampled from a footbridge using a hand-held Helley-Smith sampler with a 15 x 15 cm orifice and 0.25 mm mesh bag. A number of samples were collected in a cross section, the sampling period of each single measurement being 4 minutes. Water discharge during the sampling was obtained from the gauging station. Total energy slope was determined between the crests of the first riffles upstream and downstream of the footbridge, with the distance between the riffles of 46 m or about 10 channel widths. All of the measurements were collected during the spring snowmelt periods of years 1982-1984. Migrating bed forms or bars were not observed in the Sagehen Creek study reach at any time. Altogether 55 sets of tabular data on flow conditions and bedload transport rates for fractions ranging from 8 to 128 mm are available. These data are used to obtain plots of q_{bi}^* versus τ_i^*, with τ_i^* defined using the Manning and Strickler equations [see description of Pozdnyakov (1987) data above] to account for the effect of channel forms (riffles) on flow characteristics.

Wathen et al. (1995) studied transport of bedload in the Allt Dubhaig, a small river in Scotland. Their approach was to trap the sediment transported during flood events over a period and relate the amount and size distribution of trapped sediment to shear stress at the flood peak, rather than attempt to make instantaneous measurements of transport rate and shear stress. Integrating transport over events sacrificed detail but meant that sample sizes were far larger, and grain size information far more reliable, than would have been the case with point samples. The bedload and hydraulic data were collected during 1991-1993. Bedload was monitored using a trench dug across the full channel width and lined with two rows of plastic bins (each about 45 cm long, 30 cm wide, and 30 cm deep) bolted to each other with metal strips. The total trap capacity of over 1.5 tonnes was sufficient for most flood events, the trap being normally emptied after each event. The channel bed near the trap is predominantly composed of gravel with a secondary sand mode. The channel is almost rectangular in shape and there was no sign of migrating bed forms, therefore form drag was assumed to be minimal. The peak shear stress for each event was calculated from the depth-slope product, with the

slope measured over the distance of 60 m upstream of the trap using pressure transducers and data loggers. Transport rates normalized on bed surface composition for fractions ranging in size from 0.5 mm to 64 mm were plotted as Parker bedload parameter as W_i^* versus Shields stress τ_i^* and fitted by fractional transport curves (Wathen et al. 1995, their Fig. 7).

5.4 Results

5.4.1 Fractional transport rates

Experimental fractional bedload relations are the basic data required for the reference transport approach to predicting the incipient motion of different size fractions in a mixture. Some of the fractional transport data obtained in this study are given in Figures 5.2 and 5.3. Figure 5.2 shows plots of q_{bi}^* versus τ_i^* obtained for mixtures N-1, N-2, N-3, F, C, and B at a slope of 0.0083. Similar plots are derived for all the other slopes used in the experiments. Figure 5.3 shows plots of q_{bi}^* versus τ_i^* obtained for the mixture HR at a slope of 0.0045. It is obvious from these figures that strong intergranular effects are present in all the mixtures investigated. These effects significantly reduce mobility of fine fractions (due to sheltering from larger grains) and increases mobility of coarse fractions (due to greater exposure and instability) in mixed-size sediments compared to the mobility of the same grain sizes in uniform sediments (compare Figures 5.2 and 4.5). The wider is the range of grain sizes in a mixture, the more pronounced are the hiding and exposure effects. Similar behaviour of individual size fractions is evident for all the additional flume and field data on graded sediment transport compiled in this study. Some of the field data expressed in terms of q_{bi}^* versus τ_i^* are shown in Figures 5.4 and 5.5.

In Figure 5.6, the q_{bi}^* versus τ_i^* plots are shown for some size fractions in mixture N-2 (present study) at flume slopes ranging from 0.0041 to 0.0141. It is seen from Figure 5.6 that the fractional transport rates q_{bi}^* strongly depend on the slope as in the case of uniform sediment (see Figure 4.5). In the present experiments, for example, increase of bed slope from 0.0041 to 0.0141 caused 40-50% increase of τ_i^*

corresponding to a given value of q_{bi}^*. This is something that has never been noted before in the literature devoted to the transport of graded sediments. That is, the behaviour of individual size fractions is strongly affected by both relative position of this fraction in a mixture and bed slope. The latter factor can be explained by different resistance of the grains at different slopes as described in Section 4.3.3 of Chapter 4. Therefore, both these effects should be taken into account in consideration of fractional thresholds. More importantly, combined analysis of incipient motion data collected at different slopes (commonly applied by many researchers) is unacceptable, as it may lead to erroneous conclusions.

The experimental q_{bi}^* versus τ_i^* plots were used to determine values of critical Shields stress τ_{ci}^* corresponding to the two chosen values of reference transport rate ($q_{bi}^* = 10^{-4}$ and $q_{bi}^* = 10^{-2}$) as shown in Figures 5.2-5.5. In some cases transport data for the end size fractions appear above and below the reference levels, and an extrapolation of the data has to be made to read the appropriate values of τ_{ci}^*. The extrapolation was applied and values of τ_{ci}^* were determined only for those fractional transport data, which demonstrated well-defined trends of the q_{bi}^* versus τ_i^* relations. Although there is always some degree of uncertainty involved in extrapolating data, it is believed that, given the natural variability of the sediment transport and very steep q_{bi}^* versus τ_i^* relations for low transport rates, the extrapolation errors for the data sets selected are within the errors of the measurements.

In Figure 5.4 constructed using Oak Creek transport data from Parker and Klingeman (1982), the widely used reference transport rate of Parker et al. (1982) $W_i^* = 0.002$ is also shown for comparison with the threshold criteria employed in the present study. Given the experimentally established linear relationship between intensity of sediment motion (or probability of sediment entrainment) and dimensionless Einstein bedload parameter q_{bi}^* (Figure 4.4), one may conclude from Figure 5.4 that the Parker et al. (1982) criterion gives almost three orders of magnitude higher probability of particle entrainment for the finest fractions in the mixture compared to the coarsest fractions at incipient motion. This is consistent with the conclusion of Wilcock and McArdell (1997) that the mobilized proportion of fractions decreases with grain size at the Parker et al. (1982) reference transport conditions. That is, the widely used Parker

incipient motion method does not provide equal relative mobility of different size fractions in sediment mixtures.

5.4.2 Hiding functions

As follows from the literature review given in Section 2.6 of Chapter 2, there are two fundamentally different types of hiding functions based on critical bed shear stress concept. The first hiding function relates critical shear stress for a given grain size in a mixture (τ^*_{ci}) to that in uniform sediment of the same size ($\tau^*_{ci\,uni}$). The second hiding function defines fractional critical stress (τ^*_{ci}) with respect to the critical stress for a central value of the mixture grain size distribution, commonly the median size (τ^*_{c50}). The first approach is rather rarely used, while the second one is much better established and is widely applied to the description of the behaviour of different fractions in graded sediments.

Analysis of the present results indicates that there is no definite relationship between the determined values of τ^*_{ci} and appropriate values of $\tau^*_{ci\,uni}$ established experimentally, see Section 4.3.4 of Chapter 4, whereas the relationship between τ^*_{ci} and τ^*_{c50} is well defined, with the general trend common for all the mixtures investigated. The experimental results also indicate that for a given sediment mixture, the character of the hiding function of the form of $\tau^*_{ci}/\tau^*_{c50} = \text{function}(d_i/d_{50})$ is independent of bed slope. This is due to the fact that bed slope influences absolute values of both τ^*_{ci} and τ^*_{c50} (corresponding to a given reference transport rate), which results in a constant τ^*_{ci}/τ^*_{c50} ratio for different slopes (see Figure 5.6). It is also found that this hiding function is the same for the full range of reference transport rates chosen, which reflects the essential parallelism of the log-log q^*_{bi} versus τ^*_{ci} relations for low transport rates apparent in Figures 5.2-5.6. However, for active bedload transport the q^*_{bi} versus τ^*_{ci} relationships are known to change significantly (e.g., Paintal 1971, Misri et al. 1984, Parker 1990), and the character of the hiding function for transport rates higher than those investigated may therefore be different (Misri et al. 1984, Samaga et al. 1986, Patel and Ranga Raju 1996).

The independence of the hiding function of both bed slope and reference transport rate for near-to-threshold transport is a very important fact as it significantly simplifies

the further analysis and unifies the final results. The plots of τ^*_{ci}/τ^*_{c50} against relative size d_i/d_{50} obtained for $q^*_{bi} = 10^{-4}$ are shown in Figure 5.7. All the data appear to fall within a relatively narrow band and can be approximated by the following equations:

$$\frac{\tau^*_{ci}}{\tau^*_{c50}} = \begin{cases} \left(\frac{d_i}{d_{50}}\right)^{-e} & \text{for} \quad \frac{d_i}{d_{50}} \le 1 \\ \left[\log\left(10\frac{d_i}{d_{50}}\right)\right]^{-2.2} & \text{for} \quad \frac{d_i}{d_{50}} \ge 1 \end{cases} \tag{5.3}$$

where exponent e ranges from 0.73 to 1.13. A similar range for e between 0.81 and 1.09 was obtained for unimodal and weakly bimodal sediments by Wilcock and Southard (1988), who applied the Parker et al. (1982) reference transport method to their own and other available flume and field data.

It is seen from Figure 5.7 that the hiding function (5.3) bends up for particles coarser than d_{50}. This means that the coarsest fractions are entrained (i.e., reach the appropriate reference transport level) at a higher dimensional bed shear stress $\tau = \rho\, g\, R_b\, J$ compared to median-sized fractions. The range of variation of e in (5.3) demonstrates that in some mixtures the finer particles are entrained at lower shear stress than the median-sized grains ($e < 1$). In other mixtures the finest particles need a higher shear stress for entrainment compared to median fractions ($e > 1$). The under-representation of either the coarser grains or both the extreme finest and coarsest fractions in transport near incipient motion is common for other graded sediment data (e.g., Rakoczi 1987, Wilcock and Southard 1989, Ashworth et al. 1992, Wilcock 1992, Kuhnle 1992, 1993a, Wathen et al. 1995, Gomez 1995, Wilcock and McArdell 1993, 1997). Therefore, the Parker et al. (1982) hypothesis of near-equal entrainment mobility holds only for $d_i < d_{50}$ and only for certain mixtures.

It is also clear from Figure 5.7 that the use of the average value of the exponent e=0.93 does not provide a good fit to all the data, especially for the finest particles. Errors in the calculation of τ^*_{ci} may be as high as 40-60 %. Therefore, the exponent e in (5.3) should be expressed in terms of some other parameters determining the behaviour of fractions finer than the median grain size in a mixture.

The apparent reasons for the variation of the entrainment mobility of the fine fractions are the range of sizes (sorting) and the shape of sediment size distribution (normal/skewed, unimodal/bimodal). The influence of mixture sorting on fractional motion was suggested by White and Day (1982), Nakagawa et al. (1982), Misri et al. (1983, 1984), Samaga et al. (1986), Pender and Li (1995), and Patel and Ranga Raju (1999). The dependence of the relative size effect on the degree of bimodality was observed by Wilcock (1993) and Kuhnle (1992, 1993a, 1993b). The range and shape of size distributions in this study are characterized, as a first approximation, by their geometric standard deviation $\sigma_g = \sqrt{d_{84}/d_{16}}$. One may argue that σ_g characterizes mixture sorting and is not a very good measure for bimodal and skewed distributions. Nevertheless, as one can see from Figure 5.1, change of size distribution skewness or degree of bimodality is also reflected on the value of σ_g. Standard deviation σ_g is greater for bimodal mixtures relative to unimodal ones, as well as for unimodal distributions skewed towards the finer grains compared to normal distributions and compared to those skewed towards the coarser particles in the mixture.

Values of the exponent e determined by fitting (5.3) to individual data sets are plotted against σ_g in Figure 5.8 together with the corresponding values of d_{50}. It is seen in this figure that e systematically decreases with the increase of σ_g. In other words, the greater the value of σ_g, the less the hiding effect and the higher the degree of size selective entrainment for fine fractions. This observation is generally consistent with that of Nakagawa et al. (1982). The best-fit relationship between e and σ_g has the following equation:

$$e = 1.17\,\sigma_g^{-0.24} \tag{5.4}$$

However, a close examination of Figure 5.8 indicates that there is also an apparent dependence of the value of exponent e on median size d_{50}. This is most clearly seen in Figure 5.9 showing variation of e with d_{50}, the values of σ_g shown as the third parameter. The graph in Figure 5.9 demonstrates that for a given value of σ_g, the hiding of fine fractions is most pronounced (i.e., e reaches the maximum value) for mixtures with d_{50} around 5 mm. For smaller and larger values of d_{50}, the hiding effect is

reduced, and a higher degree of size-selectivity is observed. The relationship relating e with both σ_g and d_{50} is approximated by the following equation:

$$e = 2.0\,\sigma_g^{-0.10}\,\{0.049\,[\log(1000\,d_{50})]^3 - 0.26\,[\log(1000\,d_{50})]^2 + 0.33\log(1000\,d_{50}) + 1.20\} - 1.4 \tag{5.5}$$

where the grain size d_{50} is expressed in metres. The correlation coefficient is 0.88 for (5.5) compared to 0.74 for (5.4).

The physical interpretation of the relationship (5.5) is not clear at present. It can be related to the near-bed turbulent field and the damping effect of the granular bed, both depended on the absolute size of the bed particles. The damping effect was experimentally investigated by Klaven (1987) and Klaven and Kokovin (1987). They established from flume tests with uniform sands and gravels that pressure fluctuations caused by the flow turbulence and responsible for the particle mobilization penetrate the pores between the sediment grains. Due to damping effect the pressure fluctuation inside the bed material are weakened and happen with a time delay. As the damping effect is related to the size of pores (hence, grain size), Klaven and Kokovin hypothesised that for different grain sizes circumstances can arise which reduce or increase the mobility of bed particles. However, applicability of this hypothesis to the behaviour of different size fractions in graded sediments needs further detailed examination.

It is interesting to note that the variation of e with d_{50} in Figure 5.9 is very similar to the variation of critical Shields stress for uniform sediment τ_c^* in Figures 4.9 and 4.10 (or parameter a in Figure 4.16). This suggests that the observed increase of hiding effect for fine fractions in mixtures with d_{50} around 5 mm in Figure 5.9 is somehow related to the increase of τ_c^* for this size in Figures 4.9 and 4.10. Obviously, more investigations on the matter are needed to explain this phenomenon.

No effect of mixture sorting on the mobility of fractions coarser than the median grain size is found in this study. This may be a result of the insufficient coverage of this range of sizes by the existing data set. On the whole the results of the present study support the observation of White and Day (1982) that the position of the size fraction

within the grading curve is more important than the overall grading of the sediment mixture, i.e. τ^*_{ci}/τ^*_{c50} is more sensitive to d_i/d_{50} than d_{84}/d_{16}.

5.4.3 Mobility of median size fractions

To predict behaviour of different size fractions in a mixture using hiding function (5.3), it is necessary to estimate the critical Shields stress τ^*_{c50} for the median-sized grains. So far this was commonly made by comparing τ^*_{c50} with the standard Shields threshold curve derived for uniform sediments, but without significant success (see Section 2.6 and Figure 2.6, Chapter 2). The present study indicates that the Shields threshold diagram is an inappropriate means of accurately evaluating the threshold for uniform sediments (Section 4.3.4, Chapter 4) and therefore cannot be used as a basis for analysing the behaviour of graded sediments. Here the determined values of τ^*_{c50} are compared to the results of the experiments on incipient motion of uniform sediments presented in Chapter 4 of this thesis.

An interesting fact emerging from the comparison of Figures 5.2 and 5.6 obtained for graded sediments with Figure 4.5 and the threshold diagrams in Figures 4.9 and 4.10 obtained for uniform sediments is that for a given bed slope and reference transport rate the values of τ^*_{c50} are about the same as the critical Shields stress for uniform sediment of the same size. Similar behaviour is found for all the other relatively narrow-graded ($\sigma_g < 3$) mixtures investigated. For mixtures with a wider grading, the values of τ^*_{c50} are found to be higher than those of uniform sediment. The ratio of the critical Shields stress of size d_{50} in a mixture (τ^*_{c50}) to that in uniform sediment ($\tau^*_{c50\,uni}$) versus mixture standard deviation σ_g is shown for different data for the two chosen reference transport rates in Figure 5.10. A single relationship is fitted to both data sets in Figure 5.10:

$$\frac{\tau^*_{c50}}{\tau^*_{c50\,uni}} = 2.5\left[\log(\sigma_g)\right]^{4.0} + 1 \qquad (5.6)$$

This relationship allows the critical Shields stress for the median size fractions in unimodal and weakly bimodal sediment mixtures to be estimated from the known

mixture geometric standard deviation σ_g and value of $\tau^*_{c\,50\,uni}$ determined either from the appropriate threshold diagram in Figure 4.9 and 4.10 or from the generalized equation (4.13) using d_{50}.

There is some uncertainty regarding Goodwin Creek data (Kuhnle 1992, 1993a) largely affecting the character of the relationship (5.6) for large values of σ_g. The bed shear stress in Goodwin Creek was calculated using the hydraulic radius without correction for the bed form roughness, which could lead to some errors. On the other hand, the general reduction of the mobility of widely graded sediments has also been observed elsewhere (e.g., Egiazaroff 1965), and it can be explained by siltation reducing the overall mobility of the bed material.

5.4.4 Formalization of results

Given the relationships (4.11), (4.12), (5.3), (5.5), and (5.6), the fractional q^*_{bi} versus τ^*_{ci} relations for $q^*_{b50} \leq 10^{-2}$ (value of q^*_{bi} for $d_i = d_{50}$) can be approximated by

$$q^*_{bi} = \left(\frac{a_{50}\,\tau^*_i}{b\,\varepsilon_i} \right)^{18} J^{-5.0} \qquad (5.7)$$

where a_{50} is the particle mobility factor calculated by (4.12) using d_{50}, $b = \tau^*_{c\,50} / \tau^*_{c\,50\,uni}$ is the mixture mobility factor calculated by (5.6), and $\varepsilon_i = \tau^*_{ci} / \tau^*_{c\,50}$ is the hiding function (5.3) with the exponent e calculated by (5.5). Fractional bedload relations calculated using (5.7) are shown in Figures 5.2-5.6 and demonstrate reasonable agreement with the observed data. Although equation (5.7) is partly based on the data shown in Figures 5.2-5.6, it should be noted that (5.7) is an averaged generalized transport relationship, which is not fitted to a particular data set but is derived from the total combination of the uniform and graded sediment transport data compiled in this study. Given the absence of reliable methods for estimating behaviour of individual size fractions in sediment mixtures, the present results are rather encouraging.

Substituting the chosen values of the reference transport rate in (5.7), we arrive after rearrangements at:

$$\tau^*_{ci} = b\,\varepsilon_i \frac{0.60}{a_{50}} J^{0.278} \qquad \text{(for } q^*_{bi} = 10^{-4}\text{)} \tag{5.8}$$

and

$$\tau^*_{ci} = b\,\varepsilon_i \frac{0.77}{a_{50}} J^{0.278} \qquad \text{(for } q^*_{bi} = 10^{-2}\text{)} \tag{5.9}$$

For a single-size sediment (i=1), b=1, $\varepsilon_i = 1$, and (5.8) and (5.9) reduce to (4.14) and (4.15), respectively.

Given the equality of the Einstein bedload parameter to the intensity of sediment motion for a given grain size [Figure 4.4, equation (4.6)], expression (5.7) can also be rearranged into a general equation for the calculation of critical Shields stress for any size fraction in unimodal and weakly bimodal sediment mixtures:

$$\tau^*_{ci} = b\,\varepsilon_i \frac{I_c^{0.0556}}{a_{50}} J^{0.278} \tag{5.10}$$

where I_c is the "critical" value of intensity of sediment motion (or probability of sediment entrainment) representing the threshold.

The above set of equations (5.3)-(5.10) is derived for $1 \le d_{50} \le 124$ mm, $0.001 \le J \le 0.070$, and is applicable only for $q^*_{b50} \le 10^{-2}$ ($I_c \le 10^{-2}$).

5.4.5 Bed features

During the present flume experiments with relatively active sediment transport longitudinal ridges and troughs were developed on the bed parallel to the mean flow direction. These longitudinal bed features took the form of periodic span-wise variations in bed texture and bed topography, and were similar to those observed in uniform sediments (Section 4.3.6, Chapter 4), but significantly less pronounced and distinguished. The ridges were typically composed of finer grains compared to the troughs, with the lateral spacing between the ridges of 1.5-2.5 flow depths h ($\approx 2h$ on average). The troughs were about 1-2 median grain diameters deep. The number of troughs varied from two to five in the Armfield flume tests. The development of two

troughs was observed for the highest flows in HR Wallingford flume. Similar bed forms in sediment mixtures have been observed by others (e.g., Tsujimoto 1989, McLelland et al. 1999).

The cause of the development of the longitudinal bed forms is discussed later in Chapter 6 concerned with the flow turbulent structure.

5.5 Conclusions

Based on the graded sediment transport data examined here and the research method used, the following principal conclusions can be drawn.

Behaviour of individual fractions in mixed-size sediments is largely controlled by strong intergranular effects. These effects reduce mobility of fine fractions due to sheltering from larger grains and increase mobility of coarse fractions due to greater exposure to the flow compared to uniform sediments of the same sizes (Figures 5.2-5.5).

It is also evident that behaviour of graded sediments is significantly affected by bed slope as in the case of uniform sediments. The steeper the slope is, the higher the shear stress is needed to produce a given transport rate for a given size fraction (Figure 5.6). This is explained by the greater hydraulic resistance caused by reduced relative depth (depth to grain size ratio) for steeper slopes. This effect of bed slope (or relative depth) on the mobility of different grain sizes in sediment mixtures has never been studied before and is not taken into account by any of the existing sediment transport formulas. It also follows that combined analysis of transport data collected at different slopes (commonly applied by many researchers) is unacceptable as it may lead to erroneous conclusions.

The stability of a particle d_i in a graded bed material is largely determined by its size relative to the median grain size d_{50} (Figure 5.7). The character of hiding function in Figure 5.7 is the same for all the range of bed slopes and reference transport rates investigated, but changes for finer fractions with mixture sorting and median grain size. Although the relative size effects dominate in sediment mixtures, they do not suppress completely the size-selective entrainment. The degree of size-selectivity increases with mixture standard deviation σ_g (Figure 5.8). In other words, the wider is the range of grain sizes in a mixture, the more independent is the entrainment mobility of fractions

finer than the median grain size. Conversely, the narrower the grading is, the more significant is the influence of median-sized sediment on incipient motion of finer fractions. As the value of σ_g is related to the shape of the sediment size distribution, one may conclude from Figure 5.8 that bimodal mixtures and mixtures with a mode at the fine-grained end of the distribution (having, therefore, greater σ_g) offer a higher degree of freedom for fine fractions compared to unimodal mixtures and mixtures with normal distribution or coarse-grained mode, respectively.

It is also found that the hiding effect for fine fractions is most pronounced for mixtures with d_{50} around 5 mm (Figure 5.9). This is probably somehow related to the general increase of critical Shields stress for uniform sediment of this size (Figures 4.9 and 4.10). More data are required to find a physical explanation of these phenomena.

The comparison of the graded sediment transport data and experimental results obtained for uniform sediments indicates that in relatively narrow graded sediments ($\sigma_g < 3$) critical Shields stress τ^*_{c50} of median-sized grains is the same (at a given bed slope) as in uniform sediments of this size. For mixtures with a wider grading, τ^*_{c50} systematically increases compared to uniform material (Figure 5.10). This is apparently related to the siltation effect reducing the mobility of the entire sediment mixture.

Therefore, the relative variation of τ^*_{ci} with respect to τ^*_{c50} depends on the relative size d_i/d_{50}, mixture sorting σ_g, and absolute value of d_{50}, which is expressed by (5.3) and (5.5). The value of τ^*_{c50} in a mixture is related to that in uniform sediment of size d_{50}, as shown by (5.6). So, we have all the parameters required for calculating the fractional q^*_{bi} versus τ^*_{ci} relations by (5.7) and values of critical Shields stress τ^*_{ci} by (5.10).

Thus, the proposed method allows prediction of the incipient motion and near-to-threshold transport of different grain sizes in streambeds for a given bed slope and sediment size distribution of the surface bed material. The method refers to unimodal and weakly bimodal sediment mixtures. Incipient motion of strongly bimodal two-component sediment mixtures according to the reference-transport approach adopted is the subject of future investigations.

Table 5.1 Range of Data for Graded Sediments in Present Experiments

No.	Mix	Flume	Width B (m)	Slope J x 10^3	Depth h (m)	Velocity V (m s^{-1})	Transport Rate q_b (g s^{-1} m^{-1})
1	N-1	Armfield	0.30	4.1-14.1	0.032-0.118	0.48-0.85	0.17-26.7
2	N-2	Armfield	0.30	4.1-14.1	0.033-0.121	0.42-0.81	0.11-38.3
3	N-3	Armfield	0.30	4.1-14.1	0.026-0.128	0.41-0.76	0.031-53.3
4	F	Armfield	0.30	4.1-14.1	0.015-0.091	0.34-0.70	0.009-93.7
5	C	Armfield	0.30	4.1-14.1	0.041-0.124	0.46-0.91	0.035-34.0
6	B	Armfield	0.30	4.1-14.1	0.023-0.124	0.26-0.81	0.064-71.5
7	HR	HR Wallingford	0.80	4.5	0.088-0.150	0.63-0.98	1.37-80.9

Table 5.2 Bed Materials in Other Studies on Graded Sediment Transport

Mixture Designation	Primary Reference	Mixture Type	Size Distribution			Geometric Standard Deviation
			d_{16} (mm)	d_{50} (mm)	d_{84} (mm)	σ_g
(a) Flume data						
DAY A	Day (1980)	Weakly bimodal	0.33	1.75	5.45	4.06
MISRI N2	Misri et al. (1984)	Weakly bimodal	1.27	3.82	11.5	3.02
MIT 1ϕ	Wilcock and Southard (1988)	Lognormal	0.92	1.83	3.78	2.03
PATEL M3	Patel and Ranga Raju (1996)	~Lognormal	1.50	2.59	4.50	1.73
(b) Field data*						
Oak	Parker and Klingeman (1982)	Long fine tail	20	54	87	2.09
Ala-archa	Pozdnyakov (1987)	Long fine tail	55	124	169	1.75
Goodwin	Kuhnle (1992)	Weakly bimodal	0.8	11.7	29	6.02
Sagehen	Andrews (1994)	~Lognormal	27	58	115	2.06
Allt Dubhaig	Wathen et al. (1995)	Long fine tail	4.97	21.3	41.3	2.88

* surface bed material

Table 5.3 Summary of Data for Other Studies on Graded Sediment Transport

Mixture	Width B (m)	Slope J x 10^3	Depth h (m)	Velocity V (m s^{-1})	Transport Rate q_b (g s^{-1} m^{-1})
(a) Flume data					
DAY A	2.46	0.7-3.7	0.107-0.169	0.48-0.74	0.72-65.6
MISRI N2	0.75	3.8-4.8	0.078-0.135	0.56-0.81	0.49-16.9
MIT 1ϕ	0.60	1.0-3.3	0.109-0.112	0.43-0.73	0.023-59.4
PATEL M3	0.40	4.4-5.6	0.056-0.091	0.55-0.77	0.048-17.2
(b) Field data					
Oak	5.0-6.1	~10	0.27-0.44	0.84-1.16	0.28-111
Ala-archa	10-11	~25	0.62-0.79	1.84-2.60	3.9-178
Goodwin	25	3.3	0.3-2.0	?	~0.1-3000
Sagehen	4.85	~10	0.35-0.62	1.10-1.96	0.50-34.9
Allt Dubhaig	~8	~2	0.49-0.92	?	~0.05-5*

* bed load transport measured over flood events

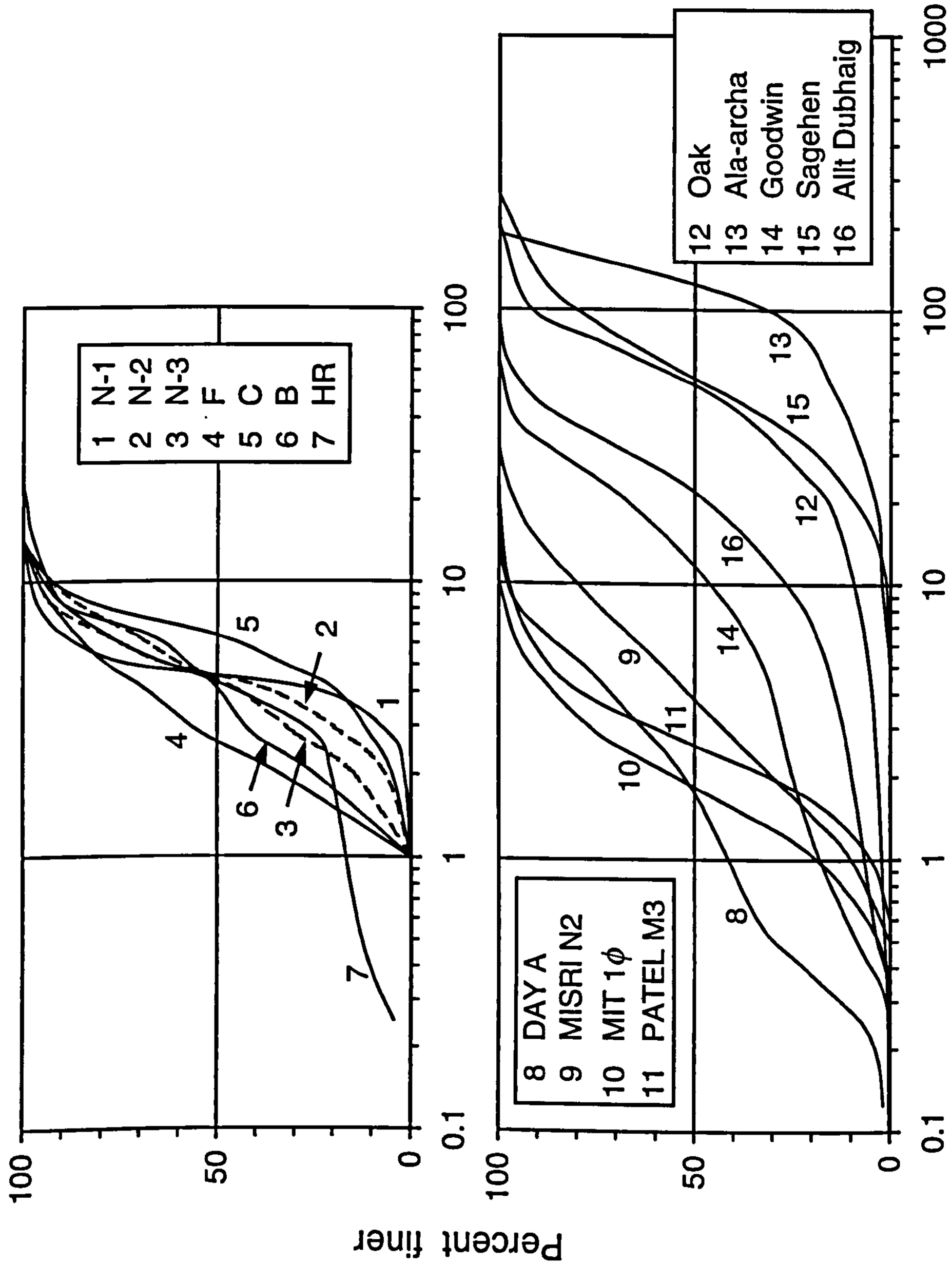

Figure 5.1 Cumulative grain size distributions for all sediment mixtures used in analysis.

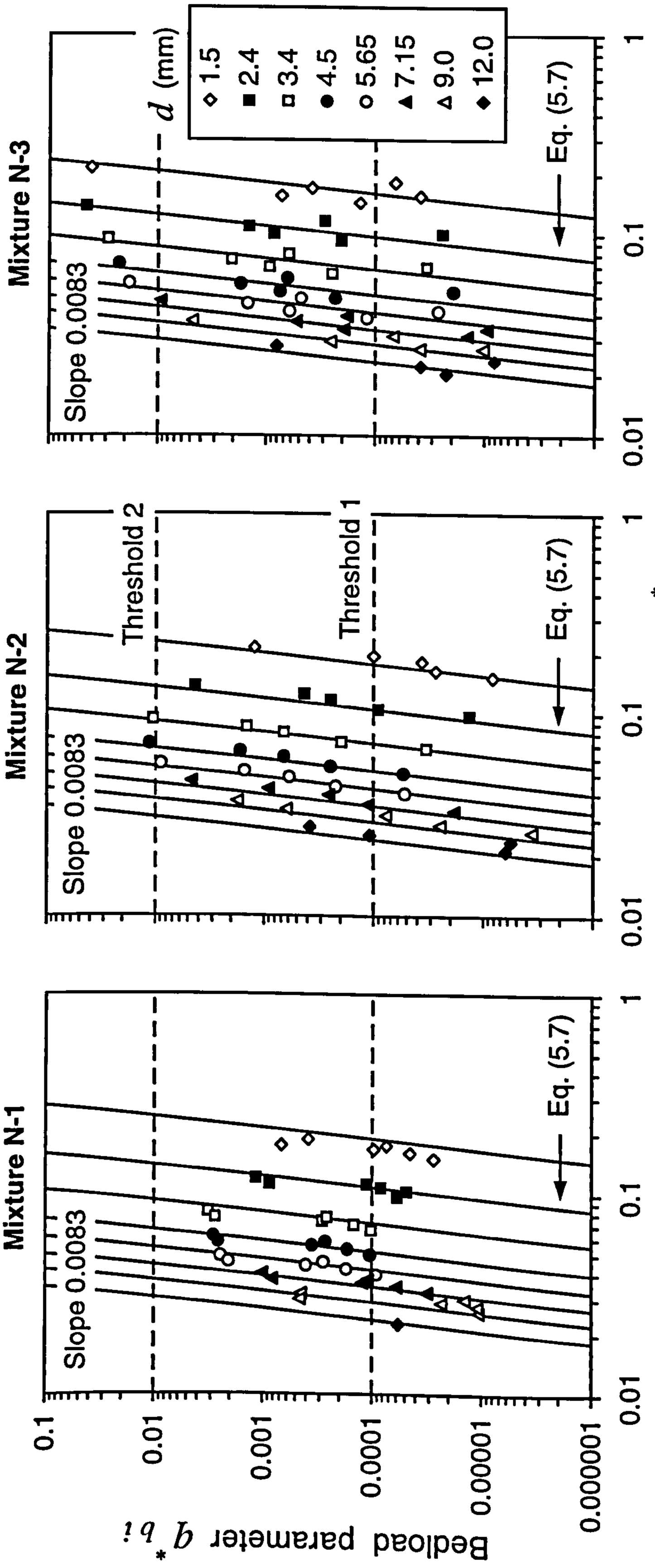

Figure 5.2 Plots of q^*_{bi} versus τ^*_i for mixtures N-1, N-2, N-3, F, C, and B at slope 0.0083.

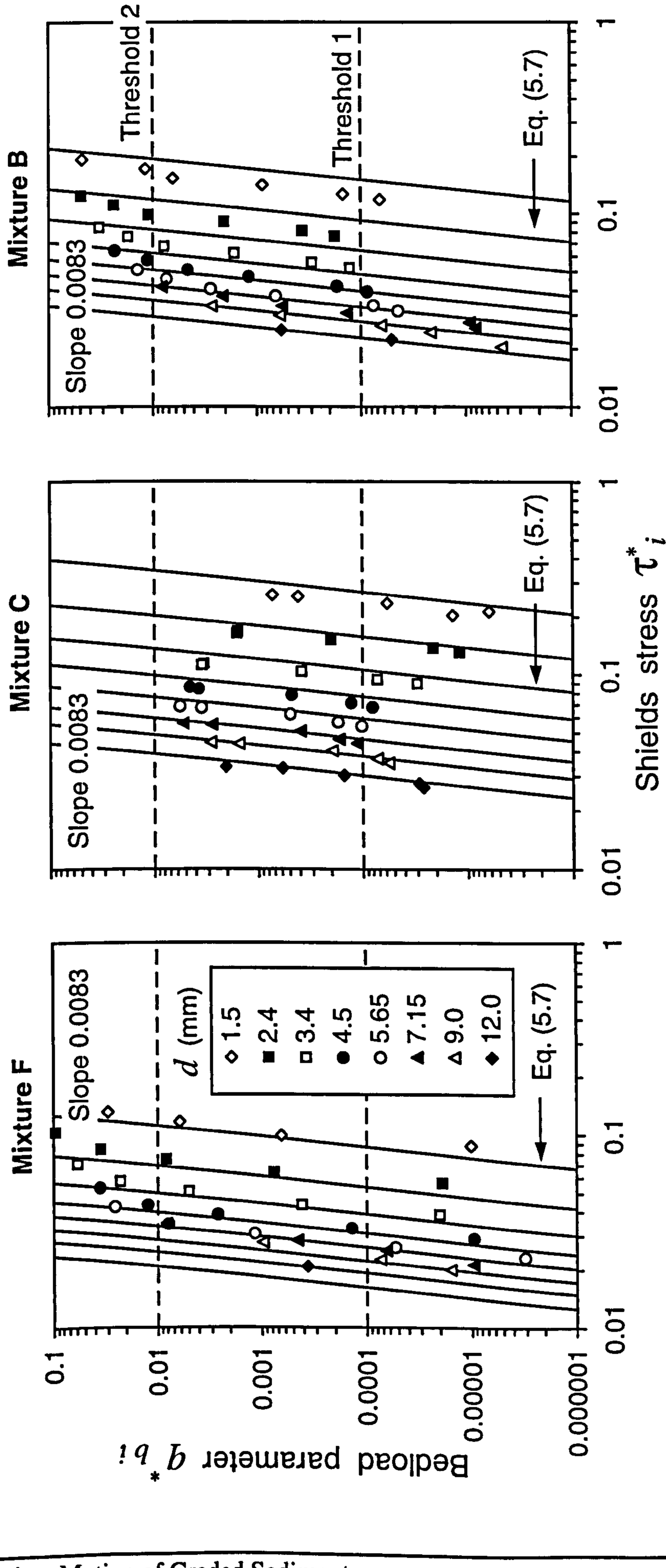

Figure 5.2 (continued).

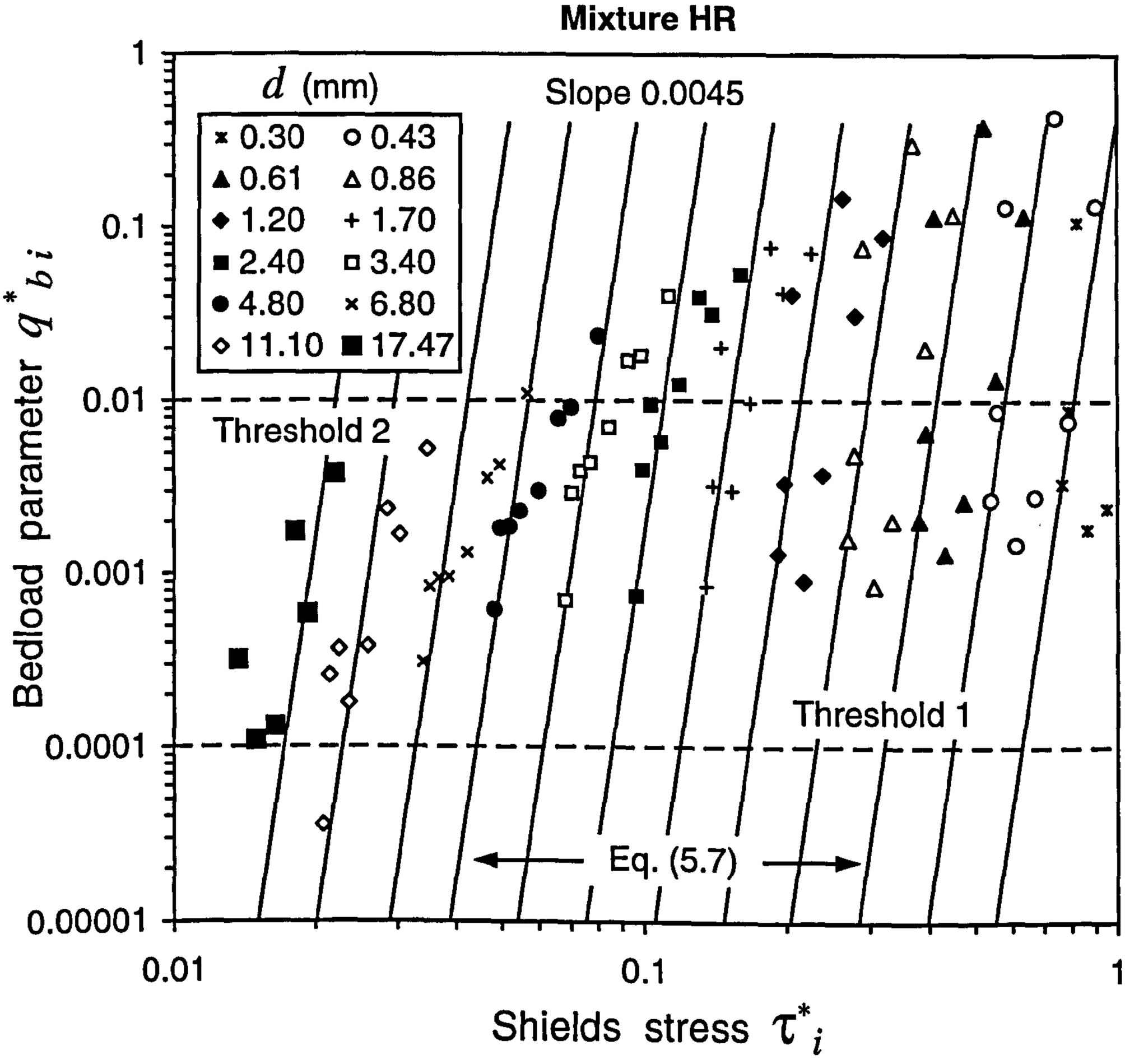

Figure 5.3 Plots of q^*_{bi} versus τ^*_i for mixture HR at slope 0.0045.

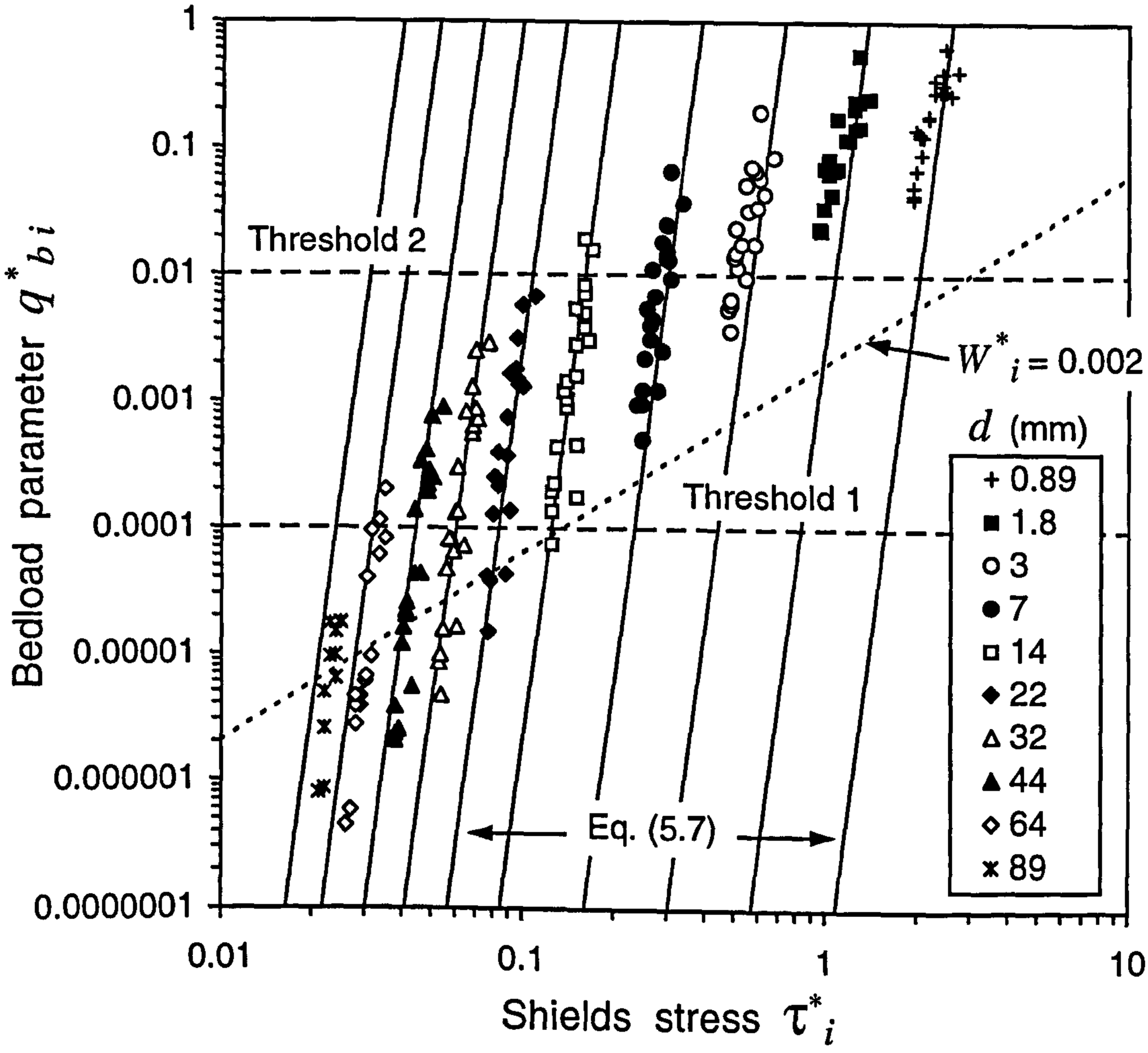

Figure 5.4 Plots of q^*_{bi} versus τ^*_i for Oak Creek (after Parker and Klingeman 1982).

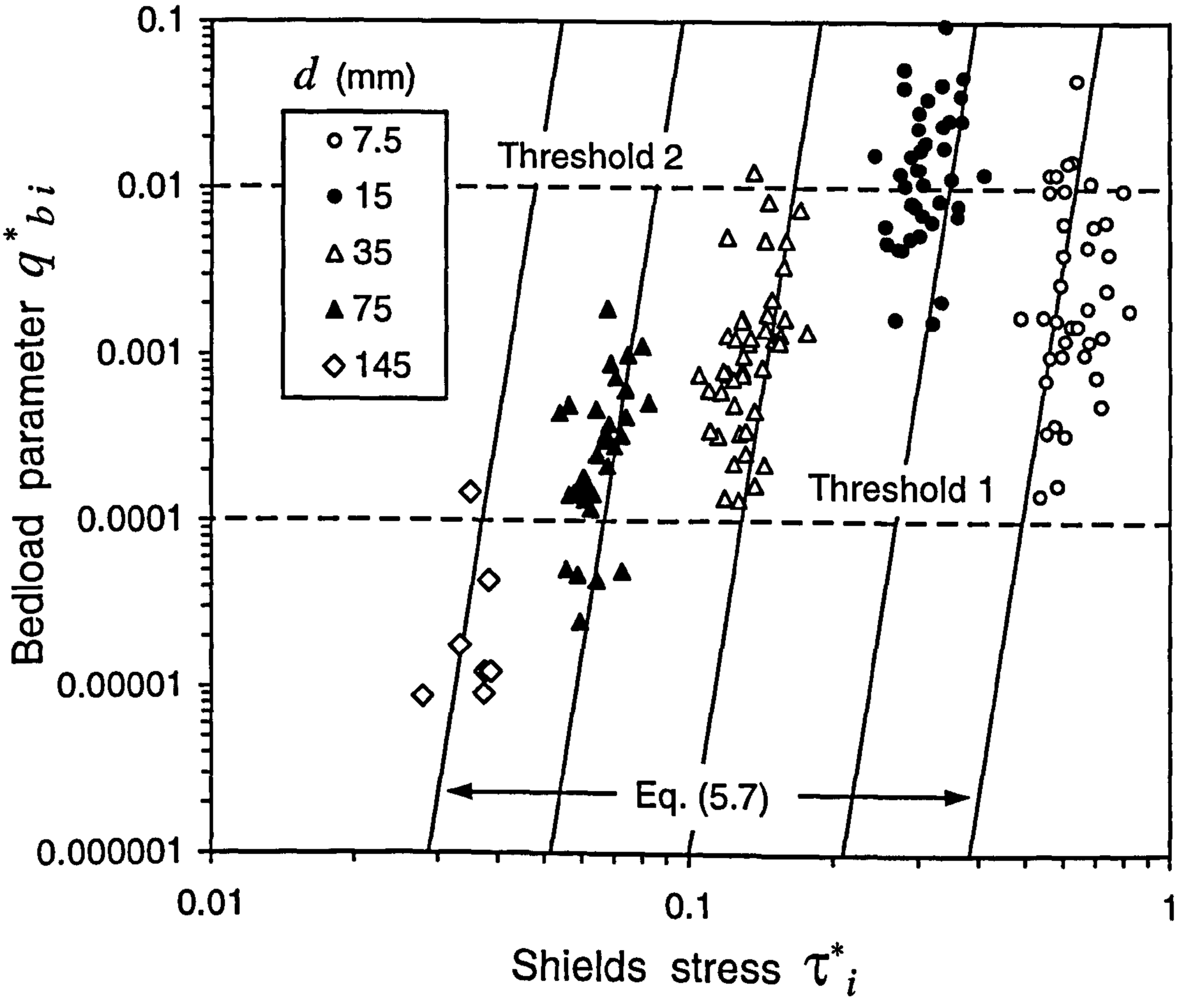

Figure 5.5 Plots of q^*_{bi} versus τ^*_i for Ala-archa River (after Pozdnyakov 1987).

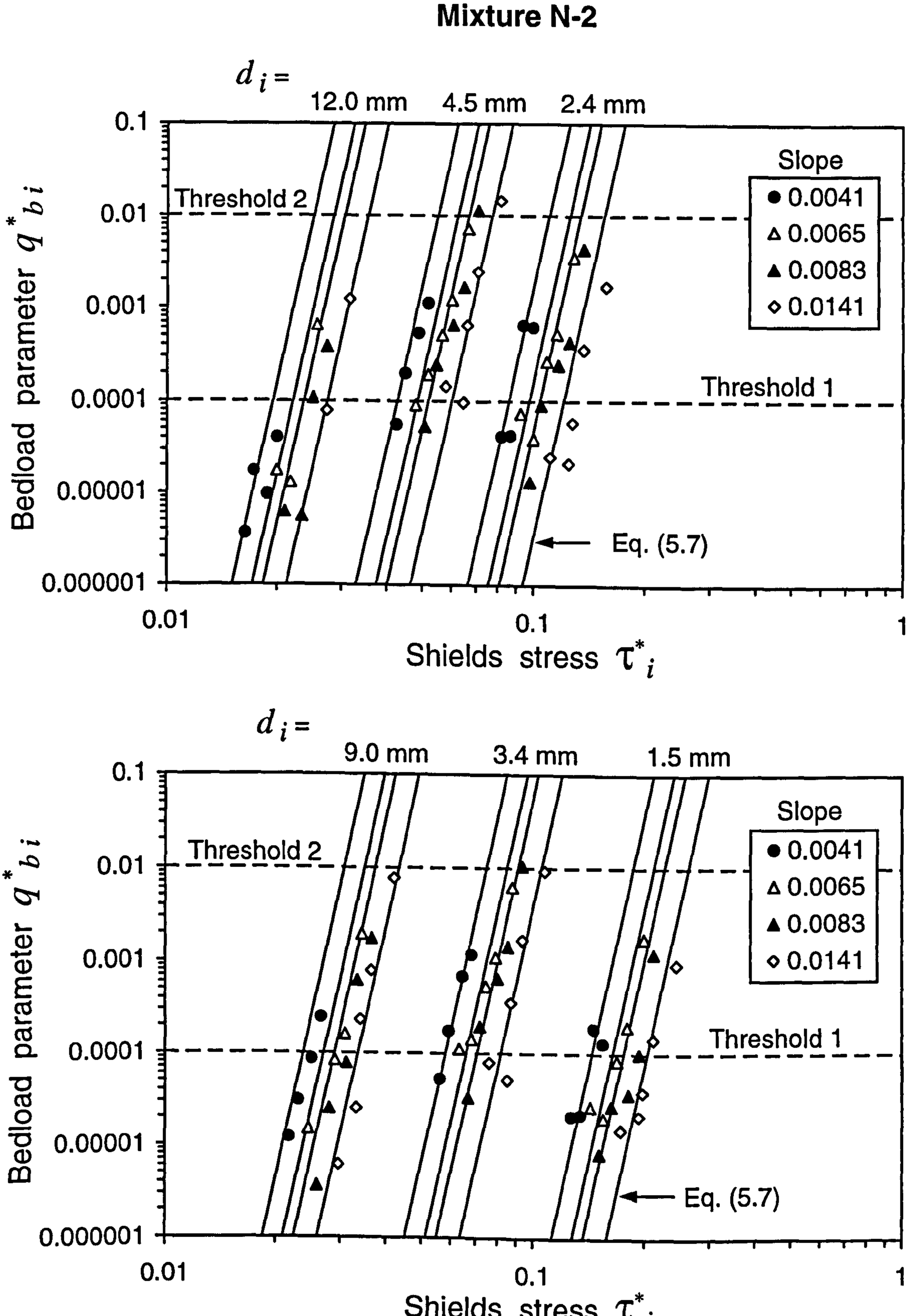

Figure 5.6 Plots of q^*_{bi} versus τ^*_i for different fractions at different slopes in mixture N-2.

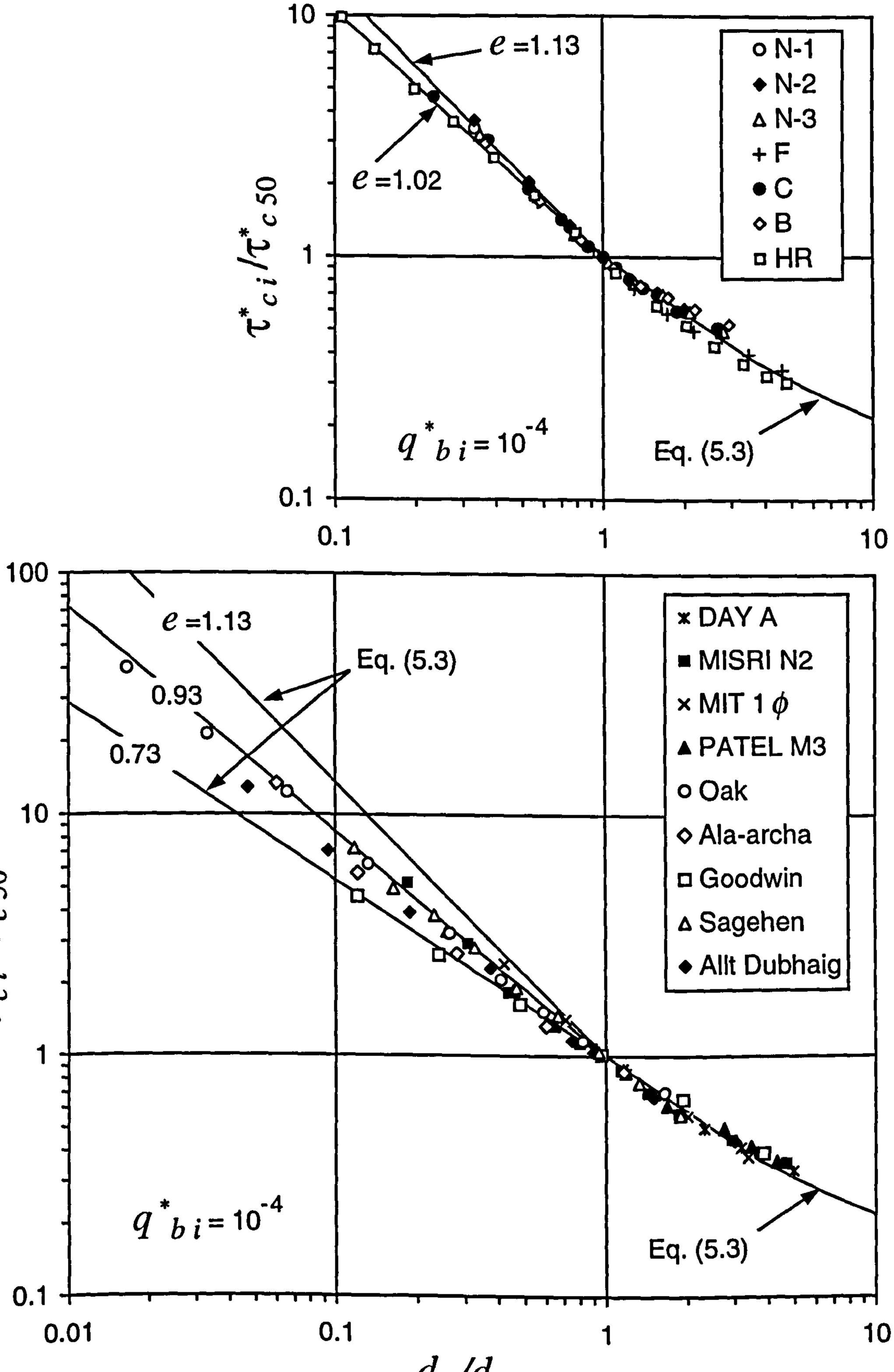

Figure 5.7 Hiding function for different sediment mixtures.

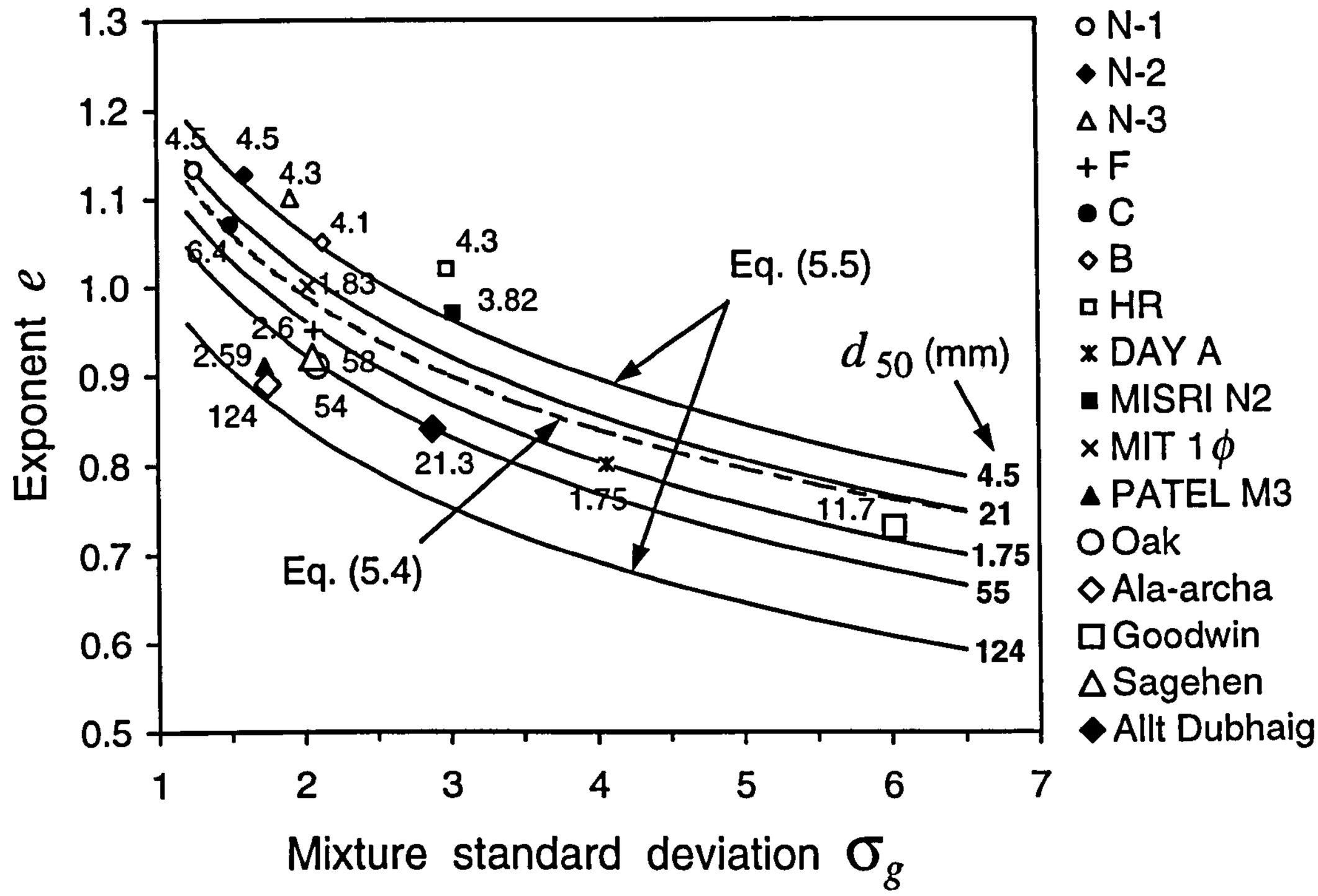

Figure 5.8 Exponent e in hiding function versus mixture standard deviation σ_g.

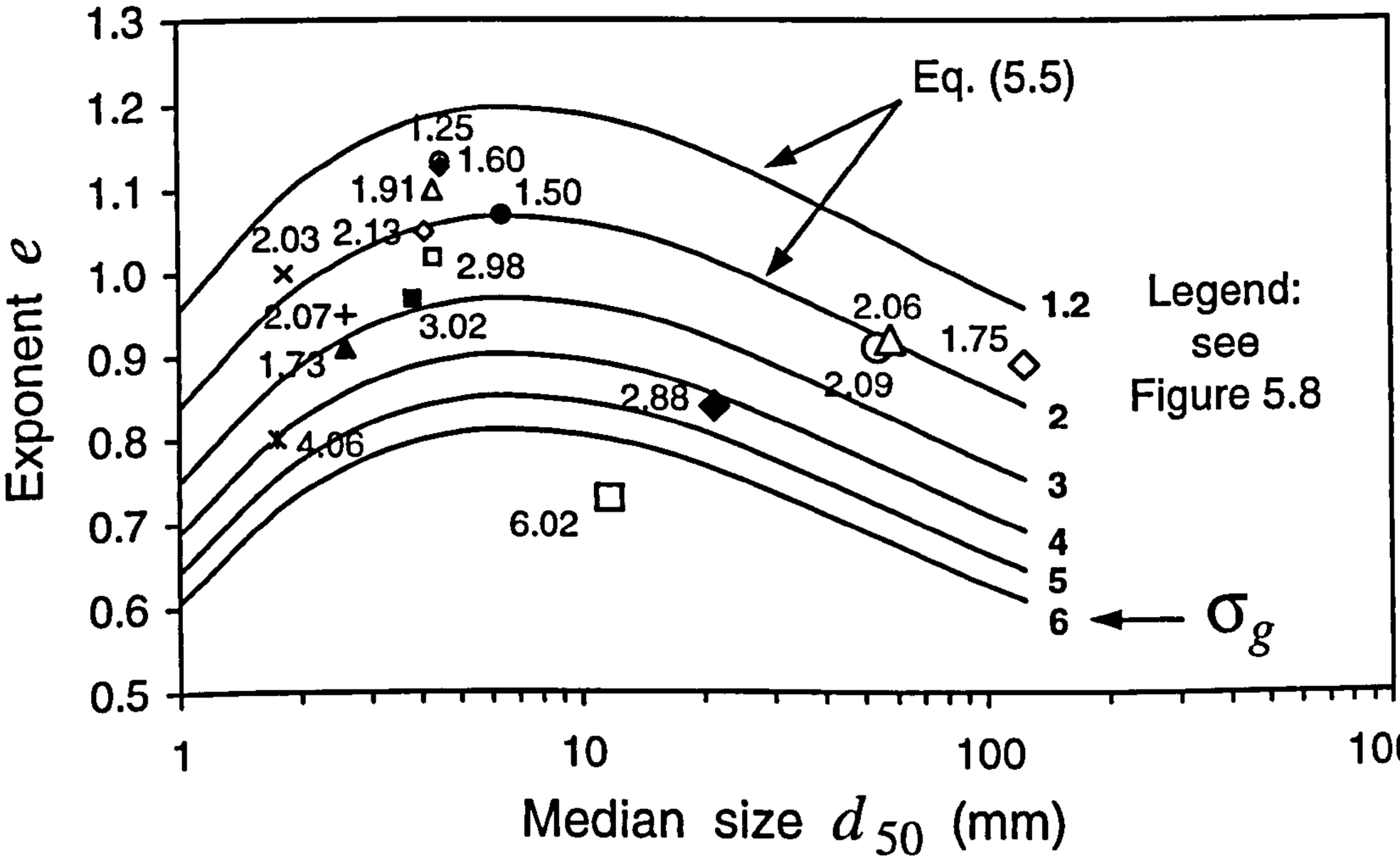

Figure 5.9. Exponent e in hiding function versus mixture median size d_{50}.

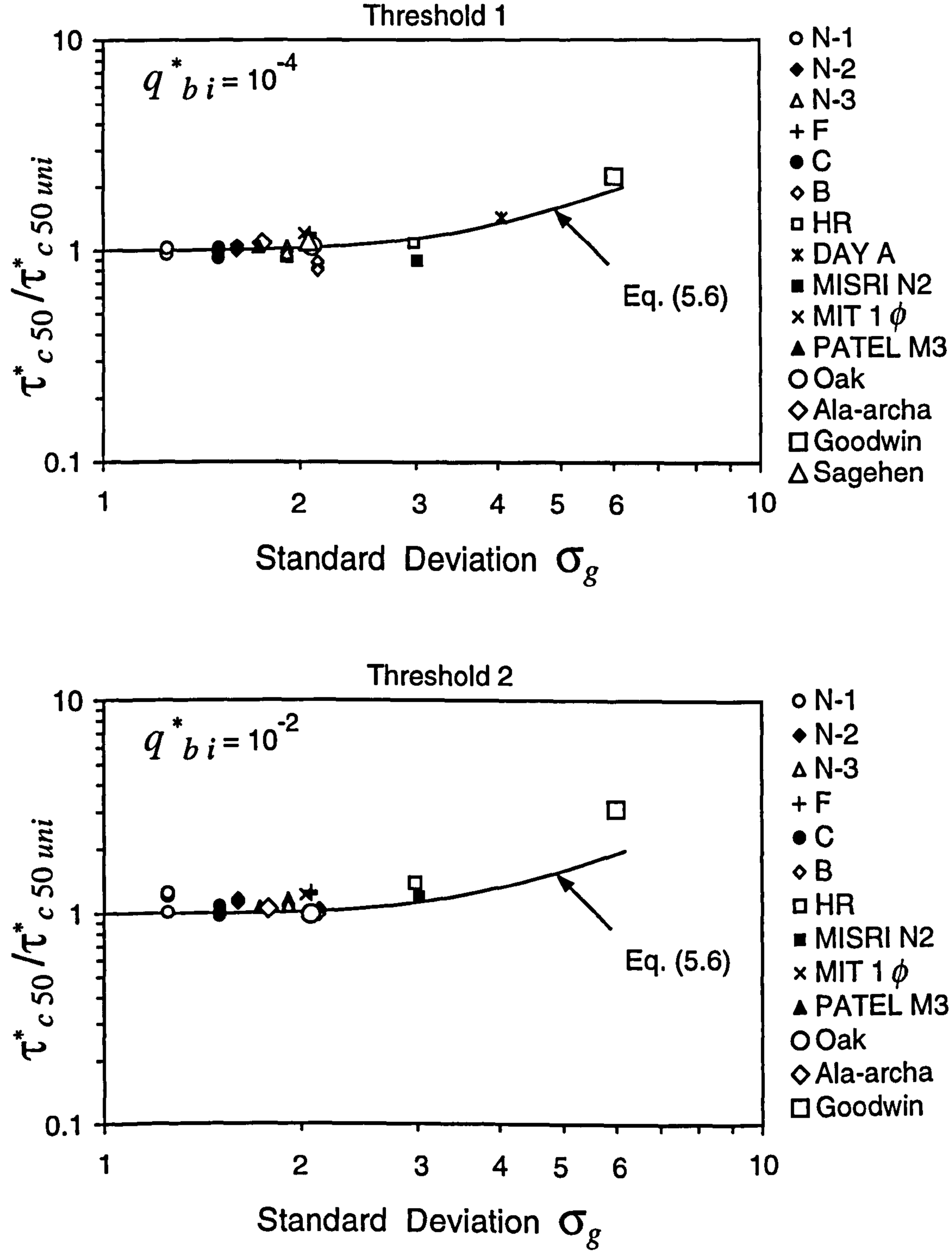

Figure 5.10 $\tau^*_{c50}/\tau^*_{c50uni}$ versus standard deviation σ_g.

6

Turbulent Structure of Open-Channel Flow over Gravel Beds

"It is much easier to describe movement of Jupiter's moons than movement of water."

(Galileo Galilei)

"... the water does not like straight lines."

(DuBuat)

6.1 Background

Turbulence in water flows is one of the major factors controlling entrainment and motion of bed particles. It is known that the instantaneous fluid velocity in turbulent flows fluctuates in magnitude and direction. These fluctuations result in varying lift and drag forces acting on the bed particles. Bed sediment is entrained when the local destabilising forces exceed those acting to stabilise it. Hence, improvement of our understanding of sediment incipient motion is not possible without knowledge of the mechanism of turbulence.

Presently there is a great deal of research activity in the field of turbulence in open-channel flows, particularly in the area of "coherent structures". These are generally considered to be repetitive quasi-cyclic large-scale (of the order of the flow depth) turbulent motions. Until the 1950's turbulent fluctuations were considered random and chaotic, which led to the expectation that all of the turbulent structures would be clarified theoretically and experimentally by means of conventional statistical tools. Velikanov (1949) was apparently the first who inferred that flow turbulence might be a "structural" and "quasi-periodic" phenomenon. On the basis of the analysis of large-scale turbulent fluctuations, Velikanov (1949) developed a theoretical model of open-channel turbulent flow which contained a sequence of depth-size "rolling" vortices.

Velikanov's structural concept of flow turbulence was later experimentally confirmed by Fidman (1953) [also discussed in Fidman (1991)], Klaven (1966, 1968), and Klaven and Kopaliani (1973). Fidman (1953) studied the kinematic structure of the flow in flumes with smooth and rough beds. He used a camera moving with the flow to record images of fluid motion within visualized turbulent flow and concluded that the maximum energy of turbulence is contained in the low-frequency turbulent fluctuations caused by the largest turbulent disturbances, the vertical and longitudinal dimensions of which scale with the flow depth. Klaven (1966, 1968) and Klaven and Kopaliani (1973) used a similar visualization technique in their flume studies with smooth and mobile gravel beds. The experiments revealed the existence in the turbulent flow of large-scale eddies with the vertical size close to the flow depth h and the length varying from about $7h$ for smooth beds to $4h$ for rough beds. These eddies are the most stable structural features and can be considered as quasi-periodic elements of the open-channel flow turbulence (Klaven 1968). Subsequently Zaitsev (1984) established from the detailed measurements of flow velocity vector fluctuations in a flume with smooth and sand beds that the large-scale turbulent eddies are actually three-dimensional and move downstream along stable paths ("macrojets") with a width close to $2h$.

An interesting set of flow visualization experiments has been undertaken by Imamoto and Ishigaki (1986a, 1986b). They investigated the turbulent structure of the open-channel flow over smooth and rough immobile beds and detected the existence of upwelling and downwelling circular fluid motions over the entire flow depth, interpreted as "depth-scale longitudinal eddies". Both the lateral and the longitudinal scale of the fluid motion was about $2h$. Tamburrino and Gulliver (1999) studied the fluid turbulence induced by a steel belt sliding on the bottom of a horizontal flume and revealed the existence of rotational fluid motion between the bed and the free surface similar to that detected by Imamoto and Ishigaki (1986a, 1986b).

It has been hypothesized that the depth-scale (or "macroturbulent") eddies are closely linked to what is today called the "bursting" phenomenon in boundary layers (Grishanin 1990, Yalin 1992). The bursting phenomenon was discovered by Kline et al. (1967) and Corino and Brodkey (1969). Using hydrogen-bubble visualization, they detected repetitive ejections of fluid away from the wall with subsequent high-speed inrushes of fluid towards the wall sweeping away the low-speed fluid remaining from the ejections. Since then intensive experimental research on the bursting processes in

open-channel flows near both smooth and rough beds has been performed by many investigators [for a review see Grass et al. (1991), Nezu and Nakagawa (1993), and Best (1993)]. It has been found that fluid ejections/sweeps have a quasi-cyclic pattern and are not restricted to the near-bed region but influence the entire flow field irrespective of bed roughness (Grass 1971, Talmon et al. 1986, Shen and Lemmin 1999). The ejected low momentum fluid travels across the entire flow depth up to the water surface while high momentum fluid moves from the water surface towards the bed (Rashidi and Banerjee 1988, Grass et al. 1991), giving rise to rolling structures which in many respects are very similar to the large-scale eddies observed by Klaven (1966, 1968), Klaven and Kopaliani (1973), Imamoto and Ishigaki (1986a, 1986b), and Tamburrino and Gulliver (1999). In addition, the streamwise spacing of the bursting events has been found to be between $2h$ and $7h$ (Sumer and Deigaard 1981, Nezu and Nakagawa 1993, Best 1993, Nikora and Goring 1999, Sechet and Le Guennec 1999) which is close to the observed length of large-scale eddies and thus partly supports the hypothesis about close linkage between these two phenomena.

In spite of these studies, however, the knowledge of turbulent flow structure remains incomplete. While an agreement appears to have been reached with regard to at least the general pattern of the bursting phenomenon in the near-bed region (Nezu and Nakagawa 1993), opinions differ about the ordered depth-scale motions in open-channel flows. Yalin (1992), for example, argues that macroturbulent eddies are not permanent and do not originate in their full size ($\approx h$). According to Yalin (1992), eddies are generated near the bed as a result of bursts with a size much smaller than h, then grow until their size becomes nearly equal to h, they are then destroyed prompting the generation of a new small eddy, and so on. The complete cycle of the eddies birth, life and destruction occurs over a distance of $\approx 6h$ which is generally in agreement with the existing field and laboratory data.

Thus, the existence of quasi-stable large-scale eddies and their relation to the turbulent fluctuations is disputable. It is still poorly understood why the high-speed and low-speed regions exist alternately in both the streamwise and spanwise directions in a turbulent flow (Nychas et al. 1973, Kirkbride and Ferguson 1995, Ferguson et al. 1996, Buffin-Belanger et al. 2000, Roy and Buffin-Belanger 2000). Some researchers explain this with reference to bursting (Yalin 1992, Nezu and Nakagawa 1993), but the

sequence of high- and low-speed regions can also be explained using the downstream movement of large-scale turbulent eddies.

So far little is known about the cause and regularity of the turbulent fluctuations. There is some evidence of the presence of low-frequency velocity fluctuations corresponding to the spatial scale of the order of the flow depth in laboratory and field streams (e.g., Komori et al. 1982, Grinvald and Nikora 1988, Clifford et al. 1992, Lapointe 1992, Nezu and Nakagawa 1993, Robert et al. 1993, Roy et al. 1996, Cellino and Graf 1999, Shen and Lemmin 1999). However, there are a number of laboratory and field data which do not reveal any regular period in turbulent fluctuations (e.g., Grinvald 1974, Nikora and Smart 1997) which suggest that coherent structures are randomly distributed in space and in time (Nychas et al. 1973, Smith 1996, Nikora and Goring 1999).

Thus, the question if there is *order* or *chaos* in turbulent flows still remains unanswered. At the same time it has been established that the coherent turbulent motions make a significant contribution to the turbulent shear stress and pressure fluctuations (Kim et al. 1971, Talmon et al. 1986, Shen and Lemmin 1999) which significantly affect bed particles and control sediment motion. Therefore there is a need for more investigations on ordered motions and coherent structures in turbulent flows. This is especially true for flows over natural sediment beds which have not been studied systematically.

The present experimental research investigates the turbulent structure of the open-channel flow over mobile gravel beds. The primary objective of the experiments was to establish whether the large-scale organized turbulent structures really exist and how they are related to the flow velocity fluctuations and character of bed particle motion. The presence of these large-scale structures may be very important in explaining the initiation of particle motion at the bed.

6.2 Experimental Procedure

The experiments on flow turbulence were conducted in the Armfield flume, University of Glasgow. Four uniform gravels ranging is size from 2 mm to 8 mm (sediments No. 2, 4, 5, and 6 in Table 3.1) used earlier in the investigation of incipient

motion of uniform sediments (Chapter 4) were employed in the flume tests discussed. The bedload sampling equipment used earlier was dismounted, the sampling slot in the flume base closed and covered with a 5 cm layer of mobile sediment to obtain a continuous sediment bed without any disturbances which might influence the turbulent structure of the flow.

The pre-experimental arrangements included a standard set of procedures: preparation of a flat bed, setting the flume slope, slow flooding of the bed from the downstream end of the flume, and gradual increase of water discharge until it reached an experimental value. The measured characteristics were the bed slope, water discharge, flow depth, mean flow velocity, water temperature, large-scale turbulent structure of the flow, and near-bed flow velocity fluctuations.

Water discharge, flow depth, and temperature were measured using the apparatus described in Section 3.2.3 of Chapter 3. The mean flow velocity was obtained from the water discharge and depth measurements. Additional measurements with the mini-propeller meter were made at a distance $0.4h$ above the bed surface to check the calculated value of the mean flow velocity.

A flow visualization technique was used to study the large-scale turbulent structure of the flow. The water was seeded with neutrally buoyant tracers and illuminated by a thin vertical light sheet parallel to the flume walls, which was positioned at different locations across the channel. The motion of the illuminated tracers in vertical and longitudinal directions was recorded using computer monitored digital video and still cameras. The cameras were mounted on a movable carriage, which during the recordings was moving with the flow (so-called "sliding filming" of the visualized flow structure). Preliminary tests demonstrated that the most clearly interpretable turbulent structures were observed when the cameras were moving along the flume at a speed equal to the mean flow velocity. Therefore, this speed was set for sliding filming during the main series of the experiments. The flow visualization apparatus is described in detail in Section 3.2.5 of Chapter 3 and is shown in Figures 3.5-3.7.

In addition, flow velocity fluctuations over 4.5 mm, 5.65 mm, and 7.15 mm gravel beds were measured using the Acoustic Doppler Velocimeter (ADV) described in Section 3.2.6 of Chapter 3 and shown in Figure 3.8. The ADV measuring section was situated 4.7 m from the flume entrance where turbulent flow was fully developed.

Because of the restriction on the flow depth for the ADV, the measurements were made for a range of depths exceeding 0.06 m and only in the near-bed region at a distance of about one grain diameter from the bed surface at different locations across the channel. Care was taken to orient the ADV probe properly to minimize errors in the measurements due to the sensor misalignment. The sampling period was 5 min, with the sampling rate of 25 Hertz, which allowed the collection of sufficient data for statistical analysis.

The experiments were conducted for steady, uniform flow at a variety of bed slopes and water depths. When necessary the flow regime was controlled by means of the tailgate at the downstream end of the flume. A summary of the experimental conditions is given in Table 6.1.

During the experiments different states of bed mobility ranging from "no sediment movement" to "medium movement" were observed, but in most cases it can be characterized as "occasional particle movement at some locations" for coarser gravel and "weak" sediment transport for finer gravel ["several particles are in motion, in isolated spots, and in countable numbers" Kramer (1935)]. Because of the generally low transport rates and the relatively short duration of the experiments (most lasted for about one hour), no sediment was re-circulated or fed into the flume. This did not cause any noticeable change of flow conditions or bed elevation and, therefore, was assumed not to influence the measured data.

Sediment transport characteristics were not measured directly in this particular study. However, the present experiments were designed to repeat a part of the earlier flume tests on incipient motion of coarse uniform sediments (Chapter 4), but now with the emphasis on studying the turbulent structure of the flow. Given that exactly the same bed material was used, the characteristics of bedload transport corresponding to different flow conditions can be estimated from the results of the previous flume tests concerned with sediment motion alone. Bed sediment mobility here is characterized by the transport intensity parameter introduced in Section 4.1 of Chapter 4, this quantifies the fraction of all bed surface particles displaced in unit time (Table 6.1).

6.3 Results

6.3.1 Large-scale turbulent structure

Altogether 52 videos of the visualized turbulent flow have been recorded using sliding filming, the light sheet being positioned at various transverse offsets. Analysis of the videos reveals the following flow pattern developed during the experiments (Figure 6.1). At the beginning of the flume neutral tracers moved approximately parallel to the water surface and bed. Then a circular motion of the tracers ("rolling" small-scale eddies) generated in the near-bed region of the flow. These eddies gradually increased in size finally occupying the entire flow depth. The development of the depth-scale rotational movement was completed at 1.5-2.5 m from the flume entrance (about 25-50 flow depths), after which the depth-scale rotation was sustained over the rest of the flume. The observed flow pattern is in contradiction to the model of the turbulent flow proposed by Yalin (1992) (constantly repeated sequence of eddy birth, growth and disruption). The flow pattern described was developed for all the sediments used and flow conditions tested (see Table 6.1). The sliding filming of the motion of the neutral tracers clearly reveals that: (a) the development of depth-scale eddies was not caused by the entrance conditions to the flume; (b) the fully developed rotational motion of fluid occupied the entire flow depth; (c) the observed circular motion took place in a vertical plane, and it was not simply a reflection of the spiral motion of secondary currents.

The longitudinal organization of these depth-scale eddies could not be reliably determined either from the videos (due to the complexity of simultaneous motion of a great number of neutral tracers) or from single video frames (due to the short exposure 1/25 s which did not allow the motion of individual neutral particles to be traced). Therefore, a still digital camera with an exposure of 1/4 s was used to obtain "frozen" pictures of the macroturbulent flow structure. The digitised images were taken at 3.5-4.0 m from the flume entrance where the turbulence was fully developed. Altogether 362 images were collected for different sediments, flow conditions, and transverse offsets of the light sheet. The analysis of the images reveals that open-channel turbulent flow consists of a continuous sequence of large-scale longitudinal eddies moving downstream at the bulk flow velocity (Figure 6.2). The eddies have an asymmetric form reflecting areas of high-forward-speed downwelling ("sweeps") and burst-like upwelling ("ejections") fluid motions. The vertical size of these eddies is close to the flow depth h.

The length of individual eddies L_E (taken as a distance between adjacent sweep or ejection areas) varies from about $2h$ to $12h$ and is around $(4\text{-}5)h$ on average. A summary of the average characteristics of the large-scale eddies is presented in Table 6.2. Here eddy period T_E is defined using eddy length L_E and mean flow velocity U as $T_E = L_E/U$. Not all the images collected are as distinct as shown in Figure 6.2. It is acknowledged that there is a great deal of subjectivity in analysing the images and measuring the dimensions of the large-scale turbulent structures. This together with the natural variability of the phenomenon is reflected in rather significant values of standard deviations of the determined characteristics of the eddies (Table 6.2). Nevertheless, the existence of an ordered sequence of regions of upwelling and downwelling fluid motions is clearly distinguishable on all the images. The higher the flow depth and velocity, the more pronounced the development of the large-scale turbulent eddies and the less ambiguous the interpretation of the images.

During some of the experiments longitudinal ridges and troughs were developed on the sediment bed (see Table 6.2). Analysis of the images of the visualized flow above both ridges and troughs does not reveal noticeable difference in the longitudinal turbulent structures. Although there might be mutual interaction of the large-scale turbulent eddies and the bed forms developed, images collected before and after the development of the ridges and troughs do not indicate any noticeable change in the eddy characteristics with the growth of the longitudinal bed features. However, it is accepted that this may be owing to rather significant variability of the phenomenon itself and limitations of the present research method which requires the light sheet to be rather wide to capture the trajectory of motion of individual neutral tracers. The characteristics of the longitudinal bed forms, their cause and the possible relationship with the large-scale eddies are discussed later.

The experimental data enables some preliminary conclusions to be drawn on the relationship between the parameters of large-scale turbulent eddies and the main flow characteristics. As one can see from Table 6.2, eddy length L_E generally increases with the flow depth h, mean flow velocity U, and slope J (for a given h). At the same time all the changes in relative eddy length L_E/h with flow conditions are within the errors of the measurements. Judging from the experimental results for 7.15 mm gravel with a relatively wide range of flow depths, L_E/h value tends to slightly decreases with an increase of h (Table 6.2). The experiments with 2.40 mm gravel conducted for different

bed slopes reveal a general increase of L_E/h ratio for steeper slopes. However, in all the cases relative eddy length is close to the value of $L_E/h \approx$4-5. Notable are the very similar periods of large-scale eddy motion $T_E \approx$0.3-0.5 s (average value $\approx$0.4 s) in different experiments, in spite of a rather wide range of experimental conditions.

The relationships of L_E with flow depth h and mean flow velocity U are shown in Figure 6.3. As the first approximation, these relationships can be expressed as follows:

$$L_E \approx 4.5\,h \tag{6.1}$$

and

$$L_E \approx 0.4\,U \tag{6.2}$$

The coefficient 4.5 in (6.1) is the average relative eddy length L_E/h, and 0.4 in (6.2) is the average time period of eddy motion T_E (in seconds). Despite the significant variability of the experimental data, these preliminary relationships can serve for approximate assessments and as a background for further investigations.

It is interesting to compare the results of the present experiments with data from other similar flow visualization studies. The only data available for coarse bed particles are those collected by Klaven and Kopaliani (1973) in an 8 m long by 0.21 m wide flume and Imamoto and Ishigaki (1986a, 1986b) in a 6 m long by 0.20 m wide flume. Their data are summarized in Table 6.3 and plotted on Figure 6.3. As one can see, the additional data generally support the results of the present experiments. There are some indications in the literature that L_E/h ratio might decrease with relative roughness (Klaven and Kopaliani 1973) and that moving bedload might alter the flow turbulence (Nikora and Goring 1999, 2000). However, to date the existing rather limited data set for flow over mobile granular beds together with a high degree of variability of the phenomenon prevents a reliable estimation of the effect of the absolute grain size, relative bed roughness, and intensity of sediment transport on the eddy characteristics. This is a task for future investigations.

6.3.2 Flow velocity fluctuations

Six sets of measurements (altogether 33 measurements) of the instantaneous flow velocity components near the bed were completed using an Acoustic Doppler Velocimeter (ADV) for three different gravel sizes (Table 6.4). The quality of the velocity data collected is characterized by the mean values of the correlation parameter of 75.5% and signal-to-noise ratio of 38.9 dB, which are consistently above the admissible limits for reliable data of 70% and 15 dB, respectively, recommended by the ADV manufacturers (SONTEK 1995). No attempts were therefore made to filter or correct the original data.

The flow conditions during the measurements were characterised by: (a) a constant value of Shields stress $\tau^* = 0.048$, and (b) a constant value of sediment transport intensity $I = 10^{-4}$ s^{-1}. The present analysis is restricted to streamwise u and vertical v flow velocity components as directly related to the rotational fluid motions observed in the flow visualization experiments (see Figure 6.2). A typical flow velocity time series is shown in Figure 6.4. The data collected indicate that flow velocity fluctuations take place in a quasi-cyclical manner, with an increase in the streamwise velocity component usually corresponding to a negative (towards the bed) vertical flow velocity component, and vice versa. This is most clearly demonstrated by Figure 6.5 showing a quadrant plot of streamwise u' and vertical v' flow velocity fluctuations. Figures 6.4 and 6.5 reflect the wave-like motion of the fluid masses known as the "bursting phenomenon". Upwelling motion of fluid away from the bed ($+v'$) causes a decrease of longitudinal velocity ($-u'$) near the bed ("ejection of fluid"). This is followed by an inrush of fluid ($-v'$) towards the bed causing an increase of streamwise flow velocity ($+u'$) near the bed surface ("high speed sweep").

To derive whether there is any periodicity in the flow velocity fluctuations, spectral analysis of the flow velocity time series has been used. Typical energy spectra for streamwise and vertical flow velocity components are shown in Figure 6.6 together with the well-known Kolmogorov's "–5/3" power law (Monin and Yaglom 1975). As one can see, both spectra generally follow the Kolmogorov's law in the high-frequency region. At the same time, there is a well-distinguishable peak in the low-frequency region corresponding to a time period $T \approx 0.4$ s. This peak is common to all the energy spectra obtained for the vertical velocity components, and can also be recognized in the streamwise velocity spectra, however, in this case it is much less stable and pronounced

(note the log-scale visually reduces the amplitude of low-frequency energy peaks and increases those for high frequencies). The period of flow velocity fluctuations of about half a second is also detectable in Figure 6.4, which shows the time series of the velocity data. As discussed previously, the same value was obtained for the period of motion of the large-scale turbulent eddies. This suggest that these two phenomena are closely linked, and the movement of the large-scale eddies (Figure 6.2) is apparently the main reason for the observed low-frequency flow velocity fluctuations (Figures 6.4 and 6.6).

Interestingly, the low-frequency periodicity in turbulent fluctuations has also been detected in some other flume studies with similar experimental conditions. For example, Komori et al. (1982) investigated flow velocity fluctuations at the free surface in a 6.1 m long by 0.3 m wide flume and discovered regular vertical fluid motions in the 0.04 m deep flow (mean flow velocity 0.07 m s^{-1}) with the period of about 1.2 s. Cellino and Graf (1999) undertook turbulence measurements in a 16.8 m long and 0.60 m wide flume with a bed composed of 4.8 mm grains. The bed slope was 0.0015, the flow depth was 0.12 m, and the flow velocity was 0.73 m s^{-1}. The turbulence spectra obtained reveal a noticeable energy peak corresponding to the period of about 0.5 s. Macauley (1999) measured turbulence characteristics in an 18 m long and 0.8-1.1 m wide trapezoidal channel with gravel bed (median grain size 3.7 mm) having slope of 0.0025. The measurements were made for the flow depth of 0.15 m and mean velocity of 0.75 m s^{-1}. Spectral analysis of the velocity data series collected showed a stable period of flow velocity fluctuations of about 0.4 s. Thus, there is a remarkable similarity in the results of these independent flume studies.

The existence of low-frequency regular velocity fluctuations was also detected in some geophysical flows (e.g., Grinvald and Nikora 1988, Clifford et al. 1992, Lapointe 1992, Nezu and Nakagawa 1993, Robert et al. 1993, Roy et al. 1996), but this is usually attributed to the effect of different bed forms and large-scale roughness elements. However, recently Buffin-Belanger et al. (2000) measured velocity fluctuations in the Eaton North River, Canada above a reasonably flat gravel bed (median grain size 33 mm) without significantly protruding pebble clusters. The average depth of flow was between 0.35 m and 0.40 m and the mean velocity of flow was 0.36 m s^{-1}. From the flow velocity measurements at different elevations above the bed, Buffin-Belanger et al. (2000) detected the presence of a cyclic and alternating pattern of large regions of faster and slower moving wedges of fluid, occupying the entire flow depth. These flow

structures had a relatively low frequency of occurrence (on average 9 events per minute) and relatively long duration (mean duration 2 s), and they were typically 3 to 5 times longer than the flow depth (Roy and Buffin-Belanger 2000). Buffin-Belanger with colleagues concluded that these wedges represent a self-organisation mechanism of river flows over gravel river beds. In the context of the results of the present flow visualization experiments, the wedges of high-forward-speed and low-forward-speed fluid can be associated with the head and tail of the depth-size eddies shown in Figure 6.2.

Given the insufficient experimental evidence and the controversy of the very existence of large-scale turbulent structures and regularity in flow velocity fluctuations, there is an obvious need of further investigations on the matter, especially for natural sediment beds. Simultaneous observation of the turbulent structures in visualized flow and the measurement of velocity fluctuations in different parts of the flow using a non-intrusive technique would significantly clarify the situation.

6.3.3 Effect of flow turbulence on sediment motion

The sequence of the fluid ejections and high speed sweeps caused by the movement of large-scale eddies is an important process in bed particle destabilisation. These burst-like upwelling and high-forward-speed downwelling fluid motions significantly increase the local Reynolds stress, as is shown in Figure 6.4 constructed from the present data [see also Kim et al. (1971), Talmon et al. (1986), Lapointe (1992), Shen and Lemmin (1999)], and when strong enough displace the bed particles most susceptible to movement.

The main visually observed feature of the process of bed particle movement is its apparent randomness and intermittency. This is attributed to the random distribution of exposure and support conditions of individual grains and the effect of the turbulent fluctuations (Grass 1970). However, as shown above, turbulent fluctuations are closely linked to the movement of the large-scale eddies and appear to be ordered in space and time. Fluid ejection and sweep events are grouped over certain bed areas occupied by moving large-scale eddies. This results in patchiness of sediment entrainment and intermittent character of bed particle transport (Grass 1971, Drake et al. 1988, Best 1992, Gyr and Schmid 1997).

The destabilising hydrodynamic forces responsible for bed particle mobilization are as follows: (a) drag force due to streamwise flow velocity component; (b) lift force due to difference between streamwise velocity near the bottom and the top of a bed particle ("dynamic lift"); (c) lift force generated by upward fluid motion ("direct lift"); and (d) impact from other moving particles. The peak impulse of the drag force and dynamic lift is associated with high speed sweeps, while the maximum destabilising impact of the direct lift is associated with fluid ejections. During high-forward-speed sweeps, the corresponding increase of dynamic lift is partly compensated for by the downwelling fluid motion (negative direct lift). During fluid ejections, both direct lift and dynamic lift (the latter reduced due to reduction of the streamwise flow velocity component) coincide in direction. The impact force from moving particles becomes significant during relatively active transport of bed sediment.

When dealing with initial motion of streambeds, entrainment due to collision impact can be neglected. The main destabilising forces exerted upon bed particles are therefore sweep-related drag and dynamic lift, and ejection-related direct lift, as is schematised in Figure 6.7. The pressure distribution on a grain surface that induces motion is the result of a combination of all of these forces. It is seen from Figure 6.7 that particles may be entrained by the sweep-related forces exerted by a passing turbulent eddy, i.e. an impulse force on the particles. The particles may also be lifted from the bed by ejection-related forces. By this mechanism even sheltered particles can be entrained.

Both sweep and ejection events are responsible for the generation of high local Reynolds stresses most significantly affecting bed particles (Figure 6.4). However, opinions differ on the prevailing mechanism of particle entrainment. For example, Grass 1971, 1983, Williams and Kemp 1971, Klaven 1987, Drake et al. 1988, Best 1992, 1993, and Dittrich et al. (1996) associate the initiation of sediment transport with sweep impacts significantly increasing drag and dynamic lift forces. On the other hand, Garcia et al. (1996), Shen and Lemmin (1999), and Sechet and Le Guennec (1999) relate mobilization of bed particles mainly with fluid ejections. Ergenzinger and Jupner (1992) used pressure sensors built in an artificial 120 mm cobble to measure fluid forces acting on the cobble (placed on a rough bed with $d_{50} = 50$ mm) at different flow conditions. They came to the conclusion that the lift force is far more important than the drag force for the entrainment of bedload. The role of the lift force in inducing coarse particle movement has been recently investigated by Allan and Frostick (1999) in a 9 m long by

0.6 m wide flume. They recorded entrainment of 3-20 mm gravel particles ($d_{50} = 8.7$ mm) using a digital video camera and applying a recently developed image-analysis method established that particles do not pivot around adjacent grains as required by drag induced entrainment but are entrained by vertical movement. They concluded that the main force at the time of entrainment was therefore lift with drag only becoming significant once the particles were lifted clear of the bed.

Obviously, the contribution of each of these destabilising forces to particle mobilization depends on particular bed surface conditions. Factors influencing this include particle size, shape, position among surrounding grains, exposure, support conditions, bed sediment packing, and granulometric composition of the bed material. The variability of these factors in natural streams and the difficulty in determining their individual effect means that they have to be accounted for statistically. This approach is used in this study (see Chapters 4 and 5).

6.3.4 Ejection-related lift force and sediment mobility

It is known that the turbulent intensity in the longitudinal direction has a maximum value near the rough bed quickly decreasing towards the water free surface, while the vertical turbulent intensity is almost constant in the near-bed region (e.g., Nezu and Nakagawa 1993). This allows the flow velocity data collected in this study at about one grain diameter above the bed to be used for assessing the change of the destabilising impact from the lift force due to vertical fluid motion (direct lift F_L) on the bed particles of different sizes.

The instantaneous lift force due to upward fluid motion is given by

$$F_L = c_p \frac{\pi d^2}{4} \rho \frac{(+v')^2}{2} \tag{6.3}$$

where c_p is the resistance coefficient of particles. The gravitational force stabilising bed particles is

$$G = g(\rho_s - \rho)\frac{\pi d^3}{6} \tag{6.4}$$

The ratio of the above forces is

$$\frac{F_L}{G} = \frac{3\, c_p (+v')^2}{4g\ (s-1)\, d} \tag{6.5}$$

The resistance coefficient c_p is different for all the surface grains, and depends on the grain shape and location among the surrounding particles. However, for rough beds composed of sediments with a similar density, shape, and degree of uniformity statistically average values of c_p should be the same. Therefore, we can write

$$\frac{F_L}{G} \propto \frac{(+v')^2}{g\ (s-1)\, d} \tag{6.6}$$

Given the highest Reynolds stresses are produced by the maximum vertical turbulent pulsations (Figure 6.4), we finally obtain

$$\frac{F_L}{G} \propto M_L = \frac{v_{95}^2}{g\ (s-1)\, d} \tag{6.7}$$

Here M_L is the dimensionless particle mobility parameter, and v_{95} is the 95th percentile of v values. The mobility parameter M_L is directly proportional to the ratio of the destabilising lift forces from upward fluid motions to stabilising forces acting on the bed particles, and, therefore, reflects the overall degree of bed sediment mobility. The greater M_L, the higher the ratio of the destabilising to stabilising forces, and the higher the bed mobility.

The values of v_{95} and M_L in the present experiments are shown in Table 6.4. Change of mobility parameter M_L with grain size at different flow conditions is also shown in Figure 6.8. As one can see from Table 6.4(a) and Figure 6.8(a), the mobility parameter M_L and, accordingly, intensity of sediment motion I gradually increase with grain size d in spite of the constant value of the Shields stress τ^*. At the same time, for the flows with the same transport intensity I (which required gradual reduction of τ^* with increase of d), the mobility parameter M_L was very similar [Table 6.4(b) and

Figure 6.8(b)]. These observations mean that for gravel-size particles, the Shields stress τ^* required to produce a given intensity of sediment motion (or sediment transport rate) decreases with increase of grain size, i.e. the coarser the gravel, the higher its relative mobility. This conclusion supports the results of the experiments on incipient motion of uniform sediments showing the gradual reduction of critical Shields stress τ_c^* for large values of grain Reynolds number Re_* (Section 4.3.4 of Chapter 4, Figures 4.9 and 4.10). As mentioned above in Chapter 4, this phenomenon can be explained by the effect of the absolute grain size on the wake eddies, which are shed behind the bed particles and which affect the near-bed turbulence field and, therefore, overall flow resistance.

It would be very interesting to assess the destabilising impact on bed particles of different sizes from the drag force F_D and dynamic lift F_{DL}. These forces are obviously an order of magnitude greater and their contribution to bed particle entrainment is therefore more significant compared to direct lift F_L. However, this requires precise measurements of the instantaneous streamwise flow velocity component at the top of the bed particles, which is not provided by the ADV capabilities. The use of the data collected at one grain diameter above the bed for this purpose would be incorrect given the significant change of the longitudinal turbulent intensities when moving away from the bed surface. This also prevents assessment of the relative change of the drag force and dynamic lift for different grain sizes using the present data, as the measurement results for the streamwise flow velocity component are very sensitive to the accuracy of the positioning of the ADV sampling volume above the bed surface, which always involves some errors given the uncertainty of defining the "surface of the rough granular bed".

6.3.5 Bed pattern and large-scale turbulent eddies

During the present experiments with relatively active transport of 2.40 mm gravel longitudinal ridges and troughs were developed on the sediment bed (see Table 6.2). These bed features were the same as those described in Section 4.3.6, Chapter 4 and shown in Figure 4.15. The number of troughs in these tests varied from two to five, with spacing of about two flow depths. The most active transport of sediment took place along the troughs, as demonstrated by Figure 4.16.

At present the development of longitudinal bed forms is usually explained by the existence of the "secondary spiral currents" initiated near the channel walls. These near-

wall currents are believed to expand across the erodible bed through the feed-back mechanism when existing spiral currents induce formation of a longitudinal sediment ridge which, in turn, creates another pair of spiral currents with axes parallel to the flume walls, and so on (Nezu and Nakagawa 1993). Adjacent currents, with opposite directions of rotation, form zones of alternating convergent-upward (corresponding to ridges) and divergent-downward (corresponding to troughs) movements of water flow promoting lateral bedload transport. There are also studies which relate the generation of secondary flows and, as a result, longitudinal bed forms in poorly sorted sediments with lateral variations in bed roughness (e.g., Tsujimoto 1989, Colombini and Parker 1995, McLelland et al. 1999).

However, as the movement of bed particles is affected by passing large-scale turbulent eddies shown in Figure 6.2, the development of the longitudinal bed features with the observed preferential transport of bed particles along the troughs can be considered as an indirect indication of the three-dimensional structure of the eddies with the eddy width of $\approx 2h$. This speculation is supported by direct measurements of Imamoto and Ishigaki (1986b) who recorded depth-scale circular motion of neutral tracers over an immobile bed in both longitudinal and transverse directions. This is also consistent with experimental results of Zaitsev (1984) and Tamburrino and Gulliver (1999), who came to the same conclusion about three-dimensional structure of the depth-size turbulent eddies.

Thus, based on the results of the present experiments and previous flow visualization studies, the general spatial structure of the open-channel turbulent flow can be represented by the model sketched in Figure 6.9. This model is similar to that proposed by Tamburrino and Gulliver (1999), but with a greater longitudinal dimension of the eddies (Tamburrino and Gulliver gave $L_E = 2h$). The downstream movement of the three-dimensional macroturbulent eddies shown in Figure 6.9 will cause quasi-periodic fluctuations of the local flow velocity vector, and in the fixed coordinate system will be seen by an observer as circular fluid motions known as "secondary currents". Hence, the existence of the organized movement of three-dimensional depth-scale turbulent eddies along stable paths may explain the commonly observed alternation of high-speed and low-speed regions in both streamwise and spanwise directions in a turbulent flow which are reflected in the character of sediment motion and bed pattern developed. As the macroturbulent eddies have been detected above both

rigid (Klaven 1966, 1968, Imamoto and Ishigaki 1986a, 1986b) and mobile beds (Klaven and Kopaliani 1973, present study), their existence is thus independent of the presence of the bed forms and may be viewed as self-organisation mechanism of open-channel turbulent flow.

6.4 Conclusions

From the results of the present study the following general picture of the macroturbulent structure of the open-channel flow and turbulence driven processes on the mobile sediment bed emerges. The turbulent flow appears to consist of not random fluid motions but rather an ordered sequence of persistent three-dimensional large-scale turbulent eddies (Figures 6.2 and 6.9). The vertical size of these eddies is close to the flow depth, the longitudinal size is between two and 12 depths (around 4-5 depths on average), and the transverse size is about two depths. These eddies move downstream at the bulk flow velocity. This causes quasi-periodic high-forward-speed downwelling ("sweeps") and burst-like upwelling ("ejections") fluid motions throughout the entire flow depth, resulting in quasi-periodic fluctuations of the flow velocity vector. The movement of the eddies takes place along relatively stable paths ("macrojets") and is responsible for the existence of alternating high-speed and low-speed regions in both the streamwise and spanwise directions. The up-and-down movement of fluid due to the eddy motion exerts fluctuating lift and drag hydrodynamic forces on the bed particles in a cyclical manner. These forces when strong enough cause displacement of bed particles most susceptible to movement. As the movement of bed sediment is affected by passing turbulent eddies, it has a patchy and intermittent character and is concentrated along the paths of eddies motion. This results in the alternation of longitudinal stripes of active and inactive sediment transport causing the development of longitudinal troughs and ridges with spacing of about two depths (Figures 4.15 and 4.16 of Chapter 4).

Given the remarkable similarity of the results of the present experiments with other flow visualization studies (Klaven 1966, 1968, Klaven and Kopaliani 1973, Imamoto and Ishigaki 1986a, 1986b, Tamburrino and Gulliver 1999), one may conclude that the observed large-scale turbulent structure is not an accidental coincidence of facts or due to the imagination of a researcher but a common phenomenon in open-channel

flows. The established organized depth-scale fluid motions appear to play an important part in the mechanism of the open-channel turbulence and bed particles transport and, therefore, should be taken into account in predicting methods.

Table 6.1 Hydraulic Conditions During Turbulence Measurements (Armfield Flume)

Experiment	Measuring Equipment	Sediment Size d (mm)	Slope J x 10^3	Flow Depth h (m)	Flow Velocity U (m s^{-1})	Transport Intensity* I x 10^4 (s^{-1})
Flow visualization	Video camera	2.40-7.15	4.1-8.3	0.025-0.100	0.41-0.98	0-2000
	Still camera	2.40-7.15	4.1-6.5	0.030-0.100	0.38-0.98	0-150
Velocity fluctuations	ADV	4.50-7.15	6.5	0.063-0.107	0.77-0.99	0.7-4.0

* estimated from data on incipient motion of uniform sediments

Table 6.2 Characteristics of Large-Scale Turbulent Eddies in Armfield Flume

Sediment Size d (mm)	Flow Width B (m)	Slope J x 10^3	Flow Depth h (m)	Flow Velocity U (m s^{-1})	Number of Images	Eddy Length L_E		Relative Length L_E / h		Eddy Period T_E		Transport Intensity* I x 10^4 (s^{-1})
						Mean (m)	Standard Deviation (m)	Mean	Standard Deviation	Mean (s)	Standard Deviation (s)	
2.40	0.30	4.1	0.0316	0.38	5	0.11	0.01	3.4	0.2	0.28	0.01	~0
			0.0402	0.46	9	0.17	0.02	4.3	0.5	0.37	0.04	0.6
			0.0458	0.53	2	0.15	0.00	3.3	0.0	0.29	0.00	10**
			0.0508	0.60	12	0.21	0.04	4.1	0.8	0.35	0.07	25**
			0.0594	0.66	8	0.28	0.06	4.6	1.0	0.42	0.09	100**
2.40	0.30	6.5	0.0300	0.46	55	0.19	0.07	6.5	2.2	0.42	0.14	2.0
			0.0316	0.48	28	0.22	0.06	7.1	1.8	0.46	0.12	10**
			0.0340	0.53	10	0.15	0.03	4.4	1.0	0.28	0.06	40**
			0.0356	0.56	12	0.21	0.05	5.8	1.5	0.37	0.10	150**
4.50	0.30	6.5	0.0593	0.69	54	0.30	0.09	5.1	1.4	0.44	0.12	0.1
			0.0630	0.77	22	0.30	0.06	4.8	1.0	0.40	0.08	0.7
5.65	0.30	6.5	0.0813	0.78	31	0.33	0.09	4.0	1.1	0.42	0.12	1.7
7.15	0.30	6.5	0.0300	0.40	13	0.20	0.04	6.8	1.3	0.51	0.10	~0
			0.0400	0.49	32	0.20	0.05	5.0	1.3	0.41	0.11	~0
			0.0500	0.61	3	0.16	0.03	3.2	0.7	0.27	0.05	~0
			0.0700	0.72	15	0.29	0.08	4.1	1.1	0.40	0.11	~0
			0.0895	0.93	12	0.32	0.06	3.6	0.6	0.34	0.06	0.1
			0.1000	0.98	39	0.39	0.07	3.9	0.7	0.40	0.07	1.0

* estimated from data on incipient motion of uniform sediments

** longitudinal ridges and troughs developed on the bed

Table 6.3 Summary of Other Flow Visualization Studies

Source	Flume Width B (m)	Camera Type	Grain Size d (mm)	Slope J x 10^3	Flow Depth h (m)	Flow Velocity U (m s^{-1})	Bed Sediment Mobility
Klaven and Kopaliani (1973)	0.21	Movie	3-14	6.7-10	0.050-0.052	0.54-0.56	No/Weak
Imamoto and Ishigaki (1986a)	0.20	Still/Video	12	2.0	0.040	0.19	Fixed bed

Table 6.4 Turbulence Characteristics in Armfield Flume (slope 0.0065)

Sediment Size d (mm)	Flow Depth h (m)	Flow Velocity U (m s^{-1})	Shields Stress τ^*	Turbulent Intensity		Vertical Velocity v_{95} (m s^{-1})	Mobility Parameter M_L Eq.(6.7)	Transport Intensity* I x 10^4 (s^{-1})
				Streamwise σ_u (m s^{-1})	Vertical σ_v (m s^{-1})			
(a) τ^*=0.048								
4.50	0.0630	0.77	0.048	0.092	0.025	0.041	0.022	0.7
5.65	0.0813	0.78	0.048	0.098	0.030	0.049	0.026	1.7
7.15	0.1066	0.99	0.048	0.117	0.036	0.060	0.032	4.0
(b) I=10^{-4} s^{-1}								
4.50	0.0649	0.82	0.049	0.092	0.027	0.044	0.026	1.0
5.65	0.0799	0.77	0.047	0.099	0.031	0.050	0.027	1.0
7.15	0.0995	0.98	0.045	0.108	0.034	0.056	0.027	1.0

* estimated from data on incipient motion of uniform sediments

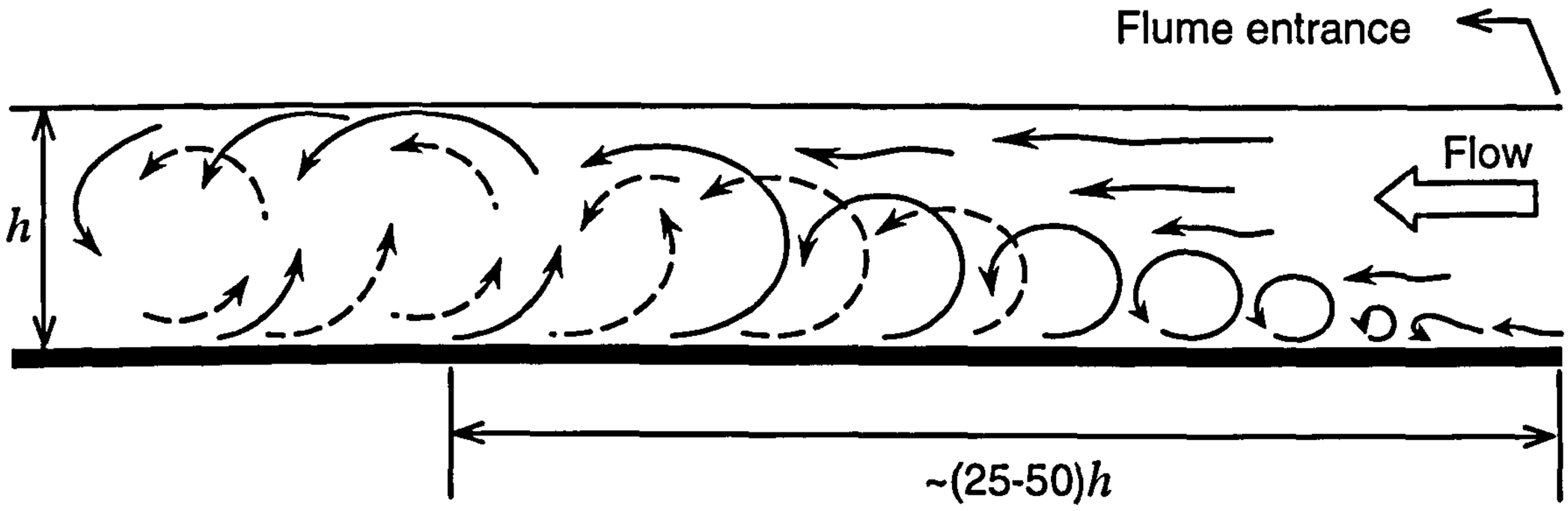

Figure 6.1 Development of rotational movement of flow in flume experiments (from videos of neutral tracers motion).

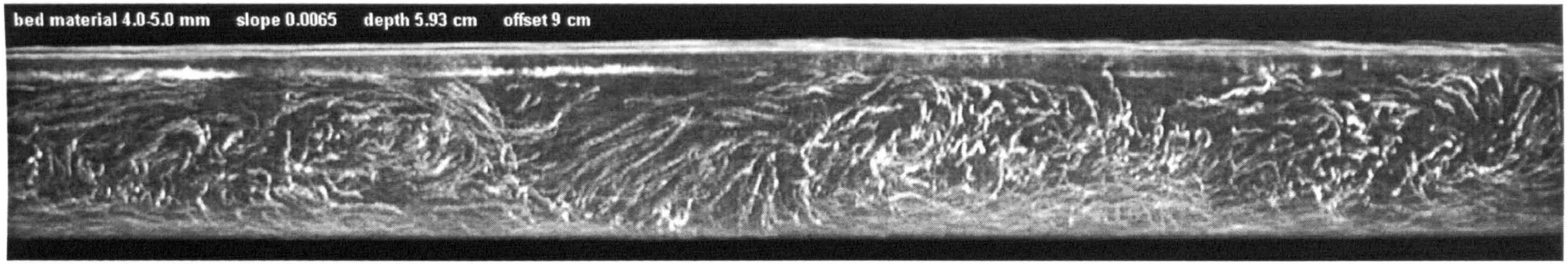

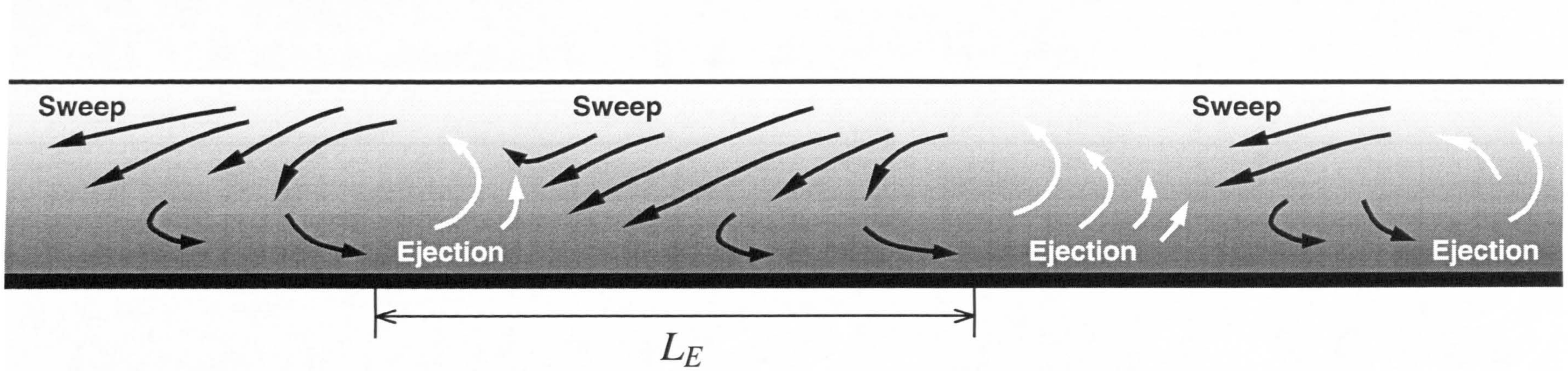

Figure 6.2 Large-scale turbulent structure of open-channel flow over mobile gravel beds (camera is moving with mean flow velocity). Flow right to left.

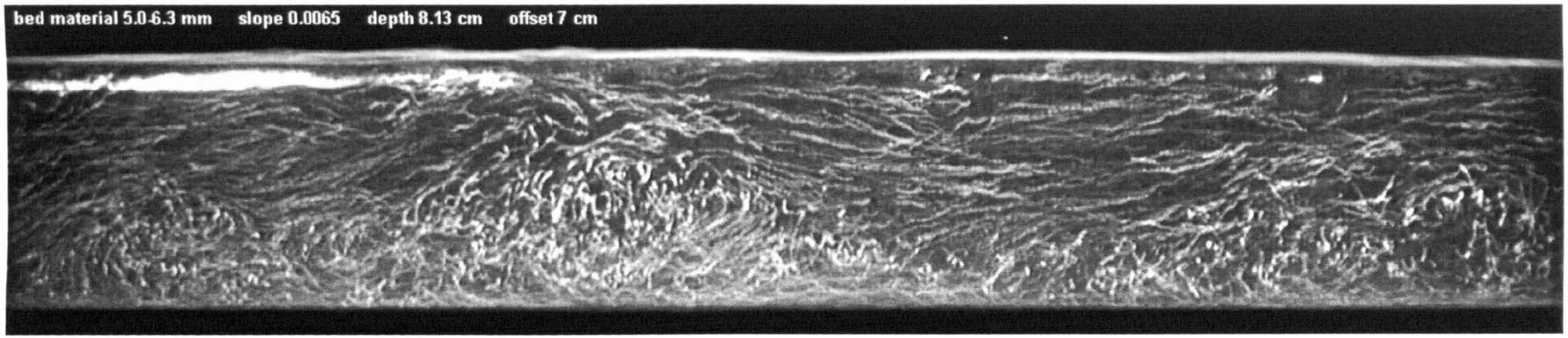

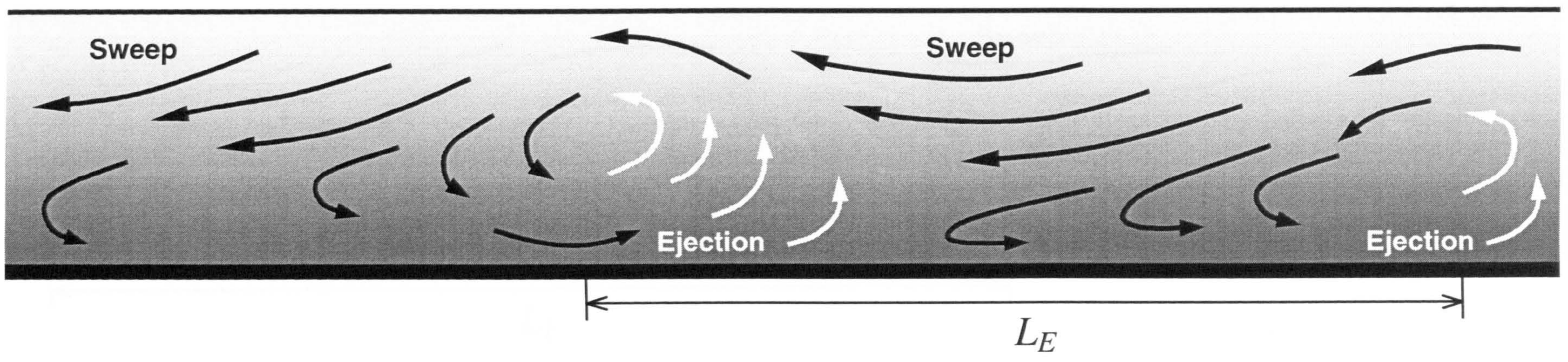

Figure 6.2 (continued).

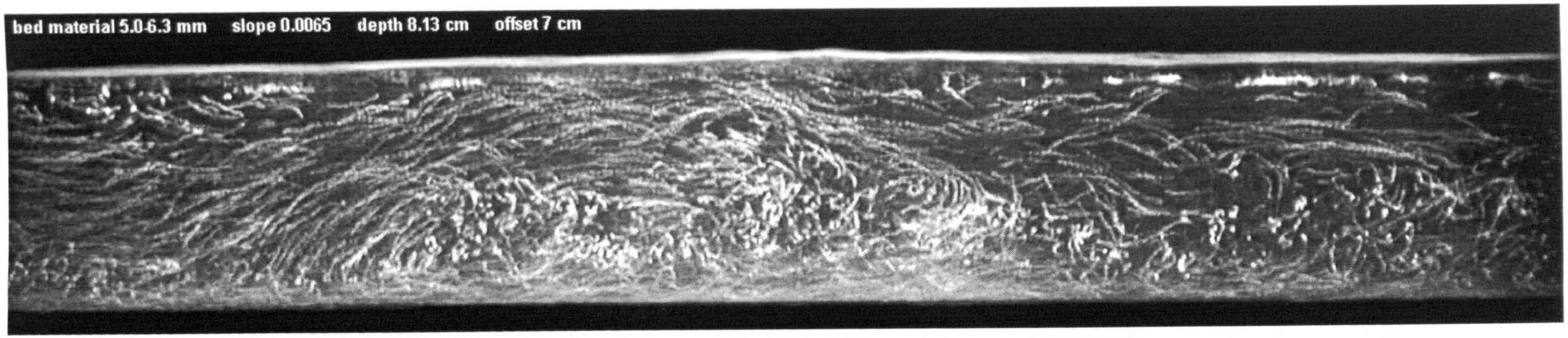

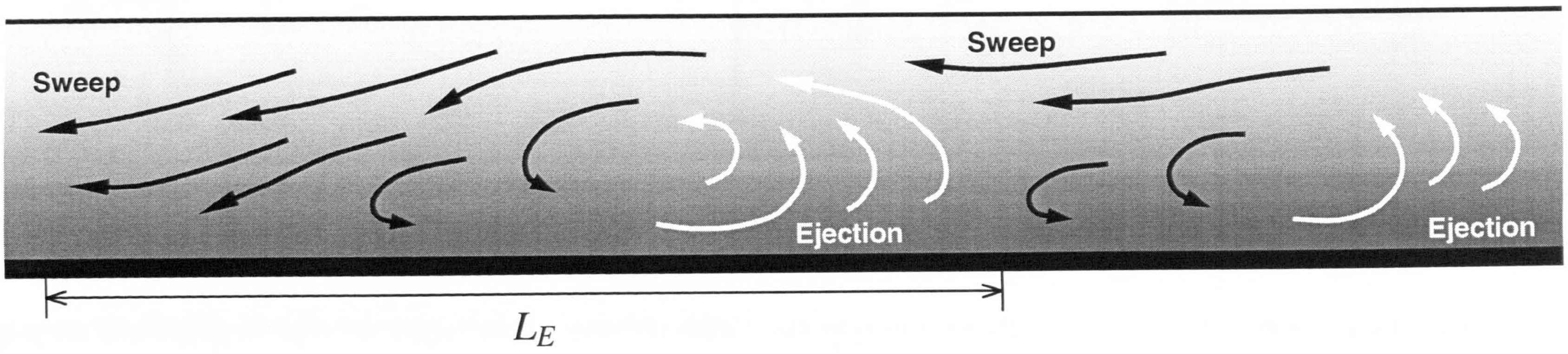

Figure 6.2 (continued).

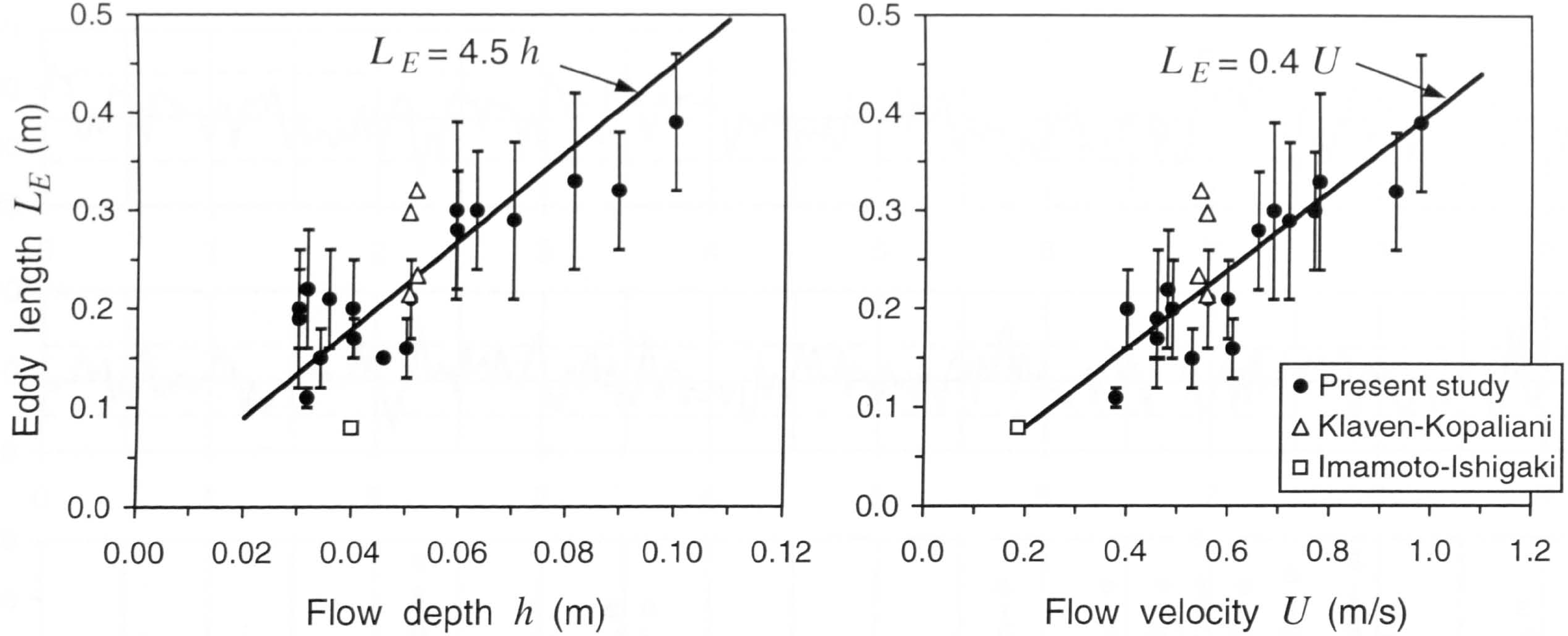

Figure 6.3 Relationship of depth-size eddy length L_E with flow depth h and mean flow velocity U. Error bars indicate standard deviations.

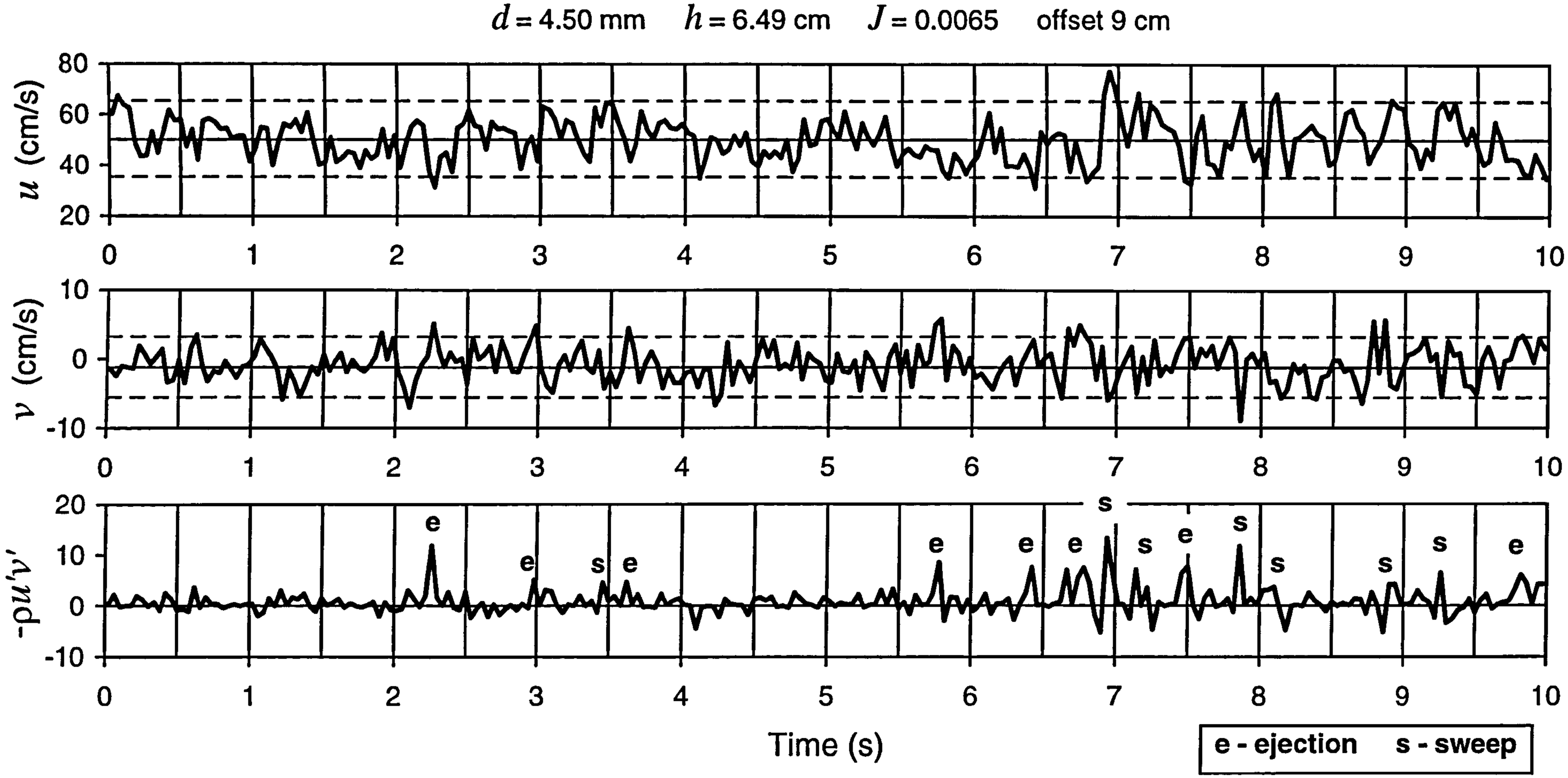

Figure 6.4 Streamwise u and vertical v instantaneous flow velocity data with 95% confidence intervals (dashed lines) and Reynolds stress $-\rho u'v'$.

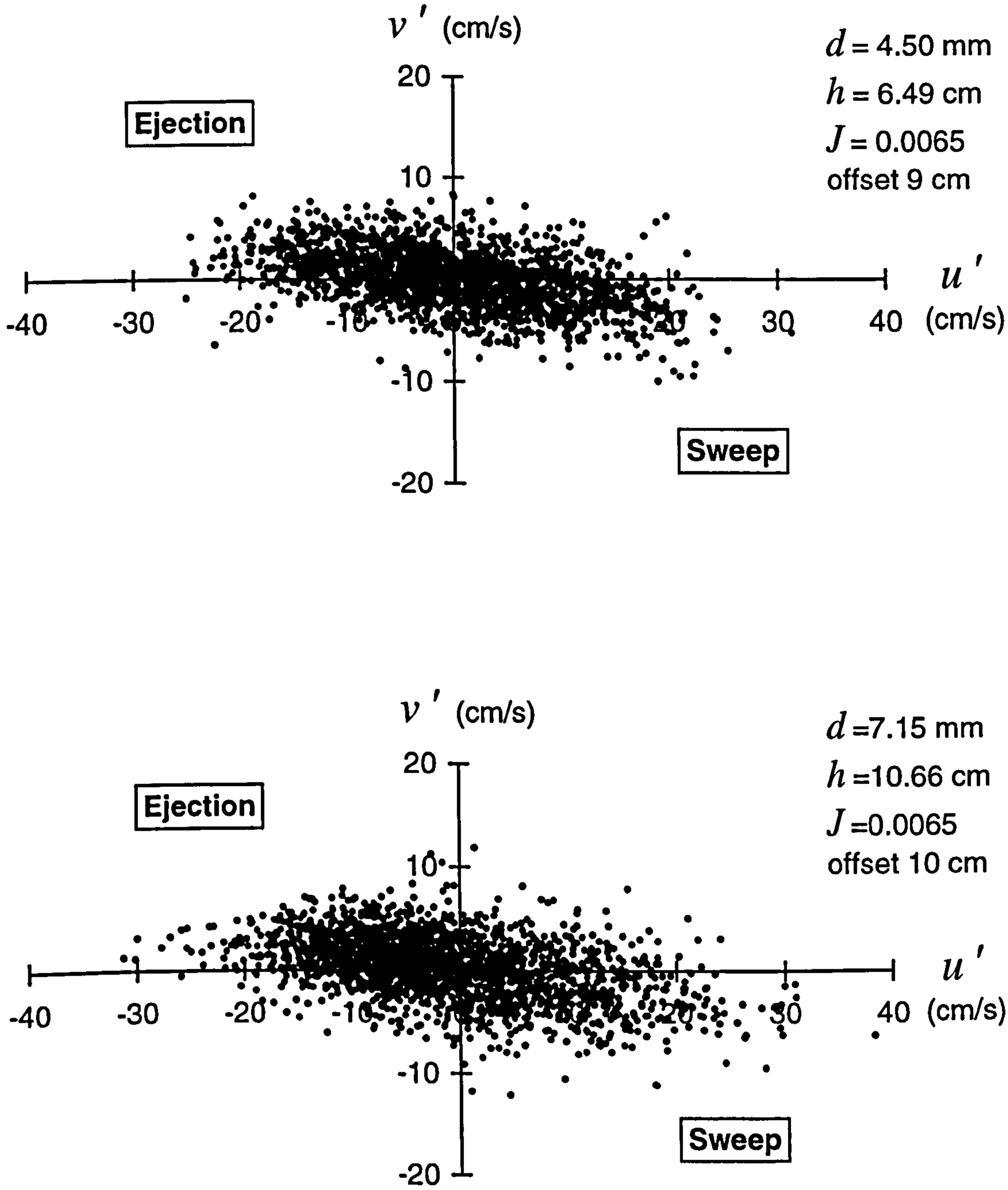

Figure 6.5 Quadrant plot of streamwise u' and vertical v' flow velocity fluctuations.

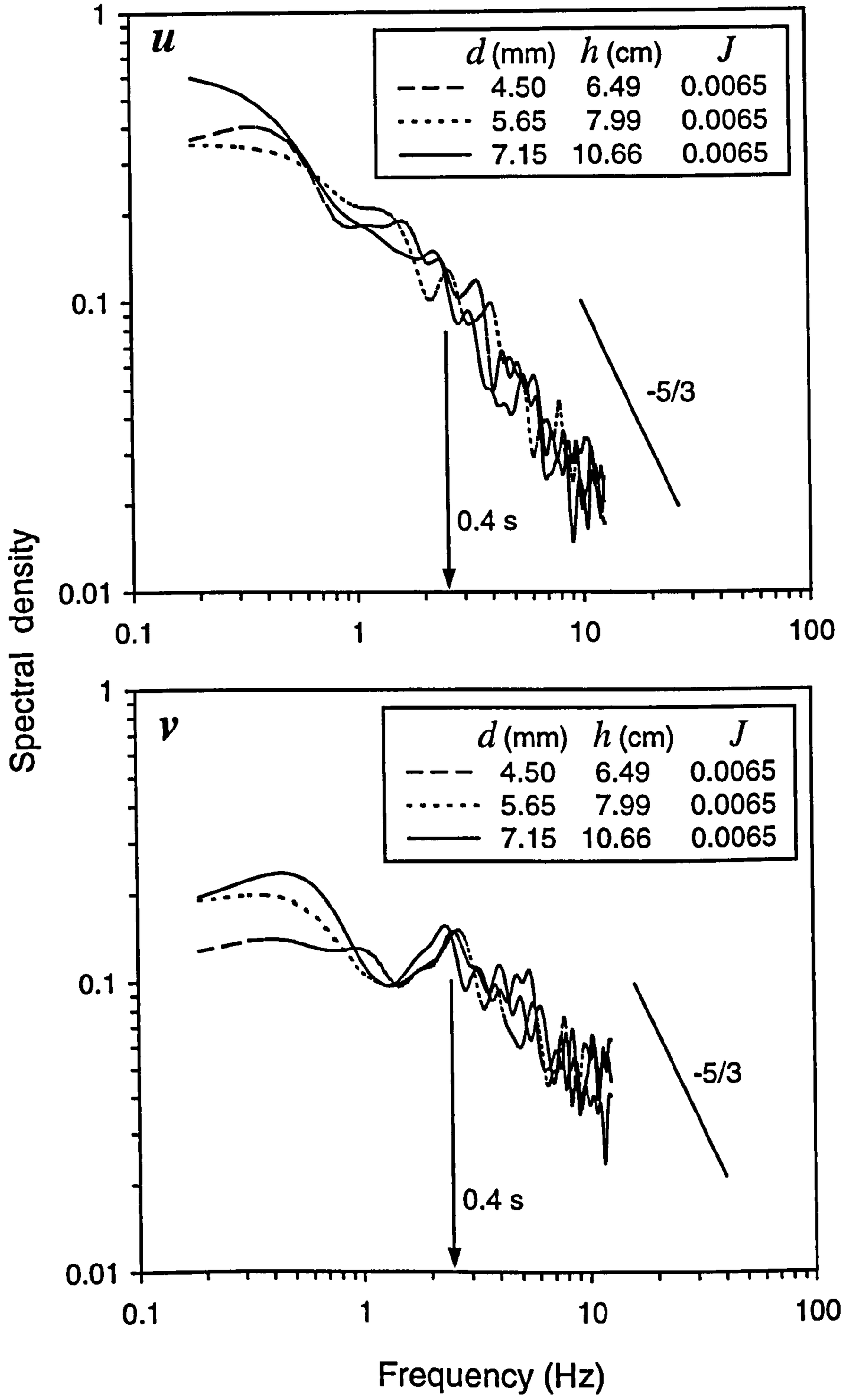

Figure 6.6 Distribution of energy spectra for streamwise u and vertical v flow velocity components (offset 9-10 cm).

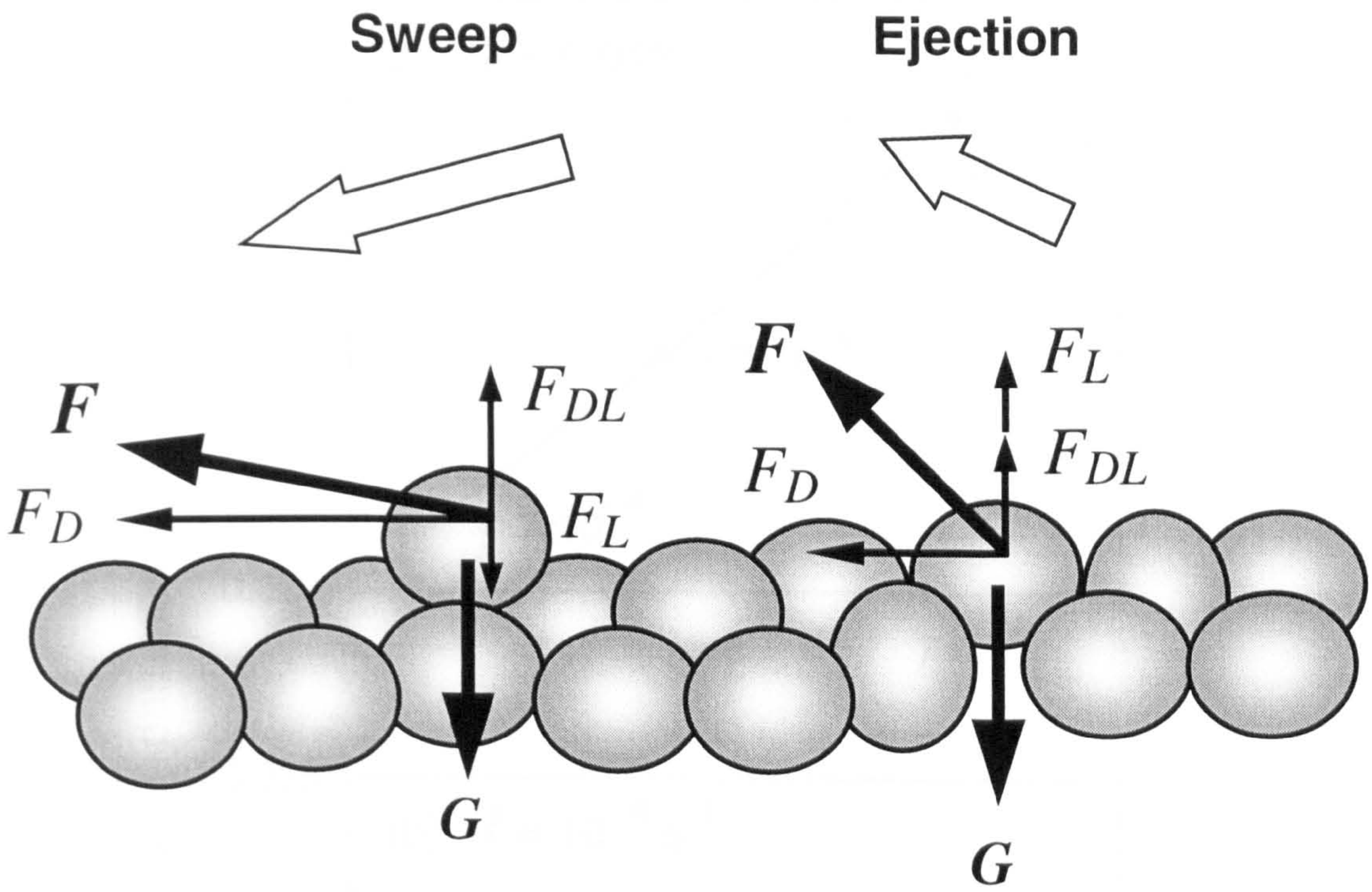

Figure 6.7 Diagram of forces acting on bed particles (F_D is the drag force, F_{DL} is the dynamic lift force, F_L is the direct lift force, F is the resultant hydrodynamic force, and G is the grain weight).

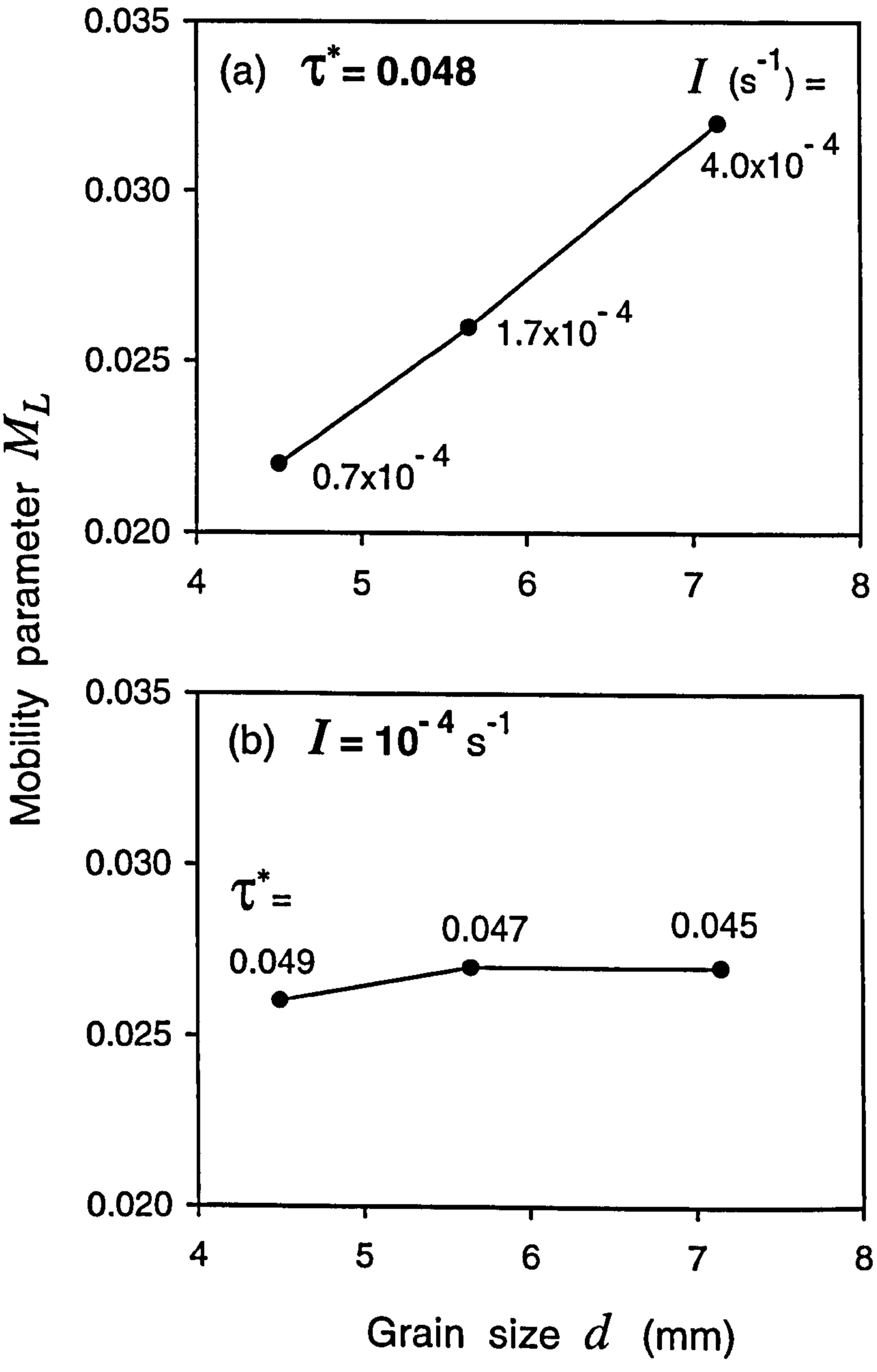

Figure 6.8 Mobility parameter M_L against grain size d for (a) constant Shields stress τ^*=0.048, and (b) constant transport intensity I=10^{-4} s^{-1}.

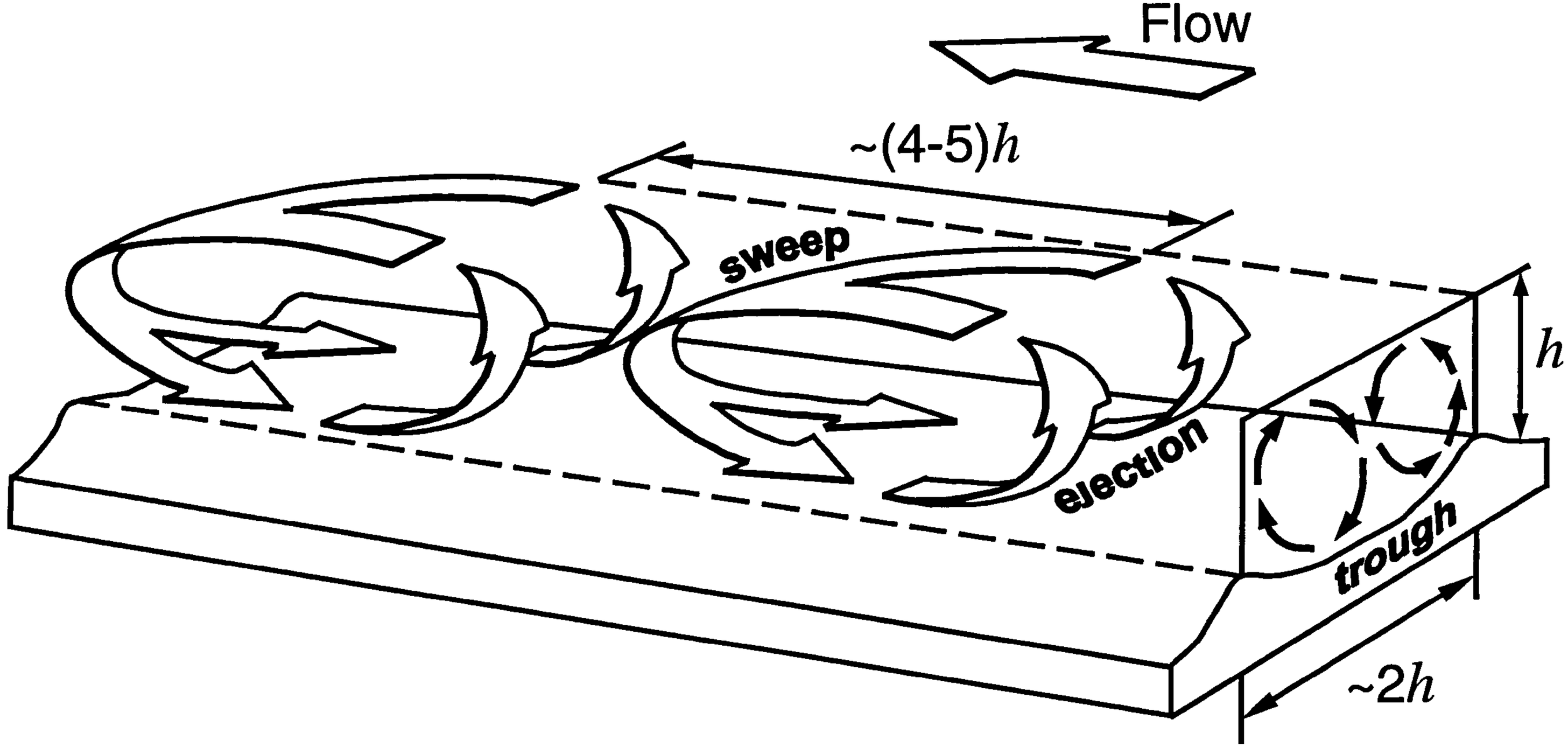

Figure 6.9 Model of three-dimensional large-scale turbulent structure of open-channel flow over a mobile bed (coordinate system is moving with bulk flow velocity).

7

Implementation and Testing of Bedload Transport Model

"To study the laws of Nature does satisfy the mind, but it also does serve an utilitarian purpose: ... The theory must be applied to the practice ..."

(DuBuat)

7.1 A New Model for Weak Bedload Transport

Many field gravel-bed streams are characterised by low bed shear stresses with inactive bedload transport most of the time (Charlton et al. 1978, Andrews 1984, 1994, Milhous 1997). Even at bankfull conditions, the bed shear stress often exceeds the critical stress for bed material movement only moderately and is rarely more than two or three times the critical value, even during severe floods (Parker et al. 1982, Wathen et al. 1995). A substantial portion of the bed material transported over a period of years is carried out under marginal transport conditions when the flow is capable of transporting relatively few bed particles at any time. Therefore, an accurate prediction of the behaviour of bed sediment in gravel-bed streams requires a proper description of the process of near-to-threshold bedload motion. However, most of the available bedload equations are derived for active sediment transport. More over, none of these accounts for the effect of bed slope on sediment mobility, which is shown in previous chapters to be an important factor for adequate prediction of near-to-threshold bedload transport.

The set of transport relationships [(4.12), (5.3), (5.5), (5.6), and (5.7)] derived in this study for the characterization of the incipient motion of streambeds represents a new surface-based model of weak bedload transport. This model describes near-to-threshold transport of uniform and graded (unimodal and weakly bimodal) natural sands and gravels on a flat bed under quasi-uniform flow conditions and is summarized below (all variables are expressed in m-kg-s units).

General bedload transport relationship:

$$q_{bi}^{*} = \left(\frac{a_{50}\, \tau_i^{*}}{b\, \varepsilon_i} \right)^{18} J^{-5.0} \tag{7.1}$$

Normalized Einstein bedload parameter:

$$q_{bi}^{*} = \frac{q_{bi}}{f_i\, \rho_s \sqrt{(s-1)\, g\, d_i^{3}}} \tag{7.2}$$

Shields stress:

$$\tau_i^{*} = \frac{\tau}{g\, (\rho_s - \rho)\, d_i} \tag{7.3}$$

Particle mobility factor:

$$a_{50} = -1.1\, [\log(1000\, d_{50})]^{3} + 4.8\, [\log(1000\, d_{50})]^{2} - 5.0 \log(1000\, d_{50}) + 4.6 \tag{7.4}$$

Mixture mobility factor:

$$b = 2.5\, [\log(\sigma_g)]^{4.0} + 1 \tag{7.5}$$

Hiding function:

$$\varepsilon_i = \begin{cases} \left(\dfrac{d_i}{d_{50}} \right)^{-e} & \text{for} \quad \dfrac{d_i}{d_{50}} \le 1 \\ \left[\log\left(10\, \dfrac{d_i}{d_{50}} \right) \right]^{-2.2} & \text{for} \quad \dfrac{d_i}{d_{50}} \ge 1 \end{cases} \tag{7.6}$$

Exponent in hiding function:

$$e = 2.0\, \sigma_g^{-0.10} \{0.049\, [\log(1000\, d_{50})]^{3} - 0.26\, [\log(1000\, d_{50})]^{2} + 0.33 \log(1000\, d_{50}) + 1.20\} - 1.4 \tag{7.7}$$

Mixture geometric standard deviation (for bed surface):

$$\sigma_g = \sqrt{\frac{d_{84}}{d_{16}}} \tag{7.8}$$

In the above equations q_{bi} is the fractional transport rate (dry weight) per unit width, f_i is the proportion of fraction i in the bed surface, d_i is the mean size of fraction i, d_{50} is the median grain size for the bed surface, ρ_s is the sediment density, ρ is the fluid density, $s = \rho_s/\rho$ is the specific density, g is the gravitational acceleration, $\tau = \rho g R_b J$ is the bed shear stress, J is the slope, $R_b = R\left(n_g/n\right)^{3/2}$ is the hydraulic radius of the bed corresponding to grain roughness, R is the hydraulic radius, $n_g = 0.048\, d_{50}^{1/6}$ is the grain roughness coefficient, and n is the overall Manning roughness coefficient of the channel.

The above bedload transport model is restricted for $q^*_{b50} \leq 10^{-2}$ (value of q^*_{bi} for $d_i = d_{50}$), d_{50}=1-124 mm and J=0.001-0.070. It can be used for predicting the behaviour of coarse-grained streambeds under marginal transport conditions, which are typical of gravel-bed streams. In the following sections an example of implementation of this model in the existing computer software ISIS Flow/Sediment is demonstrated and its performance for simulating graded sediment transport is tested.

7.2 ISIS Flow/Sediment

ISIS Flow is a computer program developed jointly by Halcrow Group Ltd, U.K. and HR Wallingford Ltd, U.K. for modelling steady and unsteady flows in open channels. ISIS Sediment is a mobile bed sediment transport module for the ISIS Flow program. By the use of this module ISIS Flow can predict sediment transport rates, bed elevations and amounts of erosion/deposition throughout a channel system with a bed composed of either uniform or graded sediments. The following is a brief discussion of the hydrodynamic and mobile bed portions of this simulation package. The discussion is not intended to provide a complete description of the package, as it addresses only those parts that are used for modelling the behaviour of graded sediments. For more detailed information about ISIS Flow and ISIS Sediment see Halcrow/HR Wallingford (1997, 1999).

7.2.1 Hydrodynamics

The modelling of the free surface flow is based on the Saint-Venant equations, which express conservation of mass and momentum of the water body one-dimensionally. Conservation of mass leads to the "continuity" equation, which establishes a balance between the rate of rise of water level and wedge and prism storage. Conservation of momentum leads to the "dynamic" equation, which establishes a balance between inertia, gravity and friction forces.

The governing equations are the continuity equation

$$\frac{\partial Q}{\partial x}+\frac{\partial A}{\partial t}=q_l \tag{7.9}$$

and the momentum equation

$$\frac{\partial Q}{\partial t}+\frac{\partial}{\partial x}\left(\frac{\beta Q^2}{A}\right)+g\,A\frac{\partial H}{\partial x}-g\,A\frac{Q|Q|}{K^2}+q_l\frac{Q}{A}\cos\alpha=0 \tag{7.10}$$

where Q is the water flow, A is the cross-section area, q_l is the lateral inflow, x is the longitudinal channel distance, t is the time, H is the water surface elevation above datum, β is the momentum correction coefficient, g is the gravitational acceleration, α is the angle of inflow, $K=A\,R^{2/3}/n$ is the channel conveyance, n is the Manning roughness coefficient, R is the hydraulic radius.

The assumption made in order to derive these equations are: (a) the flow is one-dimensional, i.e. a single velocity and elevation can be used to describe the state of the water body in a cross-section; (b) the streamline curvature is small and vertical accelerations negligible, hence the pressure is hydrostatic; (c) the effects of boundary friction and turbulence can be accounted for by representations of channel conveyance derived for steady state flow; (d) the average channel bed slope is small enough such that the small angle approximation can be used; and (e) all the functions and variables are continuous and differentiable.

The Preissmann four-point implicit finite difference scheme is employed in ISIS Flow to provide a linearisation and solution to the linear version of the Saint-Venant equations. Let f be the value of depth or discharge or a function of depth or discharge at longitudinal position $x_{k+1/2}$ and at time $t_{i+\theta}$, where k is the position index, which

increases in the downstream direction, and i is the time index. The value of f or its continuous derivatives with respect to space and time can be discretised as:

$$f(x,t)=\frac{1}{2}\left[\theta\left(f_{k+1}^{i+1}+f_{k}^{i+1}\right)+(1-\theta)\left(f_{k+1}^{i}+f_{k}^{i}\right)\right] \tag{7.11}$$

$$\frac{\partial f}{\partial x}=\frac{1}{2\,\Delta x}\left[\theta\left(f_{k+1}^{i+1}-f_{k}^{i+1}\right)+(1-\theta)\left(f_{k+1}^{i}-f_{k}^{i}\right)\right] \tag{7.12}$$

$$\frac{\partial f}{\partial t}=\frac{1}{2\,\Delta t}\left[\left(f_{k+1}^{i+1}-f_{k+1}^{i}\right)+\left(f_{k}^{i+1}-f_{k}^{i}\right)\right] \tag{7.13}$$

where θ is a weighting factor lying between 0.5 and 1, Δx is the distance step, Δt is the time step, and f_k^i is the value of f evaluated at position x_k at time t_i.

Using the above, both Saint-Venant equations can be transformed into their linear form:

$$c_1\,Q_k^{i+1}+c_2\,H_k^{i+1}+c_3\,Q_{k+1}^{i+1}+c_4\,H_{k+1}^{i+1}=c_5 \tag{7.14}$$

The values of $c_1 \ldots c_5$ are calculated for each iteration and each node in the open channel and depend on variables calculated at the previous iteration or time step.

The external boundary and initial conditions must be applied to provide a well-posed mathematical problem. For sub-critical flow, which is of primary interest, the upstream boundary condition is normally specified as a discharge hydrograph and the downstream conditions as a stage hydrograph or a stage-discharge curve.

7.2.2 Mobile bed module

The modelling of sediment bed evolution is based on the sediment continuity equation:

$$(1-p)\,B\,\frac{\partial z}{\partial t}+\frac{\partial G}{\partial x}=0 \tag{7.15}$$

where p is the bed porosity, B is the flow width, z is the bed elevation, and G is the volumetric bedload discharge. This equation assumes that the rate of change of sediment entrained in the flow is negligible in comparison with the terms expressing the rate of change in bed elevation and change in transport rate.

Equation (7.15) is discretised in the following form:

$$(1-p)B_{k+1}\frac{\Delta z_{k+1}}{\Delta t}+\frac{G_{k+1}^{i+1}-G_{k}^{i+1}}{\Delta x}=0 \qquad (7.16)$$

where Δz is the change in bed elevation over time step Δt. This equation can be solved explicitly for Δz as G_{k+1}^{i+1} is calculated by the sediment transport equation and G_{k}^{i+1} will have been determined previously.

Central to successful simulation of the mobile bed is the use of an appropriate sediment transport equation. The original version of ISIS Sediment offers a choice of three sediment transport equations for non-cohesive sediments: (a) Engelund and Hansen (1967); (b) Ackers and White (1973); and (c) the revised version of the Ackers and White equation (Ackers 1993). Among these equations, the Ackers and White total load transport function is the most appropriate for coarse sediments. The revised form of the Ackers and White function will be used later for comparative computations and its general form is given below:

$$G_{gr}=C\left[\left(F_{gr}-A_{gr}\right)/A_{gr}\right]^{m} \qquad (7.17)$$

where G_{gr} is the sediment transport parameter,

$$G_{gr}=\frac{q_b}{\rho_s\, d\, U}\left(\frac{U_*}{U}\right)^{n} \qquad (7.18)$$

F_{gr} is the particle mobility parameter,

$$F_{gr}=\frac{U_*^n}{\sqrt{g\, d\,(s-1)}}\left[\frac{U}{\sqrt{32}\log(10\,h/d)}\right]^{1-n} \qquad (7.19)$$

A_{gr} is the threshold value of F_{gr} at sediment initial motion, q_b is the total load transport rate per unit width (dry weight), d is the grain size, ρ_s is the sediment density, U is the mean flow velocity, U_* is the shear velocity, g is the gravitational acceleration, s is the specific density of sediment, and h is the flow depth. The parameters n, A_{gr}, m, and C depend on dimensionless grain diameter $d_* = d\left[g\,(s-1)/k^2\right]^{1/3}$ and are defined as: for $d_*>60$ (coarse sediment, $d>2$ mm) $n=0$, $A_{gr}=0.17$, $m=1.78$, $C=0.025$; for $1<d_*<60$ (transitional and fine sediments, $0.06<d<2$ mm) $n=1-0.56\log d_*$, $A_{gr}=0.14+0.23/\sqrt{d_*}$, $m=1.67+6.83/d_*$, $\log C=-3.46+2.79\log d_*-0.98\left(\log d_*\right)^2$.

The above transport functions are originally derived for uniform sediments and in ISIS Sediment are applied to sediment mixtures on the basis of the assumption that each size fraction is not affected by the presence of other fractions and that each fraction is distributed uniformly in the bed (classical approach). The calculated transport rate for a given size fraction is multiplied by the proportion of that fraction in the bed surface, without accounting for relative size effects.

ISIS Sediment employs a three-layer conceptualisation of the mobile bed for modelling sorting effects in graded sediments. These layers are: (a) an active layer at the surface of the channel bed; (b) a deposited layer below it; and (c) the parent bed material below the deposited layer. The quantity of sediment in each of these layers is recorded at each channel section for each sediment fraction. If there is net erosion at a section, then the deposited layer is not present. As deposition or erosion causes an exchange between the material in the active layer and the material in transport, the composition of the active layer is updated. For example, in the case of erosion from a widely graded bed material, the finer sediments will be brought into transport more rapidly than the coarser sediments. So the proportion of the active layer consisting of the coarsest fraction will increase and the proportion of the finer fractions will decrease. If some fractions are not eroded at all, then the active layer will eventually stabilise to an armoured state for which only non-mobile sediments are present in the active layer. The active layer thickness is set as a factor on the local d_{95} bed material size and does not change during the computations so that for erosion the material eroded from the active layer is replaced by an equal quantity of material taken from the layer below (the deposited layer if present or alternatively the parent material). In the case of deposition,

the material being added into the active layer is matched by an equal volume of material passed from that layer into the deposition layer.

For the modelling of mobile bed evolution, the upstream boundary conditions must be specified as sediment inflow transport rate against time, concentration against time or concentration against water flow. The bed elevation is free to move at both upstream and downstream boundaries.

The sediment transport and mobile bed evolution are calculated at each time step in the following sequence: (a) calculate the hydraulic variables of flow, stage, and velocity in the usual way; (b) starting at the upstream end of the channel, loop around the nodes calculating the sediment transport capacity and solving the sediment continuity equation for depth of erosion/deposition; (c) update the channel conveyance tables to allow for any calculated deposition or erosion ready for the next time step.

The calculated parameters include sediment mass balance, sediment transport rates, volumes of erosion and deposition, composition of the cumulative bedload, active layer composition, and bed elevation.

7.3 Development of ISIS Sediment

The model of weak bedload transport derived in this study and presented above [equations (7.1)-(7.8)] is coded and incorporated into ISIS Sediment mobile bed module. The following is the bedload transport subroutine written in Fortran 77:

```
12345678901234567890123456789012345678901234567890123456789012345678901234567890

      subroutine bedload(tau, slope, dens, densty, d50, sigma,
     +                   di, fi, qbi)

c  calculates fractional bedload transport rate (dry weight)
c  per unit width (kg/s/m)
c
c  Invocation
c     It calls: none
c     Called:   for each size fraction
c
c  Arguments
c  INPUT:
c     tau       bed shear stress (kg/m/s2)
c     slope     water surface slope (m/m)
c     dens      water density (kg/m3)
c     densty    sediment density (kg/m3)
c     d50       median size for bed surface (m)
c     sigma     geometric standard deviation for bed surface
```

```
c                 =sqrt(d84/d16)
c     di          mean diameter for i-th size fraction (m)
c     fi          proportion of i-th size fraction in bed surface
c
c  OUTPUT:
c     qbi         fractional bedload transport rate (dry weight)
c                   per unit width (kg/s/m)
c
c  Other variables
c     taustar     Shields stress for di
c     qbstar      normalised Einstein bedload parameter for di
c     a50         particle mobility factor for d50
c     b           mixture mobility factor
c     e           exponent in hiding function
c     epsi        hiding function
c     x           temporal variable
c
c  Restrictions
c     0.001m<d50<0.124 m, 0.002<slope<0.090, qbstar(d50)<0.01


      real tau, slope, dens, densty, d50, sigma, di, fi
      real qbi
      real taustar, qbstar, a50, b, e, epsi, x


c  Shields stress
      taustar=tau/((densty-dens)*9.81*di)

c  Particle mobility factor
      x=alog10(1000.0*d50)
      a50=-1.1*x**3.0+4.8*x**2.0-5.0*x+4.6

c  Mixture mobility factor
      b=2.5*(alog10(sigma))**4.0+1.0

c  Hiding function epsi
      if (di/d50.lt.1.0) then
c  Exponent e
        e=2.0/sigma**0.1*(0.049*x**3.0-0.26*x**2.0+0.33*x+1.2)-1.4
        epsi=(d50/di)**e
      else
        epsi=1.0/(alog10(10.0*di/d50))**2.2
      end if

c  Normalized Einstein bedload parameter
      qbstar=(a50*taustar/(b*epsi))**18.0/slope**5.0

c  Fractional weight bedload transport rate per unit width (kg/s/m)
      qbi=qbstar*fi*densty*sqrt((densty/dens-1.0)*9.81*di**3.0)

      return
      end
```

This subroutine allows the computation of fractional transport rates from the known bed shear stress and the composition of the surface layer. The subroutine is simple (although contains the results of the extensive three-year research) and can be easily incorporated into other existing hydrodynamic simulation packages. The

subroutine is called for each size fraction at each node and each time step. The results of the computations are then used to solve the sediment continuity equation (7.16).

The bedload transport function of Parker (1990) derived for poorly sorted mixtures of gravels and cobbles and based on the use of the hiding function has also been coded and added to ISIS Sediment. This was done to provide a comparison of the results of computations. The Parker function refers to the particle size distribution of the surface bed material and reads as follows:

$$W_i^* = \begin{cases} 13.685\left(1-\dfrac{0.853}{\phi_i}\right)^{4.5} & \phi_i > 1.59 \\ 0.0025\exp\left[14.2\left(\phi_i-1\right)-9.28\left(\phi_i-1\right)^2\right] & 1 \le \phi_i \le 1.59 \\ 0.0025\,\phi_i^{14.2} & \phi_i < 1 \end{cases} \qquad (7.20)$$

where $W_i^* = q_{bi}^* / \tau_i^{*3/2}$ is the Parker bedload parameter, $\phi_i = \tau_i^* / \tau_{ci}^*$ is the normalized Shields stress, and the reference (critical) dimensionless shear stress τ_{ci}^* is defined from hiding function $\tau_{ci}^* = \tau_{c50}^* \left(d_i / d_{50}\right)^{-e}$. This bedload function is similar to a function derived by Parker et al. (1982) referenced to the particle size distribution of subsurface bed material. The transport relationship (7.20) is acknowledged as one of the most appropriate for gravel-bed rivers and is often quoted and used by others (e.g., Wilcock and Southard 1988, Ferguson et al. 1989, Kuhnle 1993a, 1993b, Andrews 1994, Wathen et al. 1995, Wilcock et al. 1996, Andrews 2000). The problem with Parker's approach is that it does not consider the influence of bed slope on sediment mobility at near-to-threshold transport conditions as established as important in this study (see Section 4.3.3, Chapter 4 and Section 5.4.1, Chapter 5), as well as the existing uncertainties in the character of the hiding function and the value of τ_{c50}^* , which are required for fractionwise calculations (these issues are discussed in detail in Chapter 2). Here the values of $\tau_{c50}^* = 0.035$ and e=0.982 determined for Oak Creek (Parker and Klingeman 1982) are used for the comparative computations.

7.4 Test Database

The model of weak bedload transport developed in the present research was tested on the detailed graded sediment transport data collected by Glasgow and Aberdeen Universities using HR Wallingford tilting flume (Fuller 1998, Willetts et al. 1998). The flume, the experimental channel, and the measuring equipment were the same as used in the part of the present experiments with graded sediments. A detailed description of the research facilities and apparatus is given in Section 3.3 of Chapter 3 (Figures 3.9-3.14).

Bed material employed in the experiments was mixed from natural sediments and was characterised by a weakly bimodal distribution typical of many gravel-bed rivers with $d_{16} = 0.85$ mm, $d_{50} = 4.05$ mm, $d_{84} = 6.71$ mm, and $\sigma_g = 2.81$. The grain size distribution and the cumulative grading curve for the bed material are shown in Figure 7.1. The initial composition of the bed material was essentially identical to that of the mixture HR used in the present study of incipient motion of streambeds (see Table 3.2, Figures 3.15-3.16). However, during the experiments considered here the composition of the bed was constantly changing in response to the variable experimental conditions applied.

The experiments undertaken were designed to produce a partial sediment transport, i.e. the applied bed shear stress was only above threshold for part of the bed material size distribution. The aim of these experiments was to study the evolution of the graded sediment bed under different upstream sediment feed conditions. The granulometric composition of the feed sediment mixture is shown in Figure 7.1, and it is characterised by $d_{16} = 0.61$ mm, $d_{50} = 3.65$ mm, $d_{84} = 5.86$ mm, and $\sigma_g = 3.10$.

Hydraulic conditions in the six experiments used for the test computations are given in Table 7.1. The experiments were conducted for initially flat sediment bed, at a variety of bed slopes and the same initial depth of 0.15 m. Water discharge during the experiments was kept constant. In Table 7.1 the first three experiments (Nos. 4, 5, and 6) were degradation ones without sediment supply to the flume, while the other three (Nos. 8, 9, and 11) consisted of two phases: initial feed phase (with feeding sediment at a constant rate to the upstream end of the channel) and subsequent degradation phase. In the experiments Nos. 9 and 11 the feed rate was 5.0 g s^{-1}, which was close to the sediment transporting capacity of the flow, while in the experiment No. 8 the feed rate was set to half of that for the other two feed experiments.

The regularly measured characteristics were water discharge, water surface elevation, flow velocity distribution, air and water temperature, bedload transport rate, longitudinal bed profiles, bed surface texture, and bedload granulometric composition. During the experiments all the sediment sizes were transported in bedload mode under generally weak transport conditions. The measured values of q^*_{b50} were consistently lower than 10^{-2}. After each of the experiments wax samples of the bed surface were taken at different parts of the channel. These gave the final composition of the bed surface. The full description of the experimental procedures and detailed analysis of the data collected can be found in Fuller (1998) and Marion (1996).

7.5 Test Simulations

The simulation of the above experiments was undertaken using ISIS Sediment as a development template with the aim of testing the performance of the proposed model of weak sediment transport (7.1). To provide a comparison, the simulations were also made using the original version of ISIS Sediment with the Ackers-White transport equation (7.17) representing the classical approach to graded sediment calculations and using the Parker bedload function (7.20) with a hiding function representing the "equal mobility" concept.

Preliminary calculations demonstrate that these transport equations give very different results when applied to the fractionwise calculations in the experiments listed in Table 7.1. This is seen in Figure 7.2 showing the calculated and measured initial fractional transport rates from the bed surface layer with the known granulometric composition (initially the same as of the bulk bed material) in the experiments Nos. 4 and 11. These experiments have similar initial conditions, and yet almost one order of magnitude difference is seen in the measured data. This is typical of the variability of bedload transport in streams. As the measured data provide the basis for the comparison, this variability can be viewed as a general criterion for the assessing the overall performance of the empirical transport equations. It is seen from Figure 7.2 that the Ackers-White equation significantly overestimates the transport of fine size fractions ($d_i < d_{50}$) and underestimates the mobility of coarse fractions ($d_i > d_{50}$), giving no transport of particles larger than 8.0 mm. The Parker bedload function shows near equal transport mobility for different grain sizes (in accordance with Parker's

"equal mobility" concept), overestimating the transport of the end size fractions in the distribution. Nevertheless, the Parker function demonstrates significantly better results compared to the Ackers-White equation. Among the transport equations tested, the proposed one gives the best fit to the measured data. However, all the transport equations show similar results for the median size fractions (d_{50}) in the sediment mixture. The principal question emerging from the examination of Figure 7.2 is: What is the significance of the difference in the calculated fractional transport rates for the end size fractions for predicting the long-term behaviour of the graded sediment bed? The answer will be obtained from the comparative test simulations.

The numerical simulations were undertaken by dividing the 16.7 m long modelled channel into 18 sections with a constant space increment of 1.0 m (0.7 m for the last downstream section). The time increment for the simulation was 1 s. The distance and time steps were chosen according to the recommendations of the ISIS developers (Halcrow/HR Wallingford 1997) to provide an accurate resolution of the channel. The bed material was divided into ten size fractions (maximum allowed in ISIS Sediment) and was assumed to be fully mixed at the start of each simulation. The active layer thickness was set to be equal to d_{95} which is between the values of d_{90} and $2d_{84}$ suggested in the literature (Parker 1991, Hoey and Ferguson 1994, Seal et al. 1998, Ferguson et al. 1998). The channel bed slope and water depth were set equal to those in the experiments. The boundary conditions employed were: (a) constant discharge at the upstream boundary; (b) constant water level at the downstream boundary; and (c) sediment inflow (zero or a constant value) at the upstream boundary.

7.6 Results

The computational results concerned the bedload transport and mobile bed evolution are presented together with the measured data in Table 7.2 and Figures 7.3 through 7.10. Most of the results given here refer to one typical degradation experiment (No. 4) and one typical feed experiment (No. 9), which are generally representative of all the other experiments simulated.

When evaluating the results of the test simulations the following points should be remembered. Firstly, the numerical simulations are based on the assumption that initially the sediment bed is perfectly mixed and has a constant slope. However, some

grain sorting and minor variations in bed slopes are an inevitable consequence of experimental preparation. The numerical simulations represent therefore idealized averaged conditions and one would expect some differences between the computed and measured results to be inevitable. Secondly, the transport equations tested are based on statistical regression of many transport data and therefore are incapable of capturing short time scale fluctuations in total and fractional transport rates and bedload grain size composition. Finally, the results of the sediment transport computations significantly depend on the accuracy of hydrodynamic simulations, as well as numerical schematisation of the mobile bed and sediment interchange processes. Therefore, the predicted behaviour of the graded sediment reflects partly the overall performance of the ISIS Flow/Sediment simulation package.

The analysis of the results obtained and discussion of the performance of the three transport equations tested is given in the following sections.

7.6.1 Bedload yield

Measured and computed bedload yields in each of the six experiments are given in Table 7.2. As one can see, all the transport functions tend to overestimate the total amount of bedload transported. The Ackers-White and Parker equations demonstrate comparable results, which are generally about two-three times higher than the measured bedload yields. The proposed transport model shows better agreement with the measured data, with the predicted bedload yields 1.2-2.1 times the measured values.

The generally higher values of the computed bedload yield may be partly due to the fact that none of the transport functions account explicitly for the infiltration of fine sediment into the gravel bed. This phenomenon appears to be important in controlling the behaviour of fine-grained portion of sand-gravel mixtures (e.g., Frostick et al. 1984, Allan and Frostick 1999). The infiltration rates into gravel beds depend on a combination of factors including the bed material composition, supply of fine sediment, mobility of the gravel framework, and flow regime. In the flume experiments this process can be especially intensive in the early stages, because of the disorganised nature of the bed material. However, the process of fine sediment infiltration has not been studied in detail, and its inclusion into transport models is a task for future investigations.

7.6.2 Temporal variation of transport rates

The temporal variation of the measured and computed total bedload transport rates in the degradation experiment No. 4 is shown in Figure 7.3. The measured data demonstrate a typical, for the degradation conditions, rapid decline of bedload transport rates during the initial few hours of the experiment, with the following gradual steady diminishing of the rates as time progressed. The computed data generally demonstrated the similar pattern. However, the Ackers-White equation gives an almost five-fold overestimation of the initial bedload transport rates, with the computed rates approaching the measured data for the second half of the experiment. The Parker equation shows results, which are close to the measured data for the first few hours of the experiment, but afterwards significantly overestimates bedload transport. The proposed transport model demonstrates reasonable agreement with the measured data for the whole duration of the experiment.

Figure 7.4 shows typical variation of measured and computed transport rates with time in the feed experiment No. 9. During this experiment feeding of sediment was provided at a constant rate for the first 49 hours. Then feeding was stopped, and a degradation phase took place. This variation in the experimental conditions is reflected in rather complicated changes in the measured data, which show increase in transport rates after 10 hours from the start of the experiment when the front of the fed sediment reached the sediment traps, approximately constant time-averaged transport between 30 and 50 hours, and gradual decrease in transport rates after 50 hours when the feeding was stopped. The well-pronounced "saw-like" pattern of the measured data series in Figure 7.4 reflects the pulsating character of bedload transport caused by the downstream motion of the fed sediment in the form of low-amplitude (of the order of the largest grains present in the bed surface) bedload waves. These grain-scale bed forms (so called "bedload sheets") are typical of sediment mixtures (e.g., Whiting et al. 1988, Kuhnle and Southard 1988, Wilcock and McArdell 1993, Kuhnle 1996, Whiting 1996, Livesey et al. 1998) and were clearly visible in these experiments, both in photographs of the bed and in the longitudinal bed profiles (Pender and Shvidchenko 1999).

In the case of the two-phase experiment No. 9, application of the three transport equations shows rather different results. It is seen from Figure 7.4 that the Ackers-White equation again gives significant (up to a factor of 20) overestimation of initial transport rates, but for the second half of the feed phase and for the degradation phase the

computed rates demonstrate reasonable agreement with the measured data. On the contrary, the Parker equation shows acceptable results for the initial stage of the experiment, then predicts a significant rise of sediment transport rates (up to three times over the measured) apparently reflecting the arrival of the fed sediment at the downstream end of the channel. For the second half of the experiment the Parker equation demonstrates results approaching the measured data. As one can see from Figure 7.4, among the equations tested the proposed one produces generally better predictions of the total bedload transport rates. However, the computed data demonstrate about four hours earlier arrival of the front of the fed sediment and about three times higher transport rate for the first wave of the fed sediment compared to the measured data, which finally resulted in the higher predicted bedload yield (see Table 7.2). As discussed above, this can be due to the infiltration of fine sediments into the gravel bed, which could be responsible for the initial significant losses of the fine portion of the fed sediments not accounted for in the transport model. Nevertheless, the general temporal pattern of the computed data series is quite realistic.

It is uncertain what causes the significant fluctuations in the calculated transport rates demonstrated by the Parker equation and the proposed transport model (see Figures 7.3 and 7.4). This is probably the result of computational instability of the uncoupled numerical scheme utilised in ISIS Flow/Sediment for the simulation of weak transport conditions at which transport rates are highly sensitive to the values of the bed shear stress [see equations (7.1) and (7.20)]. Attempts to vary the time step of the computations, however, did not result in noticeable change of the computed parameters. The variation of the computed transport rates might also be related to some natural processes in graded sediment transport. Whatever the reason, the overall performance of the proposed transport model for the predicting bedload transport rates is considered to be encouraging.

7.6.3 Bedload composition

The measured and computed grain size distribution of the cumulative bedload washed out from the channel during the degradation experiment No. 4 and feed experiment No. 9 are presented in Figures 7.5 and 7.6, respectively. As could be expected from the comparison of the measured and calculated initial fractional transport rates shown in Figure 7.2, the Ackers-White transport equation gives too fine-grained bedload compared to the measured data, while the Parker equation shows excessive

proportion for the size fractions finer than 0.35 mm and coarser than 8.0 mm. The proposed transport model demonstrates reasonable agreement with the measured data, slightly overestimating the proportion of the grains smaller than 0.35 mm. In general, both the Parker equation and the proposed model may be judged as predicting quite realistic bedload composition, given the high natural variability of the bedload transport and uncertainty regarding the infiltration of the fine particles into the gravel bed.

7.6.4 Bed elevation

Figure 7.7 presents measured and computed temporal changes of the bed elevation at chainage 9 m, which is located in the middle part of the channel. It is seen that for the degradation experiment No. 4 the Ackers-White equation demonstrates rapid erosion of the bed during the first 30-40 hours and gradual stabilisation of the bed afterward, with the final computed elevation of the bed about 1.5 cm lower than the measured one. The Parker equation shows similar changes in the bed elevation, which is about 0.5 cm higher than that predicted by the Ackers-White equation. The results given by the proposed transport model practically coincide with the measured data.

In the case of the experiment No. 9, the temporal changes in the bed elevation reflect the variable experimental conditions applied, with initial feed phase and subsequent degradation phase. The periodic variations in the measured data are related to the downstream propagation of the low-amplitude bedload accumulations – "bedload sheets" (Pender and Shvidchenko 1999). For this experiment, the bed elevation predicted by the Ackers-White transport equation is 0.5-1.0 cm lower than the measured one, but with generally similar temporal pattern. The Parker equation produces rather unrealistic temporal changes in the bed elevation, with the initial elevation about 0.5 cm higher and the final elevation about 1.0 cm lower than the measured ones. The proposed transport model again demonstrates reasonable agreement with the measured data.

The final measured and computed longitudinal bed profiles in the above experiments are presented in Figure 7.8. As one can see, for the degradation experiment No. 4 the Ackers-White transport equation gives a bed profile noticeably lower (about 1-2 cm) than the measured one. In the case of the feed experiment No. 9 the bed profile predicted using the Ackers-White equation is rather close to the measured data at the upstream part of the channel and is about 1 cm lower at the downstream end of the channel. The Parker equation shows significant erosion of the bed in both cases, with the bed profile 1-2 cm lower than the actual one. The longitudinal bed profiles

simulated using the proposed transport model almost coincide with the measured profiles for both the degradation and feed experiments.

7.6.5 Final bed surface grading

Figure 7.9 shows the measured and computed cumulative grading curves of the bed surface developed at the end of the experiments Nos. 4 and 9 at chainage 9 m. Noticeable are the little observed changes in the bed surface composition. The apparent scatter in the measured data is rather typical as far as sampling of poorly sorted sediment is concerned. The data scatter is related to both the complicated spatial sorting pattern developed (Pender and Shvidchenko 1999) and measurement errors associated with the molten wax sampling technique used (Marion 1996).

It is seen from Figure 7.9 that in both the degradation and feed experiments the Ackers-White transport equation predicts almost total winnowing of fines from the bed surface, with the development of a coarse-grained static armour layer composed of particles larger than 4 mm in size. This is obviously incorrect. The Parker equation and the proposed transport model demonstrate comparable results, which are generally in agreement with the measured data. There is some discrepancy between the grading curves predicted by these two methods and the measured data in the feed experiment No. 9. The proposed model slightly underestimates the content of the coarse grains, and both these methods overestimate the proportion of fine sediments in the surface layer. Interestingly, a similar pattern is shown for the composition of bedload (see Figure 7.6). As mentioned above, this can be explained by unpredictable losses of fine fractions on infiltration into the gravel bed. However, it is unclear why this did not happen in the degradation experiment No. 4. Another reason for the discrepancy between the measured and predicted properties of the surface layer may be under-representation of the sand-size particles in the wax samples of the bed surface due to measurement errors. On the whole, the deviation of the grading curves predicted by the Parker transport equation and the proposed model from the measured data is comparable to the scatter in the experimental results and is therefore regarded as insignificant.

7.7 Conclusions

Summarizing the results of the test computations, the following conclusions on the performance of the transport models tested can be made.

The classical approach to the calculation of transport of different grain sizes in sediment mixtures ignores size fraction interaction and as a result does not provide an adequate prediction of long-term trends in the behaviour of graded sediments. The use of this approach represented here by the Ackers-White transport equation significantly overestimates transport of fine sediments and underestimates mobility of coarse grains in sediment mixtures. This results in overestimation of transport rates and total bedload yield, with the excessive bed erosion and the development of too coarse an armour layer compared to the actual data.

The Parker bedload equation incorporates a hiding function based on the "equal mobility" hypothesis and represents the present state-of-the-art in graded sediment calculations. This equation shows reasonable results for the bedload and bed surface compositions. However, it overestimates mobility of the end size fractions in the graded sediment tested, which results in excessive transport rates and bed erosion compared to the actual data. This may be explained by the existing uncertainties in the character of the hiding function for different sediment mixtures (Parker's "equal mobility" concept obviously does not hold for all the graded sediments), as well as the absence of reliable methods for predicting the entrainment mobility of median-sized grains required for fractionwise calculations. An additional factor influencing the computed results could be different mobility of the bed sediment at different bed slopes, which is not accounted for by the Parker equation.

The flume simulations indicate that the proposed transport model is capable of reproducing long-term behaviour of graded sediment with acceptable accuracy. Among the transport equations used, the proposed one demonstrates generally better agreement with the measured data. The advantage of the new transport model over the widely used Parker equation is a more accurate prediction of bedload transport rates and bed elevations, with the comparable results for the granulometric compositions of bedload and bed surface. The shortcomings of the proposed model are its applicability to only weak transport conditions (which, however, prevail in natural gravel-bed streams), as well as non-consideration of infiltration of fine sediment into the gravel bed. The computed transport rates and, therefore, the resultant bedload yield and bed elevations

are sensitive to the determined values of the bed shear stress. This requires accurate hydrodynamic computations, with all the necessary corrections for the bed form and sidewall effects to be made. The computed results for bedload and bed surface compositions are more stable, as these depend mainly on the relative mobility of different grain sizes within sediment mixture.

It is acknowledged that the test simulations undertaken are not enough to make a categorical conclusion on the overall performance of the present model of weak bedload transport. It is necessary to test the model on a wider range of bed sediments and flow conditions, including field data, with a comprehensive sensitivity analysis of the model parameters. The main problem for this is the absence of reliable detailed data on which the transport model could be tested. Therefore, appropriate data sets need to be collected before further testing can be made. This is a task for future research. It is anticipated that collection of additional data may result in some modification and refinement of the components of this model. Nevertheless, the generally positive results of the present test simulations of graded sediment transport in a laboratory flume are rather encouraging and indicate the overall correctness of the novel approach to the prediction of streambed mobility developed in this study.

Table 7.1 Hydraulic Conditions in HR Wallingford Flume Experiments (Test Data)

Exp No.	Bed Width B (m)	Slope J x 10^3	Flow Q ($L\,s^{-1}$)	Depth h (m)	Velocity U ($m\,s^{-1}$)	Sediment Feed Rate ($g\,s^{-1}$)	Feed Duration (hrs)	Experiment Duration (hrs)
4	0.80	2.6	106	0.15	0.74	-	-	92.6
5	0.80	2.9	117	0.15	0.82	-	-	85.6
6	0.80	2.3	107	0.15	0.75	-	-	80.0
8	0.80	2.3	102	0.15	0.71	2.5	67.0	87.0
9	0.80	2.3	101	0.15	0.71	5.0	49.2	69.5
11	0.80	2.6	111	0.15	0.78	5.0	32.0	60.5

Table 7.2 Measured and Calculated Bedload Yield

Exp No.	Measured (kg)	Ackers-White (kg)	Parker (kg)	Proposed Model (kg)
4	180	600	570	278
5	325	794	803	375
6	94	352	272	156
8	352	744	924	602
9	630	957	1174	816
11	340	933	1154	724

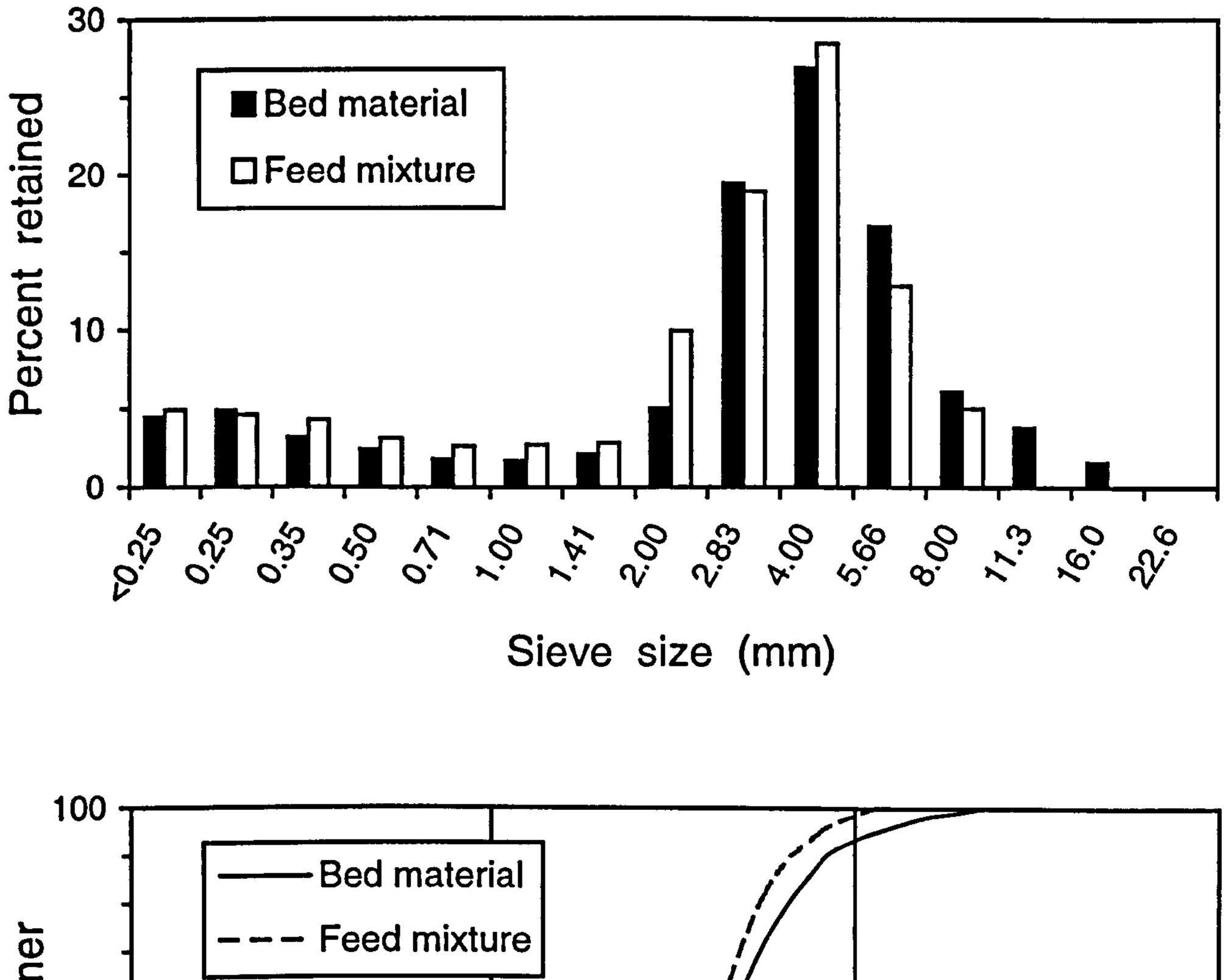

Figure 7.1 Grain size distributions (top) and cumulative grading curves (bottom) for bed material and feed mixture (test data).

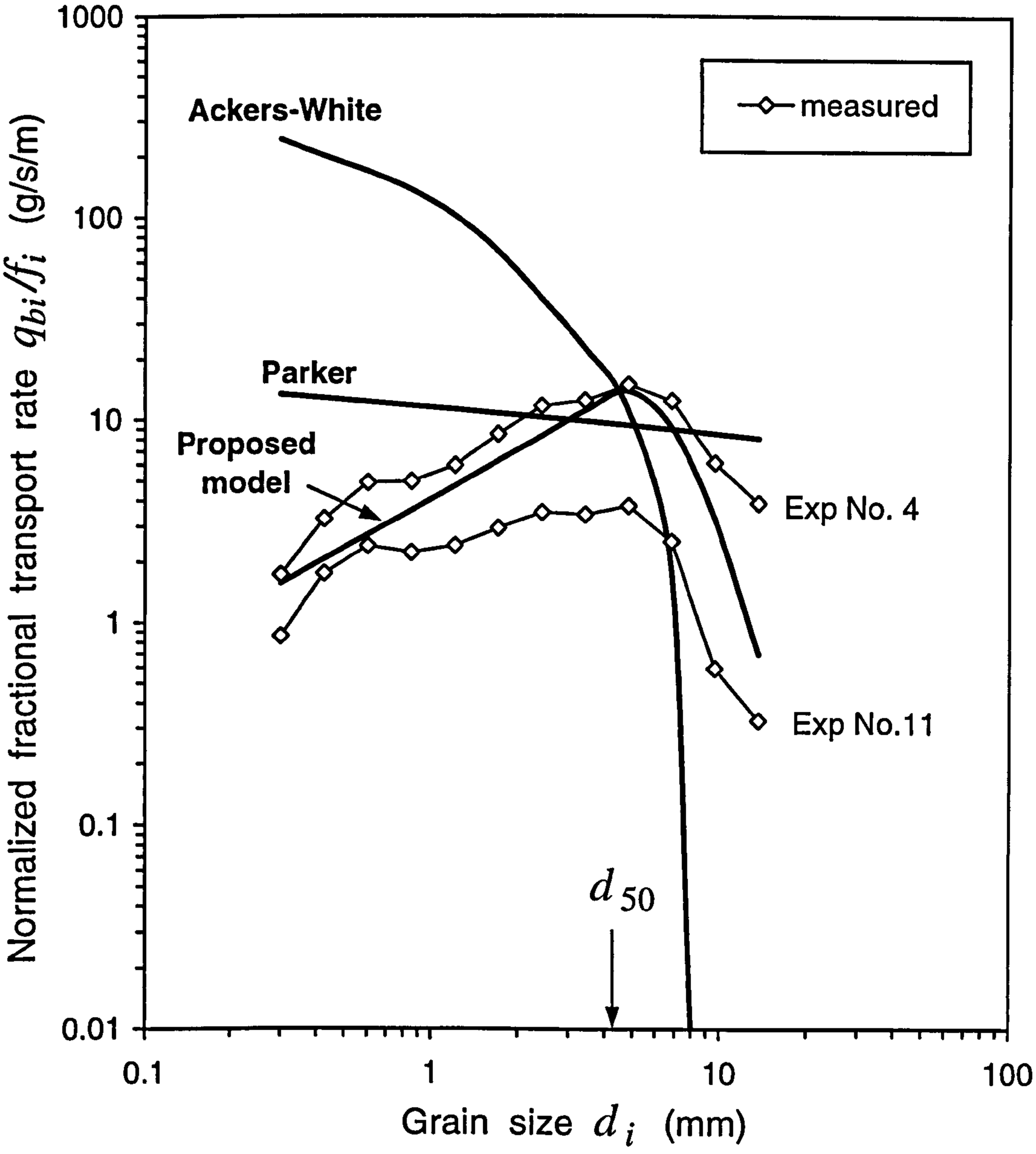

Figure 7.2 Initial fractional transport rates.

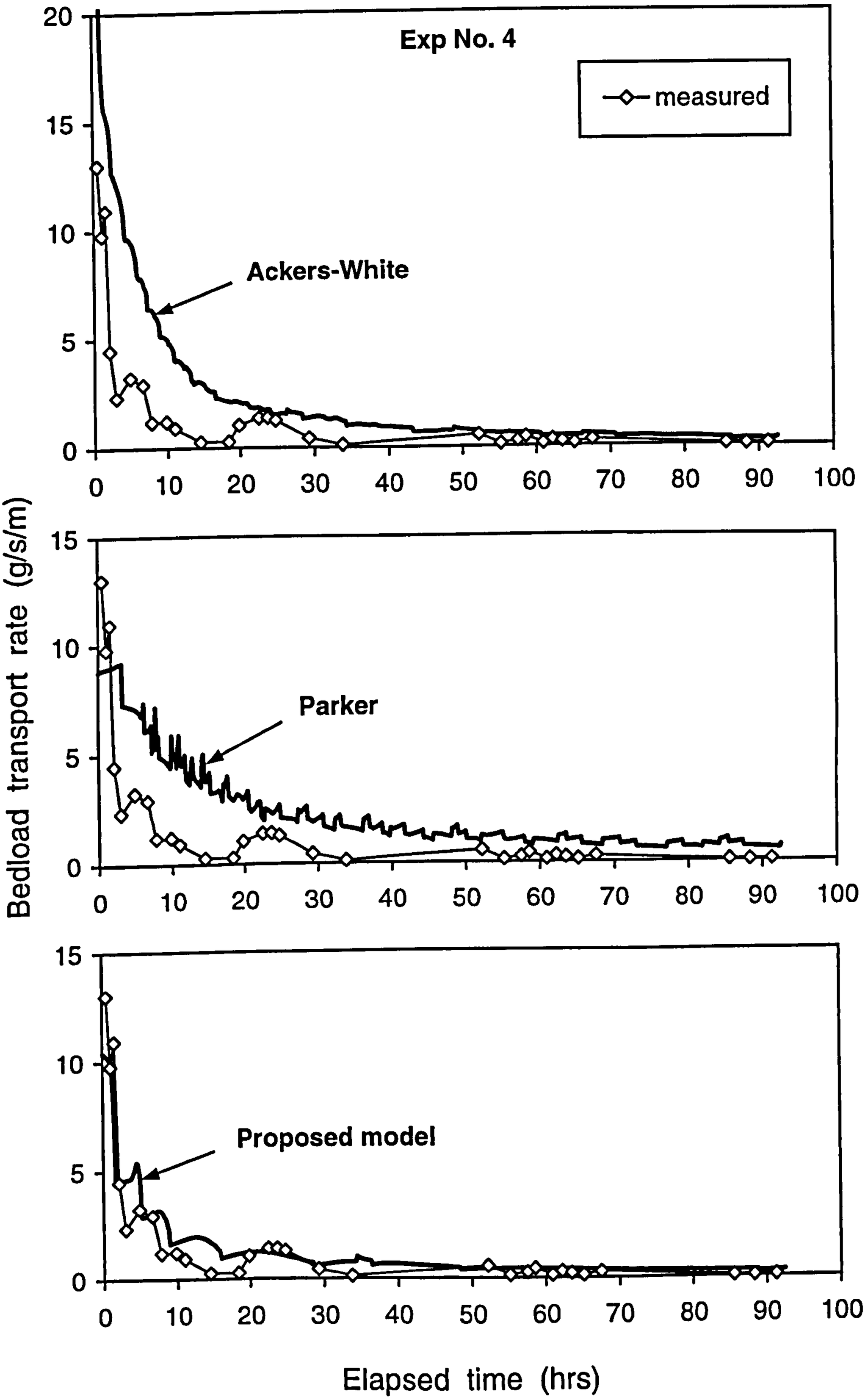

Figure 7.3 Bedload transport rates (degradation Exp No. 4).

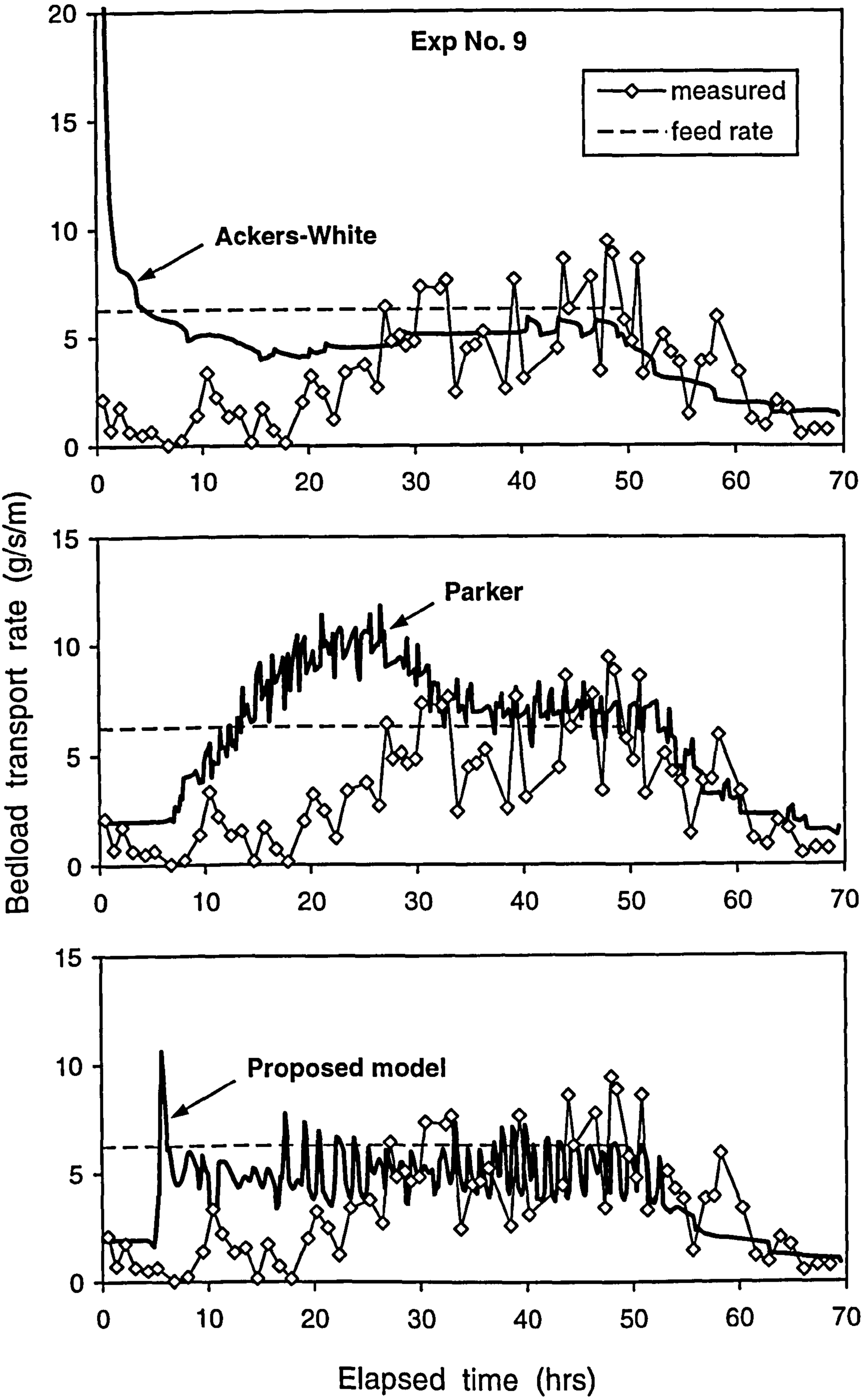

Figure 7.4 Bedload transport rates (feed Exp No. 9).

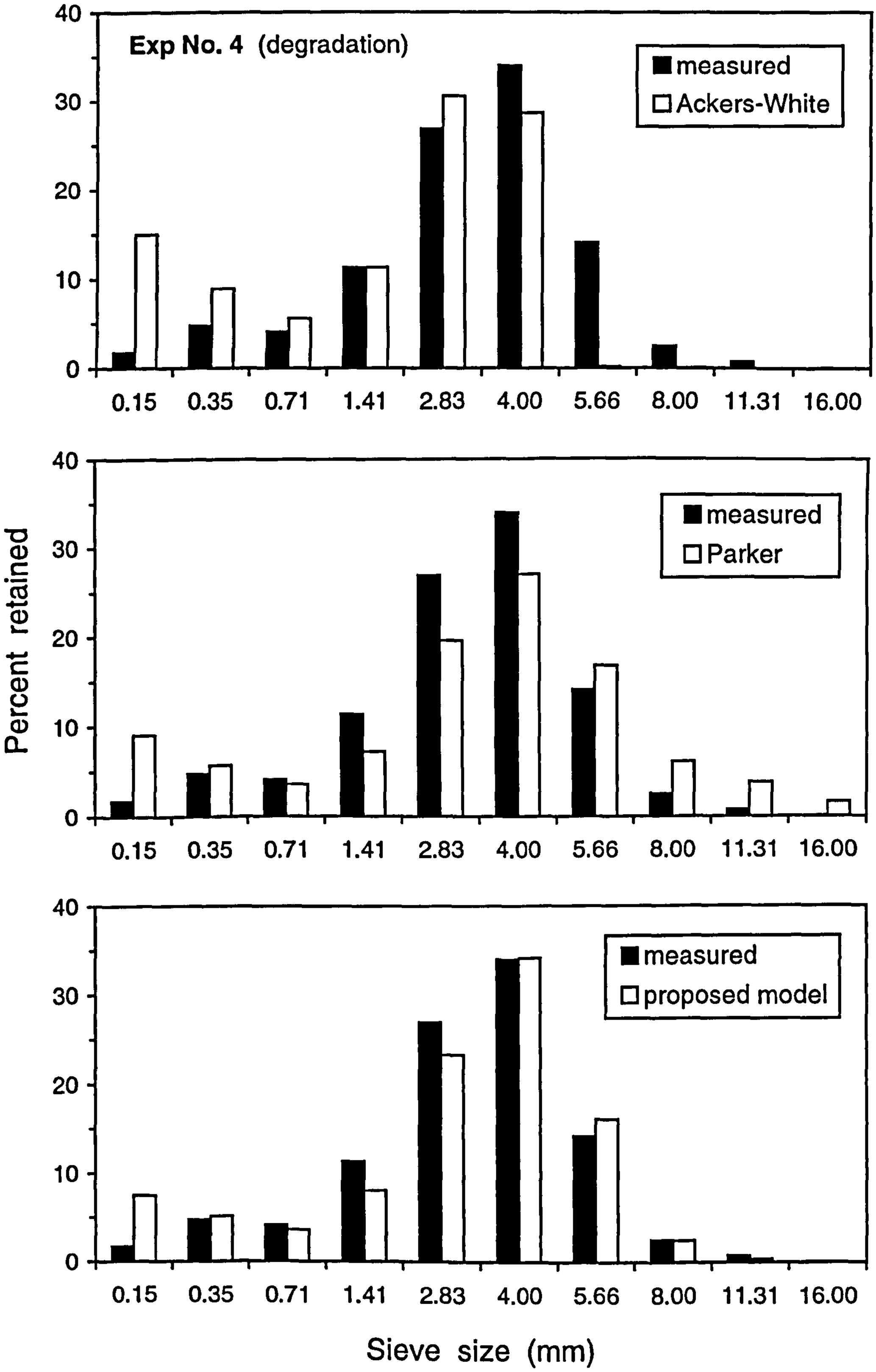

Figure 7.5 Grain size distribution of cumulative bedload (degradation Exp No. 4).

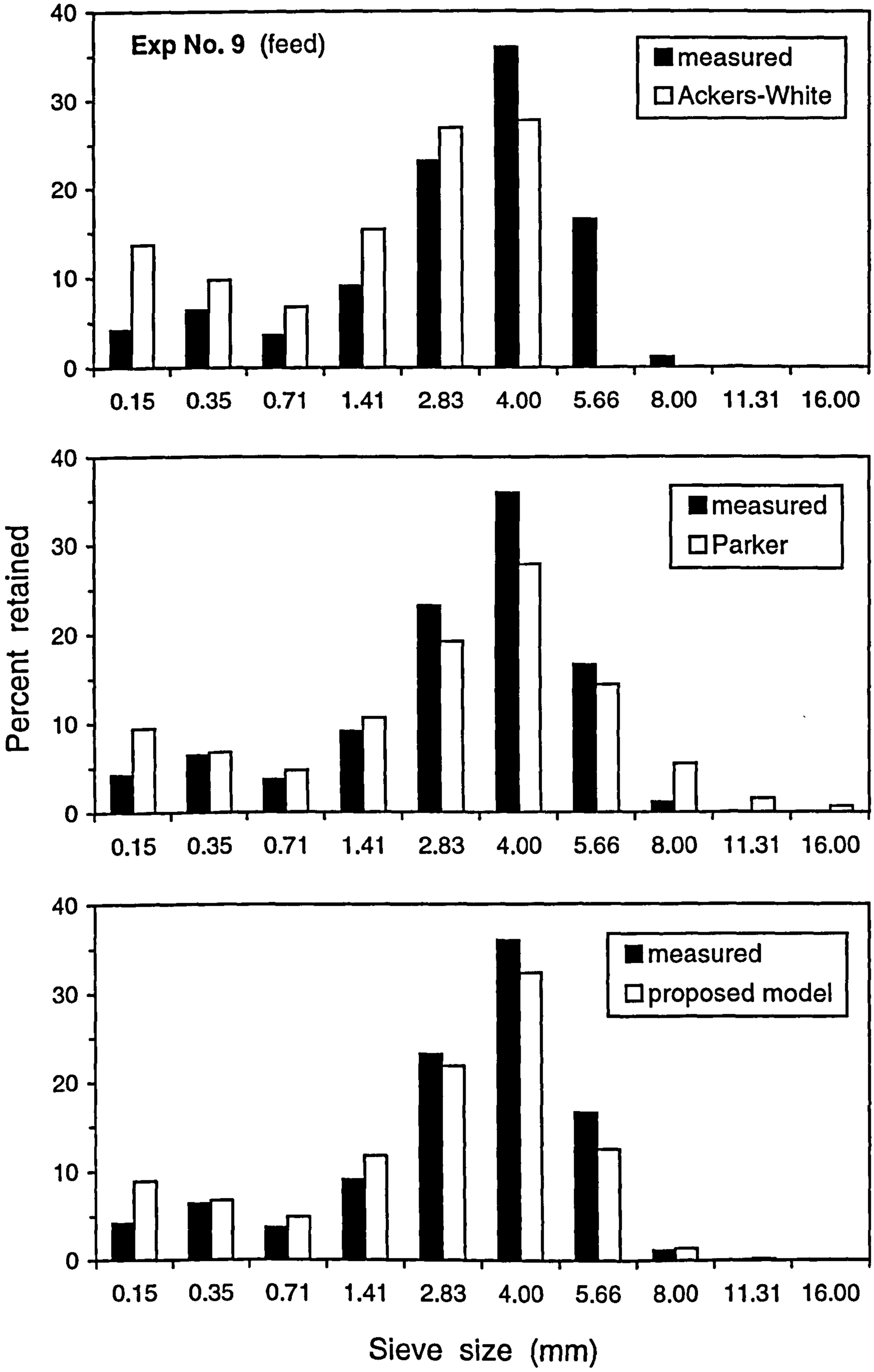

Figure 7.6 Grain size distribution of cumulative bedload (feed Exp No. 9).

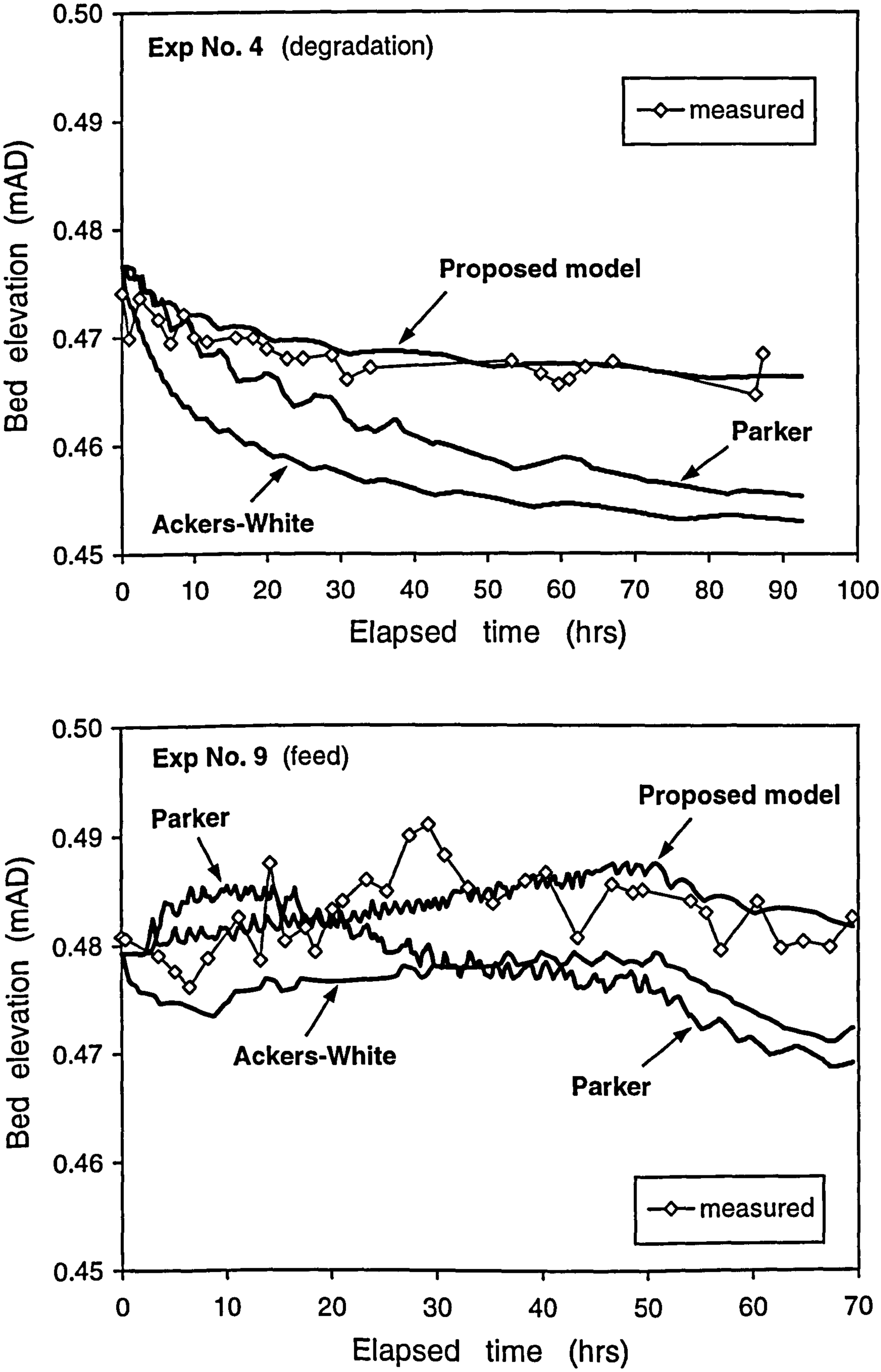

Figure 7.7 Temporal changes of bed elevation at chainage 9 m.

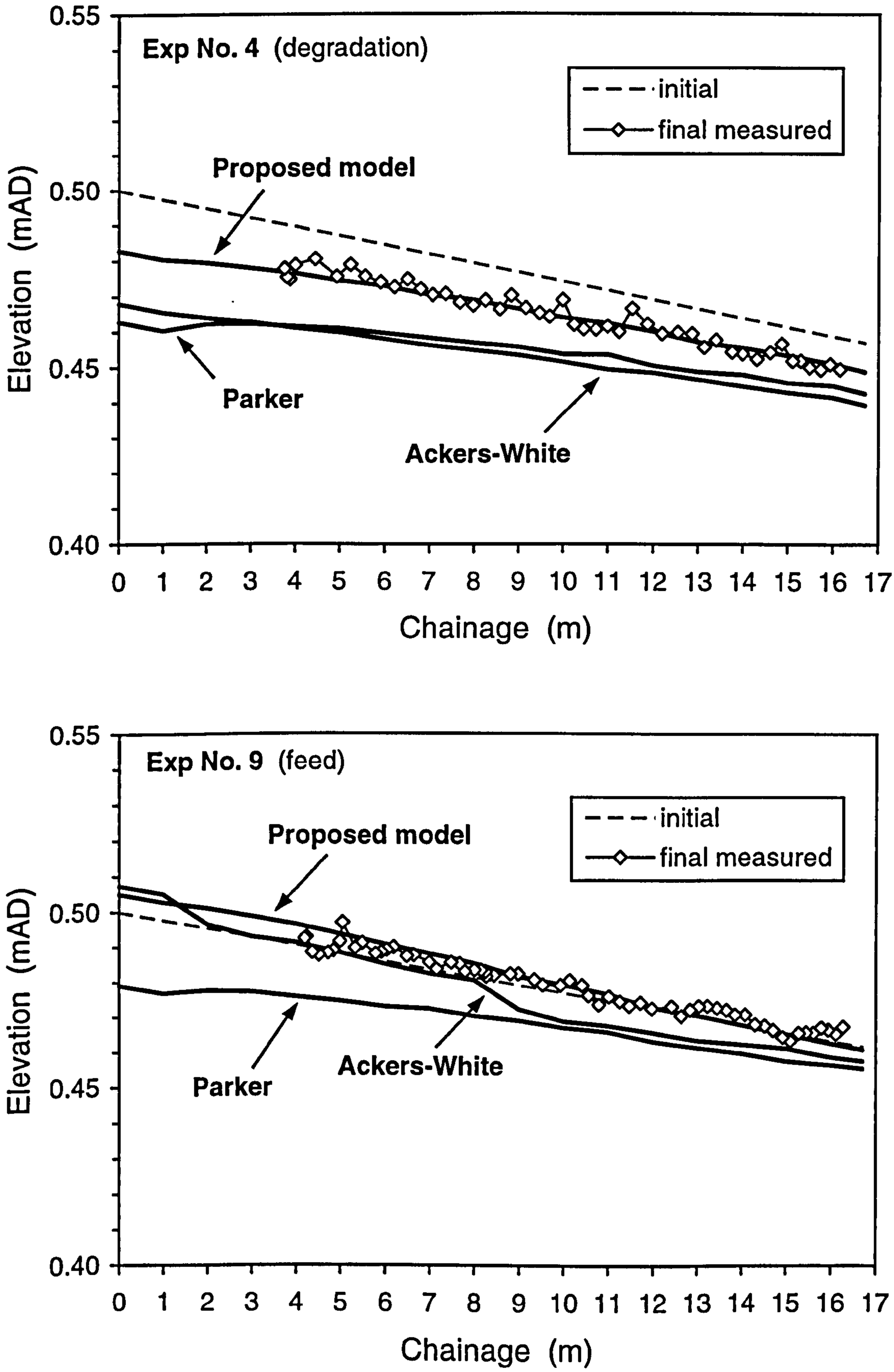

Figure 7.8 Final longitudinal bed profile.

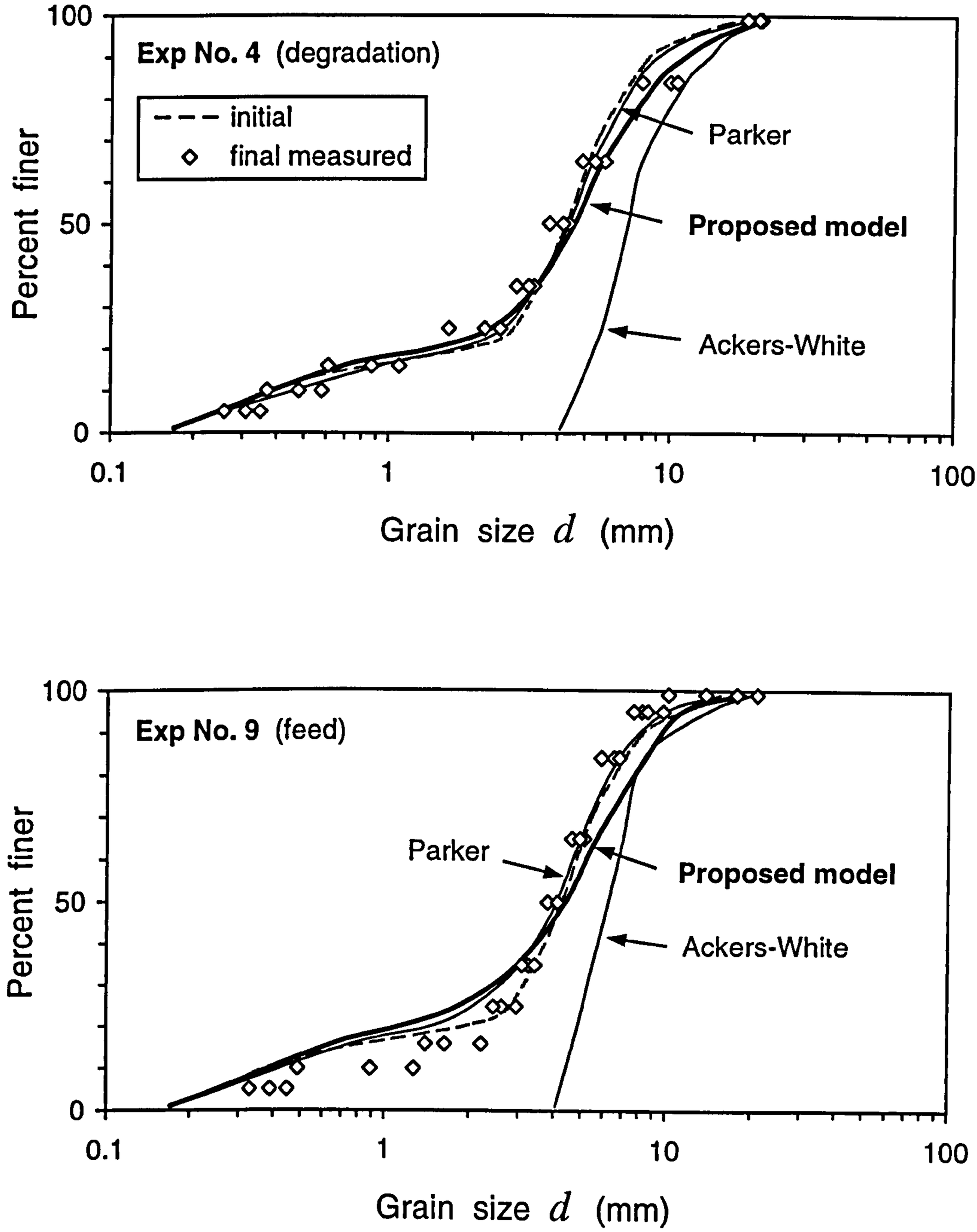

Figure 7.9 Cumulative grading curves of final bed surface at chainage 9 m.

8

Summary of Conclusions and Suggested Further Work

This thesis was an investigation of the incipient motion of streambeds. The following is a summary of the work undertaken, principal results obtained, and conclusions drawn. Some ideas and suggestions for further research are also discussed. For clarity, these are grouped into the four main areas investigated in this study: (a) incipient motion of uniform sediments; (b) incipient motion of graded sediments; (c) flow turbulence; and (d) bedload transport modelling.

8.1 Incipient Motion of Uniform Sediments

8.1.1 Summary of work

A series of laboratory experiments on incipient motion of coarse uniform sediments was undertaken in an 8 m long, 0.30 m wide by 0.30 m deep tilting flume. Natural sand and gravel sieved into eight essentially uniform fractions ranging in size from 1.0 mm to 14.0 mm were used as experimental bed materials. The experiments were conducted at a range of fixed bed slopes (0.0019-0.0287) and for a variety of water discharges with different degree of the bed particle mobility ranging from "rare displacement of single particles" to "general transport". The main measured characteristics were water discharge, flow depth, slope, fraction of bed surface particles mobilized, and bedload transport rate. A total of 312 experiments (237 hours experimental time) were performed.

To complement and extend the data set from the present experiments, an exhaustive search for additional data on the incipient motion of coarse uniform sediments was undertaken. The final compiled experimental data set covers a wide range of grain sizes (1.07-44.3 mm) and bed slopes (0.0008-0.070), and it was used to analyse the factors controlling bed material entrainment and transport.

8.1.2 Conclusions

- A new approach to the description of the incipient motion of bed sediments is proposed. This approach describes the state of the streambed mobility in terms of the fraction of bed particles mobilized in unit time (called "intensity of sediment motion" or "transport intensity"). This eliminates the subjectivity in defining threshold conditions and provides a probabilistic description of the process of sediment entrainment.
- An experimental relationship between intensity of sediment motion and dimensionless sediment transport rate is established. This relationship allows any measured transport rate to be expressed in terms of the intensity of sediment motion or, alternatively, probability of sediment entrainment.
- The experimental results indicate that the value of critical bed shear stress strongly depends on the chosen value of "critical" intensity of sediment motion. It is shown that the commonly used Shields threshold curve is more appropriate for predicting "general transport" of the bed material.
- The critical bed shear stress for incipient motion of uniform sediment appears to depend not only on the grain size, but also on the bed slope. The steeper the slope, the higher the value of the critical stress for a given grain size. This is explained by the effect of relative depth (depth to grain size ratio) on overall flow resistance.
- The value of critical dimensionless bed shear is not constant for rough turbulent flow, as is usually assumed, but gradually reduces with grain Reynolds number. This is explained by the changes in the near-bed turbulence field (and, therefore, resistance) with absolute grain size.
- The bed particle mobilization is not entirely random over the bed area but is concentrated along certain paths known as "longitudinal troughs". These are related to the effect of the kinematic structure of the flow.
- A revised Shields diagram relating critical dimensionless stress, grain Reynolds number, and bed slope is derived for different intensities of sediment motion (or, alternatively, different probabilities of sediment entrainment). The results are presented graphically and are also formulised to provide tools for easy practical calculations.

8.1.3 Further work

Further experiments on incipient motion of very coarse uniform gravels (larger than 50 mm) at moderate bed slopes (less than 0.010) are needed to extend the threshold diagram derived in this study. Given the established effect of bed slope on bed material mobility, the experiments should be conducted at fixed slopes and for a variety of water discharges with different degrees of bed material mobility. Collection of additional data on incipient motion of medium and fine sand by the method used in the present study is also desirable to extend the threshold diagram for low values of grain Reynolds number.

8.2 Incipient Motion of Graded Sediments

8.2.1 Summary of work

Incipient motion of various sand/gravel sediment mixtures was investigated in an 8 m long, 0.30 m wide by 0.30 m deep glass walled tilting flume and an 18 m long, 0.80-1.10 m wide by 0.15 m deep trapezoidal concrete channel. The bed materials used were mixed from natural sand and gravel, and were characterised by unimodal and weakly bimodal grain size distributions, with different skewness and standard deviation. The experiments were conducted at fixed bed slopes ranging from 0.0041 and 0.0141, for a variety of water discharges with different degrees of the bed mobility. The main measured parameters were water discharge, flow depth, slope, bedload transport rate, and bedload composition. Altogether 142 experiments with a total duration of 132 hours were completed.

A search of available flume and field data on graded sediment transport collected by other researchers was also undertaken to complement and extend the results of the present experimental study. In total, the compiled data set covers median grain sizes ranging from 1.75 mm and 124 mm and bed slopes ranging from 0.0007 and 0.025.

8.2.2 Conclusions

- The behaviour of graded sediments significantly depends on the bed slope as in the case of uniform sediments. The steeper the slope is, the higher the shear stress is needed to produce a given transport rate for a given size fraction. This effect has never been observed in sediment mixtures before and is not taken into account by any of the existing sediment transport formulas. It also follows that commonly

applied combined analysis of transport data collected at different slopes is unacceptable as it may lead to erroneous conclusions.

- The behaviour of individual fractions in graded sediments is largely controlled by relative size effects. These effects reduce mobility of fine fractions due to sheltering from larger grains and increase mobility of coarse fractions due to greater exposure to the flow compared to uniform sediments of the same sizes.
- Relative size effects in unimodal and weakly bimodal sediment mixtures can be adequately described by a hiding function with respect to the median grain size. The character of this function is independent of bed slope and reference transport rate, but varies for finer fractions with mixture sorting and median grain size.
- Relative size effects dominate in sediment mixtures but do not suppress the size-selective motion entirely. The greater the value of the mixture standard deviation, the more reduced the hiding effect and the higher the mobility of fractions finer than the median grain size.
- The hiding effect for fine fractions is most pronounced for mixtures with median grain size around 5 mm. This grain size also requires the greatest value of dimensionless shear stress for mobilization compared to other sizes in the case of uniform sediment.
- The mobility of median-sized grains in narrowly graded sediment mixtures (with geometric standard deviation less than three) is the same as in uniform sediment. For mixtures with a wider grading, the mobility of median fractions systematically decreases compared to uniform material, which is explained by the siltation effect.
- A practical technique for calculating the low transport and critical shear stress of individual size fractions within unimodal and weakly bimodal sediment mixtures is proposed.

8.2.3 Further work

Collection of additional laboratory and field data is needed to complement and extend the results of the present study. The data should be measured at fixed bed slopes to eliminate the effect of the slope on the sediment mobility. The issues which need detailed investigation are the mobility of median size fractions in widely graded sediments, the effect of the absolute median grain size on relative size effects, and the behaviour of fractions coarser than the median grain size in widely graded sediment mixtures. A more accurate method for describing the shape of the grain size distribution

should be developed and a wider range of graded sediments including strongly bimodal two-component mixtures should be tested.

8.3 Flow Turbulence

8.3.1 Summary of work

The turbulent structure of open-channel flow over a mobile gravel bed was undertaken in an 8 m long, 0.3 m wide by 0.3 m deep tilting flume with glass walls. Uniform gravels ranging in size from 2 mm and 8 mm were employed in the flume tests. A flow visualization technique was used and complemented by measurements of flow velocity fluctuations near the bed. The experiments were conducted for a range of water discharges at flume slopes between 0.0041 and 0.0083. During the experiments 52 videos and 362 images of the visualized turbulent flow were recorded and 33 measurements of the instantaneous flow velocity components near the bed were completed.

8.3.2 Conclusions

- Open-channel turbulent flow consists of an ordered continuous sequence of three-dimensional large-scale (or macroturbulent) eddies. These eddies have an asymmetric form, reflecting areas of high-forward-speed downwelling and burst-like upwelling fluid motions. The vertical size of these eddies is close to the flow depth, the longitudinal size is between two and twelve depths (around four to five depths on average), and the transverse size is about two depths.
- The macroturbulent eddies move downstream along relatively stable paths at the bulk flow velocity and cause quasi-periodic fluctuations of the local flow velocity components.
- The macroturbulent eddies represent a self-organisation mechanism of open-channel flow associated with the origin of "sweeps" and "ejections" in the boundary layers, alternate high- and low-speed flow regions in both the streamwise and spanwise directions, and spiral fluid motions known as "secondary currents".
- The effect of the macroturbulent eddies on the bed particle motion is reflected in the patchy and intermittent character of bedload transport, which is concentrated

along the paths of the eddy movement. This results in the alternation of longitudinal bands of active and inactive sediment transport causing the development of longitudinal troughs and ridges.

- Measurements of the flow velocity fluctuations near the gravel bed indicate that for the same value of dimensionless shear stress, the ratio of destabilising to stabilising forces acting on the bed particles gradually increases as the grain size increases. This observation supports the results of the incipient motion experiments, which demonstrated lower values of the critical dimensionless stress for higher grain Reynolds number in rough turbulent flow.

8.3.3 Further work

Given the insufficient experimental evidence and the controversy of the very existence of the organized large-scale turbulent motions and regularity of flow velocity fluctuations, there is an obvious need for further investigations of the open-channel flow macro-turbulence. These should include simultaneous observation of the turbulent structures in the visualized flow and measurement of velocity fluctuations in different parts of the flow using a non-intrusive technique (for example, Laser Doppler Anemometry). Supplementary direct measurements of the bed pressure fluctuations (using micro-pressure transducers) would significantly clarify the effect of the flow macroturbulent structures on the mechanism of bed particle mobilization. The experiments should be conducted for a variety of bed materials and flow conditions. A significant challenge in terms of experimental design would be pressure measurements at different points along, across, and inside the bed. This would provide information about the spatial and temporal bed pressure distribution and would also clarify the mechanism of damping effects of the granular bed. It would also be very interesting to undertake similar measurements in natural gravel-bed streams. Other poorly understood processes requiring detailed investigations are the effects of the absolute grain size, relative bed roughness, intensity of sediment transport, and bed forms developed on the turbulence.

8.4 Bedload Transport Modelling

8.4.1 Summary of work

The set of relationships derived in this study for predicting the near-to-threshold, or weak, bedload transport is implemented in a computer program ISIS Flow/Sediment. The modified program was tested on detailed graded sediment transport data collected by Glasgow and Aberdeen Universities during an extensive series of long experiments in the HR Wallingford tilting flume. Comparative simulations were made using the Ackers-White transport relationship representing the classical approach to calculating graded sediments without accounting for hiding and exposure effects. Also tested was the Parker bedload function incorporating a hiding function based on the Parker's "equal mobility" hypothesis.

8.4.2 Conclusions

- The results of the numerical simulations demonstrate that the classical approach, represented by the Ackers-White transport equation, fails to provide an adequate prediction of long-term trends in the behaviour of graded sediments. This approach significantly overestimates the transport of fine size fractions and underestimates the mobility of coarse grains, which results in an overestimation of transport rates and total bedload yield, with excessive bed erosion and the development of too coarse an armour layer.
- The Parker transport equation provides acceptable results in terms of the granulometric composition of bedload and surface layer of the bed. However, it overestimates mobility of the end size fractions, which results in excessive transport rates and bed erosion.
- The proposed model of weak bedload transport significantly improves the results of the numerical simulations compared to the sediment transport equations tested and demonstrates reasonable agreement with the measured bedload transport rates, bedload composition, bed elevation, and bed surface grading. The test simulations indicate the overall correctness of the approach to the prediction of streambed mobility used in this study and demonstrate that the proposed transport model is capable of reproducing long-term behaviour of graded sediment with acceptable accuracy.

8.4.3 Further work

The further work on the numerical simulation of the behaviour of streambeds should include testing of the new transport model on a variety of independent flume and field data for both uniform and graded sediments, including steady and unsteady flow conditions. The collection of additional detailed data may be needed before further testing can be made. A comprehensive sensitivity analysis of the model should also be undertaken to assess how the results of numerical simulations depend on basic hydraulic and sediment parameters and on alternative conceptualisations of sediment sorting and exchange processes. The transport model should be further developed to cover a wider range of grain size distributions, including bimodal sediment mixtures. The model should also be extended for the conditions of active bedload transport. Some modification should also be made to take into account infiltration of fine sediments into gravel beds.

References

Ackers, P. (1993). Sediment transport in open channels: Ackers and White update. *Proc. Instn Civ. Engrs Wat., Marit. & Energy, 101*, 247-249.

Ackers, P., and White, W. R. (1973). Sediment transport: New approach and analysis. *J. Hydraul. Div. Am. Soc. Civ. Eng., 99* (11), 2041-2060.

Aksoy, S. (1973). The influence of the relative depth on threshold of grain motion. *Proc. Int. Symp. on River Mechanics (9-12 January 1973, Bangkok, Thailand)*, International Association for Hydraulic Research, Delft, Netherlands, 359-370.

Allan, A. F., and Frostick, L. (1999). Framework dilation, winnowing, and matrix particle size: the behavior of some sand-gravel mixtures in a laboratory flume. *J. Sedimentary Research, 69* (1), 21-26.

Andrews, E. D. (1983). Entrainment of gravel from naturally sorted river bed material. *Geol. Soc. Amer. Bull., 94*, 1225-1231.

Andrews, E. D. (1984). Bed-material entrainment and hydraulic geometry of gravel-bed rivers in Colorado. *Geol. Soc. Amer. Bull., 95*, 371-378.

Andrews, E. D. (1994). Marginal bed load transport in a gravel bed stream, Sagehen Creek, California. *Water Resour. Res., 30* (7), 2241-2250.

Andrews, E. D. (2000). Bed material transport in the Virgin River, Utah. *Water Resour. Res., 36* (2), 585-596.

Andrews, E. D., and Erman, D. C. (1986). Persistence in the size distribution of surficial bed material during an extreme snowmelt flood. *Water Resour. Res., 22* (2), 191-197.

Andrews, E. D., and Parker, G. (1987). Formation of a coarse surface layer as the response to gravel mobility. *Sediment Transport in Gravel-bed Rivers*, C. R. Thorne, J. C. Bathurst, and R. D. Hey (eds.), John Wiley & Sons, Chichester, U.K., 269-300.

Ashida, K., and Bayazit, M. (1973). Initiation of motion and roughness of flows in steep channels. *Proc. 15th Congress of the International Association for Hydraulic Research*, vol. 1, Int. Assoc. for Hydraul. Res., Delft, Netherlands, 475-484.

Ashida, K., and Michiue, M. (1971). An investigation of river bed degradation downstream of a dam. *Proc. 14th Congress of the International Association for Hydraulic Research*, Vol. 3, Paris, France, C-30-1 – C-30-9.

Ashworth, P., and Ferguson, R. I. (1989). Size-selective entrainment of bed load in gravel bed streams. *Water Resour. Res.*, *25* (4), 627-634.

Ashworth, P. J., Ferguson, R. I., Ashmore, P. E., Paola, C., Powell, D. M., and Prestegaard, K. L. (1992). Measurements in a braided river chute and lobe 2. Sorting of bed load during entrainment, transport, and deposition. *Water Resour. Res.*, *28* (7), 1887-1896.

Bagnold, R. A. (1980). An empirical correlation of bedload transport rates in flumes and natural rivers. *Proc. R. Soc. London*, A 372, London, U.K., 453-473.

Bathurst, J. C. (1982). Theoretical aspects of flow resistance. *Gravel-bed Rivers*, R. D. Hey, J. C. Bathurst, and C. R. Thorne (eds.), John Wiley & Sons, Chichester, U.K., 83-105.

Bathurst, J. C. (1987) Critical conditions for bed material movement in steep, boulder-bed streams. *Erosion and Sedimentation in the Pacific Rim*, R. L. Beschta, T. Blinn, G. E. Grant, G. G. Ice, and F. J. Swanson (eds.), IAHS Publ. No. 165, 309-318.

Bathurst, J. C., Graf, W. H., and Cao, H. H. (1983). Initiation of sediment transport in steep channels with coarse bed material. *Mechanics of Sediment Transport*, B. M. Sumer and A. Muller (eds.), A. A. Balkema, Rotterdam, Netherlands, 207-213.

Bathurst, J. C., Cao, H. H., and Graf, W. H. (1984). Hydraulics and sediment transport in a steep flume: data from the EPFL study. *Rep. Institute of Hydrology*, Wallingford, Oxon, U.K.

Bathurst, J. C., Graf, W. H., and Cao, H. H. (1987). Bed load discharge equations for steep mountain rivers. *Sediment Transport in Gravel-bed Rivers*, C. R. Thorne, J. C. Bathurst, and R. D. Hey (eds.), John Wiley & Sons, Chichester, U.K., 453-477.

Best, J. (1992). On the entrainment of sediment and initiation of bed defects: insights from recent developments within turbulent boundary layer research. *Sedimentology*, *39*, 797-811.

Best, J. L. (1993). On the interaction between turbulent flow structure, sediment transport and bedform development: some consideration from recent experimental research. *Turbulence: Perspectives on Flow and Sediment Transport*, N. J. Clifford, J. R. French, and J. Hardisty (eds.), John Wiley & Sons Ltd, Chichester, U.K., 61-92.

Bettess, R. (1984). Initiation of sediment transport in gravel streams. *Proc. Instn. Civ. Engrs*, *77*, Part 2, Tech. Note 407, 79-88.

Bogardi, J. H. (1965). European concepts of sediment transportation. *J. Hydraul. Div. Am. Soc. Civ. Eng., 91* (HY1), 29-54.

Bogardi, J., and Yen, C. H. (1939). Traction of pebbles by flowing water. *Ph.D. dissertation*, State University of Iowa, U.S.A.

Bonnefille, R. (1963). Essais de synthese des lois de debut d'entrainment des sediments sous l'action d'un courant en regime uniform. *Bull. Du CREC*, No. 5, Chatou, France.

Brownlie, W. R. (1981). Compilation of alluvial channel data: laboratory and field. *Rep. KH-R-43B*, W. M. Keck Laboratory of Hydraulics and Water Resources, California Institute of Technology, Pasadena, California, U.S.A.

Buffin-Belanger, T., Roy, A. G., and Kirkbride, A. D. (2000). On large-scale flow structures in a gravel-bed river. *Geomorphology, 32*, 417-435.

Buffington, J. M. (1999). The legend of A. F. Shields. *J. Hydraul. Eng., 125* (4), 376-387.

Buffington, J. M., and Montgomery, D. R. (1997). A systematic analysis of eight decades of incipient motion studies, with special reference to gravel-bedded rivers. *Water Resour. Res., 33*, 1993-2029.

Bunte, K. (1992). Particle number grain-size composition of bedload in a mountain stream. *Dynamics of gravel-bed rivers*, P. Billi, R. D. Hey, C. R. Thorne, and P. Tacconi (eds.), John Wiley, Chichester, U.K., 55-68.

Carling, P. A. (1983). Threshold of coarse sediment transport in broad and narrow natural streams. *Earth Surf. Processes Landforms, 8*, 1-18.

Carson, M. A., and Griffiths, G. A. (1985). Tractive stress and the onset of bed particle movement in gravel stream channels: different equations for different purposes. *J. Hydrology, 79*, 375-388.

Carson, M. A., and Griffiths, G. A. (1987). Bedload transport in gravel channels. *J. Hydrol. (New Zealand), 26* (1), 1-151.

Casey, H. J. (1935). Uber Geschiebebewegung. *Mitteilungen der Preussischen Versuchsanstalt fur Wasserbau und Schiffbau, 19*, Berlin, Germany.

Cecen, K., and Bayazit, M. (1973). Critical shear stress of armoured beds. *Proc. 15th Congress of the International Association for Hydraulic Research*, vol.1, Int. Assoc. for Hydraul. Res., Delft, Netherlands, 493-500.

Cellino, M., and Graf, W. H. (1999). Sediment-laden flow in open-channels under noncapacity and capacity conditions. *J. Hydraul. Eng., 125*, 455-462.

Charlton, F. G., Brown, P. M., and Benson, R. W. (1978). The hydraulic geometry of some gravel rivers in Britain. *Rep. Hydraul. Res. Stat.*, Wallingford, Oxon, U.K., 48 pp.

Cheng, E. D. (1970). Incipient motion of large roughness elements in turbulent open channel flow. *Ph.D. dissertation*, Utah State Univ., Logan, U.S.A.

Cheng, N.-S., and Chiew, Y.-M. (1998). Pickup probability for sediment entrainment. *J. Hydraul. Eng.*, *124* (2), 232-235.

Chien, N. (1956). The present status of research on sediment transport. *Trans. Am. Soc. Civ. Eng.*, *121*, 833-868.

Chiew, Y.-M., and Parker, G. (1994). Incipient sediment motion on non-horizontal slopes, *J. Hydraul. Res.*, *32* (5), 649-660.

Chow, V. T. (1959). *Open-Channel Hydraulics*, McGraw-Hill Book Co., Singapore.

Church, M. (1978). Palaeohydrological reconstructions from a Holocene valley fill. *Fluvial Sedimentology*, A. D. Miall (ed.), *Can. Soc. Petrol. Geol. Mem.*, *5*, Calgary, Alberta, Canada, 743-772.

Church, M., Wolcott, J. F., and Fletcher, W. K. (1991). A test of equal mobility in fluvial sediment transport: behavior of the sand fraction. *Water Resour. Res.*, *27* (11), 2941-2951.

Clifford, N. J., Robert, A., and Richards, K. S. (1992). Estimation of flow resistance in gravel-bedded rivers: a physical explanation of the multiplier of roughness length. *Earth Surf. Processes Landforms*, *17*, 111-126.

Colombini, M., and Parker, G. (1995). Longitudinal streaks. *J. Fluid Mech.*, *304*, 161-183.

Corino, E. R., and Brodkey, R. S. (1969). A visual investigation of the wall region in turbulent flow. *J. Fluid Mech.*, *37*, 1-30.

Day, T. J. (1980). A study of the transport of graded sediments. *Rep. IT 190*, Hydraulic Research Station, Wallingford, U.K.

Diplas, P. (1987). Bedload transport in gravel-bed streams. *J. Hydraul. Eng.*, *113* (3), 277-292.

Dittrich, A., Nestmann, F., and Ergenzinger, P. (1996). Ratio of lift and shear forces over rough surfaces. *Coherent Flow Structures in Open Channels*, P. J. Ashworth, S. J. Bennett, J. L. Best, and S. J. McLelland (eds.), John Wiley & Sons Ltd, Chichester, U.K., 125-146.

Drake, T. G., Shreve, R. L., Dietrich, W. E., Whiting, P. J., and Leopold, L. B. (1988). Bedload transport of fine gravel observed by motion-picture photography. *J. Fluid Mech., 192*, 193-217.

Egiazaroff, I. V. (1965). Calculation of nonuniform sediment concentration. *J. Hydraul. Div. Am. Soc. Civ. Eng., 91* (4), 225-247.

Egiazaroff, I. V. (1967). Discussion of "Sediment transportation mechanics: Initiation of motion" by V. A. Vanoni et al. *J. Hydraul. Div. Am. Soc. Civ. Eng., 93* (4), 281-287.

Einstein, H. A. (1942). Formulas for the transportation of bed load. *Trans. Am. Soc. Civ. Eng., 107*, 561-597.

Einstein, H. A. (1950). The bedload function for sediment transport in open channel flows. *Tech. Bull. 1026*, U.S. Dep. Agric. Soil Conserv. Serv., Washington, D.C., U.S.A.

Engelund, F., and Hansen, E. (1967). *A Monograph on Sediment Transport in Alluvial Streams*. Teknisk Vorlag, Copenhagen, 65 pp.

Ergenzinger, P., and Jupner, R. (1992). Using COSSY (CObble Satellite SYstem) for measuring the effect of lift and drag forces. *Erosion and Sediment Transport Monitoring Programmes in River Basins* (Proceedings of the Oslo Symposium, August 1992), IAHS Publ. No. 210, 41-49.

Everts, C. H. (1973). Particle overpassing on flat granular boundaries. *J. Waterw. Harbors Coastal Eng. Div. Am. Soc. Civ. Eng., 99*, 425-439.

Fenton, J. D., and Abbott, J. E. (1977). Initial movement of grains on a stream bed: the effect of relative protrusion. *Proc. R. Soc. Lond. A, 352*, 523-537.

Ferguson, R. I., Prestegaard, K. L., and Ashworth, P. J. (1989). Influence of sand on hydraulics and gravel transport on a braided gravel bed river. *Water Resour. Res., 25* (4), 635-643.

Ferguson, R. I., Kirkbride, A. D., and Roy, A. G. (1996). Markov analysis of velocity fluctuations in gravel-bed rivers. *Coherent Flow Structures in Open Channels*, P. J. Ashworth, S. J. Bennett, J. L. Best, and S. J. McLelland (eds.), John Wiley & Sons Ltd, Chichester, U.K., 165-183.

Ferguson, R. I., Hoey, T. B., Wathen, S. J., Werritty, A., Hardwick, R. I., and Sambrook Smith, G. H. (1998). Downstream fining of river gravels: Integrated field, laboratory and modelling study. *Gravel-Bed Rivers in the Environment*, P. C. Klingeman, R. L. Beschta, P. D. Komar, and J. B. Bradley (eds.), Water Resources Publication, LLC, U.S.A., 85-112.

Fidman, B. A. (1953). Principal results of experimental study of the structure of turbulent flows. *Problem of Channel Processes*, N. E. Kondrat'ev and N. N. Fedorov (eds.), Gidrometeoizdat, Leningrad, Russia, 138-150 (in Russian).

Fidman, B. A. (1991). *Turbulence in Water Flows*, Gidrometeoizdat, Leningrad, Russia (in Russian).

Forchheimer, P. (1914). *Hydraulik.* Teubner, Leipzig/Berlin, Germany.

Fortier, S., and Scobey, F. C. (1926). Permissible canal velocities. *Trans. Am. Soc. Civil Engrs., 89*, 940-984.

Frostick, L. E., Lucas, P. M., and Reid, I. (1984). The infiltration of fine matrices into coarse-grained alluvial sediments and its implications for stratigraphical interpretation. *J. geol. Soc. London, 141*, 955-965.

Fuller, C. M. (1998). Bankfull and overbank flow in a straight compound channel with a graded sediment bed: degradational behaviour. *Ph.D. thesis*, Department of Civil Engineering, University of Glasgow, Glasgow, U.K.

Garcia, M., Nino, Y., and Lopez, F. (1996). Laboratory observation of particle entrainment into suspension by turbulent bursting. *Coherent Flow Structures in Open Channels*, P. J. Ashworth, S. J. Bennett, J. L. Best, and S. J. McLelland (eds.), John Wiley & Sons Ltd, Chichester, U.K., 63-86.

Garde, R. J. (1970). Initiation of motion in an hydrodynamically rough surface – critical velocity approach. *JIP (India), 27* (3).

Garde, R. J., and Ranga Raju, K. G. (1987). *Mechanics of Sediment Transportation and Alluvial Stream Problems*, Wiley Eastern Ltd., New Delhi, India.

Gessler, J. (1971). Beginning and ceasing of sediment motion. *River Mechanics*, H. W. Shen (ed.), H. W. Shen, Fort Collins, Colorado, U.S.A., 7:1-7:22.

Gilbert, G. K. (1914). The transportation of debris by running water. *U.S. Geol. Surv. Prof. Pap. 86*, 263 pp.

Gomez, B. (1994). Effects of particle shape and mobility on stable armour development. *Water Resour. Res., 30* (7), 2229-2239.

Gomez, B. (1995). Bedload transport and changing grain size distributions. *Changing River Channels*, A. Gurnell and G. Petts (eds.), John Wiley, Chichester, U.K., 177-199.

Gomez, B., and Church, M. (1988). *A Catalogue of Equilibrium Bedload Transport Data for Coarse Sand and Gravel-bed Channels*, Dept. of Geography, Univ. of British Columbia, Vancouver, Canada.

Goncharov, V. N. (1938). *Sediment transport by uniform flow*. ONTI, Leningrad-Moscow, Russia (in Russian).

Goncharov, V. N. (1954). *The fundamentals of the dynamics of fluvial streams*. Gidrometeoizdat, Leningrad, Russia (in Russian).

Graf, W. H. (1971). *Hydraulics of Sediment Transport*, McGraw-Hill Book Co., New York, U.S.A.

Graf, W. H., and Pazis, G. C. (1977). Les Phenomenes de Deposition et d'Erosion dans un Canal Alluvionnaire. *J. Hydraul. Res., 15*, 151-165.

Graf, W. H., and Suszka, L. (1987). Sediment transport in steep channels. *J. Hydroscience and Hydraul. Eng. Japan Soc. Civ. Engs., 5* (1), 11-26.

Grass, A. J. (1970). Initial instability of fine bed sand. *J. Hydraul. Div. Am. Soc. Civ. Eng., 96*, 619-632.

Grass, A. J. (1971). Structural features of turbulent flow over smooth and rough boundaries. *J. Fluid Mech., 50*, 233-255.

Grass, A. J. (1983). The influence of boundary layer turbulence on the mechanics of sediment transport. *Mechanics of Sediment Transport, Proceedings Euromech 156*, Mutlu Sumer, B. and Muller, A. (eds.), Balkema, Rotterdam, 3-18.

Grass, A. J., Stuart, R. J., and Mansour-Tehrani, M. (1991). Vortical structures and coherent motion in turbulent flow over smooth and rough boundaries. *Phil. Trans. R. Soc. Lond. A, 336*, 35-65.

Grinvald, D. I. (1974). *Turbulence of Open-Channel Flows*, Gidrometeoizdat, Leningrad, Russia (in Russian).

Grinvald, D. I., and Nikora, V. I. (1988). *River Turbulence*, Gidrometeoizdat, Leningrad, Russia (in Russian).

Grishanin, K. V. (1990). *Fundamentals of the Dynamics of Alluvial Flows*, Transport, Moscow, Russia (in Russian).

Gvelesiani, L. G. (1946). Theoretical and practical problems of sediment transport calculations. *Gidrotekhnicheskoe stroitelstvo, 4*, Gosenergoizdat, Moscow, Russia, 28-29 (in Russian).

Gyr, A., and Schmid, A. (1997). Turbulent flows over smooth erodible sand beds in flumes. *J. Hydraul. Res., 35*, 525-544.

Halcrow/HR Wallingford (1997). *ISIS Flow User Manual*, Swindon, U.K.

Halcrow/HR Wallingford (1999). *ISIS Sediment User Manual*, Swindon, U.K.

Hammond, F. D. C., Heathershaw, A. D., and Langhorne, D. N. (1984). A comparison between Shields' threshold criterion and the movement of loosely packed gravel in a tidal channel. *Sedimentology, 31*, 51-62.

Hardwick, R. I., and Willetts, B. B. (1991). Changes with time of the transport rate of sediment mixtures. *J. Hydraul. Res., 29* (1).

Hayashi, T., Ozaki, S., and Ishibashi, T. (1980). Study on the bedload transport of sediment mixture. *Proc. 24th Japanese Hydraul. Conf.*, 35-43.

Helland-Hansen, E. (1971). Time as a parameter in the study of incipient motion of gravel. *Trans. Am. Geophy. Union*, Northwest Regional Section, Corvallis, Oregon, U.S.A.

Helley, E. J., and Smith, W. (1971). Development and calibration of a pressure-difference bedload sampler. *U.S. Geological Survey Open-File Report*, Menlo Park, Calif., U.S.A.

Hey, R. D. (1988). Bar form resistance in grave-bed rivers. *J. Hydraul. Eng., 114* (12), 1498-1508.

Heyndrickx, G. A. (1948). *Het transport van bodemmateriaal door stromend water.* Drukkerij G.I.G., Brussels.

Hjulstrom, F. (1935). Studies of the morphological activity of rivers as illustrated by the River Fyris. *Bull. Geol. Inst. Univ. Uppsala, 25*, 221-527.

Ho, P.-Y. (1939). Abhangigkeit der Geschiebebewegung von der Kornform und der Temperature. *Mitteilungen der Preussischen Versuchsanstalt fur Wasserbau und Schiffbau, 37*, Berlin, Germany.

Hoey, T. B., and Ferguson, R. (1994). Numerical simulation of downstream fining by selective transport in gravel bed rivers: Model development and illustration. *Water Resour. Res., 30* (7), 2251-2260.

Ikeda, H. (1983). Experiments on bedload transport, bed forms, and sedimentary structures using fine gravel in the 4-meter-wide flume. *Rep. Environmental Research Center, University of Tsukuba*, No. 2, Tokyo, Japan.

Ikeda, S. (1981). Self-formed straight channels in sandy beds. *J. Hydraul. Div. Am. Soc. Civ. Eng., 107* (HY4), 389-406.

Imamoto, H., and Ishigaki, T. (1986a). The three dimensional structure of turbulent shear flow in an open channel. *Proc. Fifth Congress of the Asian and Pacific Regional Division of the International Association for Hydraulic Research*, vol. 1, Seoul, Korea, 139-155.

Imamoto, H., and Ishigaki, T. (1986b). Visualization of longitudinal eddies in an open channel flow. *Proc. Fourth International Symposium on Flow Visualization*, Ecole Nationale Superieure de Techniques Avancees, Paris, France, 333-337.

Karaushev, A. V. (1977). *Theory and Methods of River Sediment Computations*, Gidrometeoizdat, Leningrad, Russia (in Russian).

Kennedy, J. F. (1995). The Albert Shields story. *J. Hydraul. Eng., 121* (11), 766-772.

Keshavarzy, A., and Ball, J. E. (2000). An application of image processing in the study of sediment motion. *J. Hydraul. Res., 37* (4), 559-576.

Kim, H. T., Kline, S. J., and Reynolds, W. C. (1971). The production of turbulence near a smooth wall in a turbulent boundary layer. *J. Fluid Mech., 50* (1), 133-160.

Kirkbride, A. D., and Ferguson, R. (1995). Turbulent flow structure in a gravel-bed river: Markov chain analysis of the fluctuating velocity profile. *Earth Surf. Processes Landforms, 20*, 721-733.

Klaven, A. B. (1966). Investigation of the flow turbulent structure. *Trans. State Hydrol. Inst., 136*, Gidrometeoizdat, Leningrad, Russia, 65-76 (in Russian).

Klaven, A. B. (1968). Kinematic structure of the turbulent flow. *Trans. State Hydrol. Inst., 147*, Gidrometeoizdat, Leningrad, Russia, 134-141 (in Russian).

Klaven, A. B. (1987). The interaction of open-channel flow and noncohesive bed material and its implication for modelling of channel micro-forms. *Trans. State Hydrol. Inst., 307*, Gidrometeoizdat, Leningrad, Russia, 71-81 (in Russian).

Klaven, A. B., and Kopaliani, Z. D. (1973). Laboratory investigations of the kinematic structure of turbulent flow over a rough bed. *Trans. State Hydrol. Inst., 209*, Gidrometeoizdat, Leningrad, Russia, 67-90 (in Russian).

Klaven, A. B., and Kokovin, V. N. (1987). Some experimental results on properties of open-channel flow at the bed surface and inside the granular bed. *Trans. State Hydrol. Inst., 307*, Gidrometeoizdat, Leningrad, Russia, 82-91 (in Russian).

Kline, S. J., Reynolds, W. C., Schraub, F. A., and Runstadler, P. W. (1967). The structure of turbulent boundary layers. *J. Fluid Mech., 30*, 741-773.

Knoroz, V. S. (1953). Non-eroding velocity for fine sand. *Hydrotechnical Construction, 8*, Moscow, Russia, 21-24 (in Russian).

Komar, P. D. (1987a). Selective entrainment by a current from a bed of mixed sizes: a reanalysis. *J. Sedimentary Petrol., 57* (2), 203-211.

Komar, P. D. (1987b). Selective gravel entrainment and the empirical evaluation of flow competence. *Sedimentology, 34*, 1165-1176.

Komar, P. D. (1996). Entrainment of sediments from deposits of mixed grain sizes and densities. *Advances in Fluvial Dynamics and Stratigraphy*, P. A. Carling and M. R. Dawson (eds.), John Wiley & Sons Ltd., 127-181.

Komar, P. D., and Carling, P. A. (1991). Grain sorting in gravel-bed streams and the choice of particle sizes for flow-competence evaluations. *Sedimentology, 38*, 489-502.

Komar, P. D., and Li, Z. (1986). Pivoting analyses of the selective entrainment of sediments by shape and size with application to gravel threshold. *Sedimentology, 33*, 425-436.

Komar, P. D., and Shih, S.-M. (1992). Equal mobility versus changing bedload grain sizes in gravel-bed streams. *Dynamics of gravel-bed rivers*, P. Billi, R. D. Hey, C. R. Thorne, and P. Tacconi (eds.), John Wiley, Chichester, U.K., 73-93.

Komori, S., Ueda, H.. Ogino, F., and Mizushina, T. (1982). Turbulence structure and transport mechanism at the free surface in an open channel flow. *Int. J. Heat Mass Transfer, 25* (4), 513-521.

Kramer, H. (1935). Sand mixtures and sand movement in fluvial models. *Trans. Am. Soc. Civ. Eng., 100*, 798-878.

Krey, H. (1925). Grenzen der Ubertragbarkeit der Versuchsergebnisse. *Z. angew. Math. Mech.*, Bd. 5, Heft 6.

Kuhnle, R. A. (1992). Fractional transport rates of bedload on Goodwin Creek. *Dynamics of Gravel-bed Rivers*, P. Billi, R. D. Hey, C. R. Thorne, and P. Tacconi (eds.), John Wiley, New York, U.S.A., 141-155.

Kuhnle, R. A. (1993a). Fluvial transport of sand and gravel mixtures with bimodal size distributions. *Sedimentary Geology, 85*, 17-24.

Kuhnle, R. A. (1993b). Incipient motion of sand-gravel sediment mixtures. *J. Hydraul. Eng., 119* (12), 1400-1415.

Kuhnle, R. A. (1995). Closure to "Incipient motion of sand-gravel sediment mixtures". *J. Hydraul. Eng., 121* (5), 448-450.

Kuhnle, R. A. (1996). Unsteady transport of sand and gravel mixtures. *Advances in Fluvial Dynamics and Stratigraphy*, P. A. Carling and M. R. Dawson (eds.), John Wiley and Sons Ltd, Chichester, U.K., 183-201.

Kuhnle, R. A., and Southard, J. B. (1988). Bed load transport fluctuations in a gravel bed laboratory channel. *Water Resour. Res., 24* (2), 247-260.

Kuhnle, R. A., and Willis, J. C. (1998). Statistics of sediment transport in Goodwin Creek. *J. Hydraul. Eng.*, *124* (11), 1109-1114.

Lapointe, M. (1992). Burst-like sediment suspension events in a sand bed river. *Earth Surf. Processes Landforms*, *17*, 253-270.

Laursen, E. M. (2000). Discussion of "The legend of A. F. Shields" by J. M. Buffington. *J. Hydraul. Eng.*, *126* (9), 720-721.

Lavelle, J. W., and Mofjeld, H. O. (1987). Do critical stresses for incipient motion and erosion really exist? *J. Hydraul. Eng.*, *113*, 370-385.

Levi, I. I. (1957). *Dynamics of fluvial streams*. Gosenergoizdat, Moscow-Leningrad, Russia (in Russian).

Li, Z., and Komar, P. D. (1986). Laboratory measurements of pivoting angles for applications to selective entrainment of gravel in a current. *Sedimentology*, *33*, 413-423.

Liu, T.-Y. (1935). Transportation of the bottom load in an open channel. *M.S. thesis*, Univ. of Iowa, Iowa City, U.S.A.

Livesey, J. R., Bennett, S., Ashworth, P. J., and Best, J. L. (1998). Flow structure, sediment transport and bedform dynamics for a bimodal sediment mixture. *Gravel-Bed Rivers in the Environment*, P. C. Klingeman, R. L. Beschta, P. D. Komar, and J. B. Bradley (eds.), Water Resources Publications, LLC, Colorado, U.S.A., 149-172.

Luque, R. F., and van Beek, R. (1976). Erosion and transport of bedload sediment. *J. Hydraul. Res.*, *14* (2), 127-144.

Macauley, A. (1999). The response of graded sediment system to changes in flow regime and sediment supply. *Rep. Dept. Civil Eng., University of Glasgow*, Glasgow, U.K.

Mantz, P. A. (1977). Incipient motion of fine grains and flakes by fluids - extended Shields diagram. *J. Hydraul. Div. Am. Soc. Civ. Eng.*, *103*, 601-615.

Marion, A. (1996). Equilibrium bed material composition for well-graded sediment mixtures in a compound channel. *Rep. SR 474*, HR Wallingford, Wallingford, Oxon, U.K.

McLelland, S. J., Ashworth, P. J., Best, J. L., and Livesey, J. R. (1999). Turbulence and secondary flow over sediment stripes in weakly bimodal bed material. *J. Hydraul. Eng.*, *125* (5), 463-473.

Meyer-Peter, E., and Muller, R. (1948). Formulas for bed-load transport. *Proc. 2nd Meeting of the International Association for Hydraulic Structures Research*, Inter. Assoc. for Hydraul. Res., Delft, Netherlands, 39-64.

Milhous, R. T. (1973). Sediment transport in a gravel-bottomed stream. *Ph.D. dissertation*, Oregon State University, Corvallis, Oregon, U.S.A.

Milhous, R. T. (1997). A low shear stress gravel-bed river. *Proc. 27th Congr. of the International Association for Hydraulics Research*, Vol. 2 (theme B), New York, U.S.A., 599-604.

Miller, M. C., McCave, I. N., and Komar, P. D. (1977). Threshold of sediment motion under unidirectional currents, *Sedimentology*, *24*, 507-527.

Misri, R. L., Garde, R. J., and Ranga Raju, K. G. (1983). Experiments on bed load transport of nonuniform sands and gravels. *Proc. Second International Symposium on River Sedimentation*, Water Resources and Electric Power Press, Beijing, China, 440-450.

Misri, R. L., Garde, R. J. and Ranga Raju, K. G. (1984). Bed load transport of coarse nonuniform sediment. *J. Hydraul. Eng.*, *110* (3), 312-328.

Mizuyama, T. (1977). Bedload transport in steep channels. *Ph.D. dissertation*, Kyoto Univ., Kyoto, Japan.

Monin, A. S., and Yaglom, A. M. (1975). *Statistical Fluid Mechanics: Mechanics of Turbulence*, vol.2, MIT Press, Boston, Mass., U.S.A.

Moody, L. F. (1944). Friction factors for pipe flow. *Trans. Am. Soc. Mech. Eng.*, *66*, 671-678.

Nakagawa, H., Tsujimoto, T., and Nakano, S. (1982). Characteristics of sediment motion for respective grain sizes of sand mixtures. *Bulletin of the Disaster Prevention Research Institute*, Kyoto University, *32* (1), No. 286, 1-32.

Neill, C. R. (1967). Mean-velocity criterion for scour of coarse uniform bed-material. *Proc. 12th Congress of the International Association for Hydraulics Research*, vol. 3, Fort Collins, Colorado, U.S.A., 46-54.

Neill, C. R. (1968a). Note on initial movement of coarse uniform bed-material. *J. Hydraul. Res.*, *6* (2), 173-176.

Neill, C. R. (1968b). A re-examination of the beginning of movement for coarse granular material. *Rep. INT68*, Hydraulic Research Station, Wallingford, U.K.

Neill, C. R., and Yalin, M. S. (1969). Quantitative definition of beginning of bed movement. *J. Hydraul. Div. Am. Soc. Civ. Eng.*, *95*, 585-588.

Nezu, I., and Nakagawa, H. (1989). Self forming mechanism of longitudinal sand ridges and troughs in fluvial open-channel flows. *Proc. 23rd Congress of the International Association for Hydraulic Research, B (Fluvial Hydraulics)*, Ottawa, Canada, 65-72.

Nezu, I., and Nakagawa, H. (1993). *Turbulence in Open-Channel Flows*, A. A. Balkema, Rotterdam, Netherlands.

Nikora, V. I., and Goring, D. G. (1999). Are weakly mobile-bed flows a special class of wall-bounded flows? *Proc. 28th Congress of the International Association for Hydraulic Research* (CD-ROM), Graz, Austria.

Nikora, V., and Goring, D. (2000). Flow turbulence over fixed and weakly mobile gravel beds. . *J. Hydraul. Eng., 126*, 679-690.

Nikora, V. I., and Smart, G. M. (1997). Turbulence characteristics of New Zealand gravel-bed rivers. *J. Hydraul. Eng., 123*, 764-773.

Nikuradze, J. (1933). Stromungsgesetze in rauhen Rohren. *Forschg. Arb. Ing. Wes., 361* (English translation, Laws of flow in rough pipes, *Tech. Memo. 1292*, Natl. Adv. Comm. for Aeron., Washington, D. C., U.S.A., 1950).

Nychas, S. G., Hershey, H. C., and Brodkey, R. S. (1973). A visual study of turbulent shear flow. *J. Fluid Mech., 61*, 513-540.

Paintal, A. S. (1971). Concept of critical shear stress in loose boundary open channels. *J. Hydraul. Res., 9*, 91-113.

Parker, G. (1990). Surface-based bedload transport relation. *J. Hydraul. Res., 28* (4), 417-436.

Parker, G. (1991). Selective sorting and abrasion of river gravel, I: Theory. *J. Hydraul. Eng., 117* (2), 131-149.

Parker, G., and Peterson, A. W. (1980). Bar resistance of gravel-bed streams. *J. Hydraul. Div. Am. Soc. Civ. Eng., 106* (10), 1559-1575.

Parker, G., and Klingeman, P. C. (1982). On why gravel bed streams are paved. *Water Resour. Res., 18* (5), 1409-1423.

Parker, G., Klingeman, P. C., and McLean, D. G. (1982). Bedload and size distribution in paved gravel-bed streams. *J. Hydraul. Div. Am. Soc. Civ. Eng., 108*, 544-571.

Patel, P. L., and Ranga Raju, K. G. (1996). Fractionwise calculation of bed load transport. *J. Hydraul. Res., 34* (3), 363-379.

Patel, P. L., and Ranga Raju, K. G. (1999). Critical tractive stress of nonuniform sediments. *J. Hydraul. Res., 37* (1), 39-58.

Pender, G., and Li, Q. (1995). Comparison of two hiding function formulations for non-uniform sediment transport calculations. *Proc. Instn Civ. Engrs Wat., Marit. & Energy, 112*, 127-135.

Pender, G., and **Shvidchenko, A.** (1999). The observation of bedload sheets in laboratory experiments. *Proc. 28th Congress of the International Association for Hydraulic Research* (CD-ROM), Graz, Austria.

Petit, F. (1994). Dimensionless critical shear stress evaluation from flume experiments using different gravel beds. *Earth Surf. Proces. and Landforms, 19*, 565-576.

Petroff, C. M. (1993). The interaction of breaking solitary waves with an armoured bed. *Rep. KH-R-55*, W. M. Keck Laboratory of Hydraulics and Water Resources, California Institute of Technology, Pasadena, California, U.S.A.

Pozdnyakov, Sh. R. (1987). Methods of calculation and measurement of coarse sediment transport in rivers. *Ph.D. dissertation*, State Hydrological Institute, Leningrad, Russia.

Powell, D. M. (1998). Patterns and processes of sediment sorting in gravel-bed rivers. *Progress in Physical Geography 22*, 1, Edward Arnold, London, U.K., 1-32.

Prestegaard, K. L. (1983). Bar resistance in gravel bed streams at bank-full stage. *Water Resour. Res., 19* (2), 473-476.

Quraishy, M. S. (1943). The critical shear stress. *J. Univ. Bombay, 12*, Pt. 3, India, 37-46.

Rakoczi, L. (1975). Influence of grain-size composition on the incipient motion and self-pavement of bed materials. *Proc. 16th Congress of the International Association for Hydraulic Research*, vol. 2, Int. Assoc. for Hydraul. Res., Delft, Netherlands, 150-157.

Rakoczi, L. (1987). Selective erosion of noncohesive bed materials. *Geograf. Annal., 69A* (1), 29-35.

Rashidi, M., and Banerjee, S. (1988). Turbulence structure in free-surface channel flows. *Phys. Fluids, 31* (9), 2491-2503.

Rathburn, R. E., and Guy, H. P. (1967). Measurement of hydraulic and sediment transport variables in a small recirculating flume. *Water Resour. Res., 3*, 107-122.

Reid, I., Frostick, L. E., and Layman, J. T. (1985). The incidence and nature of bedload transport during flood flows in coarse-grained alluvial channels. *Earth Surf. Processes Landforms, 10*, 33-44.

Richards, K. (1990). Fluvial geomorphology: initial motion of bed material in gravel-bed rivers. *Progress in Physical Geography, 14*, Edward Arnold, London, U.K.,395-415.

Rijn, L. C. (1984). Sediment transport, part I: bed load transport. *J. Hydraul. Eng., 110* (10), 1431-1456.

Rijn, L. C. (1989). Sediment transport by currents and waves (handbook). *Rep. H 461*, Delft Hydraulics, Netherlands.

Robert, A., Roy, A. G., and De Serres, B. (1993). Space-time correlations of velocity measurements at a roughness transition in a gravel-bed river. *Turbulence: Perspectives on Flow and Sediment Transport*, N. J. Clifford, J. R. French and J. Hardisty (eds.), John Wiley & Sons Ltd, Chichester, U.K., 165-183.

Romanovsky, V. V. (1974). Investigation of critical velocity for sediment motion. *Trans. State Hydrol. Inst., 210*, Gidrometeoizdat, Leningrad, Russia (in Russian).

Rossinsky, K. I. (1968). Bedload motion. *Trans. State Hydrol. Inst., 160*, Gidrometeoizdat, Leningrad, Russia, 102-139 (in Russian).

Rouse, H. (1939). An analysis of sediment transportation in light of fluid turbulence. *Rep. SCS-TP-25*, Sediment Div., U.S. Dept. of Agric., Soil Conservation Service, Washington, D.C., U.S.A.

Roy, A. G., and Buffin-Belanger, T. (2000). Advances in the study of turbulent flow structures in gravel-bed rivers. *Proc. Gravel-bed River Workshop*, Christchurch, New Zealand (in press).

Roy, A. G., Buffin-Belanger, T., and Deland, S. (1996). Scales of turbulent coherent flow structures in a gravel-bed river. *Coherent Flow Structures in Open Channels*, P. J. Ashworth, S. J. Bennett, J. L. Best, and S. J. McLelland (eds.), John Wiley & Sons Ltd, Chichester, U.K., 147-164.

Samaga, B. R., Ranga Raju, K. G., and Garde, R. J. (1986). Bed load transport of sediment mixtures. *J. Hydraul. Eng., 112* (11), 1003-1018.

Seal, R., Toro-Escobar, C., Cui, Y., Paola, C., Parker, G., Southard, J. B., and Wilcock, P. R. (1998). Downstream fining by selective deposition: Theory, laboratory, and field observations. *Gravel-Bed Rivers in the Environment*, P. C. Klingeman, R. L. Beschta, P. D. Komar, and J. B. Bradley (eds.), Water Resources Publication, LLC, U.S.A., 61-81.

Sechet, P., and Le Guennec, B. (1999). Bursting phenomenon and incipient motion of solid particles in bed-load transport. *J. Hydraul. Res., 37*, 683-696.

Shamov, G. I. (1959). *Fluvial sediments*. Gidrometeoizdat, Leningrad, Russia (in Russian).

Schoklitsch, A. (1914). *Uber Schleppkraft und Geschibebewegung*, Englemann, Leipzig, Germany.

Schoklitsch, A. (1962). *Handbuch des Wasserbaues*, 3rd edn, Springer-Verlag, Vienna, Austria.

Shen, C., and Lemmin, U. (1999). Application of an acoustic particle flux profiler in particle-laden open-channel flow, *J. Hydraul. Res.*, *37*, 407-419.

Shields, A. (1936). Anwendung der Ahnlichkeitsmechanik und der Turbulentzforschung auf die Geshiebebewegung. *Mitteilungen der Preussischen Versuchsanstalt fur Wasserbau und Schiffbau*, *26*, Berlin, Germany (English translation by W. P. Ott and J. C. van Uchelen, *Rep. 167*, *Hydrodynamics* Lab., California Institute of Technology, Pasadena, California, U.S.A.).

Shvidchenko, A. (1999). Incipient motion of uniform sediments. *Proc. 28th Congress of the International Association for Hydraulic Research* (CD-ROM), Graz, Austria.

Shvidchenko, A. B., and Pender, G. (2000a). Flume study of the effect of relative depth on the incipient motion of coarse uniform sediments. *Water Resour. Res.*, *36* (2), 619-628.

Shvidchenko, A. B., and Pender, G. (2000b). Initial motion of streambeds composed of coarse uniform sediments. *Proc. Instn Civ. Engrs Wat., Marit. & Energy*, 142, 217-227.

Shvidchenko, A. B., and Pender, G. (2000c). Macroturbulent structure of open-channel flow over gravel beds. *Water Resour. Res.* (in press).

Shvidchenko, A. B., Pender, G., and Hoey, T. B. (2000). Critical shear stress for incipient motion of streambeds. *Proc. Gravel-bed Rivers Workshop 2000* (CD-ROM), Christchurch, New Zealand.

Silberman, E., Carter, R. W., Einstein, H. A., Hinds, J., and Powell, R. W. (1963) Friction factor in open channels. *J. Hydraul. Div. Am. Soc. Civ. Eng.*, *89* (HY2), 97-143.

Smart, G. M. (1984). Sediment transport formula for steep channels. *J. Hydraul. Eng.*, *110*, 267-276.

Smith, C. R. (1996). Coherent flow structures in smooth-wall turbulent boundary layers: facts, mechanism and speculation. *Coherent Flow Structures in Open Channels*, P.

J. Ashworth, S. J. Bennett, J. L. Best, and S. J. McLelland (eds.), John Wiley & Sons Ltd, Chichester, U.K., 1-39.

SONTEK (1995). *ADV Operation Manual*, San Diego, California, U.S.A., 30 pp.

Sumer, B. M., and Deigaard, R. (1981). Particle motions near the bottom in turbulent flow in an open channel. Part 2. *J. Fluid Mech.*, *109*, 311-337.

Swamee, P. K., and Ojha, C. S. (1991). Bed-load and suspended-load transport of nonuniform sediments. *J. Hydraul. Eng.*, *117* (6), 774-787.

Talmaza, V. F., and Kroshkin, A. N. (1968). *Hydromorphometric characteristics of mountain rivers*. Frunze, Kirgizstan (in Russian).

Talmon, A. M., Kunen, J. M. G., and Ooms, G. (1986). Simultaneous flow visualization and Reynolds-stress measurement in a turbulent boundary layer. *J. Fluid Mech.*, *163*, 459-478.

Tamburrino, A., and Gulliver, J. S. (1999). Large flow structures in a turbulent open channel flow. *J. Hydraul. Res.*, *37* (3), 363-380.

Taylor, B. D., and Vanoni, V. A. (1972). Temperature effects in low-transport, flat-bed flows. *J. Hydraul. Div. Am. Soc. Civ. Eng.*, *98*, 1427-1445.

Torri, D., and Poesen, J. (1988). Incipient motion conditions for single rock fragments in simulated rill flow. *Earth Surf. Processes Landforms*, *13*, 225-237.

Tsujimoto, T. (1989). Longitudinal stripes of alternate sorting due to cellular secondary currents. *Proc. 23rd Congress of the International Association for Hydraulic Research*, vol. 2, Ottawa, Canada, 17-24.

Unsold, G. (1982). Der Transportbeginn rolligem Sohlenmaterials in gleichformigen turbulenten Stromungen: Eine kritische Uberprufung der Shields-Funktion und ihre experimentelle Erweiterung auf feinkornige, nichtbindige Sedimente. *Dissertation*, Mathematische-Naturwissenschaftlichen Fakultat, Univeristat Kiel, Germany.

U.S. Waterways Experimental Station (USWES) (1935). Study of river-bed material and their use with special reference to the Lower Mississippi River. *Pap. 17*, Vicksburg, Miss., U.S.A.

Vanoni, V. A., Benedict, P. C., Bondurant, D. C., McKee, J. E., Piest, R. F., and Smallshaw, J. (1971). Sediment transportation mechanics: F. Hydraulic relations for alluvial streams. *J. Hydraul. Div. Am. Soc. Civ. Eng.*, *97*, 101-141.

Velikanov, M. A. (1949). *Dynamics of Alluvial Flows*, Gidrometeoizdat, Leningrad, Russia (in Russian).

Wathen, S. J., Ferguson, R. I., Hoey, T. B., and Werritty, A. (1995). Unequal mobility of gravel and sand in weakly bimodal river sediments. *Water Resour. Res.*, *31* (8), 2087-2096.

White, C. M. (1940). The equilibrium of grains on the be of a stream. *Proc. Royal Soc. of London*, Series A, Vol. 174, No. A 956, London, U.K., 322-338.

White, S. J. (1970). Plane bed threshold of fine grained sediments. *Nature*, *228*, 152-153.

White, W. R., and Day, T. J. (1982). Transport of graded gravel bed material. *Gravel bed rivers*, R. D. Hey, J. C. Bathurst, and C. R. Thorne (eds.), John Wiley, Chichester, U.K., 181-213.

Whiting, P. J. (1996). Sediment sorting over bed topography. *Advances in Fluvial Dynamics and Stratigraphy*, P. A. Carling and M. R. Dawson (eds.), John Wiley and Sons Ltd, Chichester, U.K., 203-228.

Whiting, P. J., Deitrich, W. E., Leopold, L. B., Drake, T. G., and Shreve, R. L. (1988). Bedload sheets in heterogeneous sediment. *Geology*, *16* (2), 105-108.

Wiberg, P. L., and Smith, J. D. (1987). Calculations of the critical shear stress for motion of uniform and heterogeneous sediments. *Water Resour. Res.*, *23* (8), 1471-1480.

Wilcock, P. R. (1988). Methods for estimating the critical shear stress of individual fractions. *Water Resour. Res.*, *24* (7), 1127-1135.

Wilcock, P. R. (1992). Experimental investigation of the effect of mixture properties on transport dynamics. *Dynamics of gravel-bed rivers*, P. Billi, R. D. Hey, C. R. Thorne, and P. Tacconi (eds.), John Wiley, Chichester, U.K., 109-131.

Wilcock, P. R. (1993). Critical shear stress of natural sediments. *J. Hydraul. Eng.*, *119*, 491-505.

Wilcock, P. R. (1997a). The components of fractional transport rate. *Water Resour. Res.*, *33* (1), 247-258.

Wilcock, P. R. (1997b). Entrainment, displacement and transport of tracer gravels. *Earth Surf. Processes Landforms*, *22*, 1125-1138.

Wilcock, P. R., and McArdell, B. W. (1993). Surface-based fractional transport rates: mobilization thresholds and partial transport of a sand-gravel sediment. *Water Resour. Res.*, *29* (4), 1297-1312.

Wilcock, P. R., and McArdell, B. W. (1997). Partial transport of a sand/gravel sediment. *Water Resour. Res.*, *33* (1), 235-245.

Wilcock, P. R., and Southard, J. B. (1988). Experimental study of incipient motion in mixed-size sediment. *Water Resour. Res.*, *24* (7), 1137-1151.

Wilcock, P. R., and Southard, J. B. (1989). Bed load transport of mixed size sediment: fractional transport rates, bed forms, and the development of a coarse bed surface layer. *Water Resour. Res.*, *25* (7), 1629-1641.

Wilcock, P. R., Barta, A. F., Shea, C. C., Kondolf, G. M., Matthews, W. V. G., and Pitlick, J. (1996). Observations of flow and sediment entrainment on a large gravel-bed river. *Water Resour. Res.*, *32*, 2897-2909.

Willetts, B. B., Pender, G., and McEwan, I. K. (1998). Experiments on the transport of graded sediment. *Proc. Instn Civ. Engrs Wat., Marit. & Energy*, *130*, 217-225.

Williams, P. B., and Kemp, P. H. (1971). Initiation of ripples on flat sediment beds. *J. Hydraul. Div. Am. Soc. Civ. Eng.*, *97*, 505-522.

Wolman, M. G., and Brush, L. M. (1961). Factors controlling the size and shape of stream channels in coarse noncohesive sands. *U.S. Geol. Surv. Prof. Pap. 282-G*, U.S.A.

Yalin, M. S. (1971). *Theory of Hydraulic Models*, Macmillan, London, U.K.

Yalin, M. S. (1972). *Mechanics of Sediment Transport*, Pergamon, Elmsford, New York, U.S.A.

Yalin, M. S. (1992). *River Mechanics*, Pergamon Press Ltd, Oxford, U.K.

Yalin, M. S., and Karahan, E. (1979). Inception of sediment transport. *J. Hydraul. Div. Am. Soc. Civ. Eng.*, *105*, 1433-1443.

Yang, C. T. (1973). Incipient motion and sediment transport. *J. Hydraul. Div. Am. Soc. Civ. Eng.*, *99* (HY10), 1679-1704.

Zaitsev, N. I. (1984). Large-scale structure of turbulent flow in a rectangular flume. *Trans. State Hydrol. Inst.*, *318*, Gidrometeoizdat, Leningrad, Russia, 3-17 (in Russian).

Zegzhda, A. P. (1938). *Theory of Similarity and Method of Design of Models for Hydraulic Engineering*, Gosstroyizdat, Moscow-Leningrad, Russia (in Russian).

Zeller, J. (1963). Einfuhrung in den Sedimenttransport offener Gerinne. *Schweiz. Bauzeitung*, *Jg. 81*, 597-602.

Appendix A

Table A.1 Measured Data for Uniform Sediments (Armfield Flume, width 0.30 m)

Run No.	Sediment *d* (mm)	Slope *J* x 10^3	Flow *Q* ($L\,s^{-1}$)	Depth *h* (m)	Sampling Duration (mins)	Bedload Yield (g)	Transport Intensity		Water Temp. (°C)
							I mean (s^{-1})	*I steady* (s^{-1})	
U1-1	1.5	1.9	3.0	0.0355	127	8.5	3.3E-05	3.3E-05	20.0
U1-2		1.9	3.5	0.0378	120	37.6	1.3E-04	1.1E-04	19.5
U1-3		1.9	3.7	0.0388	131	132.3	3.1E-04	2.6E-04	19.8
U1-4		1.9	4.2	0.0398	60	105.7	5.6E-04	5.6E-04	18.8
U1-5		1.9	4.6	0.0423	40	232.3	-	-	19.4
U1-6		1.9	5.8	0.0485	10	490.1	-	-	19.3
U1-7	1.5	4.1	1.0	0.0207	75	20.9	1.1E-04	1.1E-04	16.2
U1-8		4.1	1.3	0.0220	80	49.5	3.2E-04	2.8E-04	17.1
U1-9		4.1	1.9	0.0232	60	210.2	1.5E-03	1.5E-03	18.0
U1-10		4.1	2.0	0.0246	60	424.5	-	-	15.6
U1-11		4.1	2.4	0.0263	60	608.5	-	-	17.7
U1-12		4.1	3.0	0.0285	45	998.0	-	-	17.8
U1-13		4.1	3.5	0.0314	13	663.6	-	-	18.3
U1-14	1.5	6.5	-	0.0146	60	23.6	1.3E-04	1.1E-04	19.0
U1-15		6.5	-	0.0157	147	26.1	3.7E-05	3.7E-05	20.2
U1-16		6.5	-	0.0157	60	59.5	2.7E-04	2.7E-04	19.2
U1-17		6.5	-	0.0168	85	143.6	4.6E-04	4.6E-04	19.0
U1-18		6.5	0.9	0.0174	30	385.7	1.9E-03	1.9E-03	19.3
U1-19		6.5	1.2	0.0196	23	498.7	-	-	19.0
U1-20	1.5	8.3	-	0.0120	130	7.6	2.4E-05	1.2E-05	17.6
U1-21		8.3	-	0.0123	127	17.4	5.5E-05	5.5E-05	19.2
U1-22		8.3	-	0.0128	60	38.3	3.7E-04	3.7E-04	18.4
U1-23		8.3	-	0.0132	60	167.7	8.4E-04	8.4E-04	19.4
U1-24		8.3	-	0.0134	60	27.6	3.6E-04	2.6E-04	18.8
U1-25		8.3	-	0.0141	60	450.0	1.3E-03	1.3E-03	19.1
U1-26		8.3	-	0.0145	21	460.1	-	-	19.0
U1-27		8.3	-	0.0165	17	245.3	-	-	19.4
U1-28	1.5	14.1	-	0.0065	128	5.0	1.3E-05	6.0E-06	18.8
U1-29		14.1	-	0.0072	20	188.4	7.4E-04	7.4E-04	19.0
U1-30		14.1	-	0.0080	87	3.0	2.0E-05	6.0E-06	19.5
U1-31		14.1	-	0.0088	38	399.5	-	-	15.4
U1-32		14.1	-	0.0096	47	160.2	3.7E-04	3.7E-04	20.5
U1-33		14.1	-	0.0110	10	587.7	-	-	16.4
U1-34		14.1	1.3	0.0160	7	1795.6	-	-	17.8

Table A.1 (continued)

Run No.	Sediment d (mm)	Slope J x 10^3	Flow Q ($L\ s^{-1}$)	Depth h (m)	Sampling Duration (mins)	Bedload Yield (g)	Transport Intensity		Water Temp. ($^{\circ}C$)
							I mean (s^{-1})	*I steady* (s^{-1})	
U2-1	2.4	2.6	5.2	0.0450	60	7.5	1.2E-05	7.6E-06	17.2
U2-2		2.6	6.0	0.0490	45	31.5	5.8E-05	5.2E-05	17.8
U2-3		2.6	7.0	0.0524	50	69.4	9.7E-05	7.1E-05	17.4
U2-4		2.6	8.0	0.0570	50	150.3	2.1E-04	1.7E-04	17.3
U2-5		2.6	9.4	0.0637	15	177.7	8.0E-04	8.0E-04	17.6
U2-6		2.6	10.5	0.0683	10	433.4	2.8E-03	2.8E-03	18.4
U2-7	2.4	4.1	-	0.0322	8	-	-	0.0E+00	20.2
U2-8		4.1	-	0.0373	90	4.9	1.2E-05	5.4E-06	22.7
U2-9		4.1	-	0.0387	120	37.9	-	6.5E-05	20.2
U2-10		4.1	-	0.0426	90	83.9	1.5E-04	5.4E-05	21.5
U2-11		4.1	-	0.0428	123	573.2	1.8E-03	1.8E-03	23.5
U2-12		4.1	-	0.0450	122	179.2	-	-	24.3
U2-13		4.1	-	0.0460	65	765.6	1.5E-03	1.5E-03	23.4
U2-14		4.1	-	0.0465	60	519.9	8.3E-04	8.3E-04	23
U2-15		4.1	-	0.0492	30	1075	3.8E-03	3.8E-03	23
U2-16		4.1	-	0.0530	60	889.8	1.9E-03	1.9E-03	23
U2-17		4.1	-	0.0572	18	1636.5	1.9E-02	1.9E-02	23.2
U2-18		4.1	-	0.0625	15	1186.9	9.0E-03	9.0E-03	23.2
U2-19		4.1	-	0.0660	7	2014.4	3.3E-02	3.3E-02	22.7
U2-20	2.4	6.5	-	0.0243	60	3.0	1.4E-05	5.4E-06	22.5
U2-21		6.5	-	0.0272	60	4.3	2.3E-05	7.7E-06	22.8
U2-22		6.5	-	0.0282	60	10.3	4.7E-05	2.4E-05	22.5
U2-23		6.5	-	0.0290	90	49.9	1.7E-04	1.1E-04	21.8
U2-24		6.5	-	0.0298	60	31.1	1.0E-04	8.1E-05	22.8
U2-25		6.5	-	0.0305	91	425.5	5.7E-04	4.4E-04	22.3
U2-26		6.5	-	0.0320	60	670.4	1.6E-03	1.6E-03	22.5
U2-27		6.5	-	0.0330	60	1064.8	1.4E-03	1.4E-03	22.5
U2-28		6.5	-	0.0354	15	1531.3	1.5E-02	1.5E-02	24.0
U2-29		6.5	-	0.0395	11	2268.6	3.0E-02	3.0E-02	23.3
U2-30		6.5	-	0.0424	5	2333.4	6.9E-02	6.9E-02	23.8
U2-31	2.4	8.3	-	0.0210	60	6.5	1.4E-05	5.4E-06	23.2
U2-32		8.3	-	0.0225	60	11.1	4.1E-05	8.0E-06	23.1
U2-33		8.3	-	0.0230	60	37.0	6.5E-05	2.7E-05	21.7
U2-34		8.3	-	0.0243	60	91.8	2.6E-04	2.2E-04	22.5
U2-35		8.3	-	0.0257	60	369.8	4.9E-04	4.1E-04	22.7
U2-36		8.3	-	0.0276	30	1374.8	9.0E-03	9.0E-03	22.5
U2-37		8.3	-	0.0305	10	1370.3	2.0E-02	2.0E-02	24.1
U2-38		8.3	-	0.0330	6	1992.4	6.8E-02	6.8E-02	24.0
U2-39		8.3	-	0.0355	6	1819.5	5.6E-02	5.6E-02	22.7

Table A.1 (continued)

Run No.	Sediment d (mm)	Slope J x 10^3	Flow Q (L s^{-1})	Depth h (m)	Sampling Duration (mins)	Bedload Yield (g)	Transport Intensity		Water Temp. (^oC)
							I mean (s^{-1})	*I steady* (s^{-1})	
U2-40	2.4	8.3	-	0.0380	5	2144.8	6.1E-02	6.1E-02	24.4
U2-41	2.4	14.1	-	0.0137	65	2.5	5.0E-06	2.0E-06	20.2
U2-42		14.1	-	0.0142	60	59.7	5.2E-05	5.0E-05	20.6
U2-43		14.1	-	0.0146	64	28.5	5.4E-05	3.5E-05	19.4
U2-44		14.1	0.3	0.0154	40	281.4	3.3E-04	3.3E-04	20.5
U2-45		14.1	0.8	0.0160	30	185.5	6.0E-04	6.0E-04	20.8
U2-46		14.1	1.0	0.0167	20.33	540.9	4.8E-03	4.8E-03	19.5
U2-47		14.1	1.4	0.0175	13	674.2	1.1E-02	1.1E-02	20.7
U2-48		14.1	2.0	0.0187	7	1071.0	2.3E-02	2.3E-02	20.2
U3-1	3.4	1.9	15.0	0.0951	60	32.5	2.8E-05	2.3E-05	19.0
U3-2		1.9	18.2	0.1039	60	50.6	4.7E-05	3.9E-05	18.5
U3-3		1.9	21.5	0.1172	48	58.3	6.7E-05	6.2E-05	18.8
U3-4		1.9	24.8	0.1272	47	84.0	9.9E-05	9.9E-05	20.2
U3-5		1.9	26.3	0.1350	30	261.8	5.0E-04	4.3E-04	20.4
U3-6	3.4	2.6	14.5	0.0845	55	43.4	3.5E-05	2.8E-05	18.6
U3-7		2.6	15.8	0.0892	65	118.2	9.9E-05	6.2E-05	19.1
U3-8		2.6	18.1	0.0963	55	134.2	1.1E-04	1.0E-04	20.0
U3-9		2.6	20.7	0.1052	42	108.3	1.5E-04	8.8E-05	19.7
U3-10		2.6	23.8	0.1157	25	194.4	3.8E-04	3.8E-04	19.6
U3-11		2.6	28.7	0.1269	11	398.8	1.3E-03	1.3E-03	19.6
U3-12	3.4	4.1	8.5	0.0595	60	12.6	2.1E-05	1.5E-05	15.5
U3-13		4.1	9.2	0.0626	60	17.1	2.6E-05	1.4E-05	16.0
U3-14		4.1	10.2	0.0655	61	46.2	4.8E-05	3.3E-05	18.5
U3-15		4.1	10.8	0.0684	65	43.3	3.9E-05	2.3E-05	19.1
U3-16		4.1	11.9	0.0722	60	70.8	8.8E-05	6.0E-05	20.0
U3-17		4.1	13.7	0.0782	60	123.7	1.1E-04	7.3E-05	20.8
U3-18		4.1	14.5	0.0810	40	155.1	1.8E-04	1.8E-04	18.5
U3-19		4.1	15.8	0.0838	30	315.7	3.8E-04	3.3E-04	19.5
U3-20		4.1	16.4	0.0858	20	169.2	4.3E-04	3.9E-04	19.8
U3-21		4.1	18.8	0.0885	4	414.1	6.0E-03	6.0E-03	19.6
U3-22		4.1	17.8	0.0892	6.5	127.8	9.0E-04	9.0E-04	20.1
U3-23	3.4	6.5	5.4	0.0412	65	16.3	1.7E-05	1.4E-05	20.9
U3-24		6.5	6.7	0.0450	60	33.0	3.9E-05	3.2E-05	20.1
U3-25		6.5	7.5	0.0480	70	140.1	9.6E-05	6.4E-05	21.1
U3-26		6.5	8.0	0.0503	60	144.8	1.7E-04	1.3E-04	21.8
U3-27		6.5	8.6	0.0521	40	202.3	2.2E-04	2.0E-04	21.7
U3-28		6.5	9.4	0.0540	25	335.3	6.5E-04	6.5E-04	21.4

Table A.1 (continued)

Run No.	Sediment *d* (mm)	Slope *J* x 10^3	Flow *Q* (L s^{-1})	Depth *h* (m)	Sampling Duration (mins)	Bedload Yield (g)	Transport Intensity		Water Temp. (^oC)
							I mean (s^{-1})	*I steady* (s^{-1})	
U3-29	3.4	6.5	9.8	0.0557	17	331.5	1.0E-03	1.0E-03	21.8
U3-30		6.5	10.2	0.0572	10	427.1	1.6E-03	1.6E-03	20.9
U3-31		6.5	10.8	0.0582	6	614.9	5.0E-03	5.0E-03	21.5
U3-32	3.4	8.3	4.2	0.0330	61	12.2	9.4E-06	5.9E-06	21.4
U3-33		8.3	5.1	0.0355	60	32.4	3.8E-05	2.5E-05	20.8
U3-34		8.3	5.6	0.0386	63	106.5	9.3E-05	6.5E-05	20.3
U3-35		8.3	6.0	0.0397	60	180.2	1.3E-04	9.7E-05	20.0
U3-36		8.3	6.3	0.0412	60	200.8	2.1E-04	1.6E-04	21.0
U3-37		8.3	7.0	0.0424	15	353.3	8.1E-04	7.4E-04	20.7
U3-38		8.3	7.9	0.0461	8	733.4	2.7E-03	2.7E-03	20.2
U3-39		8.3	8.8	0.0500	6	639.6	5.7E-03	5.7E-03	21.5
U3-40	3.4	14.1	2.4	0.0226	76	14.8	8.7E-06	1.3E-06	20.6
U3-41		14.1	3.0	0.0240	60	27.4	2.7E-05	2.1E-05	22.0
U3-42		14.1	3.4	0.0250	60	125.9	8.8E-05	6.7E-05	21.1
U3-43		14.1	3.6	0.0264	62	231.4	1.7E-04	1.1E-04	20.6
U3-44		14.1	4.1	0.0273	30	378.6	6.4E-04	5.7E-04	20.6
U3-45		14.1	4.4	0.0296	15	374.5	1.9E-03	1.9E-03	21.0
U3-46		14.1	4.9	0.0310	8	691.3	2.9E-03	2.9E-03	20.6
U3-47	3.4	23.8	-	0.0127	60	7.6	1.1E-05	1.1E-05	18.6
U3-48		23.8	0.8	0.0141	55	28.7	4.1E-05	2.5E-05	18.1
U3-49		23.8	0.7	0.0144	41	59.2	9.9E-05	9.9E-05	18.5
U3-50		23.8	1.0	0.0153	62	230.0	2.4E-04	1.6E-04	18.6
U3-51		23.8	1.5	0.0163	14	241.1	1.0E-03	1.0E-03	17.0
U3-52		23.8	1.8	0.0186	10	758.9	3.8E-03	3.8E-03	18.3
U4-1	4.5	2.6	21.0	0.1142	45	5.2	8.0E-06	8.0E-06	18.4
U4-2		2.6	24.5	0.1178	45	27.4	3.3E-05	3.0E-05	18.7
U4-3		2.6	29.3	0.1360	40	179.6	2.0E-04	1.8E-04	16.6
U4-4		2.6	29.3	0.1360	46	38.3	6.5E-05	5.0E-05	18.3
U4-5	4.5	4.1	15.0	0.0825	60	25.9	1.8E-05	1.1E-05	21.0
U4-6		4.1	19.2	0.0940	60.2	237.6	1.3E-04	9.2E-05	18.3
U4-7		4.1	23.1	0.1085	68	222.5	9.8E-05	6.3E-05	19.8
U4-8		4.1	29.0	0.1223	33	391.3	5.3E-04	4.2E-04	19.0
U4-9	4.5	6.5	10.2	0.0605	67	66.9	4.2E-05	1.4E-05	19.8
U4-10		6.5	11.2	0.0633	60	168.8	8.3E-05	7.1E-05	21.1
U4-11		6.5	-	0.0657	63.5	347.0	1.8E-04	1.3E-04	20.2
U4-12		6.5	13.3	0.0681	60	334.2	2.3E-04	1.7E-04	21.7

Table A.1 (continued)

Run No.	Sediment *d* (mm)	Slope *J* x 10^3	Flow *Q* (L s^{-1})	Depth *h* (m)	Sampling Duration (mins)	Bedload Yield (g)	Transport Intensity		Water Temp. (^oC)
							I mean (s^{-1})	*I steady* (s^{-1})	
U4-13	4.5	6.5	14.7	0.0714	22	411.2	5.7E-04	5.7E-04	21.0
U4-14		6.5	15.8	0.0728	16	505.2	9.9E-04	9.9E-04	21.1
U4-15		6.5	18.6	0.0780	4	838.3	7.0E-03	7.0E-03	21.6
U4-16	4.5	8.3	7.7	0.0469	66	106.4	6.2E-05	3.0E-05	19.4
U4-17		8.3	8.4	0.0500	65	129.6	1.0E-04	6.8E-05	21.7
U4-18		8.3	9.8	0.0538	51	252.0	1.7E-04	1.5E-04	22.5
U4-19		8.3	10.5	0.0554	26	402.6	6.8E-04	5.7E-04	20.4
U4-20		8.3	11.0	0.0572	21	520.3	8.2E-04	6.7E-04	19.8
U4-21		8.3	11.6	0.0590	11	404.7	1.6E-03	1.3E-03	20.3
U4-22		8.3	12.4	0.0600	6	528.8	3.6E-03	3.6E-03	20.6
U4-23	4.5	11.5	5.6	0.0355	60	83.5	5.8E-05	3.4E-05	21.7
U4-24		11.5	6.0	0.0370	61	133.3	7.6E-05	7.1E-05	21.3
U4-25		11.5	6.3	0.0382	63	279.6	2.4E-04	1.6E-04	22.1
U4-26		11.5	7.0	0.0410	30	405.2	5.9E-04	5.0E-04	22.0
U4-27		11.5	7.3	0.0418	32	352.5	7.4E-04	4.8E-04	21.5
U4-28		11.5	8.0	0.0437	8	472.5	2.1E-03	2.1E-03	21.9
U4-29	4.5	14.1	4.3	0.0295	60	16.7	2.6E-05	2.5E-05	16.5
U4-30		14.1	4.9	0.0304	24	40.7	1.4E-04	7.0E-05	20.2
U4-31		14.1	5.2	0.0318	62	160.2	2.0E-04	1.7E-04	18.1
U4-32		14.1	5.6	0.0335	50	385.1	4.9E-04	3.3E-04	18.7
U4-33		14.1	6.0	0.0344	23	379.7	1.2E-03	9.8E-04	17.2
U4-34		14.1	6.5	0.0363	17	549.5	1.6E-03	1.6E-03	19.1
U4-35	4.5	28.7	0.9	0.0168	46	20.0	2.8E-05	1.3E-05	16.6
U4-36		28.7	1.2	0.0177	55	89.8	9.3E-05	8.6E-05	16.2
U4-37		28.7	1.6	0.0180	30	256.8	5.3E-04	5.3E-04	16.9
U4-38		28.7	1.8	0.0189	11	318.1	1.3E-03	1.3E-03	17.0
U4-39		28.7	2.8	0.0218	6	1225.3	6.7E-03	6.7E-03	16.8
U5-1	5.65	4.1	20.7	0.1015	60	13.0	1.4E-05	1.1E-05	22.7
U5-2		4.1	24.4	0.1123	60	115.5	7.7E-05	6.8E-05	21.5
U5-3		4.1	26.6	0.1218	60	109.4	1.8E-04	6.3E-05	22.7
U5-4		4.1	29.0	0.1240	60	53.0	3.1E-05	2.7E-05	23.8
U5-5	5.65	6.5	11.2	0.0660	60	26.7	2.9E-05	1.3E-05	17.7
U5-6		6.5	13.1	0.0690	60	52.9	5.6E-05	2.0E-05	19.2
U5-7		6.5	13.3	0.0717	60	69.4	6.7E-05	4.1E-05	22.6
U5-8		6.5	15.0	0.0740	30	103.8	1.2E-04	8.7E-05	21.2
U5-9		6.5	17.6	0.0805	60	360.0	1.5E-04	1.2E-04	17.2

Table A.1 (continued)

Run No.	Sediment d (mm)	Slope J x 10^3	Flow Q (L s^{-1})	Depth h (m)	Sampling Duration (mins)	Bedload Yield (g)	Transport Intensity		Water Temp. (^{o}C)
							I mean (s^{-1})	*I steady* (s^{-1})	
U5-10	5.65	6.5	19.1	0.0850	43	518.7	2.8E-04	2.4E-04	20.1
U5-11		6.5	21.0	0.0892	20	421.9	5.6E-04	3.3E-04	20.5
U5-12		6.5	24.5	0.0944	21	1449.5	1.5E-03	1.3E-03	20.3
U5-13	5.65	8.3	7.8	0.0516	24	-	1.7E-05	0.0E+00	21.2
U5-14		8.3	9.6	0.0560	60	38.5	4.1E-05	2.7E-05	21.5
U5-15		8.3	11.2	0.0601	60	135.8	5.0E-05	3.4E-05	22.1
U5-16		8.3	12.2	0.0620	60	254.2	1.2E-04	9.3E-05	21.8
U5-17		8.3	13.0	0.0650	60	318.6	1.3E-04	9.3E-05	22.2
U5-18		8.3	14.3	0.0685	30	530.8	4.1E-04	3.6E-04	21.2
U5-19		8.3	15.0	0.0697	20	475.8	5.1E-04	4.4E-04	22.6
U5-20		8.3	16.1	0.0724	15	848.1	1.1E-03	8.7E-04	21.9
U5-21	5.65	11.5	6.6	0.0430	60	18.9	1.2E-05	6.7E-06	21.7
U5-22		11.5	7.2	0.0446	60	24.1	1.5E-05	1.3E-05	21.6
U5-23		11.5	8.0	0.0465	60	146.0	5.9E-05	4.3E-05	20.3
U5-24		11.5	8.5	0.0475	60	191.7	1.0E-04	8.0E-05	21.4
U5-25		11.5	8.8	0.0497	60	276.1	1.3E-04	1.2E-04	22.3
U5-26		11.5	9.7	0.0515	60	414.2	2.1E-04	1.7E-04	22.5
U5-27		11.5	10.4	0.0530	30	673.8	4.7E-04	4.5E-04	22.5
U5-28		11.5	11.1	0.0548	30	590.5	6.1E-04	4.0E-04	22.2
U5-29		11.5	12.2	0.0565	12	1001.9	1.8E-03	1.8E-03	21.7
U5-30	5.65	14.1	5.9	0.0380	60	28.0	1.4E-05	8.7E-06	22.5
U5-31		14.1	6.2	0.0403	60	46.0	1.3E-05	4.7E-06	22.6
U5-32		14.1	6.5	0.0415	60	92.9	3.5E-05	1.4E-05	23.0
U5-33		14.1	7.4	0.0429	60	156.2	9.0E-05	9.0E-05	22.8
U5-34		14.1	8.0	0.0442	30	455.6	4.5E-04	4.5E-04	23.1
U5-35		14.1	8.1	0.0460	30	292.6	3.0E-04	2.0E-04	22.7
U5-36		14.1	8.4	0.0465	20	450.7	5.5E-04	5.5E-04	22.7
U5-37		14.1	9.1	0.0477	15	691.2	1.5E-03	1.5E-03	22.2
U5-38	5.65	15.7	5.0	0.0333	60	37.9	2.1E-05	1.3E-05	22.4
U5-39		15.7	5.1	0.0346	60	24.4	1.5E-05	1.4E-05	22.2
U5-40		15.7	5.4	0.0363	60	16.2	1.1E-05	7.3E-06	22.6
U5-41		15.7	5.6	0.0374	60	21.4	1.8E-05	1.3E-05	22.8
U5-42		15.7	6.6	0.0390	60	278.4	1.5E-04	8.0E-05	22.6
U5-43		15.7	6.9	0.0400	60	387.6	1.5E-04	1.5E-04	23.0
U5-44		15.7	7.2	0.0410	33	260.2	2.5E-04	2.5E-04	22.6
U5-45		15.7	7.8	0.0420	14	635.5	1.1E-03	1.1E-03	23.3
U5-46		15.7	8.1	0.0427	9	528.8	1.6E-03	1.5E-03	22.6

Table A.1 (continued)

Run No.	Sediment d (mm)	Slope J x 10^3	Flow Q ($L\,s^{-1}$)	Depth h (m)	Sampling Duration (mins)	Bedload Yield (g)	Transport Intensity		Water Temp. (^{o}C)
							I mean (s^{-1})	*I steady* (s^{-1})	
U6-1	7.15	4.1	28.0	0.1207	60	43.0	9.0E-06	1.0E-06	16.6
U6-2	7.15	6.5	22.4	0.0920	56	61.0	1.2E-05	9.2E-06	21.5
U6-3		6.5	-	0.0960	65	181.2	3.3E-05	1.7E-05	18.4
U6-4		6.5	26.2	0.0995	55	413.4	6.7E-05	3.4E-05	20.0
U6-5		6.5	26.8	0.1026	35	484.9	1.3E-04	1.1E-04	22.4
U6-6		6.5	28.0	0.1060	25	832.1	2.9E-04	2.9E-04	19.7
U6-7	7.15	8.3	16.0	0.0710	65	96.7	1.6E-05	4.8E-06	21.5
U6-8		8.3	18.7	0.0778	55	104.4	3.4E-05	2.7E-05	20.6
U6-9		8.3	21.0	0.0820	65	765.2	1.3E-04	9.1E-05	21.0
U6-10		8.3	23.1	0.0866	66	929.3	1.5E-04	1.3E-04	21.8
U6-11		8.3	25.2	0.0918	47	1221.1	3.3E-04	2.9E-04	22.4
U6-12		8.3	26.2	0.0961	21	1177.8	7.0E-04	5.0E-04	22.3
U6-13		8.3	28.0	0.1046	20	949.3	7.8E-04	5.5E-04	21.4
U6-14	7.15	11.5	10.8	0.0535	40	39.0	7.2E-06	7.2E-06	21.4
U6-15		11.5	11.9	0.0561	65	249.3	4.2E-05	2.5E-05	21.6
U6-16		11.5	13.0	0.0601	57	197.9	4.7E-05	2.4E-05	22.0
U6-17		11.5	13.5	0.0613	60	480.7	1.1E-04	7.7E-05	22.2
U6-18		11.5	14.2	0.0637	46	753.3	1.9E-04	1.7E-04	21.4
U6-19		11.5	15.4	0.0670	30	1087.4	5.6E-04	5.1E-04	20.8
U6-20		11.5	17.5	0.0723	13	999.6	1.1E-03	9.4E-04	21.9
U6-21		11.5	21.3	0.0766	3	1683.7	9.0E-03	9.0E-03	21.9
U6-22	7.15	14.1	10.0	0.0499	55	257.3	8.4E-05	5.4E-05	21.4
U6-23		14.1	8.6	0.0471	57	50.2	1.0E-05	3.0E-06	22.3
U6-24		14.1	9.8	0.0485	65	337.3	6.8E-05	4.5E-05	21.4
U6-25		14.1	11.2	0.0514	35	404.6	1.5E-04	1.4E-04	22.4
U6-26		14.1	11.6	0.0518	25	1036.9	4.7E-04	3.9E-04	20.7
U6-27		14.1	12.5	0.0557	17	1050.9	8.8E-04	7.3E-04	20.9
U6-28		14.1	13.2	0.0578	11	1077.9	1.3E-03	1.3E-03	21.0
U6-29		14.1	14.3	0.0595	6	1274.9	2.7E-03	2.7E-03	21.8
U6-30	7.15	23.8	4.7	0.0290	55	142.1	2.8E-05	3.2E-06	19.4
U6-31		23.8	5.1	0.0311	66	273.7	4.5E-05	1.4E-05	19.2
U6-32		23.8	5.6	0.0321	50	466.9	1.4E-04	1.3E-04	18.6
U6-33		23.8	6.2	0.0338	42	1198.0	4.4E-04	2.8E-04	20.3
U6-34		23.8	7.2	0.0349	21	882.2	8.8E-04	8.0E-04	19.8
U6-35		23.8	7.7	0.0375	5.5	1305.5	4.3E-03	4.3E-03	17.8

Table A.1 (continued)

Run No.	Sediment d (mm)	Slope J x 10^3	Flow Q (L s^{-1})	Depth h (m)	Sampling Duration (mins)	Bedload Yield (g)	Transport Intensity		Water Temp. (^oC)
							I mean (s^{-1})	*I steady* (s^{-1})	
U7-1	9.0	6.5	28.0	0.1140	60	52.4	1.9E-05	1.9E-05	18.9
U7-2	9.0	8.3	21.0	0.0910	60	65.0	1.5E-05	1.1E-05	20.6
U7-3		8.3	23.8	0.0975	60	92.0	2.0E-05	2.0E-05	21.9
U7-4		8.3	29.0	0.1040	60	195.0	5.6E-05	3.7E-05	22.0
U7-5	9.0	11.5	12.2	0.0650	60	31.6	1.3E-05	1.0E-05	22.8
U7-6		11.5	13.5	0.0677	60	75.3	1.5E-05	1.1E-05	23.4
U7-7		11.5	14.4	0.0695	60	132.8	2.9E-05	1.4E-05	22.3
U7-8		11.5	15.8	0.0720	60	97.4	3.1E-05	1.9E-05	23.2
U7-9		11.5	17.2	0.0740	60	287.7	8.7E-05	3.1E-05	23.2
U7-10		11.5	18.6	0.0765	60	307.8	1.2E-04	7.3E-05	23.8
U7-11		11.5	19.8	0.0795	20	669.4	3.7E-04	2.6E-04	23.2
U7-12		11.5	22.0	0.0825	20	472.2	2.7E-04	2.7E-04	24.3
U7-13		11.5	24.8	0.0860	8	580.2	9.3E-04	9.3E-04	23.8
U7-14	9.0	14.1	10.8	0.0580	60	45.4	2.1E-05	1.6E-05	23.8
U7-15		14.1	12.2	0.0600	60	196.9	3.7E-05	2.6E-05	22.7
U7-16		14.1	13.3	0.0623	60	236.0	3.9E-05	2.9E-05	23.8
U7-17		14.1	14.5	0.0640	60	221.7	7.1E-05	4.3E-05	22.3
U7-18		14.1	15.0	0.0658	40.3	644.7	2.7E-04	9.0E-05	24.0
U7-19		14.1	16.1	0.0675	25	453.9	2.7E-04	1.8E-04	22.7
U7-20		14.1	18.2	0.0705	15	626.6	6.7E-04	6.7E-04	22.7
U7-21		14.1	21.0	0.0745	4.5	1082.6	3.7E-03	3.7E-03	23.7
U7-22	9.0	15.7	9.8	0.0506	60	58.7	1.8E-05	1.3E-05	21.9
U7-23		15.7	11.4	0.0547	60	81.3	4.3E-05	3.4E-05	22.1
U7-24		15.7	12.4	0.0555	60	317.4	8.4E-05	5.4E-05	21.6
U7-25		15.7	13.0	0.0577	60	281.2	7.0E-05	2.6E-05	21.8
U7-26		15.7	13.2	0.0595	60	155.9	5.4E-05	4.8E-05	21.8
U7-27		15.7	14.0	0.0613	60	417.3	9.6E-05	7.6E-05	22.1
U7-28		15.7	15.8	0.0625	15	580.1	6.5E-04	6.5E-04	22.7
U7-29		15.7	15.6	0.0628	17	581.2	3.6E-04	2.9E-04	21.8
U7-30		15.7	16.4	0.0643	13	513.0	8.1E-04	7.2E-04	22.6
U7-31		15.7	17.2	0.0645	6	685.5	1.1E-03	1.1E-03	22.9
U8-1	12.0	11.5	16.7	0.0732	60	37.9	1.1E-05	3.0E-06	13.3
U8-2		11.5	20.0	0.0818	60	109.1	1.5E-05	1.0E-05	16.0
U8-3		11.5	24.5	0.0918	50	110.9	2.1E-05	2.1E-05	17.2
U8-4		11.5	29.0	0.1002	60	421.3	4.6E-05	4.6E-05	18.7
U8-5		11.5	28.0	0.1005	55	1241.8	2.1E-04	1.3E-04	19.1

Table A.1 (continued)

Run No.	Sediment *d* (mm)	Slope *J* x 10^3	Flow *Q* ($L\ s^{-1}$)	Depth *h* (m)	Sampling Duration (mins)	Bedload Yield (g)	Transport Intensity		Water Temp. (^oC)
							I mean (s^{-1})	*I steady* (s^{-1})	
U8-6	12.0	14.1	21.0	0.0788	60	403.9	5.7E-05	4.2E-05	21.4
U8-7		14.1	22.0	0.0830	60	237.8	5.2E-05	2.2E-05	19.4
U8-8		14.1	24.6	0.0837	60	770.7	1.2E-04	6.2E-05	20.8
U8-9		14.1	25.4	0.0860	57	837.0	1.9E-04	1.8E-04	22.2
U8-10		14.1	26.6	0.0890	23	1090.2	4.2E-04	4.2E-04	22.1
U8-11		14.1	29.0	0.0900	18	896.4	6.0E-04	3.2E-04	22.6
U8-12		14.1	29.0	0.0950	19	890.9	3.0E-04	3.0E-04	20.4
U8-13	12.0	17.8	14.3	0.0623	35	29.0	1.6E-05	1.6E-05	20.3
U8-14		17.8	15.3	0.0630	60	357.8	5.7E-05	3.2E-05	20.8
U8-15		17.8	16.3	0.0658	35	255.6	5.3E-05	5.3E-05	21.3
U8-16		17.8	17.8	0.0672	55	955.2	1.6E-04	8.8E-05	21.2
U8-17		17.8	19.2	0.0693	13	1440.4	1.9E-03	1.1E-03	21.0
U8-18		17.8	18.8	0.0715	21	614.2	3.4E-04	3.4E-04	22.1
U8-19		17.8	21.7	0.0735	6	1560.5	1.8E-03	1.8E-03	21.4
U8-20		17.8	20.0	0.0741	17	1278.7	1.2E-03	1.0E-03	21.4
U8-21	12.0	28.7	7.8	0.0428	60	305.9	6.1E-05	1.4E-05	21.6
U8-22		28.7	10.2	0.0442	27	1454.2	5.1E-04	4.4E-04	20.6
U8-23		28.7	9.1	0.0446	62	868.8	2.5E-04	9.7E-05	21.4
U8-24		28.7	8.4	0.0448	46	76.4	2.5E-05	8.0E-06	22.5
U8-25		28.7	9.5	0.0479	40	902.3	2.2E-04	1.8E-04	22.6
U8-26		28.7	11.9	0.0515	6	1782.2	3.7E-03	3.7E-03	23.0
U8-27		28.7	13.0	0.0545	5	1673.8	6.7E-03	6.7E-03	23.1

Appendix B

Table B.1 Measured Data for Graded Sediments (Armfield Flume, width 0.30 m)

Run No.	Sediment Mixture	Slope J x 10^3	Flow Q ($L\,s^{-1}$)	Depth h (m)	Sampling Duration (mins)	Bedload Yield (g)	Water Temp. (^{o}C)
N1-1	N-1	4.1	21.5	0.1011	75	112.1	21.0
N1-2		4.1	25.1	0.1110	60	203.6	16.6
N1-3		4.1	26.0	0.1176	60	266.1	18.6
N1-4		4.1	30.4	0.1191	45	573.9	22.2
N1-5	N-1	6.5	11.2	0.0610	60	128.2	20.2
N1-6		6.5	12.7	0.0643	60	717.9	18.8
N1-7		6.5	-	0.0692	30	538.0	20.6
N1-8		6.5	16.4	0.0758	10	823.5	14.6
N1-9		6.5	18.1	0.0805	6	986.5	16.3
N1-10	N-1	8.3	9.0	0.0502	60	155.9	19.5
N1-11		8.3	9.6	0.0540	60	256.5	15.2
N1-12		8.3	11.1	0.0567	43	393.7	16.6
N1-13		8.3	11.4	0.0593	60	420.4	19.7
N1-14		8.3	-	0.0596	11	703.5	16.4
N1-15		8.3	13.2	0.0643	8	580.6	20.2
N1-16	N-1	11.5	-	0.0374	60	149.3	18.0
N1-17		11.5	7.0	0.0416	60	487.0	19.1
N1-18		11.5	-	0.0404	53	244.3	19.4
N1-19		11.5	7.7	0.0434	18	580.4	17.7
N1-20		11.5	8.4	0.0454	11	533.4	19.0
N1-21		11.5	9.9	0.0500	4	961.1	19.1
N1-22	N-1	14.1	4.6	0.0322	60	128.2	20.2
N1-23		14.1	5.5	0.0355	60	289.6	20.2
N1-24		14.1	6.7	0.0402	30	607.9	20.4
N1-25		14.1	6.7	0.0411	10	510.7	20.0
N1-26		14.1	8.7	0.0428	4	925.8	20.8
N2-1	N-2	4.1	17.3	0.0943	80	87.3	22.8
N2-2		4.1	20.5	0.1010	70	277.1	19.9
N2-3		4.1	24.8	0.1125	45	520.9	21.6
N2-4		4.1	29.5	0.1214	25	602.8	21.2
N2-5	N-2	6.5	8.5	0.0630	65	127.6	21.0
N2-6		6.5	11.6	0.0690	60	221.3	21.2
N2-7		6.5	14.0	0.0764	55	573.9	20.9
N2-8		6.5	17.2	0.0823	22	538.4	21.3

Table B.1 (continued)

Run No.	Sediment Mixture	Slope J x 10^3	Flow Q ($L\ s^{-1}$)	Depth h (m)	Sampling Duration (mins)	Bedload Yield (g)	Water Temp. (^oC)
N2-9	N-2	6.5	20.5	0.0935	5	828.1	21.1
N2-10	N-2	8.3	-	0.0508	90	91.3	21.7
N2-11		8.3	-	0.0552	70	351.2	21.4
N2-12		8.3	8.7	0.0624	37	499.8	22.1
N2-13		8.3	8.5	0.0675	20	744.6	21.2
N2-14		8.3	14.0	0.0750	4	913.9	21.4
N2-15	N-2	14.1	-	0.0327	60	165.8	21.0
N2-16		14.1	-	0.0370	65	169.1	21.2
N2-17		14.1	-	0.0380	40	572.1	20.8
N2-18		14.1	-	0.0410	15	813.1	20.2
N2-19		14.1	-	0.0480	2.5	860.8	20.3
N3-1	N-3	4.1	14.5	0.0825	60	80.3	18.3
N3-2		4.1	16.7	0.0918	60	122.4	20.2
N3-3		4.1	21.0	0.1038	60	496.2	21.1
N3-4		4.1	23.8	0.1167	27	684.6	21.2
N3-5		4.1	29.2	0.1280	15	628.3	20.2
N3-6	N-3	6.5	7.7	0.0621	68	144.9	21.7
N3-7		6.5	9.4	0.0674	55	265.1	21.7
N3-8		6.5	11.6	0.0717	60	400.8	22.2
N3-9		6.5	15.6	0.0804	11	569.8	21.3
N3-10		6.5	19.0	0.0850	4	834.2	23.0
N3-11	N-3	8.3	-	0.0485	60	167.7	21.6
N3-12		8.3	-	0.0527	65	33.1	21.0
N3-13		8.3	7.0	0.0530	43	540.2	21.6
N3-14		8.3	9.8	0.0585	28	804.7	20.0
N3-15		8.3	8.8	0.0628	51	465.7	21.8
N3-16		8.3	16.1	0.0766	2.5	1199.4	21.5
N3-17	N-3	14.1	-	0.0258	100	27.7	21.5
N3-18		14.1	-	0.0292	20	440.9	20.8
N3-19		14.1	-	0.0310	60	92.3	22.0
N3-20		14.1	-	0.0345	60	519.9	22.1
N3-21		14.1	-	0.0412	5	950.2	21.4
F-1	F	4.1	-	0.0453	75	14.6	17.9
F-2		4.1	-	0.0500	120	9.3	21.1
F-3		4.1	5.8	0.0564	60	147.7	22.9

Table B.1 (continued)

Run No.	Sediment Mixture	Slope J x 10^3	Flow Q ($L\,s^{-1}$)	Depth h (m)	Sampling Duration (mins)	Bedload Yield (g)	Water Temp. ($^{\circ}C$)
F-4	F	4.1	7.5	0.0614	30	401.6	21.7
F-5		4.1	11.6	0.0723	15	766.3	21.2
F-6		4.1	15.0	0.0825	5	1025.3	21.6
F-7		4.1	19.3	0.0914	3	785.6	21.2
F-8	F	6.5	-	0.0379	60	25.3	23.5
F-9		6.5	-	0.0443	60	308.1	23.6
F-10		6.5	-	0.0481	40	557.8	23.8
F-11		6.5	6.7	0.0543	6	781	22.5
F-12		6.5	10.8	0.0638	3	1450	21.8
F-13	F	8.3	-	0.0283	120	18.3	23.3
F-14		8.3	-	0.0322	60	277.5	22.4
F-15		8.3	-	0.0386	21	1151.2	22.6
F-16		8.3	4.9	0.0441	4	1031.1	23.8
F-17		8.3	9.1	0.0558	2	1686.7	23.3
F-18	F	14.1	-	0.0151	180	12.5	23.0
F-19		14.1	-	0.0176	70	8.9	22.6
F-20		14.1	-	0.0186	60	276.6	22.9
F-21		14.1	-	0.0232	14	536	22.6
F-22		14.1	-	0.0310	3	1100.8	22.0
C-1	C	4.1	21.0	0.1020	60	18.9	21.0
C-2		4.1	24.8	0.1120	62	44.9	22.1
C-3		4.1	29.0	0.1236	65	104.8	19.2
C-4	C	6.5	20.0	0.0896	135	477.8	23.0
C-5		6.5	21.0	0.0937	67	299.4	22.7
C-6		6.5	25.2	0.1000	25	869.1	24.0
C-7		6.5	26.2	0.1050	20	700.1	22.0
C-8		6.5	30.0	0.1093	3	889.8	22.7
C-9	C	8.3	13.6	0.0700	130	491	23.3
C-10		8.3	16.8	0.0740	60	337.4	22.7
C-11		8.3	17.5	0.0826	40	639.4	23.5
C-12		8.3	21.0	0.0908	10	1133.5	22.0
C-13		8.3	25.2	0.0929	5	998.7	24.0
C-14	C	14.1	5.6	0.0410	70	225.1	22.4
C-15		14.1	-	0.0452	30	973.9	22.1
C-16		14.1	9.8	0.0506	35	619.3	22.7

Table B.1 (continued)

Run No.	Sediment Mixture	Slope J x 10^3	Flow Q ($L\ s^{-1}$)	Depth h (m)	Sampling Duration (mins)	Bedload Yield (g)	Water Temp. ($^{\circ}C$)
C-17	C	14.1	10.2	0.0585	4	1195.3	21.4
C-18		14.1	15.0	0.0673	4	1223.6	21.9
B-1	B	4.1	-	0.0557	60	47.1	18.4
B-2		4.1	7.5	0.0654	100	62.2	21.8
B-3		4.1	12.2	0.0757	60	225.5	21.0
B-4		4.1	17.3	0.0900	60	332.4	22.7
B-5		4.1	22.5	0.1015	15	672.5	23.0
B-6		4.1	28.0	0.1102	5	726.2	20.7
B-7		4.1	30.1	0.1238	4	581.5	22.5
B-8	B	6.5	5.0	0.0466	60	87.2	22.3
B-9		6.5	6.2	0.0509	90	51.8	23.2
B-10		6.5	7.0	0.0529	60	292.9	23.1
B-11		6.5	9.8	0.0608	20	550.8	23.4
B-12		6.5	15.0	0.0745	11	785.5	22.8
B-13		6.5	17.8	0.0834	5	925.0	23.5
B-14	B	8.3	3.0	0.0388	125	137.8	23.7
B-15		8.3	3.5	0.0417	65	137.5	23.1
B-16		8.3	6.5	0.0472	40	578.9	22.8
B-17		8.3	8.0	0.0519	15	1033.8	23.4
B-18		8.3	10.5	0.0593	5	842.8	23.2
B-19		8.3	13.5	0.0676	3	1281	24.4
B-20	B	14.1	-	0.0232	30	530.1	22.6
B-21		14.1	-	0.0239	56	81.2	23.6
B-22		14.1	-	0.0291	10	893.4	22.9
B-23		14.1	4.2	0.0368	10	967.8	22.9
B-24		14.1	8.7	0.0471	2	1286.2	22.8

Table B.2 Size Distribution of Bedload as Percentage of Total (Armfield Flume)

Run No.	Size Range							
	1.0-2.0 (mm)	2.0-2.8 (mm)	2.8-4.0 (mm)	4.0-5.0 (mm)	5.0-6.3 (mm)	6.3-8.0 (mm)	8.0-10.0 (mm)	10.0-14.0 (mm)
N1-1	0.2	1.6	15.7	50.8	25.9	2.1	3.7	0.0
N1-2	0.1	0.8	14.6	54.6	23.3	5.8	0.8	0.0
N1-3	0.04	0.86	12.8	53.2	25.1	7.1	0.9	0.0
N1-4	0.1	1.1	15.2	52.3	22.4	6.6	2.3	0.0
N1-5	0.1	1.2	16.5	57.7	22.2	2.3	0.0	0.0
N1-6	0.1	0.8	14.6	54.9	23.1	5.8	0.7	0.0
N1-7	0.1	1.4	17.4	54.1	20.7	5.1	0.9	0.3
N1-8	0.1	1.4	16.3	56.5	18.8	5.8	1.1	0.0
N1-9	0.1	0.6	12.8	56.4	21.4	7.4	1.3	0.0
N1-10	0.1	1.0	13.6	57.1	22.8	4.6	0.8	0.0
N1-11	0.1	0.5	11.8	55.9	25.9	5.3	0.5	0.0
N1-12	0.1	0.4	10.7	55.0	28.2	5.1	0.5	0.0
N1-13	0.1	0.7	12.8	54.5	25.6	5.9	0.4	0.0
N1-14	0.1	0.6	14.8	57.3	20.7	4.9	1.4	0.2
N1-15	0.05	0.7	15.15	55.9	21.7	5.3	1.2	0.0
N1-16	0.1	0.6	11.9	61.2	24.0	2.2	0.0	0.0
N1-17	0.05	0.4	9.75	56.4	27.6	5.5	0.3	0.0
N1-18	0.1	0.6	10.8	56.8	25.5	6.2	0.0	0.0
N1-19	0.03	0.33	11.4	54.2	26.2	7.4	0.44	0.0
N1-20	0.04	0.26	10.1	53.4	27.9	7.4	0.9	0.0
N1-21	0.03	0.35	10.55	56.97	25.03	5.89	0.95	0.23
N1-22	0.2	0.5	11.0	58.0	27.0	3.3	0.0	0.0
N1-23	0.04	0.31	8.56	53.39	30.59	6.25	0.86	0.0
N1-24	0.05	0.12	7.07	51.11	31.55	8.39	1.45	0.26
N1-25	0.1	0.3	7.6	52.0	32.2	7.5	0.3	0.0
N1-26	0.03	0.28	8.91	51.15	26.20	10.77	2.66	0.0
N2-1	0.7	4.6	16.9	39.9	23.6	8.7	4.0	1.6
N2-2	0.2	1.3	15.6	39.0	29.0	10.0	2.8	2.1
N2-3	0.6	6.8	21.0	35.8	22.5	10.2	2.7	0.4
N2-4	0.2	3.1	17.4	35.8	23.4	15.6	3.7	0.8
N2-5	0.5	4.6	20.0	36.5	29.4	6.2	2.8	0.0
N2-6	0.2	1.3	13.8	40.6	28.8	13.0	0.0	2.3
N2-7	0.3	3.1	18.3	38.3	23.4	13.1	2.9	0.6
N2-8	0.3	2.6	16.0	38.6	27.4	12.7	2.4	0.0
N2-9	0.4	2.6	13.3	33.6	26.0	17.9	4.3	1.9

Table B.2 (continued)

Run No.	Size Range							
	1.0-2.0 (mm)	2.0-2.8 (mm)	2.8-4.0 (mm)	4.0-5.0 (mm)	5.0-6.3 (mm)	6.3-8.0 (mm)	8.0-10.0 (mm)	10.0-14.0 (mm)
N2-10	0.3	1.6	11.5	40.9	30.9	13.5	1.3	0.0
N2-11	0.2	2.2	13.8	38.3	26.5	16.6	1.8	0.6
N2-12	0.1	2.2	17.2	37.9	26.3	14.0	2.1	0.2
N2-13	0.1	1.4	13.7	34.6	24.5	18.2	6.1	1.4
N2-14	0.2	2.3	16.3	39.0	23.5	15.1	2.8	0.8
N2-15	0.2	1.1	10.1	40.7	31.5	15.6	0.8	0.0
N2-16	0.3	1.0	6.9	29.1	34.8	24.4	3.5	0.0
N2-17	0.1	0.5	8.9	35.3	30.4	18.9	5.9	0.0
N2-18	0.1	0.8	11.1	35.2	26.2	20.6	5.3	0.7
N2-19	0.1	0.6	9.5	33.0	25.4	21.5	8.2	1.7
N3-1	4.9	13.8	20.3	23.8	21.2	11.3	4.7	0.0
N3-2	2.1	10.8	23.8	28.3	21.1	8.1	3.6	2.2
N3-3	10.4	18.4	19.1	22.2	16.6	10.1	3.2	0.0
N3-4	8.9	17.6	18.7	19.8	17.0	11.7	5.2	1.1
N3-5	3.1	12.9	21.5	27.3	17.5	12.6	3.7	1.4
N3-6	1.7	11.1	25.1	31.3	21.7	9.1	0.0	0.0
N3-7	2.1	9.9	25.5	32.5	22.8	6.0	1.2	0.0
N3-8	1.7	10.1	20.6	30.2	22.4	10.9	3.7	0.4
N3-9	1.4	9.3	22.0	28.0	24.3	12.5	1.8	0.7
N3-10	7.1	15.4	18.2	21.7	17.3	12.4	5.8	2.1
N3-11	4.1	12.2	24.2	36.4	19.2	3.9	0.0	0.0
N3-12	6.3	7.9	18.1	16.6	23.3	14.2	13.6	0.0
N3-13	4.8	11.3	20.3	26.1	22.0	11.8	2.1	1.6
N3-14	1.1	8.4	19.9	26.2	23.2	14.0	6.0	1.2
N3-15	0.6	5.3	18.7	30.8	23.6	15.1	5.1	0.8
N3-16	7.1	15.8	16.3	20.7	17.1	14.8	6.7	1.5
N3-17	6.9	14.1	14.8	14.4	17.7	7.9	8.3	15.9 (?)
N3-18	1.7	11.2	24.3	32.4	21.6	7.2	1.2	0.4
N3-19	0.9	2.3	9.7	28.0	35.3	22.1	1.7	0.0
N3-20	0.6	5.3	20.7	29.9	24.1	13.8	4.3	1.3
N3-21	4.3	12.2	17.2	22.1	20.9	13.7	7.7	1.9
F-1	32.9	32.2	21.2	8.9	4.8	0.0	0.0	0.0
F-2	25.8	29.0	21.5	17.2	6.5	0.0	0.0	0.0
F-3	44.0	33.8	15.6	5.5	1.1	0.0	0.0	0.0
F-4	35.2	34.3	18.4	9.5	2.1	0.2	0.3	0.0
F-5	32.2	30.3	19.6	12.0	4.6	0.8	0.5	0.0

Table B.2 (continued)

Run No.	Size Range							
	1.0-2.0 (mm)	2.0-2.8 (mm)	2.8-4.0 (mm)	4.0-5.0 (mm)	5.0-6.3 (mm)	6.3-8.0 (mm)	8.0-10.0 (mm)	10.0-14.0 (mm)
F-6	35.3	26.7	19.2	11.9	6.2	0.6	0.1	0.0
F-7	17.9	25.4	24.4	18.7	10.9	1.7	0.8	0.2
F-8	20.2	36.8	30.0	13.0	0.0	0.0	0.0	0.0
F-9	12.8	41.7	28.5	12.8	3.5	0.7	0.0	0.0
F-10	20.1	35.6	25.1	13.9	4.9	0.2	0.2	0.0
F-11	28.9	31.7	21.0	12.5	5.3	0.4	0.2	0.0
F-12	21.6	25.8	23.1	17.6	9.5	1.9	0.4	0.1
F-13	12.6	27.3	35.0	19.1	6.0	0.0	0.0	0.0
F-14	26.8	36.1	23.8	9.2	3.4	0.7	0.0	0.0
F-15	21.4	32.9	24.1	14.8	6.3	0.4	0.1	0.0
F-16	22.2	29.9	23.4	14.8	9.0	0.6	0.1	0.0
F-17	30.8	24.8	18.5	13.0	9.0	3.3	0.4	0.2
F-18	33.6	32.8	21.6	8.8	3.2	0.0	0.0	0.0
F-19	20.2	23.6	31.5	19.1	5.6	0.0	0.0	0.0
F-20	17.8	46.3	25.0	8.6	2.0	0.3	0.0	0.0
F-21	19.8	30.1	26.3	16.5	6.8	0.5	0.0	0.0
F-22	13.7	24.3	25.5	20.5	12.9	2.4	0.4	0.3
C-1	0.5	0.5	3.7	17.0	25.9	36.0	16.4	0.0
C-2	0.0	0.2	2.5	15.2	29.8	41.2	11.1	0.0
C-3	0.2	0.3	2.6	10.6	23.5	48.6	10.3	3.9
C-4	0.1	0.8	2.9	8.3	16.5	53.4	16.1	1.9
C-5	0.1	0.2	2.3	8.8	20.1	48.1	17.8	2.6
C-6	0.2	1.2	4.3	11.3	19.4	42.5	13.4	7.7
C-7	0.06	0.14	1.8	8.4	20.4	51.0	14.0	4.2
C-8	0.6	2.3	4.9	11.3	18.0	39.5	15.9	7.5
C-9	0.1	0.2	1.3	8.5	17.9	49.2	16.3	6.5
C-10	0.03	0.24	2.10	9.13	20.3	49.3	14.1	4.8
C-11	0.1	0.8	3.9	11.9	20.5	40.7	13.3	8.8
C-12	0.1	0.9	5.0	13.1	20.6	40.8	14.7	4.8
C-13	0.1	0.5	2.7	9.1	18.9	43.6	15.6	9.5
C-14	0.05	0.13	1.38	10.17	24.43	51.00	11.82	1.02
C-15	0.1	1.0	7.2	18.1	21.7	35.6	11.7	4.6
C-16	0.03	0.06	0.71	4.52	14.21	50.88	21.19	8.40
C-17	0.02	0.17	2.97	13.25	20.55	41.93	13.77	7.34
C-18	0.03	0.10	0.92	5.21	13.78	43.97	23.67	12.32

Table B.2 (continued)

Run No.	Size Range							
	1.0-2.0 (mm)	2.0-2.8 (mm)	2.8-4.0 (mm)	4.0-5.0 (mm)	5.0-6.3 (mm)	6.3-8.0 (mm)	8.0-10.0 (mm)	10.0-14.0 (mm)
B-1	15.1	42.5	24.6	11.2	6.6	0.0	0.0	0.0
B-2	31.4	35.0	15.3	13.2	5.1	0.0	0.0	0.0
B-3	13.6	28.5	18.1	17.0	15.1	7.7	0.0	0.0
B-4	13.1	25.8	18.1	17.7	17.4	7.5	0.4	0.0
B-5	22.5	24.5	13.1	12.7	12.4	13.4	1.1	0.3
B-6	20.4	21.3	12.3	13.2	14.3	15.3	3.2	0.0
B-7	15.7	20.1	12.7	12.5	15.1	20.5	3.1	0.3
B-8	6.1	26.7	29.9	24.5	10.8	2.0	0.0	0.0
B-9	14.9	20.3	15.8	26.1	19.1	3.8	0.0	0.0
B-10	13.2	32.8	20.8	17.1	12.2	3.4	0.5	0.0
B-11	14.3	29.4	17.7	16.3	13.1	8.4	0.8	0.0
B-12	11.8	23.5	15.2	13.8	15.0	17.2	2.3	1.2
B-13	7.6	21.8	16.8	14.3	16.5	19.0	2.8	1.2
B-14	8.4	28.3	18.7	18.4	15.4	8.6	2.2	0.0
B-15	9.9	30.2	22.4	18.6	13.8	5.1	0.0	0.0
B-16	8.5	24.8	18.1	19.1	17.5	11.2	0.8	0.0
B-17	13.0	27.9	18.0	15.4	15.4	9.8	0.5	0.0
B-18	9.8	24.6	16.4	15.5	16.7	14.9	1.9	0.2
B-19	15.7	20.1	12.3	12.6	12.5	22.5	3.4	0.9
B-20	26.28	31.56	15.05	12.64	10.54	3.85	0.08	0.00
B-21	5.8	22.8	19.1	20.9	23.4	8.0	0.0	0.0
B-22	13.3	33.5	19.5	16.1	12.5	4.4	0.5	0.2
B-23	5.0	16.6	15.5	18.1	19.9	22.1	2.2	0.6
B-24	6.6	9.1	10.1	13.7	16.8	31.8	8.6	3.3

Table B.3 Size Distribution of Final Bed Surface as Percentage of Total (Armfield Flume)

Run No.	Size Range							
	1.0-2.0 (mm)	2.0-2.8 (mm)	2.8-4.0 (mm)	4.0-5.0 (mm)	5.0-6.3 (mm)	6.3-8.0 (mm)	8.0-10.0 (mm)	10.0-14.0 (mm)
N1-1	0.4	2.4	15.7	47.7	18.6	8.9	3.4	2.9
N1-2	0.3	2.3	15.0	48.4	18.5	9.2	3.7	2.6
N1-3	0.3	2.4	15.3	47.6	17.3	9.5	4.3	3.3
N1-4	0.4	2.7	15.6	47.5	18.2	8.0	4.4	3.2
N1-5	0.5	2.7	16.3	50.8	17.7	7.4	2.4	2.2
N1-6	0.5	3.0	16.3	49.7	18.1	8.3	3.0	1.1
N1-7	0.6	3.1	15.6	48.8	16.0	9.1	4.4	2.4
N1-8	0.9	3.1	15.3	47.5	17.4	8.5	4.1	3.2
N1-9	0.7	3.1	17.6	48.3	16.4	7.7	3.0	3.2
N1-10	0.3	1.8	13.0	44.3	20.5	11.1	4.4	4.6
N1-11	0.5	2.5	16.7	48.1	17.9	8.7	3.7	1.9
N1-12	0.5	2.4	14.4	47.3	19.2	10.2	3.2	2.8
N1-13	0.3	2.2	15.4	49.1	18.0	9.5	2.6	2.9
N1-14	0.8	3.6	17.0	49.0	16.1	8.9	2.8	1.8
N1-15	0.6	3.0	16.9	45.8	17.1	10.3	3.0	3.3
N1-16	0.3	2.3	14.7	51.8	18.2	7.7	2.8	2.2
N1-17	0.8	2.7	15.9	49.4	18.1	7.5	3.7	1.9
N1-18	0.2	1.9	14.2	48.3	21.0	9.2	3.7	1.5
N1-19	0.4	2.7	16.6	50.0	16.7	9.3	3.3	1.0
N1-20	0.4	2.0	15.6	45.3	18.8	11.8	4.4	1.7
N1-21	0.4	2.6	17.6	49.2	17.0	8.5	2.5	2.2
N1-22	1.0	3.7	17.2	50.1	16.9	7.9	2.4	0.8
N1-23	0.2	1.5	13.5	50.9	20.3	8.7	3.8	1.1
N1-24	0.1	0.9	11.9	47.3	19.9	12.8	4.1	3.0
N1-25	0.3	1.7	14.6	51.5	19.6	8.1	3.1	1.1
N1-26	0.2	2.1	15.4	51.2	17.1	8.0	3.5	2.5
N2-1	-	-	-	-	-	-	-	-
N2-2	0.8	4.9	15.5	28.8	17.4	16.6	8.9	7.1
N2-3	2.7	8.1	16.6	26.9	15.9	14.3	8.1	7.4
N2-4	2.5	7.5	16.6	26.9	15.7	15.7	8.5	6.6
N2-5	2.4	7.7	17.3	28.5	17.4	15.1	6.4	5.2
N2-6	1.0	4.4	15.2	29.3	17.8	16.8	9.4	6.1
N2-7	2.3	7.2	16.3	27.0	14.7	17.9	7.5	7.1
N2-8	2.4	7.1	17.1	27.6	16.3	15.9	6.7	6.9
N2-9	1.6	5.8	15.9	25.1	14.9	16.8	9.8	10.1

Table B.3 (continued)

Run No.	Size Range							
	1.0-2.0 (mm)	2.0-2.8 (mm)	2.8-4.0 (mm)	4.0-5.0 (mm)	5.0-6.3 (mm)	6.3-8.0 (mm)	8.0-10.0 (mm)	10.0-14.0 (mm)
N2-10	-	-	-	-	-	-	-	-
N2-11	1.8	6.4	17.2	27.1	16.8	17.4	8.6	4.7
N2-12	1.7	7.0	17.3	28.6	17.4	14.7	7.6	5.7
N2-13	2.6	7.7	17.4	28.3	15.9	15.0	7.1	6.0
N2-14	5.2	11.2	20.1	26.5	14.7	12.6	5.2	4.5
N2-15	0.7	3.9	15.4	30.5	20.0	16.8	7.5	5.2
N2-16	0.4	2.0	14.7	36.0	21.6	15.3	6.5	3.5
N2-17	0.5	2.8	15.3	31.6	19.0	18.0	8.8	4.0
N2-18	0.6	3.9	18.9	32.4	16.8	16.2	7.0	4.2
N2-19	0.7	4.5	17.3	30.4	16.2	16.6	8.9	5.4
N3-1	3.9	6.9	10.3	14.5	14.1	17.7	15.4	17.2
N3-2	9.5	12.8	14.6	16.3	13.7	13.4	11.7	8.0
N3-3	9.2	12.4	12.5	14.6	12.3	15.4	11.3	12.3
N3-4	9.0	11.0	12.3	13.7	12.0	16.4	13.4	12.2
N3-5	10.6	13.9	13.3	14.1	11.9	13.5	9.1	13.6
N3-6	8.2	12.9	14.0	15.4	12.9	15.1	11.7	9.8
N3-7	9.1	13.7	14.0	15.0	12.7	14.1	9.7	11.7
N3-8	7.9	12.3	13.7	15.6	12.3	13.7	11.9	12.6
N3-9	7.9	13.4	13.8	15.0	11.7	13.8	12.4	12.0
N3-10	13.1	14.1	14.1	14.7	11.9	14.5	8.9	8.7
N3-11	6.9	13.3	17.3	19.2	14.5	13.9	8.2	6.7
N3-12	3.0	6.7	11.7	17.4	16.1	18.5	11.6	15.0
N3-13	11.2	15.7	15.0	14.6	11.3	14.5	10.6	7.1
N3-14	9.8	14.1	13.8	14.2	11.5	15.0	9.9	11.7
N3-15	6.3	11.6	14.6	17.5	14.2	16.5	10.5	8.8
N3-16	10.7	14.0	15.0	15.7	12.0	13.2	8.9	10.5
N3-17	9.0	13.4	14.8	15.9	13.8	13.8	10.0	9.3
N3-18	8.9	14.4	14.9	15.7	13.7	15.5	10.1	6.8
N3-19	4.8	8.3	13.7	17.6	15.2	16.4	12.2	11.8
N3-20	8.1	13.2	14.6	15.8	12.2	13.4	11.6	11.1
N3-21	9.7	14.9	16.2	16.3	12.4	11.7	8.5	10.3
F-1	29.8	18.0	13.7	10.7	8.1	7.1	5.4	7.2
F-2	29.1	18.9	15.2	11.9	8.5	7.2	5.4	3.8
F-3	32.2	19.6	14.2	11.0	6.9	5.9	5.1	5.1
F-4	36.9	20.3	13.8	10.3	7.0	5.5	3.2	3.0
F-5	34.9	18.3	12.6	10.0	7.5	6.9	5.1	4.7

Table B.3 (continued)

Run No.	Size Range							
	1.0-2.0 (mm)	2.0-2.8 (mm)	2.8-4.0 (mm)	4.0-5.0 (mm)	5.0-6.3 (mm)	6.3-8.0 (mm)	8.0-10.0 (mm)	10.0-14.0 (mm)
F-6	35.9	20.4	13.4	9.8	6.8	5.9	4.0	3.8
F-7	27.8	19.7	14.3	11.4	8.4	8.1	4.8	5.5
F-8	32.9	20.7	14.5	11.4	7.1	5.8	4.0	3.6
F-9	29.7	20.7	15.1	11.9	7.8	5.9	4.4	4.5
F-10	30.9	19.3	14.4	10.7	8.6	6.4	5.1	4.6
F-11	36.5	20.2	13.0	10.5	7.4	5.3	3.8	3.3
F-12	37.3	19.5	13.1	9.3	7.4	5.5	3.5	4.4
F-13	28.5	19.6	15.5	12.7	7.9	7.0	5.1	3.7
F-14	34.3	20.0	14.1	10.3	6.7	6.1	4.7	3.8
F-15	34.0	18.6	12.9	10.9	8.1	6.3	4.3	4.9
F-16	33.3	21.2	13.9	10.6	7.3	6.4	4.1	3.2
F-17	36.4	21.2	12.8	9.9	6.3	6.5	4.3	2.6
F-18	34.0	20.2	15.0	11.2	8.1	4.2	4.7	2.6
F-19	32.6	19.6	15.2	11.4	7.4	6.4	3.5	3.9
F-20	36.0	20.5	13.5	10.4	6.3	6.0	4.1	3.2
F-21	29.7	20.6	14.3	11.9	7.6	6.3	4.5	5.1
F-22	31.4	21.1	13.7	10.6	6.9	6.0	5.9	4.4
C-1	0.9	2.1	5.5	11.9	15.7	36.3	19.2	8.4
C-2	0.6	1.6	4.9	10.6	17.1	33.6	19.2	12.4
C-3	1.9	2.7	5.8	11.8	15.6	34.5	17.0	10.7
C-4	0.9	2.3	5.8	11.6	15.7	31.2	20.9	11.6
C-5	1.0	2.9	6.1	12.6	17.0	35.3	15.7	9.4
C-6	2.1	4.5	7.7	13.6	15.8	30.6	16.0	9.7
C-7	1.0	2.4	5.9	12.1	15.9	30.2	21.3	11.2
C-8	1.8	4.2	8.1	14.9	17.5	30.7	13.2	9.6
C-9	1.2	2.6	6.7	12.5	17.6	32.3	18.3	8.8
C-10	0.9	2.4	6.7	12.1	14.9	31.9	18.3	12.8
C-11	1.9	4.4	8.1	14.3	16.8	29.5	15.4	9.6
C-12	3.2	5.5	9.3	14.3	15.6	31.3	13.9	6.9
C-13	2.2	4.5	8.1	13.7	16.4	29.7	16.8	8.6
C-14	0.8	2.4	6.0	13.1	17.3	34.4	16.6	9.4
C-15	2.0	6.3	10.7	15.0	16.3	27.8	14.0	7.9
C-16	0.04	0.42	2.63	8.95	16.15	35.72	20.99	15.10
C-17	1.1	4.3	9.0	15.0	16.1	27.6	14.6	12.3
C-18	0.8	1.9	5.5	14.1	18.1	32.9	15.8	10.9

Table B.3 (continued)

Run No.	Size Range							
	1.0-2.0 (mm)	2.0-2.8 (mm)	2.8-4.0 (mm)	4.0-5.0 (mm)	5.0-6.3 (mm)	6.3-8.0 (mm)	8.0-10.0 (mm)	10.0-14.0 (mm)
B-1	19.4	14.3	8.0	9.2	11.3	23.0	7.0	7.8
B-2	21.3	14.4	8.1	8.1	10.4	22.3	8.9	6.5
B-3	20.5	14.3	8.7	9.1	10.0	24.8	6.3	6.3
B-4	20.5	14.3	8.4	8.4	9.0	24.8	6.9	7.7
B-5	23.7	15.2	8.4	8.1	8.7	21.7	7.3	6.9
B-6	22.8	14.8	7.9	7.8	9.4	22.7	7.6	7.0
B-7	22.0	15.1	8.4	8.7	9.1	23.1	7.2	6.4
B-8	23.1	16.1	8.6	8.8	9.6	21.0	6.6	6.2
B-9	17.4	14.7	9.3	9.2	11.3	22.5	9.8	5.8
B-10	18.0	13.0	8.0	8.5	10.0	24.8	9.3	8.4
B-11	22.4	14.5	7.9	8.7	10.4	25.0	6.1	5.0
B-12	20.6	13.7	7.8	7.8	9.0	26.2	8.2	6.7
B-13	20.3	13.4	7.8	8.0	9.2	24.5	10.0	6.8
B-14	14.4	11.4	8.1	9.2	11.1	28.1	9.3	8.4
B-15	17.5	13.7	9.0	9.0	10.6	25.4	8.4	6.4
B-16	21.4	14.8	8.2	8.8	9.4	21.8	8.6	7.0
B-17	22.3	14.6	9.1	10.2	10.8	16.6	10.2	6.2
B-18	19.8	13.6	7.7	7.7	8.8	29.3	6.4	6.7
B-19	23.6	17.1	8.7	8.7	8.4	20.6	7.1	5.8
B-20	25.6	15.1	8.1	6.5	10.1	21.3	6.3	7.0
B-21	20.2	16.1	9.7	8.4	12.1	22.4	6.2	4.9
B-22	24.0	16.0	8.1	6.9	10.5	21.7	6.6	6.2
B-23	15.6	14.7	9.5	8.5	12.7	25.3	8.1	5.6
B-24	20.7	19.0	9.8	8.1	10.8	22.0	5.8	3.8

Appendix C

Table C.1 Measured Data for Mix HR (HR Wallingford Flume)

Run No.	Bed Width B (m)	Slope J x 10^3	Flow Q ($L\ s^{-1}$)	Depth h (m)	Sampling Duration (mins)	Bedload Yield (kg)	Water Temp. (^oC)
HR-1	0.80	4.5	19.6	0.044	immobile bed		10
HR-2	0.80	4.5	22.6	0.050	immobile bed		10
HR-3	0.80	4.5	38.6	0.077	weak motion of grains <5 mm		10
HR-4	0.80	4.5	49.0	0.088	326	21.3	10
HR-5	0.80	4.5	52.5	0.091	230	49.8	10
HR-6	0.80	4.5	56.4	0.095	216	77.8	10
HR-7	0.80	4.5	65.0	0.100	159	42.8	10
HR-8	0.80	4.5	74.5	0.105	3	11.0	10
HR-9	0.80	4.5	73.5	0.110	189	76.6	10
HR-10	0.80	4.5	83.7	0.122	10.5	15.5	10
HR-11	0.80	4.5	104.5	0.130	39	47.8	10
HR-12	0.80	4.5	140.0	0.150	6.8	20.2	10

Table C.2 Size Distribution of Bedload as Percentage of Total (HR Wallingford Flume)

Run No.	Size Range							
	<0.25 (mm)	0.25-0.36 (mm)	0.36-0.5 (mm)	0.5-0.71 (mm)	0.71-1.0 (mm)	1.0-1.4 (mm)	1.4-2.0 (mm)	2.0-2.8 (mm)
HR-4	0.51	0.68	0.60	0.58	0.54	0.71	1.01	3.16
HR-5	0.32	0.54	0.58	0.56	0.50	0.55	1.16	5.12
HR-6	0.83	3.93	5.24	5.85	4.66	4.04	4.36	7.29
HR-7	0.11	0.09	0.08	0.09	0.07	0.12	0.87	5.95
HR-9	0.01	0.08	0.10	0.12	0.11	0.33	1.85	8.41
HR-10	0.69	2.94	4.26	4.80	4.51	3.57	4.01	7.35
HR-11	0.05	0.04	0.09	0.20	0.36	0.90	2.65	7.09
HR-12	0.17	0.47	0.64	0.71	0.87	1.04	1.85	4.93

Table C.2 (continued)

Run No.	Size Range							
	2.8-4.0 (mm)	4.0-5.6 (mm)	5.6-8.0 (mm)	8.0-9.5 (mm)	9.5-12.7 (mm)	12.7-15.9 (mm)	15.9-19.1 (mm)	19.1-22.2 (mm)
HR-4	21.88	42.35	23.07	3.12	1.16	0.63	0.00	0.00
HR-5	27.71	38.12	19.11	1.54	2.56	0.50	1.13	0.00
HR-6	22.23	23.46	12.88	2.42	2.17	0.64	0.00	0.00
HR-7	33.22	38.50	17.52	1.45	1.42	0.20	0.31	0.00
HR-9	35.12	33.57	16.01	1.82	2.01	0.21	0.25	0.00
HR-10	23.26	24.11	11.89	1.61	3.43	1.64	0.91	1.02
HR-11	30.02	33.58	17.06	1.94	2.93	1.99	0.37	0.73
HR-12	27.11	35.42	18.00	2.11	3.73	1.61	0.98	0.36